FINITE ELEMENT ANALYSIS OF AIRCRAFT TYRES

BY

MOHAMMAD H. BEHROOZI

A thesis submitted to the College of Engineering and Physical Sciences of the University of Birmingham for the degree of

DOCTOR OF PHILOSOPHY

School of Mechanical Engineering

College of Engineering and Physical Sciences

The University of Birmingham

February 2014

FINITE ELEMENT ANALYSIS OF AIRCRAFT TYRES

Mohammad Behroozi

Supervised by

Dr Oluremi Olatunbosun

February 2014

THE UNIVERSITY OF BIRMINGHAM
Edgbaston, Birmingham, West Midlands B15 2TT, United Kingdom

Abstract

In this thesis, the Finite Element (FE) Analysis of aircraft tyres is presented. The modelling and simulations of detailed construction of tyre enable tyre manufacturers to evaluate new designs and development before a prototype is fabricated, and aim to reduce the research costs and efforts to optimise the current structure design in tyres. In addition, the other objective is to develop a user friendly environment so that the complicated Finite Element implementations are more effortlessly accessible to designers and engineers who are not quite familiar with the base knowledge of solving analysis and optimisation problems by Finite Element. Eventually, the results from Finite Element analysis enable tyre designers to obtain tyre models with higher fidelity for design synthesis and vehicle/aircraft dynamicists to understand tyre mechanical behaviour on ground manoeuvres.

To achieve abovementioned objectives, the following approaches are proposed. The finite element approach is selected to be used for modelling of the tyre macro-mechanical behaviour such as deformations and force and moments generated in contact patch as well as the micro-mechanical ones where occurs inside the tyre structure such as stress and strain of the compounds and contact pressure. The finite element tyre models are correlated to a number of design checks and standard tests such as profile growth after inflating tyre, sidewall deformation when tyre is loaded, footprint, contact pressure, and load-deformation data so that the results from finite element model can be trusted. In addition, a standard approach toward modelling of the aircraft tyres is proposed from the CAD sketching to the material modelling of tyre compounds and analysis configuration.

On the other hand in order to develop a tyre model with higher fidelity, the air is modelled as the tyre inflator for a better prediction of the vertical stiffness and footprint area. Moreover, the FE configuration parameters such as mesh size and tyre geometry are investigated for optimisation of the runtime and improvement of the mechanical behaviour for a more accurate replication of the physical testing. To obtain the results usable for modelling of the tyre mechanical behaviour on ground, the rolling tyre is simulated on the runway to replicate the taxiing manoeuvres, which includes operations such as extreme

cornering, braking, and heat build-up in free rolling condition to characterise the tyre performance on aircraft ground manoeuvres for engineers in Airbus.

Finally, TAIS (Tyre Analysis Interface System) is developed based on the design requirements from Dunlop Aircraft Tyres. TAIS is an input/output interface in tyre analysis for non-expert FE users and benefits from material database builder which was initially developed in order to obtain the tyre mechanical properties.

In this research, two tyres (a military aircraft tyre and a civil aircraft one) are employed for experimentation in order to evaluate the tyre modelling accuracy. When the tyres are validated, a number of simulations are run to characterise the tyre performance in generation of forces and moments across the contact patch using a steady-state approach. Last not the least, the tyre is freely rolled on the runway using an explicit approach to investigate the energy dissipation in material hysteretic loops heat generation due to the tyre viscoelasticity.

The following statements present the contribution aspects of this research. As the beginning, a standard approach for analysis and design synthesis of aircraft tyres was proposed. This was aimed to be developed based on generalisation concept so that the analysis approach is not limited to a specific brand or tyre size. Moreover, the capability of tyre inflator modelling was also introduced to obtain higher fidelity tyre models for a better prediction of deformed shape and inflation pressure change in tyre when the vertical loading is applied. Heat generation of rubber compound in cyclic deformation due to viscose behaviour and hysteretic loops was implemented in a fully coupled thermal-displacement analysis, solved in an explicit approach. In addition, the Tyre Analysis Interface System was developed as a tailor-made analysis environment for inexpert designers to enable them performing the design analysis in a shorter and more efficient way.

Acknowledgement

In the first place, I would like to express my greatest gratitude to Dr Oluremi Olatunbosun for his supervision and guidance from the very early stage of this research as well as sharing his extraordinary experiences throughout the work. I would also like to give him my special thanks for trusting me and opening my eyes to the world of professionals and support me compassionately to grow up step-by-step in my educational and personal life like a father to his son.

It is a pleasure to sincerely thank my senior colleagues, Dr Xiaoguang Yang and Dr Emanuel Bolarinwa, for scientific discussions, giving valuable advices, and sharing brilliant ideas as well as being good friends in my personal life while living in Birmingham.

I would like to extend my thanks to Dr Wei Deng and Mr Martin Pye from Dunlop Aircraft Tyres Ltd for their technical and laboratory supports. I would also like to acknowledge all the engineers and directors from Dunlop, Airbus, Midlands Aerospace Alliances, and West Midlands Aviation for their contributions in discussions, useful evaluations, and collaborations to bring the ATFEM project to a successful completion. I highly appreciate to the decision committee in European Union to grant funds to this project and made this remarkable collaboration possible.

My parents deserve special mention for their continuous support and prayers. My Father in the first place is the person who put the fundament of my learning character, showing me the joy of intellectual pursuit ever since I was a child, and my Mother is the one who sincerely raised me with her caring and gentle love.

Words fail me to express my appreciation to my wife Samaneh whose dedication, love and persistent confidence in me, has taken the load off my shoulder. I owe her for being unselfishly let her intelligence, passions, and ambitions collide with mine.

Table of Contents

List of Figures

List of Tables

List of Nomenclature

f_r	Rolling resistance coefficient
R_x	Rolling resistance force
M	Weight on the wheel
C	Constant reflecting loss and elastic characteristics of the tyre material
D	Outside diameter
H	Tyre section height
W	Tyre section width
t	Track Depth
h	Height of the centre of gravity above the road
α	Instantaneous slip angle
v	Instantaneous lateral sliding velocity
u	Vehicle longitudinal speed
s	Slip ratio
r	Effective tyre rolling radius
ω	Tyre angular velocity
v_{sx}	Sliding Velocity
x_s	Sliding displacement
γ	inclination angle or camber
k_z	vertical stiffness
F_z	vertical load
z	Vertical deformation
k_y	Lateral stiffness
F_y	lateral load
y	Lateral deformation
c_α	Cornering stiffness
F_α	Cornering force
F_{zo}	Reference vertical load
$c_{F\alpha}$	Cornering stiffness
k_x	longitudinal stiffness
F_x	longitudinal load
x	longitudinal deformation
σ_x	Longitudinal relaxation length
σ_y	lateral relaxation length
c_s	longitudinal slip stiffness
c_α	cornering stiffness
k_x	longitudinal stiffnesses
k_y	lateral stiffnesses

Vw	Wheel Spin Velocity
Vt	Trajectory Velocity
FyRD	Cornering Force
FxRD	Tractive Force
Fz	Normal Force
Mz	Aligning Moment
Tw	Wheel Torque
My	Rolling Moment
Mx	Overturning Moment
IA	Inclination Angle
SA	Slip Angle
k_{axial}	Equivalent axial (bending) stiffnesses
$k_{lateral}$	Equivalent lateral (bending) stiffnesses
A	Cross-sectional area
E	Elastic modulus
L	Length
S_{comp}	Comprehensive Slip
S_{long}	Longitudinal Slip
S_{lat}	Lateral Slip
μ	Instantaneous friction coefficient
μ_{sta}	Static friction coefficient
μ_{dyn}	Dynamic friction coefficient
S^*	Critical friction coefficient
F_z	Vertical load
C_s	Longitudinal tyre stiffness
α^*	Critical slip angle
C_α	Lateral tyre stiffness
r_{eff}	Effective rolling radius
Y	Output variable F_x, F_y, and M_z
V_{sx}	Sliding velocity
X	Input variable $\tan\alpha$ or κ
B	Stiffness factor
C	Shape factor
D	Peak value
E	Curvature factor
S_H	Horizontal shift
S_V	Vertical shift
F	Generated force in spring
Δx	Deformation in spring
K	spring stiffness
σ	stress

ϵ	strain
τ	shear stress
Υ	shear strain
G	shear modulus
B	Bulk modulus
V	volume of the substance
P	uniform hydrostatic pressure
I_1, I_2, and I_3	strain tensor invariants (first, second and third)
λ_1, λ_2, and λ_3	principal stretch ratios
λ	stretch ratio
L_0	initial length
ϵ	Engineering strain
W_e	potential energy per unit volume
λ_i	principal stretches
c_{ij}	deviatory behaviour that governs the isochoric shear behaviour
D_i:	the compressibility and is ignored for fully incompressible rubber
n	chain density per unit of volume
k	Boltzmann constant
T	absolute temperature
jG_0	initial shear modulus
λ_m	locking stretch
K_b	Boltzmann constant
η	dashpot viscosity
k	springiness constant
λ	rate of relaxation
σ_m	Maxwell stress
$J(t)$	compliance modulus
σ_0	constant applied stress
ϵ_0	constant applied strain
G'	storage moduli
G''	loss moduli
σ_∞	equilibrium stress term
$K(t)$	creep function
$F(t)$	relaxation function
$G(t)$	time-dependent shear modulus
G_∞	long term shear modulus in relaxation test
F_t	tensile load
A_0	nominal cross-section area
L_t	length
L_0	initial length
K_{uu}	mechanical stiffness

$K_{\theta\theta}$	thermal coefficients
$K_{u\theta}$	Combination of mechanical stiffness and thermal coefficients
θ	temperature variables
$[M]$	Mass matrices
$[C]$	Damping matrices
$[K]$	Stiffness matrices
$\{\varphi\}$	eigenvector
β	eigenvalue
F_μ	friction forces
p	average pressure across the element contact surface
τ_μ	resultant of the shear stresses across the element surface
$\tau_{\mu x}$	shear stress components along the x coordinate on the element surface coordinate system
$\tau_{\mu x}$	shear stress components along the y coordinate on the element surface coordinate system
τ_{max}	maximum allowable shear stress on the element surface
θ_I	Initial temperature
K	Fluid bulk modulus
$V(p,\theta)$	Current fluid volume
$V_0(\theta)$	Fluid volume at zero pressure and current temperature
$V_0(\theta_I)$	Fluid volume at zero pressure and initial temperature
$\rho(p,\theta)$	current fluid density
$\rho_0(\theta)$	density at zero pressure and current temperature
ρ_R	Reference fluid density

List of Abbreviations

EEA	European Economic Area
EC	European Commission
UK	United Kingdom
IATA	International Air Transport Association
BEA	Bureau Enquêtes-Accidents
CAA	Civil Aviation Authority
NHTSA	National Highway Traffic Safety Administration
FAA	Federal Aviation Administration
JIS	Japanese Industrial Standards
TSO	Technical Standard Order
ISO	Organisation Internationale de Normalisation
TERATYRE	Aircraft tyre test benches vehicle
NFM	Neyrpic Framatome Mécanique
FE	Finite Element
FEA	Finite Element Analysis
GUI	Graphical User Interfaces
CAE	Computer Aided Engineering
API	Application Programming Interface
ODB	Output Database
DATL	Dunlop Aircraft Tyres Limited
TAIS	Tyre Analysis Interface System
EPM	End per Meter
RRR	Revolutionarily Reinforced Radial
CAB	Combat Aviation Brigade
EASA	European Aviation Safety Agency
CAD	Computer Aided Design
MSRP	Manufacturers' Suggested Retail Price
ITF	Inter-Tread Reinforcing Fabric
SSF	Static Stability Factor
TAIS	Tyre Analysis Interface System
DOE	Design of Experiment
MF	Magic Formula
CFD	Computational fluid dynamics
DATL	Dunlop Aircraft Tyres Limited
HPC	High-Performance Computation
TAIS	Tyre Analysis Interface System

Chapter 1: Introduction

1.1. Motivation

Air travel has been measured as the second most popular mode of transport in the 27 European Union Countries (EEA members), responsible for equivalent rate of 22.9% of external trade value in both export/import in 2010 (EC, 2012). Air travel is also the most popular route for passengers both to and from the UK. In 2012, air routes were selected by passengers for 80 per cent of all visits by UK residents who are travelling overseas, and for 73 per cent of all inbound visits (ONS, 2013). The significance of air transport comes not only from connecting peoples, countries and cultures, but also speeding up the access to global markets and generating trade and tourism.

The biggest challenge ahead of the air transportation industry is to prioritise safety as the number one issue in this industry. A total number of 414 fatalities were reported in 2012 within 15 fatal accidents (IATA, 2013). As a case in point, during a Concorde take-off operated by Air France in 2000, a burst tyre occurred and ruptured the wing fuel tank. Leaking fuel was then ignited and the engines exploded. The aircraft crashed shortly afterwards and 113 passengers were killed (BEA, 2002). There are seven significant safety risks in aviation: loss of control, runway excursions, controlled flight into terrain, runway incursion, airborne conflict, ground handling and fire (CAA, 2011). Ground related issues instigated the highest number of fatalities amongst the aircraft safety incidents (CAA, 2011), which is typically associated with safety in tyre/terrain behaviour during taxiing, take-off and landing.

The main functionality of the tyres is to support the aircraft's weight while it is on the ground. The tyre rolling during taxiing generates tremendous heat in the rubber compounds owing to large sidewall deflection, and this will result in sharp local temperature rise (Clark

& Dodge, 1984) and (Clark & Dodge, 1982). Tyres also have a high tread wear ratio due to the extreme side slip angles encountered during taxiing and abrupt low to high rolling speed in landing, when a stable and cushioned ride is expected. The take-off manoeuvre is of further concern due to having to reach the highest ground speed of the aircraft while sustaining greatest load mainly due to its unburned fuel. A tyre failure upon landing can occur due to misalignment of tyre on landing gear or tyre overheating and skidding due to applying the brakes severely to stop the aircraft in a shorter distance on the runway. Last but not the least, the landing impact should also be absorbed by the tyre in conjunction with the landing gears mechanism (Michelin, 2006).

Within a take-off manoeuvre, the Airbus A380 needs to reach a safe take-off speed, that is so called V2 speed (Bellonte, 2005), of 157 knots (290 km/h) (Watson, 2005) on the runway. That can be converted into a rolling speed of 1098 rpm for a Bridgestone's standard radial aircraft tyre 1400x530R23 (Bridgestone , 2006) with nominal size of 1.4 m in diameter. This ground speed in addition to the weight of the aircraft brings a high rate of wear in tread as well as heat build-up issues in the side wall.

To provide more quantitative perception of the tyre operating condition, a sharp heat build-up equivalent to steady state temperature increase to 90° C under 32% sidewall deflection is produced in the tyre bead at a speed of 30 knots (55.56 km/h) during taxiing to the runway (Goodyear, 2011). This temperature can be increased to a value of 105°C at higher taxiing speed and sidewall deflection (Goodyear, 2011), which is a deterioration point for most car tyres (NHTSA, 2001). These facts inspire tyre designers towards a challenging design, which not only should comply with the desired performance required by aviation authorities, but come up with innovative solutions in order to accelerate the competitiveness factors such as

safety parameters and number of re-treading cycles among the other suppliers for the range of encountered loads, speeds and operating conditions.

The above-mentioned extreme requirements direct the tyre design toward a highly engineered product in order to adapt it for such demanding conditions. For these demands, tyres are designed as a composite of rubber toppings strengthened with fabric and steel cords. Each topping is reinforced at different angles and symmetrically orientated with different levels of strength where the majority of tyre mechanical behaviours are built. Hence, the tyre mechanical performance is engineered by tyre specialist through variation of those parameters in response to those extreme safety demands and based on adjustment of rubber compounds' properties.

The concerns toward safely operating aircraft tyres tends to very costly design and manufacturing processes in order to meet strict regulation, particularly given the fact that these tyres are operational for 1500 to 1800 landings (Rayna, 2004), depending on different tyres. However, the tyre tread wears away quickly to below permitted threshold in approximately 250 to 300 landings (Rayna, 2004), and hence the tyre is sent out for re-treading corresponding to its regular maintenance standards (FAA, 2006). It is due to frictional shear stress during landing principally driven by speed difference between the landing speed (150 knots or 278 km/h for Boing 777-300 (Feiertag, 2011)) and zero rolling speed at the instant of contact with the runway. The large deflection produced in the sidewall and wide contact patch due to aircraft weight can increase the tread wear. Therefore, aircraft tyres are engineered with stronger structure for longer life to be re-treaded in order to cut down on cost with reducing the total number of tyres that need to be replaced within a specific time interval.

1.2. Research theme

The manufacturers of aircraft tyre are forced to pass a number of firm specifications that are legislated by either the well-known Federal Aviation Administration (FAA) in United States for safety oversight of approximately 7300 US commercial airlines and air operators (FAA, 2013), or other regional authorities such as the Japanese Industrial Standard JIS K6251 & JIS K6257 in Japan. The FAA's approved standard performance for certification of most aircraft tyre's range and manufacturer can be found on the FAA website in the Regulatory and Guidance Library, and is regularly updated in response to new technologies and safety requirements, and is the so called Technical Standard Order TSO-C62. The safety requirements by TSO-C62 are the outcome of extensive engineering investigations in order to meet both normal and emergency situations. Accordingly, the TSO-C62 certificate can be issued for an appropriate tyre size and type that are acquired by aircraft's manufacturer in extreme manoeuvres as specified in table 1.1.

Table 1.1. The conditions to check the tyre endurance by FAA TSO-C62 (FAA, 1997)

TSO-C62 specification		
Dynamometer Test	100% Load Take off cycles	50
	100% Load Taxi cycles Min Speed: Min Distance:	8 40 mph 35,000 ft
	120% Load Taxi Min Speed: Min Distance:	2 40 mph 35,000 ft
	150% Load Take off cycle	1
Overpressure Test		4 times its rated inflation pressure for 3 seconds
Operating temperature range of tyre material properties		-40° F and 160° F

Aircraft tyres have a thicker sidewall and crown that result in a stiffer structure in bending and tensile deformation in order to ensure about following the strict safety requirements demanded by aviation authorities. Aircraft tyre manufacturers typically produce tyres for both commercial and military usage. Apart from general criteria of aircraft tyres, each type of aviation demands a number of exclusive configurations for tyre. Design of commercial tyres faces challenges such as environmental concerns, durability, and efficiency in construction; however, military usage explores over-strengthened material characteristics for extreme hazardous manoeuvres with insignificant negotiation on its environmental impact and efficiency. These complexities in structural layup and large number of plies resulting from the safety and load carrying requirements have serious cost implications for the design and manufacturing processes of aircraft tyres. The significance of mechanical strength for tyres in aviation owing to stringent safety regulations is emphasised in its design while the trend of car tyre design is highly oriented toward low weight structure, low rolling resistance, and efficiency concepts. Hence, safety questions constitute the key subject in the assessment of the aircraft tyre's performance.

To address safety issues required by legislation (ISO, 1998), the ultimate strength of aircraft tyres is typically evaluated with destructive tyre tests under excessive, although unusual, loading conditions such as high rolling speed, vertical load, or extraordinary inflation pressure. The burst test is one of the important safety requirements concerning aircraft tyre robustness in taking off and landing manoeuvres and is covered by legislation. The burst test is usually associated with the tyre operation under low inflation pressures, while the aircraft is taxied speedily for a long time, and the heat build-up in the internal tyre compounds

deteriorates material strength. Operating in such condition can either cause tyre burst or increase the rate of fatigue in the carcass (Dunlop, 2008).

Aircraft tyres are also tested in rolling condition under varying vertical load, inflation pressure, side slip angle and longitudinal speed in order to extract the dynamic behaviour during taxing for the handling performance analysis of aircrafts on the runway. The measured characteristics such as braking (longitudinal) and cornering (lateral) forces as well as self-aligning moment can contribute to the assessment of the aircraft behaviour in the virtual simulating environments. These measurements can be obtained using either the indoor flat track or drum tyre test rig or the outdoor specialised trailer test facilities like TERATYRE, built by NFM Technologies and owned by Airbus (NFM Technologies, 2009). The stationary indoor test facilities such as MTS FLAT-TRAC dynamometer rig have the capacity to conduct test in high longitudinal speed up to 320 km/h, but limited to the slip angle measurement up to 30 degrees. On the other hand, the TERATYRE test can be performed within a higher range of slip angles, but is limited in the rolling speed capacity owing to measurement using an over-weighted instrumented vehicle. In addition to the fact that both rigs have limitations in practice, the costs involved to carry out such tests are tremendously high.

As previously discussed, the temperature increase in rubber compounds can deteriorate the material strength and speed up the trend toward a material failure mode such as burst and bulge in the sidewall rubber due to overheating of tread area. The indoor dynamometer test facility can be employed to measure the heat build-up and temperature rise. However, the FAA's advisory documents (FAA, 2000) report that the dynamometer is not a satisfactory tool in prediction of temperature distribution and final temperature because of its inherent

incapability to simulate the actual runway condition and thermodynamic interaction between tyre and runway. This is due to the fact that the actual road condition and surface temperature is not implementable on this equipment.

The above-mentioned themes in aircraft tyre research stimulate the usage of an efficient tool which can be tailored for any specialised preliminary analysis of tyre performance before the actual product is manufactured and tested in the real-world. Improvement in tyre design and manufacturing process is a vital optimisation phase in most research and development departments with a view to reducing product development costs and efforts, and concurrently, enable tyre manufacturers to deal with intense competition within the market. Although iterative approaches have been used in the past in the design of aircraft tyres, modern approaches based on computer simulation are now increasingly being used to reduce the prohibitive costs of the iterative design approach. The Finite Element (FE) Analysis is a powerful computer simulation tool which has been adopted in a vast spectrum of industrial applications including the tyre manufacturing, for studying the behaviour of engineering systems under a variety of loading conditions. The FE approach is particularly useful when mathematical methods required for solution are not simply derivable because of complexity in the tyre geometry, loading, and material properties. In addition, empirical and semi-empirical methods are limited to the adaptability of suggested formulation to the assumed situation, and extrapolation is not necessary a valid function. Furthermore, although easy to use, these methods' drawback is the inability to consider design details as much as the FE approach can, while the FE approach's drawback is typically related to inefficiency of its solution and the convergence issues that may be encountered.

The FE approach is capable of simulating tyre behaviour under various operating conditions for analysis of its performance using investigatory approaches such as static loading, implicit/explicit dynamic force and moment generation, frequency and time domain analysis, failure examination, thermal analysis, and coupled studies of preceding analyses. Moreover, adoption of user friendly processes and methods has also encouraged tyre developers to utilize FE tools increasingly. The user-friendly menu-driven programmes ease the practice of CAE tasks rather than either complicated command-driven systems or inadequate graphical user interfaces (GUIs) for designers and those technical specialists who are unfamiliar with the FE approach and use of computer-based analyses.

In this research, Abaqus FEA – developed by Simulia and owned by Dassault Systèmes, is employed for FE-based simulations. Abaqus is one of the most common FE tools which has been widely used in the tyre industry with regard to its versatile capability in modelling composite layers with a considerable focus on the tyre structure to a larger extent than what is available in other FE packages. It is also equipped with the Abaqus Scripting Interface which is an application programming interface (API) to the models and data used by Abaqus. The Abaqus Scripting Interface is an extension of the Python object-oriented programming language (Dassault Systèmes Simulia Corp, 2012); Abaqus Scripting Interface scripts are Python scripts and are capable of creating and modifying tyre models, submitting Abaqus input deck (INP files) to solver, and reading/writing/viewing from/to the output database (ODB files).

1.3. Aims and Objectives

The main goal of this thesis is to develop a comprehensive modelling and simulation approach for analysis of mechanical behaviour in aircraft tyres. This research work develops

Finite Element modelling capability at Dunlop Aircraft Tyres Ltd (DATL) in order to improve tyre design process and develop tyre model for landing gear system and aircraft modelling/simulation required by customers such as Airbus. The analysis is used to principally evaluate and support developments of new tyre designs in DATL. Furthermore, the dynamic and thermal simulations of rolling tyres provides forces and moments (F&M) and tyre thermal behaviour, which are generated across the contact patch when the tyre is rolled, steered, and braked during aircraft ground manoeuvres in taxiing, landing, and take-off. The other goal is to develop a virtual environment of tyre analysis for non-expert users to deep knowledge of tyre modelling and simulation. This interface offers a simplified user friendly environment that operates the complications of modelling in background and allows the tyre designer and engineers to vary the design parameters and provide a quick implementation of the required simulations before a prototype is fabricated.

In order to achieve the set goals in this research, a number of objectives are expected to be defined and obtained. Benchmarking available approaches to model the mechanical behaviour of tyre was conducted to select a comprehensive tyre model and a number of criteria are set for selection of a suitable modelling approach. The same benchmarking was planned to be carried out on available material models. To develop a model with higher fidelity, the inflator air is also modelled so that the tyre mechanical behaviour such as footprint and contact patch is predicted with higher accuracy. Moreover, the finite element method requires fine tuning of the configuration parameters to reduce the chance of divergence through the FE simulation. The fine tuning of FE models contains two steps: the mesh size investigation to find appropriate mesh size/type and setting up the solver configuration parameters. Eventually, the temperature build-up in rubber compounds and

generated forces in cornering and braking were the objects that were set to obtain through this research.

The other important objective to obtain in the thesis is to modelling tyre in slip conditions, which enables users such as aircraft ground dynamicist to accommodate the aircraft handling and ride models with accurate enough tyre force and moment models. Therefore, the modelling approach was aimed to be capable of predicting tyre dynamic behaviour as well as its mechanical behaviour commonly in static conditions.

This research also aimed to develop a user friendly interface to provide analysis tools using finite element to inexpert users and tyre designer to the deep knowledge of Finite Element Method. However, it is necessary the specific objectives discussed in the previous paragraphs is achieved firstly. The goal is to develop a tyre modelling environment that the design and analysis tools are easily accessible with least efforts so that the tyre designers will have their focus on product development rather than solving the FE problems.

1.4. Contributions

A list of contributions is outlined in this section as below:

- Modelling of ideal gas as inflator increases the model accuracy in prediction of the contact area and pressure; this is discussed in the second section of chapter five in more details how this simulation is carried out and the implementation is available in the same chapter, but section five. However, the importance of inflator modelling and the contribution of this simulation into the field of aircraft tyre modelling is discussed in third section of chapter 3.

- Yeoh model for the rubber compound and nylon cord provides a reasonable prediction of material behaviour with quite faster implementation in comparison to complicated high degree material models; the procedure which was lead to this selection is comprehensively discussed in chapter four.
- Simulation of burst pressure can be used as a predictor tool rather than physical burst testing in early product development and is capable to predict where the failure occurs; the burst simulation was performed in chapter 5 section five with relative explanation on its importance in certification of aircraft tyres.
- Tyre Analysis Interface System facilitates the task of tyre analysis using finite element method for inexpert designers in the field of FE analysis; this contribution is described in details in chapter 6 as the necessity of this tools and the originality of the algorithm to obtain such interface are discussed in both chapters 3 and 6.
- Thermal-displacement coupled modelling of viscose heat dissipation in free rolling tyre is capable to predict the heat generation in cyclic deformation; the current developments of thermal models are explained within the third section of chapter 3 and this method to obtain this contribution is further discussed in details within the fifth section of chapter 5.
- The solution of FE tyre models with many layups and material/geometrical nonlinearities is converged and overcomes the convergence issues encountered; the challenge ahead of modelling such big and complicated problem in discussed in the second section of chapter 5.
- The thesis propose two different partitioning geometry with low and high detailed compound for the rubber region that offers a faster implementation by low detail model versus more accurate approach with high fidelity rubber region; the third

section in chapter 5 describes the way that the partitioning direction is contributed in the field of tyre modelling.

- Modelling cords helps to achieve aircraft tyre models with better convergence and higher accuracy in prediction of mechanical behaviour. In this thesis, the nylon cords were tested and implemented in FE package by the nonlinear hyperelastic materials, which was necessary due to the large deformation encountered in aircraft applications; the detailed approach to obtain this contribution is discussed throughout the chapter 4.
- The 2D FE model of aircraft tyres successfully predicts the tyre behaviour under symmetrical loading conditions like what occurs in burst test. This implementation is much faster in comparison to 3D model setup and less convergence issues is encountered; this contribution is briefly explained in the implementation section of chapter 5.
- The optimized mesh size/tyre provides an FE model with a better prediction of mechanical behaviour and helps to a better convergence and as faster implementation as possible; this contribution is also presented in the third section of chapter 5.

In addition, here are the list of contributions in the form of publications and presentations performed during this research:

1. M. Behroozi, O. A. Olatunbosun, W. Ding, "*Finite Element Analysis of aircraft tyre – effect of model complexity on tyre performance characteristics*", Materials & Design, (June 2011), doi:10.1016/j.matdes.2011.05.055

2. Mohammad Behroozi, Oluremi Olatunbosun, "*Simulation of heat build-up in aircraft tires under high speed free rolling using an explicit approach*", Tire Technology Conference, February 2013, Cologne, Germany.

3. Mohammad Behroozi, Oluremi Olatunbosun, "*Prediction of Aircraft Tyre behaviour under Extreme Loading Condition using ideal gas inflator*", Tire Society conference 2012, Cleveland, Ohio, United States, 2012.

4. M. Behroozi, O. A. Olatunbosun, "*TIRE ANALYSIS INTERFACE SYSTEM (TAIS), A virtual prototyping tool for tire development*", Tire Technology Conference, February 2012, Cologne, Germany.

5. M. Behroozi, O. A. Olatunbosun, "*Simulation of Dynamic Characteristics of Aircraft Tires*", Tire Technology Conference, February 2011, Cologne, Germany.

6. M. Behroozi, O. A. Olatunbosun, "*FE Analysis of Aircraft Tire*", Tire Technology Conference, February 2010, Cologne, Germany.

1.5. Thesis outline

In this chapter, the motivation of conducting the current research was discussed, and the research theme and the necessity of such research were explained. Furthermore, the overall aims and objectives were presented in the third section to ensure the research is directed in line with the specified goals.

In chapter 2, the history of aircraft tyres is presented and the current research interests towards tyre modelling are discussed as well as the importance of using modelling approaches in simulation of the tyre behaviour. In addition, the description of tyre construction is provided for a better understanding of the rubber and cord composition that

helps to understand tyre behaviour due to its construction. Eventually, the tyre primary terms are introduced and defined to be known when it is used in the following chapters.

The necessity of a user friendly interface for tyre analysis and the modelling objectives are initially explained in chapter 3. Furthermore, the existing and recent research on the field of tyre analysis is studied. The purpose of literature review was to set the direction of this research. Moreover, criteria to assess the usefulness of the available tyre models are discussed in order to select the suitable model for simulation of tyre mechanical behaviour which is in line with the research objectives.

In chapter 4, the importance of material modelling is presented and the involved material behaviours in aircraft tyres are investigated. Furthermore, available models for elasticity, hyperelasticity, and viscoelasticity are presented and appropriate models are selected based on the accuracy and simplification. Finally, the test instrumentation and procedure are introduced and the selected models are parameterised and employed as material models in modelling and simulation.

In chapter 5, finite element modelling and analysis of aircraft tyres are presented and implemented. In addition, a study on the effect of different partitioning methods for rubber region in FE model was carried out. The partitioning was based on the level of detailed to represent the tyre components for simplified and detailed representation of rubber compounds in civil and military aircraft tyres. Then, a correlation study is carried out to evaluate the finite element performance in prediction of tyre behaviour. Finally, a number of simulations are conducted to calculate the tyre forces and moments that are generated in taxiing manoeuvre and braking condition as well as the heat build-up in tyre cross-section when it rolls on runway at different speeds and loads.

In chapter 6, TAIS (Tyre Analysis Interface System) is developed based on the requirements and demands from DATL. TAIS is an input/output interface in tyre analysis for non-expert FE users and benefits from material database builder which was initially developed in order to obtain the tyre mechanical properties.

Finally, the conclusion and future work are presented in chapter 7. In this chapter, the results of the modelling and simulation are summarised and a number of possible modifications for future study is offered.

Chapter 2: Aircraft Tyre Design

2.1. Introduction

The history of key developments and inventions in aircraft tyres is initially presented within the next section for a better understanding of the challenges in design and modelling of high strength aircraft tyres in comparison to passenger car tyres. Following section two, the tyre industry interest towards using modelling and simulation tools is discussed in section three. In order to address the concerns regarding the selection of an appropriate modelling method, it is required to primarily study the structure of aircraft tyres in details for a better understanding of tyre design potentials and challenges that come across in the modelling practice. Therefore, common structures of aircraft tyre are primarily studied in section four, and the challenges toward the modelling of aircraft tyre behaviour and its mechanical properties are described within this section. In section five, the standard framework for modelling and analysis are presented and the common terminologies used in tyre industry are defined.

2.2. History of the aircraft tyres

The pneumatic tyre idea was officially patented by John Boyd Dunlop in 1888 (Dunlop, 2013), although the basic pneumatic tyre was practically developed by Thomson (Thomson, 1847) and subsequently superseded owing to increasing popularity of Dunlop's patent. Dunlop's tyre was made of a small-sized and thin cross section with high inflation pressure, and initially used for bicycle applications. The public interest to use the pneumatic tyres in the transportation industry was rapidly increased and several awards were soon granted in race competitions to these types of tyres (Dunlop Tyres, 2013).

After the Wright Brothers built the first functioning flyer in 1903, bicycle tyres were utilised as the ground stand on pioneer aeroplanes. In 1909, Goodyear developed the first

pneumatic tyre that was specifically designed for the forerunner aircrafts (Goodyear aviation, 2013). The woven cotton cloth was the common material in those days to provide the reinforcement for the primitive tyres. However, synthetic cords gradually replaced the cotton one as a fibre support so that the number of viable cord's End per Meter (EPM) reduced. As the aircrafts became bigger and heavier, stronger tyres with high strength cords were designed and employed for the military and commercial aviation industries. Later, the progression in the technology of the tyre's rubber and cord materials led to mature bias-ply (cross ply) tyres, and resulted in elimination of the short life span of cotton cloth tyres.

An abrupt change was triggered in the production of aircrafts in early second decade of the 20th century due to the shortened transportation time in shipping consignments and, more importantly, strengthened tyre structure for safer landing/taking-off manoeuvres for military usage. Reaching 11,000 aircrafts produced during the First World War, there was a rise in market demand for more aircraft tyres with higher reliability and better resistance to failure in emergency landings. This encouraged the tyre manufacturers to invest in test facilities in order to evaluate the requirements for designed application. Goodyear built the first aircraft tyre testing machine in 1910 (Goodyear aviation, 2013) to improve the research capabilities. Owing to the fact that the tyre structure endures for noticeably longer period than the tread due to wear during ground manoeuvres (landing/take-off/taxiing), the retreadable aircraft tyre industry was born in Akron, Ohio, in 1927, and became possible by another Goodyear invention (Goodyear aviation, 2013).

After the Second World War, the tyre's limited operating life was increasingly challenged by airliners in order to reduce the operating and maintenance costs. Therefore, the tyre lifetime concerns were deliberately emphasised together with the safety issues of aviation

tyres due to updated standards compelled by aviation authorities. Although bias tyres were built extremely strong to fulfil the high safety standards, disadvantages in its mechanical performance on runway, which caused a shorter service life and a higher rate of heat build-up inside its thick sidewall block during the ground manoeuvres, motivated designers to come up with innovative solutions such as radial tyres. In response to the increasing demands for performance, the radial tyres that were formerly used on cars for at least 30 years were re-designed in construction in order to adapt the tyre's applicability in the aviation industry. Michelin first introduced steel-belted radial tyres and filed its patent, July 4th 1946 (Michelin, 2013). The term "radial" denotes the under tread ply cords oriented at a 90 degree angle to the wheel circumferential direction, and the tyre casing is strengthened by a belt of steel cords that are laid over the circumference of the tyre. In 1981, the world's first operational radial aircraft tyre was mounted on the French Air Force fighter jet, the Mirage III (Michelin, 2013). Later in 1983, Michelin equipped the first commercial aircraft, Airbus A300, with radial tyres (Michelin, 2013).

The Concorde tragedy on 25 July 2000 compelled aircraft manufacturers towards a greater emphasis on tyre safety to provide improved casing integrity which reduces the chance of scattering tyre fragments after external object damage. In 2005, Bridgestone developed the *Revolutionarily Reinforced Radial* (RRR) technology designed to improve tyre durability and safety under the harsh operating conditions, which utilised high strength nylon cords in its construction (Bridgestone, 2013). The RRR technology acquired the Combat Aviation Brigade (CAB), Federal Aviation Administration (FAA), and European Aviation Safety Agency (EASA) authorization to be used for Airbus A380, the world's biggest aircraft, and Airbus A350. This technology became popular thereafter for use on more aircrafts for its better

durability, efficiency, and high resistance to damage in traversing an external object or debris as well as offering enhanced service life. These days, advances in the material characteristics of rubbers and cords in addition to the ply configuration technology has speeded up the transition from bias ply to radial ply tyres to achieve higher safety and efficiency standards in aircraft tyres.

2.3. Interests in tyre modelling and simulation

As discussed in the previous chapter, the current trends in the aircraft tyre industry toward improved performance and reduced final product price has encouraged manufacturers to achieve lower design and manufacturing costs to survive and stay economically competitive in such a rapidly growing market. The modelling environments such as Abqus or Ansys support tyre designers in the development process from developing preliminary geometry sketch and the belt's configuration using the Computer Aided Design (CAD) approaches to simulating its behaviour under the operating physical conditions using Computer Aided Engineering (CAE) tools. The capabilities of CAD/CAE tools are greatly enhanced by the recent advances in computational tools such as increasingly powerful hardware and dedicated Finite Element (FE) analysis packages, adopted for successive phases of tyre simulation.

In this research, both CAD and CAE tools are employed to investigate the influence of tyre construction and alternative material characteristics on tyre safety and checking its performance. Moreover, the procedures of compulsory safety assessment for the certification of tyres can be simulated in a virtual prototyping environment to reduce the costly and time-consuming processes of physical prototyping. This kind of virtual tools can significantly reduce the number of dedicated personnel, preliminary investment, and

prolonged experiment preparation required for physical prototyping so that the risk of high volume investment is minimised and the *manufacturers' suggested retail price* (MSRP index) is reduced by lessening the number of physical prototypes required in the trial and error (various submissions and corrections) product development.

The modelling and simulation of tyre behaviour can contribute to a great extent in a better understanding of its physical parameters on preliminary conceptual design. A significant number of modelling approaches have been developed heretofore by either well-known individual researchers or research institutions from basic parameter models to very sophisticated ones. The complexity in modelling of the tyre mechanical behaviour is purposely associated with the application for which the performance is demanded. The application study for deciding on an appropriate modelling approach essentially reflects opinions and requirements of tyre manufacturers, aircraft manufacturers, airliners, and aviation authorities with different mechanisms. The tyre manufacturer's desire is to achieve reduced costs in design and manufacture by implementing quicker parametric study of tyre configuration and material properties for brand-new designs. This is however balanced against the requirement by the airliners and supply chain to assess the resistance against failure modes and lifetime quality of the brand-new designs, in order to stay competitive and efficient in maintenance and operating costs. Aviation authorities are interested in developing models to ensure the safety of tyre for the claimed properties and added features in improvement of tyre mechanical performance under various operating conditions before the costly and time consuming assessment procedures. An appropriate model for aircraft tyre reflects the aircraft manufacturer's desire to predict the tyre

mechanical performance in different runway manoeuvres, which is used to predict the tyre capability to help the aircraft manoeuvrability.

2.4. Tyre construction

In this section, the regular aircraft tyre features and construction are defined and investigated based on the tyre label as it can be seen in figure 2.1. Each term is defined according to the legal manufacturer's standard tyre care manual and the importance of each term is separately discussed. This is primarily to study the aircraft tyre performance limits and legalised operating boundaries and subsequently to gain the comparative knowledge on the various tyre structures. This section starts with the influence of the aircraft tyre configuration on its performance and efficiency, and the operation restrictions are determined and inspected and ends with clarification of the tyre marking meaning in terms of the tyre performance and limits of operating conditions.

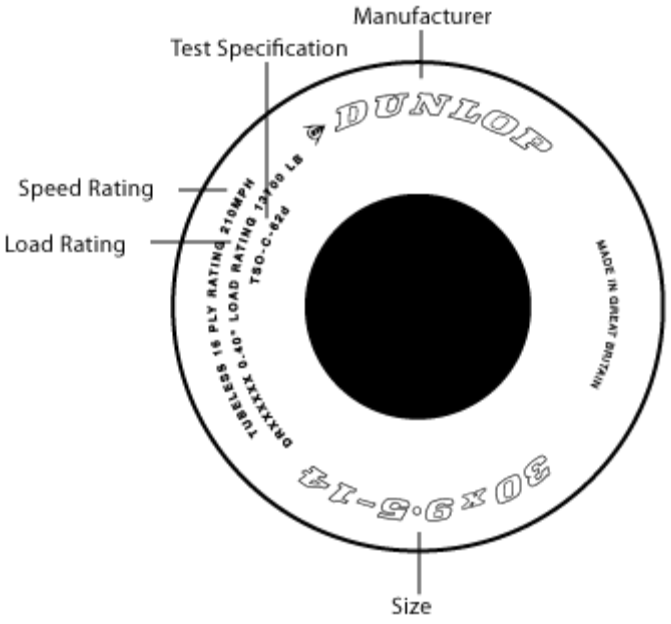

Figure 2.1. Tyre marking on a Dunlop DATL sample tyre (Dunlop, 2013)

2.4.1 Aircraft tyre compounds

In this section, the common aircraft tyre constructional components are defined and the advantage of each in the whole structure is described. The corresponding terms in figure 2.2, which are associated with a Dunlop aircraft tyre structure, are described in the following.

Figure 2.2. Tyre component terms (Dunlop Aircraft Tyre Limited, 2013)

2.4.1.1 Tread

The tread is a specially compounded rubber that is formulated to resist wear, cutting, chunking, providing high friction level and minimises the side effects caused by the heat build-up specifically in taxiing. Some aircraft tyre designs feature grooves circumferentially moulded around the tread to disperse water from the tread area in contact with the runway. The tread is engineered to help the tyre in reducing the risk of excessive skid by improving the grip between the tread surface and runway.

2.4.1.2 Casing plies

The fundamental strength of the tyre is delivered by the casing plies. Casing plies are layers of fabric cord coated with high modulus rubber on both sides (Dunlop Aircraft Tyre Limited, 2013). Casing plies are enveloped around the beads and consequently is well secured from being separated from its place.

2.4.1.3 Belt plies

A rubber-topped layer of cords that is located between the body plies and the tread. Cords are most commonly made from steel but may also be made from fiberglass, rayon, nylon, polyester or other fabrics (Michelin, 2014).

2.4.1.4 Beads

The bead wire connects the tyre to the rim and secures the air cavity from air leakage. Beads consist of a package of high tensile and high strength steel wires. Each bead is coated in rubber compound topping and is the key construction design feature in the tyre to determine the tyre rim size.

2.4.1.5 Chafers (Apex strip)

Chafers or apex strip as indicated in figure 2.2 are made of high strength nylon material and are fitted around the bead seat area to resist chafing damage to both tyre and rim flange (Dunlop Aircraft Tyre Limited, 2013).

2.4.1.6 Sidewall

Sidewall commonly refers to the region between the tyre shoulders and the bead. The sidewalls are coated with a layer of special rubber preserved with anti-oxidants (Dunlop Aircraft Tyre Limited, 2013). The sidewall protects the casing plies from the environmental effects and provides resistance to material scratching externally.

2.4.1.7 Inner Liner

Tubeless tyres have a layer of rubber merged to the inside of the tyre and the bottom casing ply from bead to bead along the internal boundary to resist the permeation of nitrogen and moisture into the casing (Dunlop Aircraft Tyre Limited, 2013).

2.4.1.8 Under-tread (Breaker overlay)

The under-tread or breaker overlay as indicated in figure 2.2 is a layer of rubber topping without embedded reinforcement. It is designed to improve the bond between tread/ ITF and the casing plies. During the re-treading process, the layer acts as the interface for the application of fresh tread rubber (Dunlop Aircraft Tyre Limited, 2013).

2.4.2 Bias-ply versus radial

The typical structural layup, compound and composition of the tyres that are used on aircrafts in recent years are presented in this section in order to compare differences of the aircraft tyre performance with ones used on passenger cars, busses, trucks, or similar earthbound vehicles, which is to help for a better understanding of the modelling challenges ahead. As stated on the timeline of aircraft tyres in the previous section, two dominant configurations of plies are recognised and are popular worldwide among the aircraft tyre industry, known as *bias-ply* (cross-ply) and *radial-ply* technologies. Both configurations were initially used on car tyres, and later, re-engineered for a durable adaption to the extreme conditions such as high speed and sudden stress that the aircraft tyre encounters in take-off and landing.

2.4.2.1 Bias-ply (cross-ply) tyres

In the bias tyre technology, the parallelised cords, encased in the rubber topping, are arranged at an angle with respect to the circumferential direction. The bias tyres are

composed of the described laminated plies, which overlap each other in a symmetrical arrangement. The overlapped plies are interdependent and distributed throughout the tyre's cross section, and accordingly, a thick sidewall is formed and characterised by high bending stiffness owing to the number of overlapped plies. The crosshatch construction provides stronger sidewalls and the inflated tyre shapes are smoothly rounded due to the symmetry in cords arrangement throughout the cross section (figure 2.3).

a. Layer-cut perspective schematic ***b. cross section***

Figure 2.3. Construction of bias-ply tyre (Michelin, 2013)

In this layup arrangement, which has been historically accounted as the first well-known and most popular configuration amongst aircraft tyres, the stiffer sidewall experiences less radial deformation and consequently a less wide contact patch is formed under the same vertical load in comparison with configurations made of softer sidewall construction. A medium to high frequency recurring deformation and relaxation in the thickly enveloped sidewall under low to high rolling speed conditions generates excessive heat in the rubber material and makes the cooling challenging by conduction due to the rubber's high thermal

capacity and low thermal conductivity within the bulky sidewall thickness. Although the cross-ply tyres are strong in its sidewall owing to the thick carcass, the tyre exhibits in more deformation across the contact area in comparison to other tyre configuration so that a higher amount of wear across the contact patch can be potentially produced (Michelin, 2013); that is, the strong sidewall movements contribute to lower relaxation length and consequently a higher slip ratio across the contact patch, and the higher slip ratio quickly wears away the tread block. Although radial-ply tyres were later introduced to the aircraft tyre market, the bias-ply tyres are still popular owing to their undoubted contribution to aviation safety and reliability as well as slightly lower prices.

2.4.2.2 Radial tyres

The drawbacks of bias-ply tyres, mostly because of its bulky structure and inferior wear characteristics, has directed engineers toward an optimised layup configuration where the sidewall deformation is more controlled and each layup is allocated to be responsible for a specific mechanical behaviour (figure 2.4). In radial tyres, the layers are divided into sidewall (carcass) and belt plies, where in such configuration the layers are usually oriented perpendicular to and parallel with (or slightly oriented to) the tread centre line respectively. Sidewalls in radial tyres are less stiff compared to the carcass and sidewall in bias-ply tyres so that radial structure suggests more flexibility to bumps and radial deflection. Referring to this feature, radial-ply arrangement would probably not be of a great interest to be used on aircrafts as much as cars that encounter unevenness on the road constantly. Nevertheless, it offers a reduction in amount of wear due to higher flexibility in the carcass and less dependency between belt and carcass in comparison to the bias-ply configuration since they are less influenced by steer angles, which can improve tyre durability.

Figure 2.4. Construction of radial-ply tyre (Michelin, 2013)

The sidewall stiffness under vertical loading is directly associated with the sidewall's bending stiffness, due to the compound strength and the inflator gas' bulk modulus, which latter is determined by varying temperature and pressure conditions. The tyre radial stiffness is decreased in radial configuration due to a softer structure in sidewall and as a result a wider footprint is formed so that the cornering performance is potentially improved. The tread is nevertheless reinforced with either higher strength cords or strong steel belts, which allows stiffer cornering characteristics and less sliding velocities. This feature can also improve the wear characteristics and provide longer tread life eventually due to wider contact patch improved by shrinkage in sliding area across the contact patch as well as the reduced contact pressure, as the major players in tyre wear.

Since it is desired that aircraft tyres are designed for longer operating life, the radial-ply tyre configuration suggests improved lifetime characteristics and offers a better match to the airliner's expectation for greater productivity. On the other hand, radial tyres demonstrate

stronger structural strength in comparison to cross-ply configuration especially at higher load and larger size grades. This parameter can be customised to desired engineering specifications for each aircraft inasmuch as the sidewall and tread stiffnesses are separate within the radial configuration. In other words, the radial configuration suggests more flexibility in design configuration in order to cope with the special requirements in heavier load, bigger size, and higher speed tyre grades.

The latter capability of radial-ply is owing to its tailor-made reinforcement for sidewall and tread that can be independently engineered to cope with encountered operating condition. As another advantage of using the radial-ply tyres, less material in its construction results in it running cooler, hence a more durable tyre with longer life is achieved. The current trend (Tyre Press, 2014) in aviation also shows how increasingly airliners and aircraft manufacturers are moving toward using more radial-ply tyres in their fleet. In fact, some radial tyres for a particular application can achieve twice as many landings before each re-treading exercise as bias tyres (Massy, 1991).

The radial tyre construction design delivers an overall lower weight in aircraft tyres due to reduced compounds in its structure to maintain the same amount of strength needs in comparison with the similar size bias-ply tyres for its usage in equal desired conditions. In a particular application, a 20 per cent weight saving by radial construction has been identified (Massy, 1991). It apparently becomes even more important since the weight related issues are always of fundamental importance in low weight design of aeroplanes.

Operational-wise, radial tyres exhibit a stronger load bearing capacity under both overload and under-inflated conditions. In addition, a generally reduced number of failure modes have been statistically proved for the radial tyres. According to (Massy, 1991), a nearly 10

per cent growth in the contact patch area improves the floatation mechanism due to the softer sidewall deformation (softer vertical stiffness) and moderates the hydroplaning characteristics of aeroplanes on wet taxiways.

2.4.2.3 Tyre type focus for analysis

Above-mentioned advantages of radial tyres has urged the tyre industry to turn their attention away the bias tyres towards more usage of the radial tyres, particularly in bigger size aircrafts, due to the extended lifetime of the radial tyres, which means consequently overall more landings per tyre that helps airliners to stay economic in such a competitive market. However, the radial tyre advantages in comparison to the bias-ply tyre become less apparent in the smaller size tyres because of overall increased stiffness, reduced aspect ratio, and improved radial characteristics in smaller size bias-ply tyres. Hence, the bias-ply tyres are more popular in smaller size aircrafts due to comparable strength and less expensive final price.

Radial tyres that are the subject of an increasing interest in this industry are targeted for the simulation and analysis in this thesis. Nevertheless, it is established in continuation of this chapter that the hypothesised methodology for tyre modelling, once developed for the analysis of radial tyres within this research, is constructed on the basis of universality as the major criteria; i.e. having established the generality of a method, it ought to be adequately flexible to be exploited for any type of tyre geometry including the cross-ply tyres, without either adding restrictive conditions or even minor needs for adaption of the modelling approach.

2.4.3 Tyre aspect ratio

The tyre aspect ratio is universally defined as the ratio of the sidewall height to the cross-section width when the tyre is inflated to the rated pressure and unloaded condition (H/W) (Gillespie, 1992), as illustrated in figure 2.5. This ratio is commonly printed and displayed on the sidewall by the tyre manufacturer in addition to the rest of the tyre's standard characteristic digits, coming after the tyre width and followed by the rim radius size.

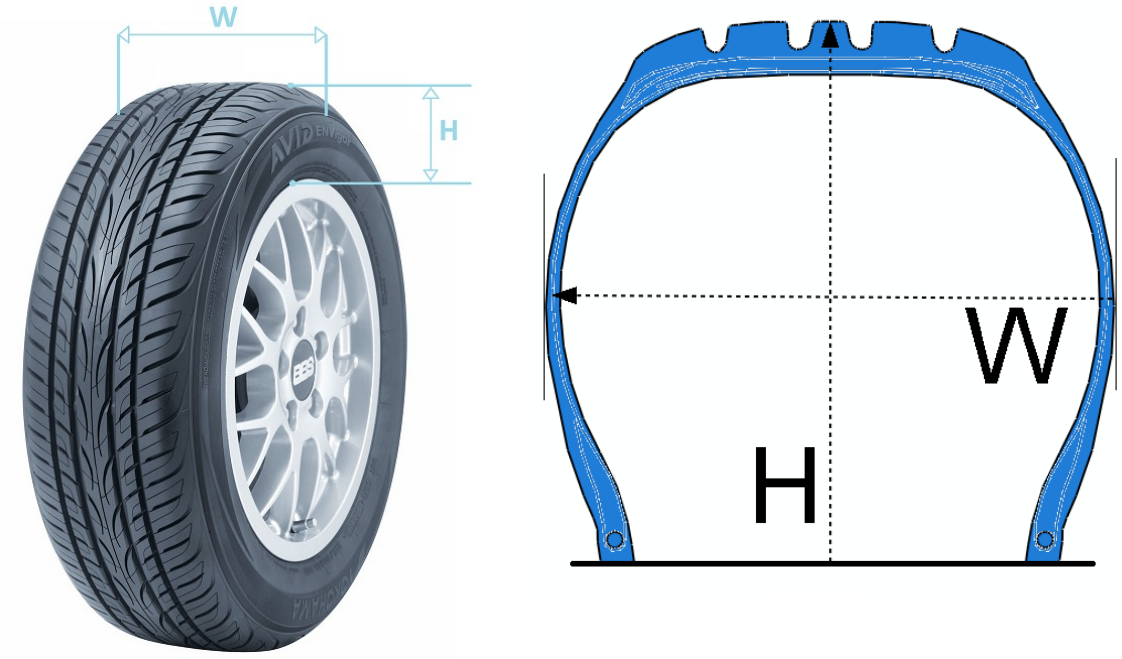

a. Perspective view of the tyre width and sidewall height (Yokohama tire, 2014)

b. Cross-section view of the tyre width and sidewall height

Figure 2.5. Tyre height and width in the aspect ratio definition

By definition, the lower aspect ratio (H/W) conveys the meaning that the tyre designs come with a shorter sidewall height, a wider cross-section width, or a combination of both parameters. A design of lowering the aspect ratio can be the shorter sidewall height at similar cross-section width. According to the beam theory, a stiffer sidewall is formed against bending moments when the tyre is exposed to the lateral force across the contact patch. Thus, the tyre responds quicker to the cornering manoeuvre and less bending

deflection is formed laterally. The tyre with reduced aspect ratio will not only transmit the generated force and moments across the contact patch more aggressively from the tread block to the wheel hub, but the steering input commands are followed quicker with reduced response time, and consequently, the steering feeling is improved (Way, et al., 2009).

The low aspect ratio tyres can also improve the cornering traction by another mechanism. Due to possibly wider cross-section, as a general rule, a wider contact patch is formed and a reduced contact pressure in magnitude is generated for the tyres with similar vertical load. The stiffer footprint provides decreased distortion in tread block and the forces and moments are transferred even more quickly through the tyre to wheel hub.

Although the low aspect ratio tyres seem to provide a great advantage to tyre dynamics, steering performance and, generally speaking, the handling characteristics, it impacts the vertical performance, and a harsher, less comfortable ride is expected owing to stiffer sidewall bending. Professor Clark from University of Michigan also investigated the influence of the aspect ratio on the rolling resistance (Clark, 1974). The equation 2.1 indicates a linear relationship between the rolling resistance coefficient and the square root of aspect ratio.

$$f_r = \frac{R_x}{M} = C\frac{M}{D}\sqrt{\frac{H}{W}} \qquad \text{Equation 2.1}$$

where:

- f_r Rolling resistance coefficient
- R_x: Rolling resistance force
- M: Weight on the wheel
- C: Constant reflecting loss and elastic characteristics of the tyre material
- D: Outside diameter
- H: Tyre section height

- W: Tyre section width

In the automotive industry, the low aspect ratio tyres are commonly used for performance and luxurious cars. However, in aircraft application, the aspect ratio is one of the design specifications for tyre selection procedure at particular speed requirement set by the manufacturer.

2.4.4 Tyre rim diameter

The selection of tyre rim size in car industry is principally based on the loading conditions that a vehicle encounters in a wide range of usages and conditions. In addition, there is a growing interest amongst the car consumers in the selection of tyre size among the acceptable sizes that can be fitted to a particular vehicle (Morris, 2014), denoting the owner's desire to upgrade the performance of the vehicle according to the tyre's mechanism in lowering of the vehicle static stability factor (SSF)[1] as well as the enhanced appearance (Daws, et al., 2007). The latter statement dominates the arguments around the tyre size in the car market; however, the tyre size in aircraft application is dependent on the static loading when the aircraft is taxiing at low speed without braking (Torenbeek, 1982).

2.4.5 Load rating

This parameter refers to the maximum tyre load that is allowed for the aircraft standard operation at the rated inflation pressure (Skiba, 1999). The load and centre of gravity in aviation are strictly controlled, and as a result, it is not difficult to check whether the aeroplane exceeds the standard load rating of tyres during normal airline operation. The amount of load allowed for an aircraft tyre is determined based on the strength of the reinforcement that is used in its structure.

[1] The Static Stability Factor (SSF) of a vehicle is half the track width, t, divided by h, the height of the centre of gravity above the road.

2.4.6 Speed rating

The speed rating is the other parameter that influences the selection of aircraft tyres. The aircraft tyres are designed to survive in operating at high landing and take-off speeds. The pilots are constantly warned on the tyre maximum speed since the tyre may fail if the take-off or landing speed exceeds its maximum capacity. Slightly exceeding this rated speed would not be harmful for the tyre, but surpassing the rated speed excessively can cause extreme heat generation and centrifugal force in tread and may create a potential loss in tread block (Wakefield & Dubuque, 2009).

2.5. Tyre terms definition

In this section, the tyre terms are presented and future formulation and standard coordinate setup are referred to the term definition provided in this section.

2.5.1 Tyre state terms

The tyre position and the state of its motion are defined in the following.

2.5.1.1 Slip angle

The slip angle is phenomenologically defined as the deformation that is built up in the tyre when the vehicle is steered in cornering condition. During cornering, the wheel heading direction is inclined with regards to the vehicle longitudinal speed and the tyre contact patch is exposed to a transverse deformation in response to the inclination. The tyre contact patch that encounters this condition and the generated slip angle is shown in figure 2.6. In figure 2.6.a, the deformation of contact patch is demonstrated and the slip angle is known to be the angle between the direction of heading and the direction of travel which is oriented along the contact patch deformation. The overall contact patch deformation in lateral direction Y (in figure 2.6.b) is build up because of two deflections: the tread package

deformation and belt deformation in reaction to lateral force Fy generated in contact patch as shown in figure 2.6.b. The first deformation resulted in developing the distance between point C and E while the latter deformation built the distance from point E to B. This angle can be directly measured from the wheel hub orientation around the king pin or calculated based on the difference between the stationary wheel plane and the rotated state.

The mechanism of deformation in contact patch due to wheel head steering and generated side force is a complex phenomenon that varies from a tyre to another. This deformation is important for calculation of forces and moments generated across the contact patch when the aircraft tyres are subjected to extreme cornering during taxiing. However, this phenomenon is known as a time and rate dependent procedure. This is due to the sidewall, carcass, and contact patch flexibility in response to the wheel slip angle commands. As a result, the generated force is relaxed to its final magnitude while the corresponding deformation in sidewall, carcass, and contact patch is developed gradually within the whole tyre structure from the rigid wheel hub to deformable sidewall and contact patch, so that the previous definition is no longer valid for such transient condition. In multi-body dynamics, instantaneous slip angle can be defined as the lateral sliding speed of contact patch due to cornering divided by the vehicle longitudinal speed at that moment, as presented in equation 2.2 for small deformations (Pacejka, 2012).

$$\alpha = \frac{v}{u} \qquad \text{Equation 2.2}$$

where the v is the instantaneous lateral sliding velocity and u explains the vehicle traveling speed.

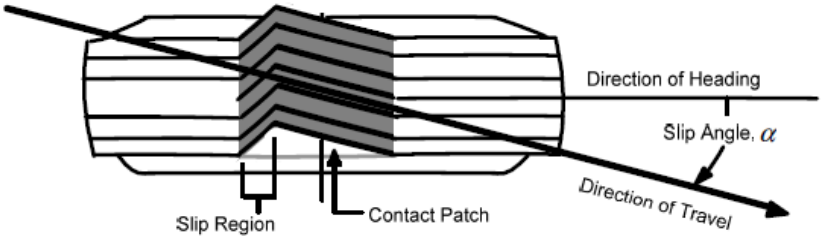

a. contact patch deformation from the top view (Gillespie, 1992)

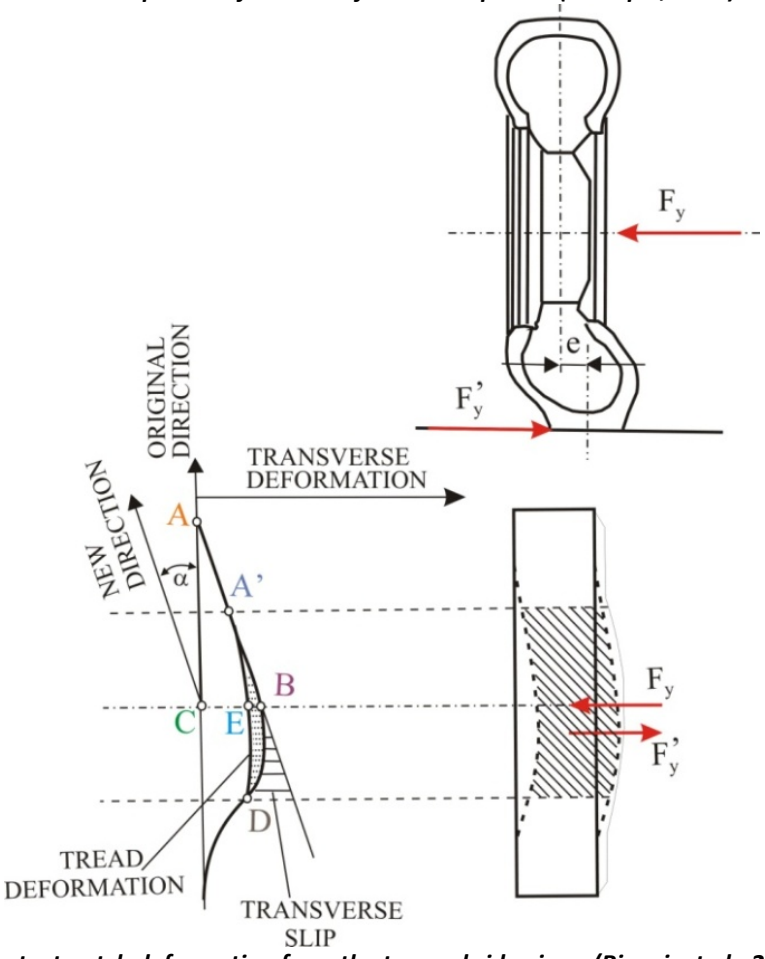

b. contact patch deformation from the top and side views (Rievaj, et al., 2013)

Figure 2.6. Slip angle generated in contact patch in a cornering manoeuvre

2.5.1.2 Slip ratio

Tyre slip ratio is defined as the ratio of the difference between tyre rotational speed and vehicle longitudinal velocity and the wheel rotation speed or vehicle ground speed. The difference in denominator definition (between the tyre speed and vehicle speed) is to

ensure the definition does not undergo singularity (divide by zero) condition that generates incorrect inputs for most of the force and moment models. The tyre in zero slip ratio condition is commonly referred to as the tyre in free rolling condition when there is no rolling torque is applied. During braking, the tyre is locked up in extreme braking condition that sets the denominator (tyre speed) in the slip ratio formulation to zero and a singularity can be generated. This results in using vehicle speed instead of tyre speed. The similar condition applies in driving mode when the vehicle speed can be zero in extreme condition and denominator is preferred to be defined by the tyre speed. The slip angle definition in braking and driving modes is shown in the following equation (Pacejka, 2012).

$$\begin{cases} s = \frac{|u - r\omega|}{u} & in\ braking\ mode \\ s = \frac{|u - r\omega|}{r\omega} & in\ driving\ mode \end{cases} \qquad \text{Equation 2.3}$$

where the s denotes the slip ratio, r is the effective tyre rolling radius, and u and ω are the vehicle speed and the tyre angular velocity. The mechanism of tyre profile deformation under braking condition is illustrated in figure 2.7. The mechanism of deformation is further explained in appendix A under the brush model description. Similar transient concept applies to the instantaneous slip ratio generation in contact patch despite the fact that fewer elements in tyre are engaged to build the transient behaviour.

The slip ratio has an important role in calculating the braking and traction forces generated across the contact patch. In aircraft application, the slip is a relevant parameter only in the braking mode since the aircraft is stopped by braking torques applied from wheel hub while in the driving mode it is not propelled by any driving torque from the wheel.

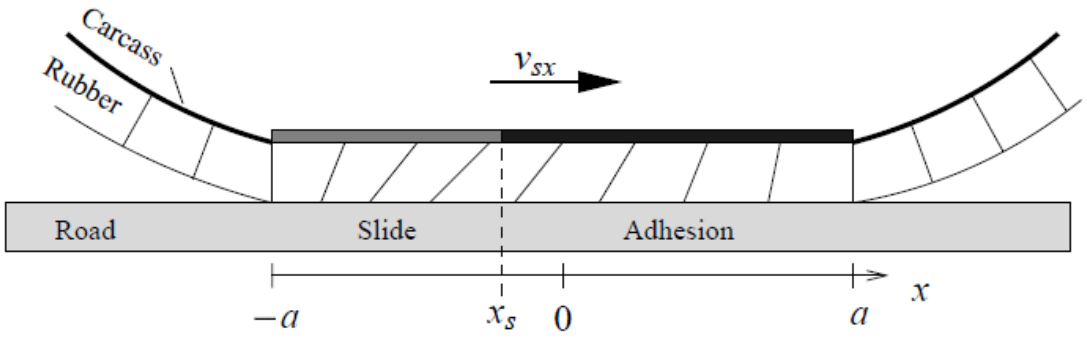

Figure 2.7. Slip ratio generated tread longitudinal deformation in contact patch in a braking manoeuvre (Svendenius & Wittenmark, 2003) (Vsx: Sliding velocity)

2.5.1.3 Inclination angle

The inclination angle or camber is the orientation between the tyre plane original position and the inclined tyre with respect to the normal vector from the road as illustrated in figure 2.8. The inclination angle is not an important parameter in aircraft tyre application since the landing gear mechanism does not allow inclined compliance due to the potential imposed asymmetry which might cause instability at high speed take-off/landing.

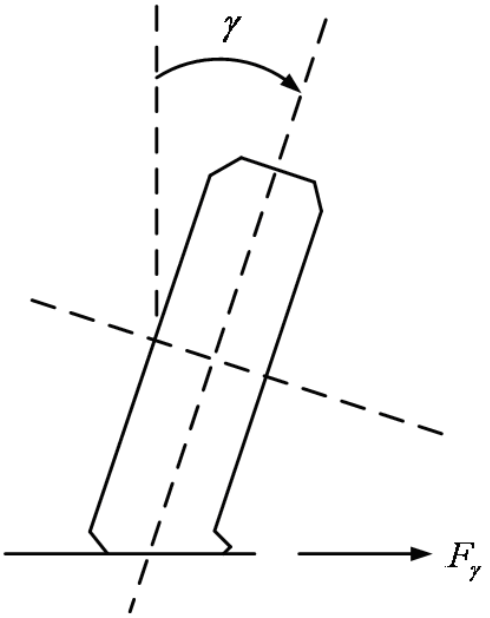

Figure 2.8. Inclination angle and tyre possible deformation (Gillespie, 1992)

2.5.2 Tyre mechanical properties

The terms and parameters that define the tyre static and mechanical properties are defined as the following.

2.5.2.1 Vertical stiffness

The tyre vertical stiffness or radial stiffness refers to the instantaneous ratio of the applied load and vertical deformation (Pacejka, 2012) of the tyre under normal loading condition. The stiffness is expressed through the following equation:

$$k_z = \frac{\partial F_z}{\partial z} \qquad \text{Equation 2.4}$$

where k_z represents the vertical stiffness and F_z and z are the vertical load and deformation respectively.

This vertical stiffness can be represented through a linear relation between the applied vertical loads and generated radial deformation in tyre cross section for small deformation ranges. Nevertheless, the aircraft tyres are subjected to high loading condition particularly before taking-off due to unburned fuels and this can result in large deformation in sidewall and carcass and the tread crown consequently. The tyre deformation demonstrates nonlinear behaviour with respect to the proportionally applied vertical load in large tread deformation (Yang, 2011). This nonlinearity in vertical stiffness can be transferred to a point of discontinuity and drastic change where the tyre tread meets the rim due to excessive radial deformation. The vertical stiffness in a tyre can be measured and characterised using a simple extraction of the load-deflection curve under a static loading procedure for non-rolling tyres in a traditional approach. However, the vertical stiffness is dependent to the speed and temperature in a modern way of definition (Pacejka, 2012).

2.5.2.2 Lateral stiffness

Lateral stiffness which can be mistaken for the cornering stiffness is the property of the tyres that is related to the lateral deformation of the tyre. The lateral stiffness is defined as the ratio of the applied lateral force to the deformation in lateral direction. The combination of the lateral slip and lateral deformation should not be used to determine the lateral stiffness and pure lateral deformation is the key parameter for the calculations of forces and moments. To measure the lateral stiffness, the tyre is placed perpendicular to the moving road belt on the test track. Then, the road belt is run at very low speed, and the resistance force against the moving belt is measured as the lateral force. The equation 2.5 (Pacejka, 2012) is employed to calculate the lateral stiffness as follows:

$$k_y = \frac{\partial F_y}{\partial y} \qquad \text{Equation 2.5}$$

where k_y represents the lateral stiffness and F_y and y are the lateral load and deformation respectively. The relation between the deformation and the generated load manifests nonlinearity in its behaviour in large lateral deformation. Although this parameter corresponds to a tyre's physical behaviour in lateral direction, it does not provide a useful direct contribution in obtaining the cornering forces and generated moments since this deformation does not replicate a realistic motion in real-world tyre experience.

2.5.2.3 Cornering stiffness

The cornering stiffness together with the vertical stiffness is the frequently used stiffnesses in vehicle ride and handling analysis. The cornering stiffness is the key parameter to estimate the generated lateral force in contact patch due to the steered tyre in cornering condition. By definition (Pacejka, 2012), the cornering stiffness is the ratio of the generated lateral force for a tyre that encounters cornering to the instantaneous slip angle (not

affected by transient response). This parameter describes the tyre contact patch deformation that occurs in cornering and it is a criterion to decide how stiff the tyre behaves in lateral direction. Unlike the other stiffnesses of which linear behaviour slightly deviates in higher load to nonlinear region, nonlinearity in the generated forces happens at any vertical load and high slip angles. The cornering stiffness of a tyre subjected to lateral force generated in cornering is expressed through the following equation:

$$c_\alpha = \frac{\partial F_\alpha}{\partial \alpha} \qquad \text{Equation 2.6}$$

where c_α denotes the cornering stiffness and F_α and α are the cornering force and slip angle respectively. Furthermore, the cornering force is highly dependent on the vertical load. At zero load condition, tyre can spin around its plane axis without resistance that denotes the zero cornering stiffness for the tyre. This magnitude increases at higher loads through a nonlinear trend, as shown in figure 2.9 at a constant slip angle. This phenomenon occurs owing to a better road grip because of wider contact patch in higher vertical loads. F_{z0} in figure 2.9 is defined as the reference vertical load. The cornering stiffness parameter may follow quite different trends on different tyres as depicted in this figure for car and track tyres.

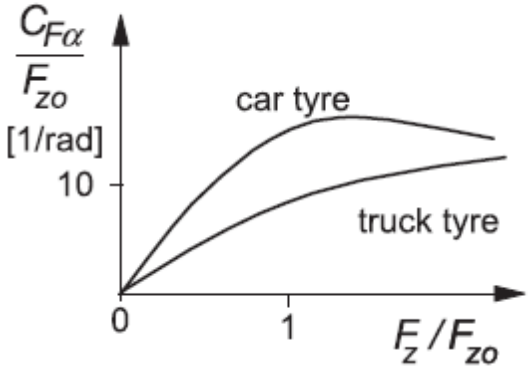

Figure 2.9. Normalised cornering stiffness versus vertical load (Pacejka, 2012)

2.5.2.4 Longitudinal stiffness

Longitudinal stiffness follows similar definition to the lateral stiffness, but towards the wheel plane heading direction. The longitudinal stiffness is explained as the ratio of the longitudinal force due to braking or traction conditions to the imposed deformation in longitudinal direction. This definition can be expressed in the following equation (Pacejka, 2012):

$$k_x = \frac{\partial F_x}{\partial x} \qquad \text{Equation 2.7}$$

where k_x denotes the longitudinal stiffness and F_x and x are the longitudinal load and deformation respectively. Because of the special application in aircraft tyres, this parameter does not attract much interest for modelling.

2.5.2.5 Relaxation length

Relaxation length is a concept that represents the phase delay behaviour of the tyre in response to the commands such as slip angle or slip ratio. This phenomenon is interpreted as the gradual tyre casing deformation to transfer the wheel hub motions to the contact patch, where the actual response is generated. A time lag exists between the steer commands from the steering wheel and the generated forces and moments in contact patch, which depends on the size of contact patch and road grip as a function of inflation pressure, vertical load and road-tyre friction. The relaxation length is defined as the phase (time) lag converted to the distance that a tyre needs to roll before the forces are relaxed up to 63% of its steady state value. In most references (Pacejka, 2012), the relaxation length is represented through the following well-known forms in longitudinal and lateral directions in terms of stiffnesses, as show in equations 2.8 and 2.9.

$$\sigma_y = \frac{c_\alpha}{k_y}$$ Equation 2.8

$$\sigma_x = \frac{c_s}{k_x}$$ Equation 2.9

where the σ_x and σ_y are the longitudinal and lateral relaxation length, c_s and c_α depict the longitudinal slip stiffness and the cornering stiffness, and k_x and k_y are the longitudinal and lateral stiffnesses.

2.5.2.6 Tyre-Road friction

The friction is a fully nonlinear instantaneous property of the tyre-road interaction that describes the normalised longitudinal force in varying longitudinal sliding condition as the most effective parameter in generating longitudinal force and its nonlinear behaviour. The friction is a phenomenon that is dependent on the mechanism of deformation which defines where the sticky/sliding region occurs in contact patch, the conditions such as sliding velocity and temperature, and microscopic/macroscopic behaviour of contact surfaces in the tire-road interaction. The deformation mechanism can influence the generation of the sliding velocities and the inclusive physics can include the contact patch pressure and the present temperature in contact interface, the heat generation and temperature distribution across the contact area. Moreover, the type of road and the tyre tread material, pattern, and geometry play important roles in a tyre's frictional behaviour. The braking force or braking efficiency in terms of the slip ratio in percentage is illustrated in figure 2.10.

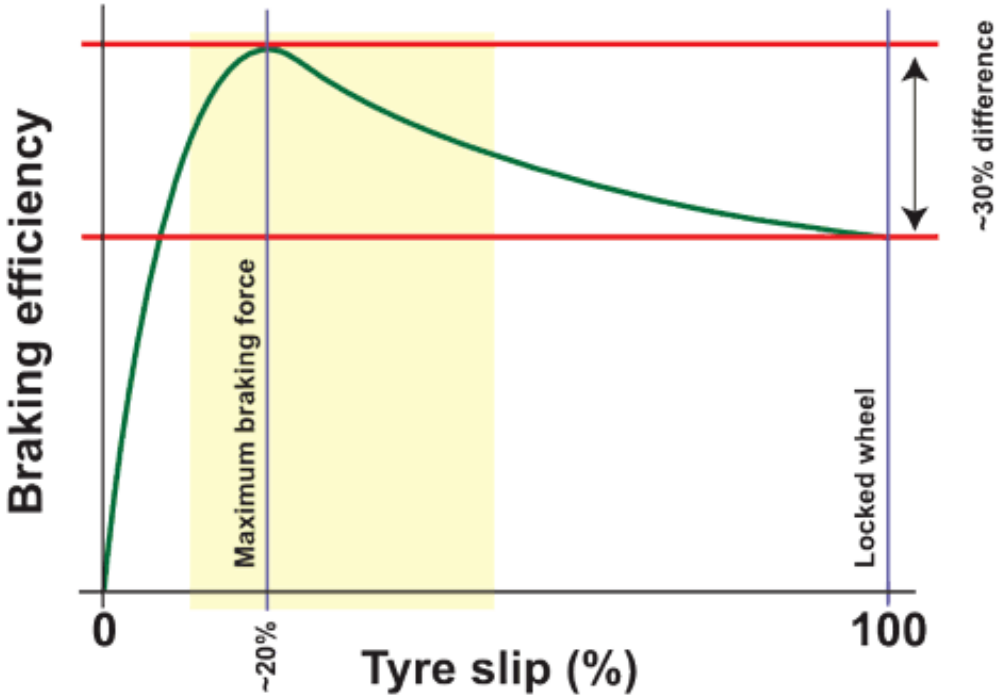

Figure 2.10. Normalised coefficient of friction versus tyre slip (Driving Fast Inc., 2013)

2.5.3 SAE legacy for coordinate system

In order to standardise the coordinates for a uniform representation of the forces and moments, a number of standard coordinates have been introduced so far by various technical centres and authorities. SAE standard coordinate system (SAE legacy) is probably the most popular form that has been frequently used in literature. A schematic of this coordinate is represented in figure 2.11.

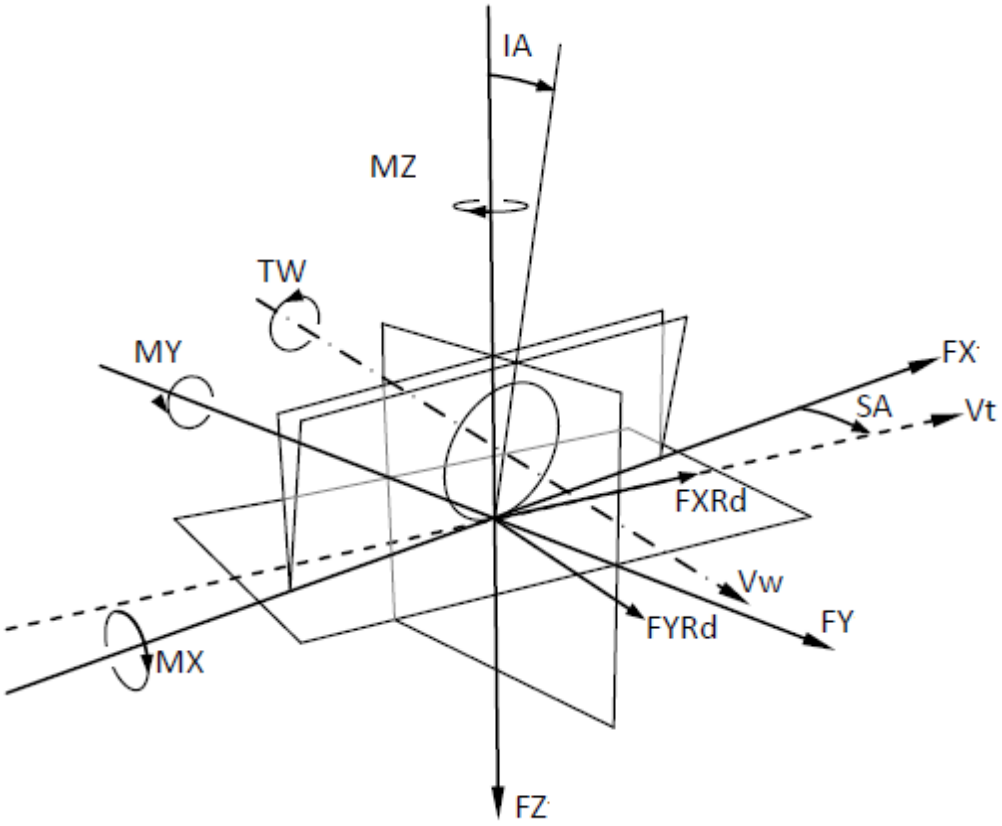

Figure 2.11. The SAE standard coordinate system (Gillespie, 1992)

The description of the coordinate symbol of figure 2.11 is listed in table 2.1. This coordinate system is used in calculation and postprocessing of data from chapter 5.

Table 2.1. Definition of the parameters in figure 2.11

Parameter	**Description**
Vw	Wheel Spin Velocity
Vt	Trajectory Velocity
Fy	Lateral Force
FyRD	Cornering Force
Fx	Longitudinal Force
FxRD	Tractive Force
Fz	Normal Force
Mz	Aligning Moment
Tw	Wheel Torque
My	Rolling Moment
Mx	Overturning Moment
IA	Inclination Angle
SA	Slip Angle

2.6. Summary

In this chapter, the history of aircraft tyres was investigated to address the progression and importance of this industry. Then, the current research interests towards the tyre modelling and simulation were discussed and the importance of using modelling approaches in simulation of the tyre behaviour was explained. A description of tyre construction was provided to direct toward a better understanding of the rubber and cord composition which helps to understand the tyre behaviour due to design parameters and construction. Finally in section five, the tyre primary terms were introduced and defined to be used in the following chapters.

Chapter 3: Literature Review

3.1. Introduction

In this chapter, the research objectives are initially introduced in section two. Following the section two, tyre modelling approaches for the mechanical and coupled thermo-mechanical behaviour are discussed and the approaches' advantages and disadvantages are compared as overview of the relevant background to provide a better understanding of tyre deflection mechanism. The challenges, limitations, and outlooks for the FE modelling in tyre application are also discussed through the relevant references within this section.

3.2. Modelling objectives

The modelling objectives that are expected to be achieved in this thesis are listed below:

- *Interface development*: In this thesis, one of the important objectives of the research was to add the capability of modelling and simulation of new designs of aircraft tyres by development of a simplified interface tool, which is later called Tyre Analysis Interface System (TAIS). This tool was developed to enable tyre designers and non-expert development engineers to analyse the mechanical performance of new tyre designs without having a deep knowledge in FE modelling techniques.
- *Standardization of analysis procedure*: Moreover, the tyre analysis procedure was standardised for consistency when used for different tyre designs. In order to check the consistency and repeatability of the analysis procedure. To achieve this goal, two tyres were employed for modelling and analysis, and their accuracy was evaluated through a number of correlation studies. For selection of the most appropriate modelling approach in this research, a deep investigation was carried out through different tyre and material models as a part of modelling objectives, and different modelling approaches were benchmarked.

- *Optimised analysis procedure*: Ease of use of selected tyre model was the other objective that was planned to be achieved through a deep research and development in modelling parameters, tyre construction, and its behaviour. To obtain the requirements of this objective, tyres with detailed representation of rubber compound as well as simplified options were investigated. In addition, some tyre simulations that can be executed through 2D FE models for a faster implementation of design check procedures. The consistency of the modelling parameters for a better accuracy was investigated as well.
- *Improvements in simulation accuracy*: The next objective was to develop a tyre model with higher precision in prediction of the mechanical properties such as design check through tyre cross-section growth when the tyre is inflated to a certain pressure, as well as the footprint and sidewall deflection when the vertical load is applied. To obtain a better fidelity, more physics such as the inflator air behaviour was added into the tyre simulation to model the considerable changes in tyre performance. Furthermore, the tyre was aimed to be modelled with highest level of geometry details and material nonlinearity to cover the tyre behaviour in nonlinear regions.
- *Extrapolation*: Eventually, the tyre models were planned to be capable of going further in terms of simulations when new manoeuvres are demanded for prediction of tyre behaviour. The tyre model is expected to predict the tyre dynamic and thermal behaviour as well as the static and steady-state mechanical behaviour where a physical test is not available.

3.3. Research direction and literature review

3.3.1 Thermal models

The research objectives were briefly discussed in chapter one, and in its continuation, the modelling objectives and aims were presented with more details in this chapter. In this section, relative literatures are reviewed to identify gaps in the literature which the research was aimed at filling. The concentration of this section is to investigate the literature to find similar works in aircraft tyres and comprehensive tyre modelling approaches. In the next section, available literatures on different tyre models are presented and the most appropriate approach is selected based on explained criteria and comparison of different approaches.

Many researchers have addressed modelling of car tyres so far that will be described in the next section. However, available researches on aircraft tyres are extremely limited in public domain essentially due to confidentiality and restrictions in access to the experimental data and material library in order to stay competitive in such growing market. In addition, because of extra care that is spent on the strength of tyre in aviation industry for a better safety, the tasks regarding the optimisation of tyre performance has been of lower priorities.

In past years, many aircraft tyre manufactures search for approaches to reduce the costs and efforts in tyre development. A number of valuable research works was conducted by Samuel Clark in University of Michigan at Ann Arbour in 80 decade that were led and funded by NASA research centre at Langley (Clark & Dodge, 1985), (Clark & Dodge, 1984), and (Clark & Dodge, 1982). In this research, a thermocouple was buried in the tyre carcass before it was being treaded in order to measure the temperature changes in carcass. The heat

generation in tyre in free rolling, steered, and braked conditions was studied based on stress approximation in the contact patch. In this study, the tyre was assumed to be axisymmetric and the results were populated circumferentially for generalisation in three dimensional tyre model. The mechanical work in contact patch was then converted to generated heat and the heat distribution was calculated using thermal diffusion equations in cross section based on finding from the thermocouple measurement. The heat generation in their model was based on strain energy loss in cyclic deformation of tread and sidewall as well as the induced contact friction which is superimposed into the strain energy loss equations. The results of correlation study demonstrated a good accuracy between the predicted distribution temperature and its value across the cross-section. Higher investment for such specially made tyres is required due to unsolved challenges ahead of design. Therefore, the models with more applicability across a wide range of tyres sizes/types support more affordable development and analysis and are more desirable by manufacturers.

In continuation to the previous researches in University of Michigan, a research on temperature distribution of a passenger car tyre was carried out in The Computational Mechanics Company in Austin, Texas (Yavari, et al., 1993). A simplified Finite Element method was used to estimate the temperature distribution due to viscoelasticity and energy loss in hysteretic loops. The heat source was decoupled from large deformation behaviour of the tyre tread and sidewall. The latter assumption was provided an acceptable agreement with test results, but it is not applicable to the aircraft tyres with large deformation in sidewall and tread block. Furthermore, the deformation mechanism was independently implemented in a separate Finite Element code and the heat flux and temperature increase model was conducted based on one-way coupling algorithm in an irreversible

thermodynamic process. The heat flux in circumferential direction was ignored in this modelling approach.

Another research was performed in Kumho tyre for prediction of temperature distribution in a passenger car tyre section (Park, et al., 1997). The similar Finite Element methodology was employed, but the deformation and viscoelastic dissipation models were coupled in the simulation. This research suggested that the quadratic elements are capable to provide a higher precision in prediction of thermal properties than linear elements due to the nonlinear nature of this phenomenon which can be captured using the nonlinear formulation of quadratic elements. This simulation was conducted in a steady-state and the heat flux and temperature gradient was neglected in circumferential direction. In addition, in steady-state approach, the elements are deformed due to static loading before the rolling simulation to help a better convergence by starting the steady state simulation from the equilibrium condition.

The tyre temperature prediction model was developed in Goodyear based on Finite Element approach (Ebbott, et al., 1999). In this research paper, a similar approach to Kumho tyre's method was followed and a semi-coupled mechanism of thermal and deformation equations was used for predicting the temperature across the tyre section. As a result, the rolling resistance was also predicted and correlated with test results. The temperature model was still dependent to the one-way calculation of deformation and was not fully coupled.

Similar approaches with more improvements as explained in the following were conducted in more research works that were following the same line of implementation in Finite Element commercial packages. In (Lin & Hwang, 2004) a decoupled temperature and

deformation model was used in non-axisymmetric three dimensional tyre model. In (Futamura & Goldstein, 2004), the deformation index was introduced to simplify the thermo-mechanical model in steady-state simulation into a simpler problem. Similar modelling approaches were developed and published through the following research papers: (Lee, et al., 1997), (Teodorescu, 2000), (Narasimha Rao, et al., 2006), (Shida, et al., 1999), (Fevrier, 2013), (Yin, et al., 2006), (LaClair & Zarak, 2005), (Assaad, et al., 2008), (Luchini & Popio, 2007), (Giessler, et al., 2010).

As a summary to above paragraphs, the developed thermal models were mostly focused on the off-line temperature distribution independent from the tyre deformation cycles. In few cases, quasi-static or semi-coupled approaches have been selected by researcher to investigate the long term heat generation and temperature build-up in tyre section. In addition, more researches have been conducted based on the co-simulation approach in which the thermal equations are separately solved and the results of solution are fed to the deformation model at the same time step. Although the latter approach leads to more efficient solution, the linearity is assumed in co-simulation approach for the thermal-displacement interaction while it can be broken due to the extreme nonlinearity in material property and deformation modes in response to temperature change and vice versa. Therefore, a fully coupled deformation/thermal approach provides a more reliable solution to the problem. This shortcoming in the current research leads to the propose using a fully coupled approach to gain the reliability and model fidelity in presence of nonlinear material properties and its changes due to nonlinear thermal effects. The other gap in modelling of thermal phenomena is the limited direction in heat conduction. In most researched as mentioned in above paragraphs, the heat transfer is assumed to be a radial phenomenon ,

which is a reasonable assumption when the heat is generated due to frictional forces in contact patch, while the internally induced heat due to damping dissipative energy can be distributed along the tyre section in all directions.

In this research, a fully coupled thermal-displacement model in an explicit approach was utilised to calculate the temperate increase in free rolling condition. The tyre lateral/longitudinal slip is neglected to reduce the conditions so that the heat build-up is a parameter of hysteretic loops and induces damping dissipative energy. In this approach, the circumferential heat flux is considered in the simulation of aircraft tyres with nonlinear large deformation models and nonlinear viscoelasticity to calculate the energy dissipation per cycle of tyre rotation. In addition, the tyre is loaded and rolled on the road in explicit time domain simulation, which enable the simulation to vary the vertical force simultaneously and element deformation is taken into account in the dissipation model.

3.3.2 Inflator model

In most of recent researches, the tyre inflation pressure is considered as a constant parameter that is applied on the inner chamber of the tyre (Bolarinwa & Olatunbosun, 2004), (Yang & Olatunbosun, 2012), (Burke & Olatunbosun, 1997), (Faria, 1992), (Korunović, et al., 2007), etc. However, the inflation pressure cannot be assumed as a constant parameter as it varies by 20% when the rated load is applied in some cases that will be described in chapter 5 with observation of relative experiments. There is no research publication or specific application was found which is accessible to the public domain to address the inflation pressure change issue independently. However, Abaqus/Standard and Abaqus/Explicit can provide hydrostatic fluid element in a way that the air is trapped inside

an enclosure of those elements. This method is capable to replicate the trapped inside the tyre tube, and the air leakage (air flow in/out) is allowed during the simulation.

3.3.3 Tyre Analysis interface

Due to needs in DATL to employ a user friendly tool for analysis of the tyre performance in different aspects from the component behaviour to overall mechanical performance before the actual prototype development, the exploration was started among available researches to find a method to overcome the complexity of engagement with high level details in the FE codes and tyre module in Abaqus. Although a number of unpublished in-house Finite Element codes have been already developed by tyre manufacturer or independent institutes (Oertel & Wei, 2012), a practical approach which is openly accessible by developers and expert Abaqus users is not available for public domain. Therefore, an approach to develop the tyre analysis interface (later is called TAIS) using the commercial package Abaqus was exclusively proposed within this research at University of Birmingham to fill the gap in available research resources.

3.4. Tyre modelling approaches

As discussed in the previous chapter and introduction, the selection of a methodology is desirable to help designers analyse the final product before it is actually prototyped and manufactured. This approach is preferred to enable tyre and aircraft manufacturer predict the tyre mechanical, dynamic, and thermo-mechanical behaviour in both micro-scale (such as stresses) and macro-scale (such as deformation) levels. In this section, the available modelling approaches are briefly introduced and further investigated in Appendix to address the demands and fulfil the requirements from both tyre and aircraft manufacturers' standpoints and eventually the most suitable method is picked.

To target the goals planned for this research from both tyre and aircraft manufacturers' perspectives, it is essential to prioritise the technical specifications and associate a baseline modelling framework with the scheduled technical goals. From a tyre manufacturer's perspective, the requirements for the tyre modelling are mainly associated with the tyre design issues. A structural analyst is expected to investigate the influence of proposed developments in tyre configuration to gain an improved performance for the maximum stress and strain values, produced across the section between the plies in addition to the produced shear stress across the contact patch and tyre seating for a better understanding of the tread/runway and tyre/rim interaction mechanism respectively under the encountered loading conditions.

Mimicking the real-world tyre test procedures is the other aspect that the tyre manufacturers would try to discover. The significance of such analysis, which is carried out through the modelling and simulation methods, is to predict the tyre mechanical performance such as the generated forces and moments in addition to its strength against a number of standard tyre test procedures in aircraft industry that is explained in the following chapters. It is desired to examine the tyre performance and its failure modes through a virtual modelling environment and the proposed modelling approach should be able to tackle the requirements to replicate either the destructive or non-destructive tests. These analyses are intended to lead the tyre designer toward an optimised ply layup configuration and material selection on the basis of required performance specified by the local and global aviation authorities, aircraft manufacturers, and airliners.

Although the microscopic characteristics and layup configuration of tyres are placed at the centre of the tyre manufacturers' analysis interest, the aircraft specialists further

concentrate their focus on evaluation of the tyre's macroscopic behaviour under the encountered load, speed, sliding velocities, and runway conditions. The tyre mechanical behaviour, essentially the forces and moments generated across the contact patch, are employed by analysts to simulate the dynamic behaviour of aircraft in the cornering manoeuvre while taxiing on the runway and take-off/landing under braking manoeuvre. Furthermore, the right modelling approach to represent the tyre forces and moments is of even more importance since the real-world characterisation tests such as TERATYRE outdoor trailer or indoor flat track machine involve expensive costs. The costs include the efforts to test a number of candidate tyres, personnel time for the Design of Experiment (DOE), and the machine's usage fee. A method that would provide aircraft ground designers with the forces and moments of selected tyres prior to it being physically tested can be a big step forward in terms of resources required and the costs involved.

The foremost criteria for the tyre modelling approaches were presented in above paragraphs in respect of the general tyre and aircraft manufacturers' concerns. However, more specifications are taken into consideration for a comprehensive study on the selection of a modelling approach. The criteria, set by the end-level users, include the items below to guarantee the delivery of a quality approach eventually:

- *Flexibility (adaptability)*: this is to ensure that the model can interactively adapt to the physical complexity which a particular analysis would demand for. The physical complexities for a typical analysis can include static or dynamic, steady state or transient, thermal, multi-phase modelling capacity, and degradation modelling such as tyre wear rate and crack growth simulation.

- *Design synthesis*: A proper modelling approach is desired to help designers in the whole design process; i.e. to ease obtaining the design outlook (design definition level), collection of knowledge from tyre's operating conditions (inventory level), interpretation of the operating boundaries in order to feed into the design definition (analysis level), conceptualisation and organization of possible configurations (concept level), review and refinement of the tyre's new configuration drawings to greater levels of precision (final detailed concept plan), and finally assessment of the design whether the issues were addressed and programme requirements were met.
- *Parameter calibration process*: To attain a repeatable modelling approach, it is essential to minimise the calibration of parameters in final modelling tuning. The modelling approach should be able to address the predictions before any major tuning of parameters. Therefore, once the end-level model is set up and the material properties and geometrical details are put in place, a good assessment of mechanical behaviour can be achieved.
- *Detailed modelling*: the tyre structure, of which ply layup configuration can play an important role in tyre performance, is desired to be modelled with highest construction detail as well as comprehensive material property for both rubber and reinforcement. This is to investigate the layers' interaction for possible separation and stress distribution across the tyre section for the material and reinforcement configuration optimisation.
- *Accessibility to results*: The preferred approach is expected to be able to predict a wide range of microscopic and macroscopic behaviour as an output of the analysis and major physical parameters.

- *Generality*: To avoid extrapolation of results, the picked model is desired to predict the physical property within a wide input domain.

Some of the criteria that make important contribution in modelling method selection are not essentially desired for the modelling purpose that is being followed in this research. The runtime due to the model computational efficiency for the real-time implementations and relative issues regarding the post-processing time, direct integration with aircraft ground dynamics simulation packages, and the complexity of the physics and the number of effective parameters involved are of the lowest priorities.

The hierarchy chart of the available modelling approaches is presented in figure 3.1. The mathematical methods are generally categorised into the physical and empirical models. The physical models are also subcategorised into the methods with involved physics, but numerically solved and the methods with physical backgrounds and directly solved. The latter subcategory relates to the modelling methodologies where the physics, geometry, and nonlinear effects would allow a direct or indirect solution for the problem and how many equations and variables are needed to reach the modelling objectives.

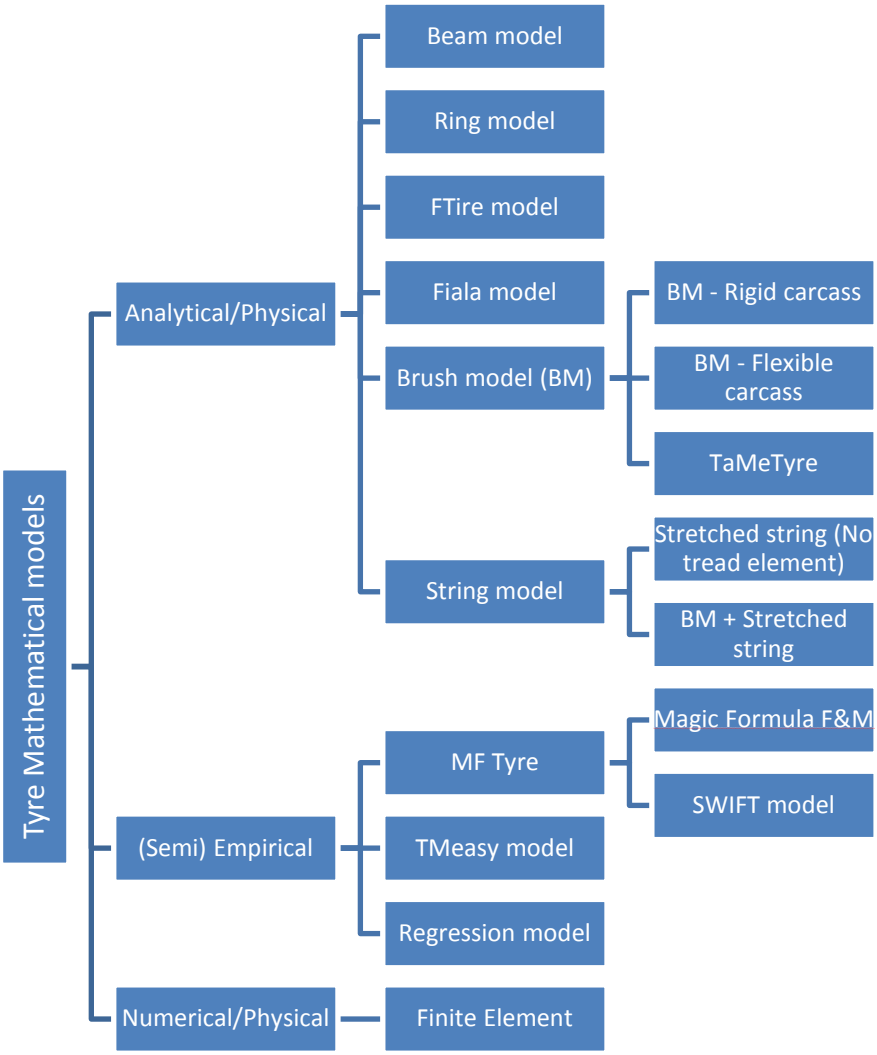

Figure 3.1. The hierarchy chart of available modelling approaches

By overall observation of the features and capabilities available in each category which are deliberately discussed in Appendix, the Finite Element was selected as the most relevant approach for the desired functionality, while examined and compared in terms of their advantages and disadvantages in Appendix. In the following section, the Finite Element approach is further discussed in details and the corresponding analyses using this tool are explained.

3.4.1 Finite Element model

Finite Element (FE) method is a well-known numerical approach to solving large-sized problems with complex physical problems. In this method, the geometry is discretised into elements interconnected at nodes as the elementary components of an FE model, as it can be seen in figure 3.2. The full geometry of a tyre can be usually imported into or created in FE codes, unlike the simplified geometry that is employed in other physical models. However, FE approach has the flexibility to model simplified models comparable with other physical models. Therefore, FE models are available in different levels of complexity based on the desired functionality.

FE model is capable of replacing a simple tyre beam model with a refined model in constructional detail. This model delivers physical modelling with desirable technical features and has a great flexibility to add required physics as analysis required. For instance, thermal effects can be added to the analysis for both frictional and viscous phenomena and coupled with a displacement model. Providing the material properties and tyre/terrain friction model are available externally, the FE based models are capable of mimicking the comprehensive real-world testing within a shorter period of time in comparison to experimentation for tyres with various structures. Analysis type-wise, FE model can be implemented for a wide range of simulations from static, quasi-static, dynamic, steady state, and time based transient to linear perturbation procedures for frequency based analyses. Like other physical models, extrapolation can produce a reasonable on-trend approximation of behaviour in nonlinear regions for time and frequency based static, steady state, and transient analyses. For tyre behaviour that extends into nonlinear regions, the computation of behaviour is handled by augmented nonlinear physics corresponding to the nonlinear

region. The more advanced the physical modelling in nonlinear region is arranged, the more accurately the model compensates for the nonlinearity.

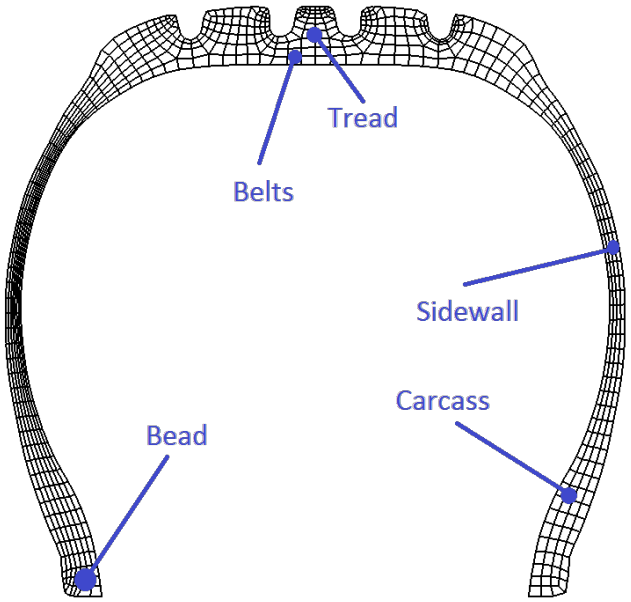

Figure 3.2. A meshed cross-section with constructing elements

A considerable number of researches have been carried out so far on the simulation of rolling tyre to capture its mechanical behaviour under loading, cornering and slip conditions. The efforts to use FE approach for simulating the tyre behaviour was initiated from the discretised revolved shells theory, reflected in (Haisler & Stricklin, 1970), (Tillerson & Haisler, 1970), (Tielking, 1984), and (Kaga, et al., 1977). In these models, the orthotropic shell elements were used in conjunction with the material properties of the rubber and cord in order to describe the ply structure. The research was progressed by researchers with more advanced elements and techniques to provide a better estimation of the deflection mechanism and tyre-road interaction through research papers such as (Ridha, et al., 1985) with focus on the footprint mechanics , (Tseng, 1987) on stress and strain distribution, (Oden, et al., 1988) on modelling of advanced viscoelastic material property for the rubber behavioural model, (Chang, et al., 1988) with concentration on three-dimensional FE models

with reduced calculation costs, (Tseng, et al., 1989) with focus on the tyre/rim interaction mechanics, (Faria, 1992) with advances in nonlinearities such as viscoelastic rubber property and complex contact problem in the contact patch, (Ebbott, 1996) on fracture mechanics analysis, and (Danielson & Noor, 1997) on introduction of efficient cylindrical elements.

Initial works in University of Birmingham were triggered to study the tyre dynamic response by Andrew Burke, (Burke & Olatunbosun, 1997), (Burke & Olatunbosun, 1997), and (Olatunbosun & Burke, 2000), using the FE code MSC.NASTRAN. In their research, the tyre cross section was cut into segments and each segment was tested separately to characterise each part of the tyre section individually. Then, the shell elements were assigned to each region of tyre section and predefined material property from tensile tests was assigned to each section. This method employs the finite element approach to discretise the section into segments of rubber and reinforcement compound and the segments boundary elements were merged in order to unify the boundary reactions. In this approach, the general mechanical behaviour of each segment is determined using the test and the FE model is not capable of identifying the boundaries of rubber and fibre/steel cords interaction. Consequently, the calculated stress across the tyre section represents the equivalent distribution of stress and tension because of the averaged behaviour of each composite segment – where the cords are wrapped into rubber toppings. The cross-section was eventually revolved including both shell and beam elements to build the three dimensional model (figure 3.3), and the developed model was rolled on the road to study the normal and traverse physics of tyre in cleat testing. The models were then examined against the cleat test on the simulated drum experiment and demonstrated a good accuracy

for the performance in vertical frequency response in comparison with experimental data from the real drum test rig as demonstrated in their results.

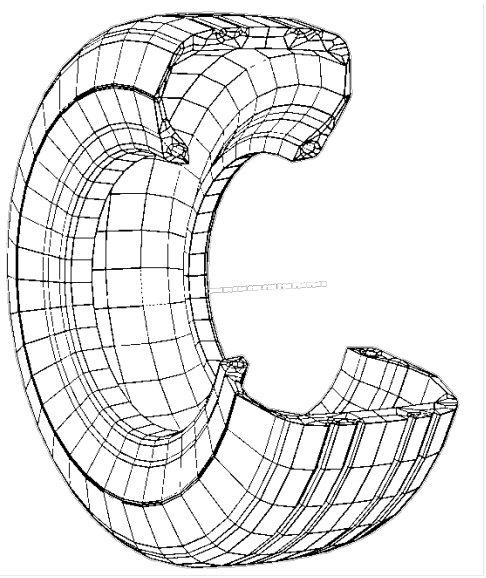

Figure 3.3. A meshed cross-section with constructing elements

As an upgrade to the above method, more researches were carried out by Bolarinwa and Yang, (Bolarinwa, 2004), (Bolarinwa & Olatunbosun, 2004), (Olatunbosun & Bolarinwa, 2004), (Bolarinwa, et al., 2004), (Yang, et al., 2009), (Yang, 2011), and (Yang & Olatunbosun, 2012), in order to bring the finite element method into simulation of detailed geometry using Simulia/Abaqus. This FE package uses the “rebar element” concept to simulate the behaviour of the reinforcement embedded in the rubber. Rebar elements are used to define layers of uniaxial reinforcement in membrane, shell, and surface elements (such layers are treated as a smeared layer with a constant thickness equal to the area of each reinforcing bar divided by the reinforcing bar spacing). In FE modelling methodology, rebar elements are considered as an embedded surface with negligible thickness in comparison with its topping thickness in order to increase the strength of the whole layer. The host region often plays its role to give a stable shape to the whole body whereas the embedded region is

mostly constructed of very thin layers. This strategy gives a much closer representation for modelling composite materials such as tyres than the layup approach which is more suitable for composites with the same range of thickness in layers (Behroozi, et al., 2012). In tyre modelling, reinforcements are actually cord plies embedded in rubber in which the cords are woven in several directions. The following data are necessary inputs for modelling tyre behaviour using the rebar approach: cords spacing (space between centres of two consecutive cords), cords cross section area, cord material property, and cords orientation inside a ply.

Abaqus/CAE is a well-known FE code that features a number of standard modules for tyre analysis. Two main approaches are introduced in Abaqus/CAE to tackle the difficulties in tyre behaviour modelling and simulation namely: “Composite Layup” and “Rebar Elements” approaches. The latter was described above. However, the composite layup is used to model a part that contains many plies, in which each single ply is defined by a material, a thickness, and a reference orientation. This configuration is used when the model contains several layups and each single layup is composed of several plies. A ply represents a single piece of material that is placed in a mould during the composite’s manufacturing process. Composite layups in Abaqus/CAE are actually designed to help analysers manage a large number of plies in a typical composite model. This modelling approach has been found to be convenient for composite parts which are mostly used in aircraft body structure. The physical modelling methods investigated so far are focused on the macroscopic behaviour of plies that is represented as stiffness and damping. These properties are not directly correlated to the tyre constructional details such as the cord strength and orientation enveloped in rubber toppings. FE models are capable of assessing the quality of

reinforcement arrangement directly by inclusion of the material property, rubber and reinforcement geometry and compound interaction characteristics into the model. As a result, major steps in the design synthesis, as already discussed, is addressed by fulfilment of the criteria for the mechanical performance after alteration of the ply configuration in both its geometry and material property. The expertise and knowledge that can be achieved through sensitivity analysis of ply configuration can help designers to obtain the idea how the parameter alteration can affect the overall performance and increase the efficiency in the way that design synthesis is organised for. With this capability, the time consuming and expensive tyre tests are substituted with the FE simulations (in a virtual environment) that mimic the real-world testing procedure.

The FE model can produce an excellent accuracy in virtual static testing and deflection mechanism and quite good accuracy for the steady state dynamic and transient testing for delivering the generated forces and moments, depending on the friction modelling precision provided in the model. The supporting results are presented and discussed in chapter 5. Tread pattern definition, ride analysis, and enveloping are supported in the physics through the FE modelling owing to its great capability to accept the geometrical details and mimic the nonlinear material behaviour. Supported tyre physics and analysis are listed in table 3.1.

Table 3.1. Available analysis and supported physics in Abaqus

Supported physics		**Supported analysis**
Flexible Solid		static
Rigid Solid		Steady-state dynamic transport
Temperature		Dynamic explicit
Fluid (CFD)		Dynamic implicit
Hydrostatic elements		Frequency
Electric Field		Forced vibration
Magnetic Field		Cyclic loading
Soil model as flexible road		Quasi-static
		Combined of displacement/Temp/Electric

The FE model, with advantages discussed above, has a couple of drawbacks that affects its functionality for a number of applications. Firstly, the FE model is computationally expensive mainly because of the number of parameters created in association with model elements required to describe its physical state multiplied by the refinement level of geometry discretisation. This multiplication results in a matrix for solvers and requires considerable calculation time, so that FE models are not usually appropriate for real-time simulations.

On the other hand, accurate material properties to describe the physical behaviour of rubbers, fibre cords, belt structures, and bead are required for accurate tyre modelling. The characterisation steps can be more challenging if the fibre or steel cords arrangement is unknown to the modeller and the tyre needs to be cut in radial segments of cross section in order to identify the cords orientation and density as well as the geometrical details. The specification of material properties also requires substantial time and efforts if the properties are not provided by the supplier. As a result, the tyre property characterisation may need destructive experiments that are sometimes not desirable in circumstances where a limited number of tyres are available for modelling in addition to the time and money costs and special cutting facilities.

Similar to the other physical tyre models, the simplified FE model employs Coulomb-Mohr friction to determine the tyre/road interaction as a default module in most FE codes. For, an industrial-level accuracy in the prediction of the generated forces and moments across the contact patch, the friction mechanism in tyre-road interaction should be fundamentally investigated for prediction of accurate forces and moments. This needs a physical approach that captures the most relevant physical parameters such as the tread surface temperature, sliding velocities in tyre-road interaction, contact pressure, small shear forces across the

contact patch, and eventually the tread pattern. A lot of research effort has been spent so far by (van der Steen, 2010), (Hunnekens, 2008), (Korunović, et al., 2007), (Korunović, et al., 2011), and (Holscher, et al., 2004) in order to characterise powerful physical and empirical friction models to be employed in FE model.

The last point to discuss is the general concerns with regards to the numerical stability in FE solution. The FE simulation in highly nonlinear regimes such as very high speed, load, extreme cornering condition, and unusual geometrical deformation may influence the convergence in solution. As a result, the final solution is influenced by the quality of the numerical methods and special arrangements should be made in tuning the effective convergence factor of numerical methods using the trial and error procedures. Moreover, the Abaqus FE package is chosen as the FE solver in this research according to its capability in solving nonlinear problems and specific function assigned for tyre modelling and simulation that is not simply accessible in other FE packages. This software employs the popular and well-known material modelling approaches to simulate material behaviour and can add desired physics to deal with the greater complexity and nonlinearity required to solve the problem.

3.5. Summary and model selection

In this chapter, the modelling objectives were explained in 5 categories as presented in section 2: Interface development, Standardization of analysis procedure, Optimised analysis procedure, Improvements in simulation accuracy, and Extrapolation; and the step to achieve these goals was briefly described.

Next in section 3, the researches in the field of tyre analysis were investigated. The purpose of literature review was to enable to set the direction of this research. Therefore, it should

identify gaps in the literature which the research was aimed at filling. It was recognised that the current researches had limitation in linking the thermal and displacement behaviours. This issue was decided to be addressed by implementation of a fully coupled physics including the thermal and deformation phenomena through an explicit approach for solution. In addition, the most available thermal models considered limits in distribution of temperature through the tyre thickness in radial direction which a common assumption to deal with the thermal problems. However, the internally generated heat in this problem can be spontaneously transferred in all directions so that a model is required to address this issue. The tyre pressure change was another aspect that have not been addressed in most FE simulations, while a considerable 20% inflation pressure change has been observed through the loading procedure which potentially changed the tyre mechanical performance and needs special attention. In continuation, it was discussed that an accessible approach to develop the analysis interface specifically developed for tyre is lacking in research. These gaps were planned to be addressed within the next chapters.

In section 4, criteria to assess the productivity and efficiency of the available tyre models are discussed in order to select the most useful model which is fitted to research objectives. In continuation, the available tyre models were briefly introduced and their features were individually discussed in details in Appendix. The models were categorised as physical, empirical and purely numerical method based on the origin and background of their governing equations.

In this thesis, the Finite Element approach was decided to be employed as the base method for simulation and analysis of tyre behaviour. This selection was made through the benchmarking procedure through the available modelling approaches and checking through

the list of goals and objectives to be achieved to understand if the selection is capable to meet the expectations. The selection procedure is further explained within the following paragraph.

According to the explained criteria for the model selection and comparing the achievements of models to satisfy the objectives, the physical models suggest the most appropriate match for the application that is required in this research. The model flexibility to add more physics, access to high level of information as analysis output with minimal input information, the ability for being used in design synthesis, and the fidelity of results over a wider range of inputs within the model validity and assumption make them a powerful proposal. The most important drawback in physical models denotes their challenging and time-consuming setup especially for the Finite Element method. However, this time inefficiency should not influence the selection of physical models as long as the results are not expected to be delivered in real time. The model result is delivered to the designers as soon as it is available for analysis and the time is not a big issue accordingly.

In summary, FE model, as a numerical-physical model among other physical models, gives an powerful capability to the designer in order to analyse tyre mechanical behaviour such as the imposed deformations, stress analysis across the section and contact patch, and force and moment generation in the presence of other physics such as temperature variation in the contact patch. Despite limitations in time and facility needed to extract the material and frictional characteristics, FE modelling can be used to provide an excellent explanation for the mechanical phenomena in rolling tyres in linear and nonlinear regions in addition to its great capability in replicating real testing conditions as a strong design evaluation tool available to the designer.

Chapter 4: Material Modelling

4.1. Introduction

Material modelling is regarded as one of the most important aspects in the tyre FE modelling since it shapes the macroscopic mechanical behaviour (such as forces and deformations) of tyre components linked to the micro-mechanical construction that happens in molecular scale. In this chapter, essential prerequisites for the Finite Element modelling and analysis are discussed in terms of the material behaviour. In order to setup an FE model for simulation, the material properties and reinforcement configuration should be determined. Since the tyres under study in this research are directly acquired from Dunlop Aircraft Tyres Limited, which will be called DATL hereafter, the tyre cross-section sketch and data related to material configuration were supplied, and consequently, the section cutting step to identify the cord orientation, spacing per cord end, and diameter was avoided. However, the material properties were required to be characterised using in-house facility in DATL. As for the case study in this research, two DATL tyres were selected and acquired from DATL: 30x11.5R14.5 that is a small size military aircraft main tyre primarily used on Tornado, and H41x16.0R20 which is a civil aircraft main tyre for Embraer ERJ-190. The specifications of both tyres are listed in table 4.1 according to the DATL online database (Dunlop, 2013).

The available material models for rubber, reinforcement, and steel bead are discussed in the next section. The available tyre modelling methods are evaluated based on a number of criteria in order to satisfy requirements of the tyre FE modelling. The selection criteria include the following factors: the model is expected to meet unusually large deformation in the belt compound and excessive distortion within the elements; the material behaviour experiences several nonlinearities at such extent of sidewall deformation; the material

behaviour demonstrates tracking of a hysteretic path, i.e. there is a delay in response to the external loads or displacements because of inherent viscous effects in material especially for rubber. The latter behaviour appears in non-static tests when the time becomes an effective factor in the load-displacement graphs. This phenomenon is called differently in various literatures, but the delay with respect to material response to force is so-called viscoelasticity while it is called relaxation length in overall tyre force and moment generation.

Table 4.1. Specification of DATL tyres under study

Specification	**30x11.5R14.5**	**H41x16.0R20**
Application	Military	Civil
Chinned	No	No
Ply Rating	24	22
Tubed/Tubeless	Tubeless	Tubeless
Aspect Ratio	0.66	0.66
Speed rating (mph)	250	225
Max Load (lbs)	25000	32825
Unloaded inflation pressure (psi)	245	187
Loaded inflation pressure (psi)	255	195
Inflation Pressure Type	Standard	Standard
Inflated Dimension for minimum Width (in)	11	15.2
Inflated Dimension for maximum Width(in)	11.5	16
Inflated Dimension for Shoulder Width(in)	10.2	14.4
Inflated Dimension Minimum Outside diameter(in)	28.75	40.15
Inflated Dimension Minimum Outside diameter(in)	29.75	41
Inflated Dimension Shoulder Outside diameter(in)	27.6	38.9
Loaded Radius (in)	12.51	17.18
Rim Dimension Between Flanges Width (in)	9.75	10.5
Rim Dimension Ledge Diameter(in)	14.5	20
Rim Dimension Flange Height (in)	1.25	1.4
Rim Dimension Minimum Ledge Width (in)	2.75	2.8

Later in this chapter, the obtained material properties are evaluated and characterised based on the selected approach.

4.2. Material modelling

In this section, diverse macroscopic behaviour of compound materials are defined and compared based on the real-world physical response of compounds. In continuation to this section, different modelling approaches to depict the material behaviour are studied and the most accurate mathematical model that delivers a good stability in solution is selected to mimic the deformation mechanism in compounds.

4.2.1 Material property of compounds

For components of an aircraft tyre, different mechanical behaviours are observed and can be classified in categories based on the deformation mechanism with respect to the applied load. In this section, the material compressibility is firstly discussed. The behaviour of a material in deformation is associated with sole components and four dominant performances are identified among the compounds materials: elasticity, hyperelasticity, viscoelasticity, and viscoplasticity, which are investigated through the following sub-sections.

4.2.1.1 Compressibility

The rubber compounds used in the tread block, sidewall and carcass, are subjected to a large deformation under the aircraft weight, and as a result, the rubber volume changes in response to the applied load. The volumetric change is measured using either the bulk modulus when the rubber elements are surrounded by hydrostatic forces or normally the Poisson's ratio when multi-axial loading is applied. The elastomers show intrinsic flexibility against shear loads. However, most elastomers such as rubber-like materials inherently resist volumetric changes against the hydrostatic forces and exhibit very small compressibility to such an extent that rubber is approximately assumed incompressible for

simplification (Hughes, 2000). According to this property, the rubber is trapped and highly resists against the volumetric changes when subjected to hydrostatic loading, which causes singularity in FE simulation. In this thesis, both rubber compressibility and incompressibility are purposely modelled in this research for the rubber section that is highly confined with hydrostatic forces.

4.2.1.2 Linear elasticity

Elasticity is a macroscopic mechanical behaviour in solid mechanics which characterises the return of material from its deformed shape when subjected to external loading, to its original state before the load application. A linear behaviour of elasticity under the applied force and generated displacement (or vice versa) is valid for small elastic strains typically under 5% of deformation in materials, particularly metals. The directional linear elastic property in a material can be represented by orthotropic (orthogonal direction dependency), isotropic (non-directional dependency), or fully anisotropic (full-directional dependency) behaviour. The linear elasticity in a material is also subject to temperature variation.

4.2.1.3 Hyperelasticity

The nonlinear time-independent behaviour of rubber-like material is commonly referred to as the hyperelastic behaviour. In this section, the hyperelasticity is firstly discussed from the physical point of view, and then, the overall behaviour is studied under the applied loading conditions.

Rubbers are a branch of polymers that are amorphous and composed of long and heavy molecular chains. These chains with undeformed shapes are extremely twisted and positioned in random directions among the unified rubber structure. When the rubber

structure is under a tensile load, the chains turn into more straightened and untwisted shape. The chains are restored to their original arrangement upon removal of the generated tension. The rubber structure is also reinforced by establishing connection between molecular chains through the vulcanization process (Treloar, 1974), (Holzapfel, 1996).

Considering twisted shape of the chains, large deformation in rubber structure is allowed while the molecular chains are excessively stretched and distorted in tension. The capability of chains to revert back to their initial shape forms the elastic foundation in the rubber structure. Moreover, the rubber volume is scarcely changed since the applied tension that straightens the molecular chains rarely changes its volume. Untwisting of the twisted chains contributes in a highly nonlinear and complicated mechanism, so that the nonlinear behaviour of tensile load and corresponding deformation in rubber can be interpreted (Boyce & Arruda, 2000).

According to abovementioned intermolecular physics, the hyperelasticity is defined as an isotropic property mostly used for elastomers or rubber-like materials when the nonlinearity is attributed to elastic materials, subjected to the tensile test. The hyperelastic constitutive law dictates that a material exhibits instantaneous elastic behaviour when subjected to excessive strain and nonlinearity of deformed geometry in finite-strain applications. The hyperelastic trend of a sample rubber is shown in figure 4.1.a and compared with the linear elastic trend. Figure 4.1.b also shows the material behaviour in tension and compression regions. The observed behaviour for rubber in tension demonstrates that the material is initially softened and then becomes progressively stiffer at higher strain. Nevertheless, the response of rubber structure to compression represents remarkably stiffer behaviour contrary to the behaviour in tension since the compression of

twisted chains requires more effort than untwisting them. Yet, the linear region can be identified in low strain values before it progressed to the nonlinear region.

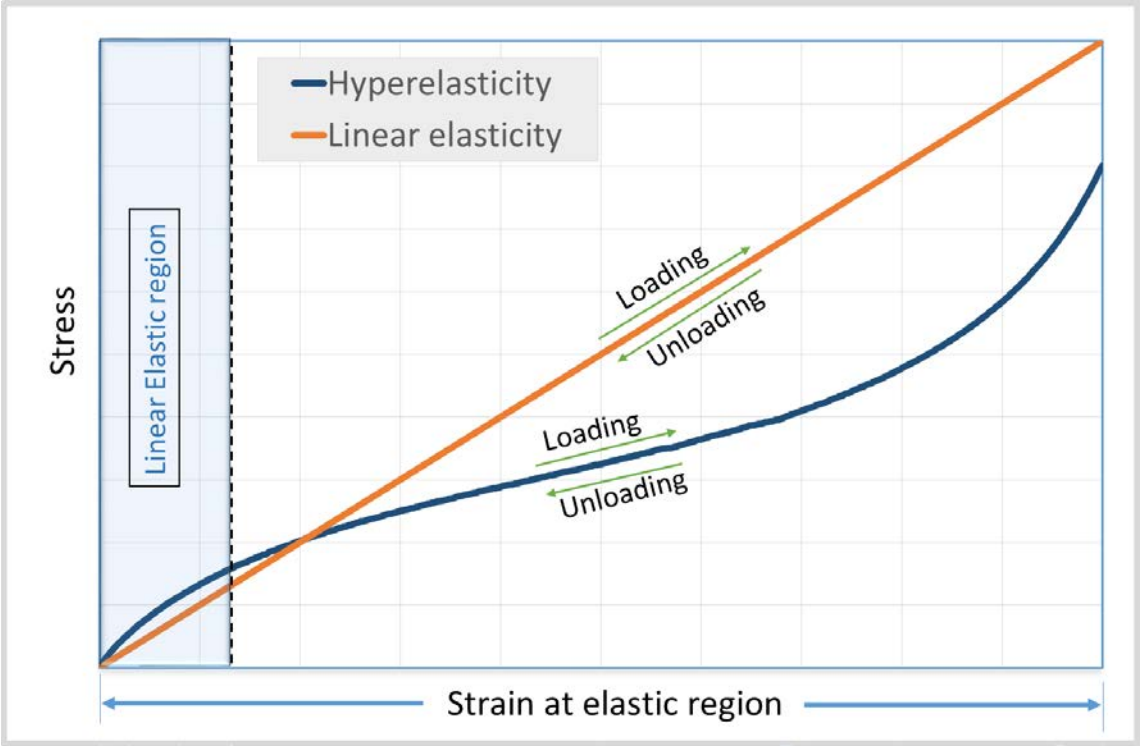

a. Hyperelasticity in comparison with linear elasticity

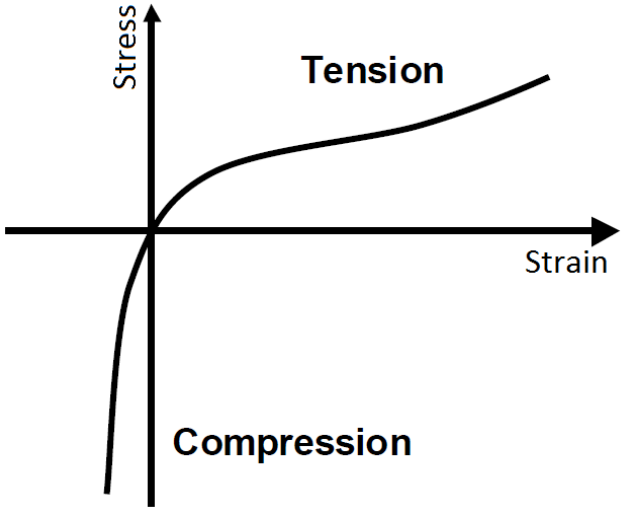

b. Hyperelasticity in tension and compression region

Figure 4.1. Hyperelasticity in trend

4.2.1.4 Viscoelasticity

Viscoelasticity is a mechanical behaviour that explains both elastic and viscous phenomena of elastomers and rubber-like materials. This behaviour is frequently referred to as the linear or non-linear time-dependent performance of stress-strain relation in those materials under loading/unloading conditions; it means that the previous response of material to stress-strain loading or unloading conditions can directly affect the current magnitudes of produced stress-strain values. The elastic deformation of elastomer bands is similar to that seen in other materials. However, viscosity explains the material resistance in response to the shear loading and the rate of distortion (Ferry, 1980). Elastomers are composed of hydrogen and carbon molecules with different arrangements, which are bonded sequentially together in a large structure to form the heavy chain of polymer molecules. On a microscopic scale, viscoelasticity in elastomers is fundamentally explained as the internal friction associated with the resistance in adjacent molecules sliding relative to each other. This slide is exposed to bonding/unbonding of intermolecular cohesion while the massive polymer chains are subjected to translation and deformation (Sills, et al., 2007).

The intermolecular mechanism of deformation in elastomers contributes in a number of phenomena in macroscopic scale, which are listed below:

- *Creeping*: this phenomenon occurs when the elastomer is subjected to a constant tensile force and non-stop strain growth is observed with time in direction of the applied load.
- *Relaxation*: this phenomenon is seen where the strain is held at a constant level and the stress in elastomer decreases with time.

- *Phase lag*: the phase lag or time delay between the applied stress and resulting strain or vice versa is developed in elastomer's behaviour in response to the cyclic load. A phase lag with more delay is achieved when the rubber is excited with higher rates at higher frequencies.
- *Dynamic stiffness*: Owing to the time delay in response to the imposed dynamic strain/stress, an instantaneous stress/strain response is not achievable. As a result, the instant stiffness is not equal to the saturated stiffness when enough time is allowed for the material to obtain the settled condition. The dynamic stiffness is also a frequency dependent phenomena and its magnitude increases at higher frequencies.
- *Loss modulus*: the phase lag between the stress and strain is produced in response to the cyclic load, which indicates a hysteretic behaviour in stress-strain (or load-deflection) curves. The loading and unloading curves follow different paths in the stress-strain graph. The hysteresis effect is principally generated due to internal friction of molecules in the viscous flow for elastomers and the energy is dissipated in the form of heat. The ratio of heat generated in a hysteresis loop with respect to the maximum kinetic energy through the full cycle is commonly referred to as the loss modulus.
- *Temperature dependency*: Elastomers become less stiff when exposed to temperature change. The temperature rise in the material constantly breaks and reforms the molecules bonds, so that the conformations through the material degrade. This concept can also be expressed as the gradual flowing of elastomer molecules into the conformations that are favoured over others due to thermal

behaviour of intermolecular bonds while the material is under loading (Baeurle, et al., 2006).

A typical hysteresis loop in viscoelastic material is illustrated in figure 4.2. Unlike the hyperelastic properties, the loading and unloading paths follow different tracks.

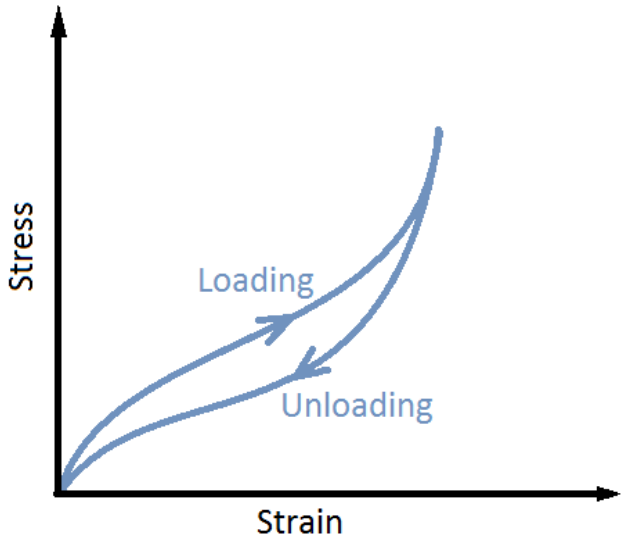

Figure 4.2. Hyperelasticity in in tension and compression region

4.2.1.5 Viscoplasticity

Viscoplastic property is attributed to inelastic viscous behaviour of materials. In other words, viscoplastic response of solids to cyclic loads is classified as a rate-dependent phenomenon in which hysteresis loops are formed in stress-strain curves while the solid undergoes unrecoverable deformation in large elongations. According to the nature of materials that exhibit viscoplasticity in deformation, creep develops progressively when a solid is subjected to cyclic loads. A schematic of viscoplastic behaviour is demonstrated in figure 4.3, where the solid elongation exceeds the plastic threshold and permanent deformation remains in strain. In addition, a general trend of a sample viscoplastic solid is

shown in figure 4.4. More explanation of this behaviour can be found in (Bergstrom & Boyce, 2000).

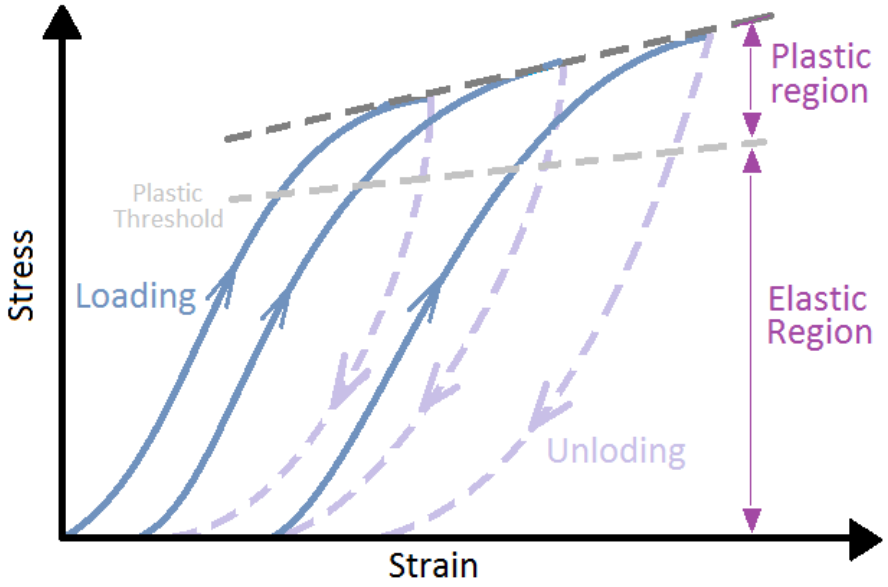

Figure 4.3. Schematic viscoplasticity in stress-strain diagram

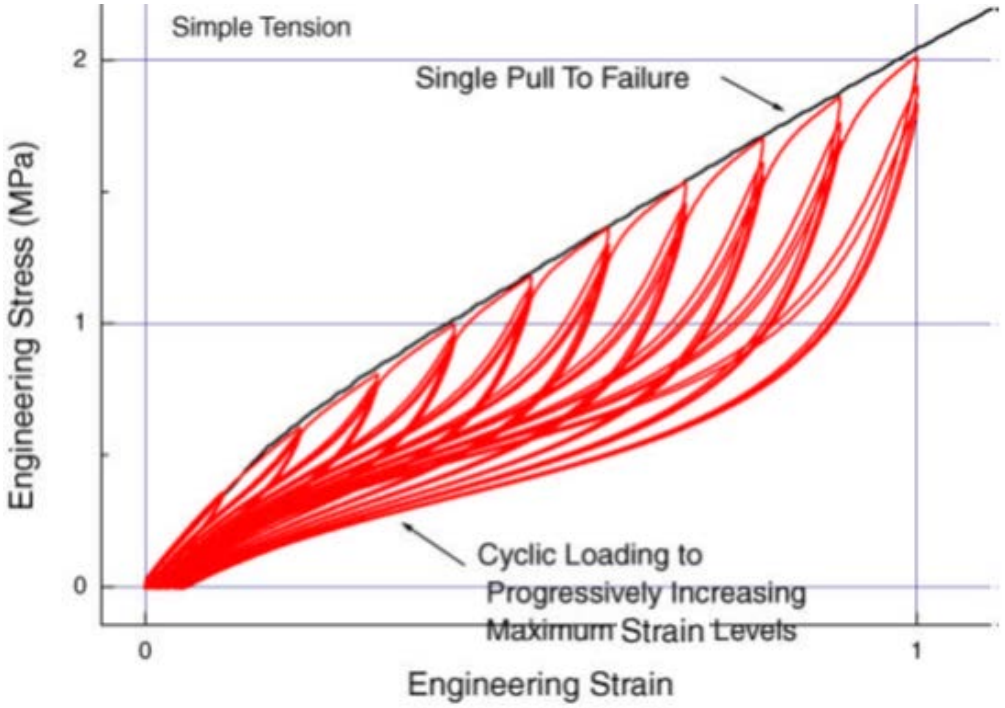

Figure 4.4. The behaviour trend of a sample viscoplastic solid in the stress-strain diagram (Miller, 2002)

4.2.1.6 Material assignment to compounds

Now that the possible material characteristics have been introduced in previous sections, the tyre compound mechanical behaviours are associated with material characteristics. Tyre structure is typically constructed from three main materials: vulcanised rubber, steel, and fibre/nylon cords. The aim of this section is to review the physical behaviour of compounds and determine appropriate characteristics for modelling the behaviour of tyre components and implementation in Finite Element codes.

Rubber

Hereafter, the term "rubber" refers to the one that has been vulcanised through the industrial procedures. The vulcanisation of rubber depicts the successive processes that results in improvement of rubber durability and elastic performance. Through the vulcanisation process, the crude rubber is mixed with sulphur and exposed to high temperature, so that the sulphur molecules fill the gap between big polymer chains and reinforce the integrity of rubber molecules together. Accordingly, the polymeric conformation is strengthened and the mechanical behaviour is less susceptible to thermal effects. Rubbers are also filled with carbon black that enhance the abrasion and tear characteristics although it increases the hysteresis effect and degrades the influence of creep/relaxation phenomena (Mark & Erman, 2005). Other fillers are also used and some oils are added to obtain desired properties in rubber.

The microscopic mechanisms that result in viscoelasticity in elastomers are similar to those in rubber. Aircraft tyre undergoes a large deformation under static weight and cyclic load in taxiing, thermal induction and temperature build-up, and high rolling speed in take-off and landing. Hence, the tyre compounds exhibit nonlinear large deformation behaviour that can

be expressed as hyperelasticity particularly in ongoing quasi-static events, where no return cycle is practiced for modelling and the strain rate is gently kept under an acceptable level. Furthermore, the hysteresis loop is induced by cyclic load and heat is generated. The latter behaviour is linked to the viscoelastic properties in elastomers and resembles the viscous behaviour in dynamic excitation. When the tyre rolls, the rubber compound is continuously deformed and recovered, so that the relaxation and creep phenomena are constantly occurring specifically in sidewall and tread block where largest deflection in rubber is made.

The plasticity is rarely identified in conjunction with viscoelasticity under normal operating conditions of aircraft tyres. Nevertheless, the viscoplastic properties should be considered when rubber tearing, scratching, or similar failure modes are experienced under destructive conditions.

Finally, the thermal dependency affects the mechanical behaviour of the material and consequently tyre overall performance; however, this effect is indirectly modelled in conjunction with either viscoelasticity or hyperelasticity as an augmented parameter. To sum up, viscoelasticity in cooperation with hyperelasticity constitutes the dominant behaviour of the broad spectrum of rubber used in aircraft tyre's operating conditions.

Reinforcement cords

Traditionally, rubbers are reinforced with cords with high strength metal or non-metal specifications. In most car tyres these days, steel cords enveloped in rubber toppings and usually angled parallel to the tyre rotary axis are considered as common material, used in construction of radial tyre configuration. The steel used in belt construction reduces the contact patch deformability and the tyre size barely changes in response to inflation pressure. Although the steel provides benefits in terms of excellent durability and strong

resistance to tyre failure, large elongation results in plastic deformation, which is not allowed in aircraft tyre application. An aircraft tyre with layers of steel belts on top of each other is most likely capable of sustaining the load prevalent in an aircraft without the deformation reaching the plastic region. On the positive side, the use of steel in tyre belt will provide the required strength. However on the negative side, the tyres of the same size but with steel cord rather than nylon one weighs more, which is a disadvantage for usage in aircraft tyre despite providing the strong structure and limited deformation required to improve the reliability and time response characteristics when undergoing dynamic loading. However nylon cords have higher tenacity and are less subjected to shrinkage. In addition, nylon cords provide an improved fatigue resistance and higher resonance frequency and generate less flat spotting due to the flexibility (Fung & Hardcastle, 2001).

Cord fibres for aircraft tyre application should provide high strength and survive under extreme static, dynamic, and impact loading. In addition, the cords are expected to be highly resistant against cutting loads and have acceptable thermal stability. Moreover, for special application in aviation where the tyre bending and deformation can result in extreme levels of elongation, the reinforcement cords are required to sustain the large deformation across the tyre section without compromising the dimensional stability and elastic recovery.

Due to the weight issues and possible moisture corrosion, the idea of using steel cords in aviation is not recommended and supported by aviation authorities. A replacement with comparable toughness and acceptable weight is not easily obtainable. Searching through the material database, fibreglass, polyester, and nylon cords have been accepted and utilised in tyres although there is a constant challenge to bond fibres and rubber together.

The polyester fibres have been very successful in passenger car tyres and light duty truck application because of its price competitiveness relative to the other ones and satisfactory stiffness for less heavy duty applications. Nevertheless, where large elongation and very high toughness is demanded such as application in aircraft tyres, the nylon cord fibres are broadly used among the other cord materials (Jain & Asthana, 2002). This is due to the high strength that nylon cords offer and lightweight owing to its low density, which makes it a great match for application as reinforcement in aircraft tyres.

The nylon cord can undergo large deformation, so that the hyperelasticity is an essential characteristic to represent its behaviour. According to the experimental result that is obtained and discussed in the material testing section later in this chapter, the nylon cords are able to recover under more than 100 per cent elongation. Although the nylon is fabricated of polymeric chains and commonly used as small diameter cords, the viscoelastic effects are not noticeable in their behaviour. For that reason, the viscoelasticity effect is neglected for the cords in this research. However, in case that the cords are stretched more than permitted, elongation in cords enters the plastic region. Aircraft tyres are carefully designed to avoid reinforcement fibres sustaining permanent deformation since plastic deformation affects the failure modes, by changing the mechanical performance from designed behaviour.

Bead

The bead is ordinarily constructed of high strength steel wire to secure the tyre from debeading and support the tyre profile. Since the bead is designed to function as a support, minimum elongation is desired under high loading conditions. On the other hand, the steel enters inelastic region for strains higher than 5 to 6 per cent, which is not a desired

behaviour due to the need to ensure bead seat stability on the rim and to ensure the tubeless tyre holds air without leakage. The linearity in stress versus strain in steel wires is the dominant behaviour owing to the designed mechanical performance. Similar to what happens in reinforced compounds under large deformation, the bead is pulled into the plastic region in case the steel wires are excessively distorted. However plastic deformation of the bead is most unlikely since the other components are designed to fail well before permanent deformation occurs in the bead. Therefore, linear elasticity is assumed to be the dominant characteristics in bead elements.

4.2.2 Material models

The material behaviour of tyre compounds, as explained in the previous section, can be modelled using two approaches: the phenomenological and physical.

- The *physical based* models employ micro-mechanical arrangements in a network of idealised molecule chains in interaction together from the statistical mechanics theories. In these models, the relation of stress and strain in material is directly derived from the inter-molecular structure and the overall mechanical behaviour is estimated through the solution of the governing equations. The physical models are less computationally efficient in comparison to the phenomenological methods in view of the fact that intermolecular details of chains network must be represented and a larger set of equations are needed for solution. As a result, the temporal variation of physical parameters such as the connecting bonds, molecular weight, and chain length can change the predicted overall behaviour without advance observation of possible specifications. In addition, the estimation capability of formulated molecular behaviour is possible through using predefined physical

parameters. As a general drawback of this method, the tyre compounds are required to be experimentally characterised for the parameter identification usually with both destructive and non-destructive tests.

- The *phenomenological* methods acquire their name from the behavioural study of the material response to applied loading conditions; i.e. the overall material behaviour is presented by empirical or semi-empirical functions. In this method, well-known polynomial formulations with more or less complexity are utilised as a function of principal stress or strain invariant. This method provides the benefit of a low calculation cost due to the direct polynomial formulation used to represent the material behaviour. Unlike the time-consuming parameter calibration procedures in physical models, the parameters in these models are rather quickly tuned in order to optimise the fitting problem. The best fitting functions and approaches are expected to reduce noise over-crossing and avoid overlearning issues while the fitting error is minimised and the correlation factor R^2 between the experimental dataset and model results is maximised. Nonetheless, the empirical model robustness is of a challenging debate as its accuracy merely depends on the conditions that are modelled for, so that unforeseen uncertainty in parameters can potentially generate inaccuracy due to a shift or deviation in shape from the original experimental trend.

To evaluate the accuracy of these models, they are examined against the following criteria:

- The change in modes of deformation in rubber should not influence the accuracy and generality of the model; e.g. if the hyperelastic model is calibrated with unidirectional experimental tension data, the model is still expected to provide acceptable predictions for shear or equibiaxial loading condition.

- The S-Shape curvature of rubber stress-strain behaviour is desired to be reproduced upon proposed strain energy density function.
- The tyre three dimensional FE models usually have a number of nodes and elements and form a large sized stiffness matrix. To minimise the cost of numerical performance for calculation of deformation in the elements, the hyperelastic models are expected to replicate the hyperelastic material behaviour by using a minimum number of characterising parameters for fitting in the strain energy density function.

4.2.2.1 Models for linear elasticity

The Hooke's law (Hooke, 1676) is probably the most common model that is used to describe the springiness, expressed as:

$$F = -K.\Delta x \qquad \text{Equation 4.1}$$

where F is the generated force because of one dimensional deformation in spring, Δx, and K is so-called the spring stiffness. The Hooke's law can be generalised to linear elasticity in materials by re-arranging the equation to express the stress and strain in material instead:

$$\sigma = E\epsilon \qquad \text{Equation 4.2}$$

where the σ denotes the stress, ϵ refers to engineering strain and E is known as Young's modulus or Elastic modulus. Equation 4.2 describes one-dimensional axial elasticity, which can be extended to lateral/torsional and volumetric deformations correspondingly:

$$\tau = G\Upsilon \qquad \text{Equation 4.3}$$

where the τ and Υ are the shear stress and strain respectively, and G denotes the modulus of rigidity or shear modulus. The resistance of a substance under uniform compression is referred to as the Bulk modulus and expressed as:

$$B = -V\frac{dP}{dV} \qquad \text{Equation 4.4}$$

where the B is the Bulk modulus, V is the volume of the substance, and P denotes the uniform hydrostatic pressure.

4.2.2.2 Models for hyperelasticity

As discussed, the large deformation stores strain potential energy in rubber and the behaviour of large molecular chains during the energy storage determines the nonlinear behaviour of strain-stress curves. The modelling of material under large deformation is to estimate the rubber behaviour based on approximation from a physical or phenomenological background in a shorter form instead of using the full set of stress-strain data, which is more appropriate for being employed in Finite Element codes. The first step in modelling hyperelasticity in most hyperelastic constitutive equations is to express them directly as a function of the strain tensor invariants (I_1, I_2, and I_3) or principal stretch ratios (λ_1, λ_2, and λ_3) as the input parameters and the strain energy density function or strain energy potential (potential energy per unit volume), W_e, as the output according to the continuum mechanics. Then, the resultant behaviour can be extracted from the derivatives of the energy functions through the Lagrangian and Eulerian methods. The mathematical backgrounds of these relations are frequently reported in references such as (Treloar, 1975), (Chen & Saleeb, 1982), (Haupt, 2000), and (Muhr, 2005). This relation can be expressed as shown below:

$$W_e = f(I_1, I_2, I_3) \qquad \text{Equation 4.5}$$

where I_1, I_2, and I_3 are the three invariants of Cauchy-Green deformation tensor and expressed in terms of the principal stretch ratios λ_1, λ_2, and λ_3 by (Chang, et al., 1991):

$$\begin{cases} I_1 = {\lambda_1}^2 + {\lambda_2}^2 + {\lambda_3}^2 \\ I_2 = \lambda_1\lambda_2 + \lambda_2\lambda_3 + \lambda_1\lambda_3 \\ I_3 = {\lambda_1}^2{\lambda_2}^2{\lambda_3}^2 \end{cases} \qquad \text{Equation 4.6}$$

The stretch ratios are also defined as:

$$\lambda = \frac{L}{L_0} = \frac{L_0+u}{L_0} = 1 + \epsilon \qquad \text{Equation 4.7}$$

where:

- λ: stretch ratio
- L: deformed length
- L_0: initial length
- u: deformation magnitude
- ϵ: engineering strain

and principal stretches are the eigenvalues of the stretch ratio tensor. A general form of the strain energy potential function in equation 4.5 can be represented for an isotropic incompressible elastomer as (Holzapfel, 2000):

$$W_e = \sum_{i+j+k=1}^{\infty} c_{ijk}(I_1 - 3)^i(I_2 - 3)^j(I_3 - 1)^k \qquad \text{Equation 4.8}$$

where c_{ijk}, i, j, and k are the model parameters which have dissimilar configurations in different hyperelastic models and may be specified using the experimental data. Assuming the incompressibility in rubber deformation, the multiplication of stretch ratios becomes

$\lambda_1\lambda_2\lambda_3 = 1$, and as a result, the $I_3 = 1$ reduces the size of equation 4.8 to represent the equations solely to the first and second invariants as follows:

$$W_e = \sum_{i+j=1}^{\infty} c_{ij}(I_1 - 3)^i(I_2 - 3)^j \qquad \text{Equation 4.9}$$

As discussed, most of the constitutive models for hyperelasticity inherently are recognised based on the type of particular function used to represent a relationship between the strain energy density function and either stain invariants or stretch ratios. Although most of hyperelastic models have their origin from the phenomenological backgrounds, some models were also developed based on the microscopic circumstances from the mechanistic behaviour of molecular chains.

A substantial number of literatures have investigated the development of rubber hyperelastic models to address the computational costs in the Finite Element codes. Despite their originality from either phenomenological or physical background, hyperelastic models seek to find appropriate and applicable relations between the applied boundary and loading conditions and the resultant behaviour of material in response to the prevailing conditions.

The constitutive models of hyperelasticity are classified based on their origin as illustrated in figure 4.5 according to the following literatures: (Ogden, 1997), (Ogden, 1972), (Ogden, et al., 2004), (Ogden, et al., 2006), (Ogden & Roxburgh, 1999), (Yeoh, 1990), (Yeoh & Fleming, 1998), (Boyce & Arruda, 2000), (Gent, 2001), (Gent, 1996), (Gent & Thomas, 1958), (Dostal, 1939), (Isihara, et al., 1951), (Kaliske & Rothert, 1997), (Swanson, 1985), (Carroll, 2011), (Miehe, et al., 2004), (James & Guth, 1943), (Wang & Guth, 1952), (Nah, et al., 2010), (Rivlin, 1992), (Arruda & Boyce, 1993), (Mooney, 1940), (Bergstrom & Boyce, 2001), (Guo & Sluys, 2006), (Meuniera, et al., 2008), (Bechira, et al., 2006), (Marlow, 2003), (Sasso, et al., 2008),

(Kuhn & Grün, 2003), (Flory, 1967), (Flory & Erman, 1982), (Flory, 1977), (Miehe, et al., 2004), and (Göktepe & Miehe, 2005).

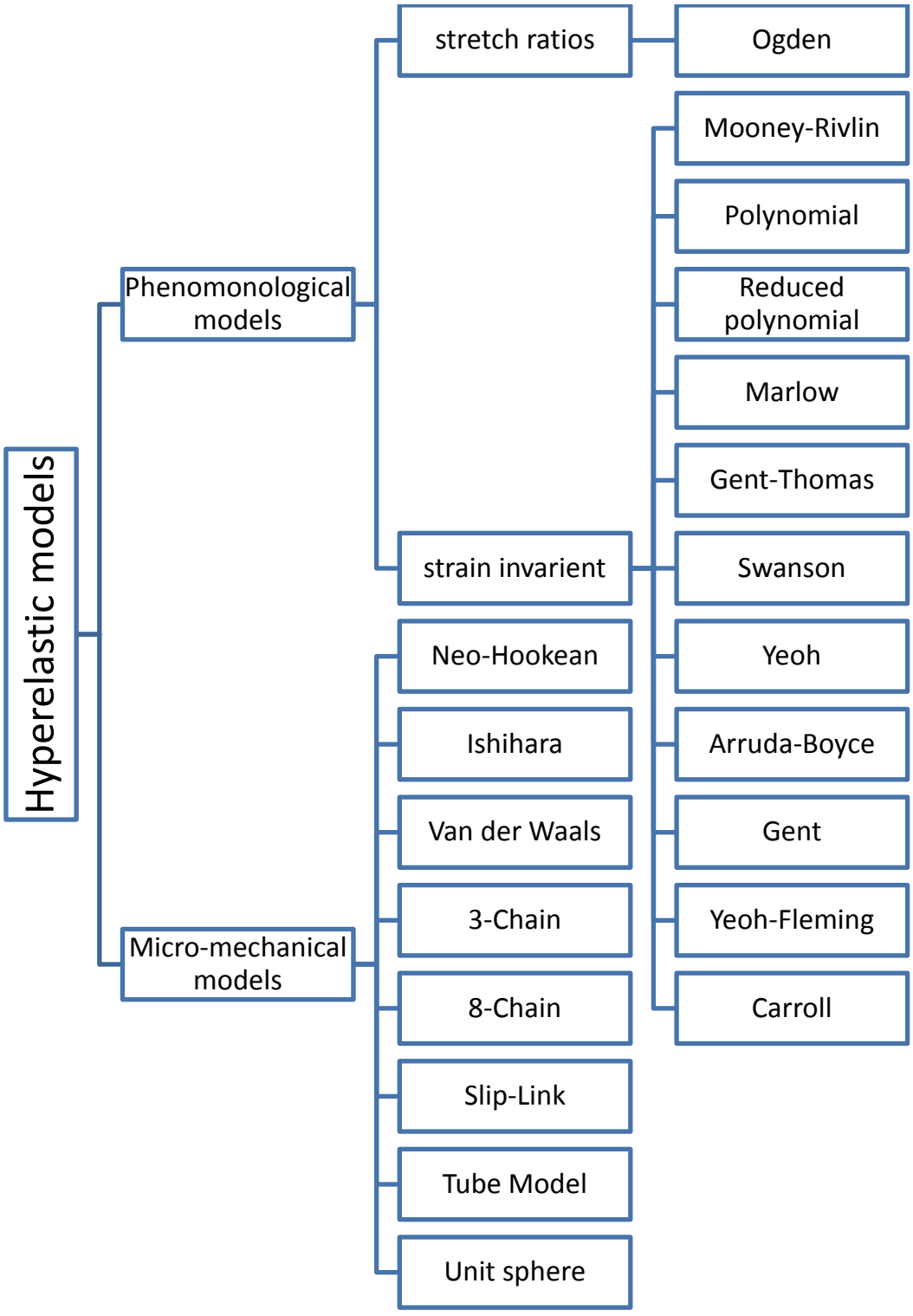

Figure 4.5. Available hyperelastic models for rubber

A selection of well-known and popular phenomenological and micro-mechanical physical-methods are introduced based on a logical hierarchy order from the most general relationship to reduced models as follow:

Ogden model

Ogden developed a number of phenomenological models of elastomers (Ogden, 1972) for the strain energy potential as a function of stretch ratios, as expressed through the following equation:

$$W_e = \sum_{i=1}^{N} \frac{2\mu_i}{{\alpha_i}^2}\left(\bar{\lambda}_1^{\alpha_i} + \bar{\lambda}_2^{\alpha_i} + \bar{\lambda}_3^{\alpha_i} - 3\right) + \sum_{i=1}^{N} \frac{1}{D_i}(I_3 - 1)^{2i} \qquad \text{Equation 4.10}$$

where α_i and μ_i describe the shear behaviour of material and $\bar{\lambda}_i$ is expressed as:

$$\bar{\lambda}_i = {I_3}^{-1/3}\lambda_i \qquad \text{Equation 4.11}$$

where the λ_i represents the principal stretches. The best accuracy for the models is achieved when infinite number of terms is expanded in strain energy potential function. Nevertheless, the model sophistication is increased. The $\frac{1}{D_i}(I_3 - 1)^{2i}$ in Ogden models represents the compressible terms in the equation that can be omitted for the incompressible rubber because of the assumption of $I_3 = 1$.

The first issue that appears in the Ogden model is the number of constants and coefficients to be parameterised, which brings complexity and computational costs for a fitting programme and reduces the efficiency of the modelling in the characterisation procedure. The next issue is the necessity for comprehensive experimental data in three directions which is not easily obtainable for a number of applications and which requires more time and results in more destructive test procedures. However, a model that is being developed

based on the Ogden model is capable of predicting the elongation behaviour in different directions and deformation modes. Consequently, Ogden model is popular and well-developed for biomedical application where a high level of precision is required.

Polynomial model

This model suggests the most general form of strain energy potential as a function of the strain invariants and compressibility parameters (Rivlin & Sawyers, 1976) and was represented in its classical form as:

$$W_e = \sum_{i+j=1}^{N} c_{ij}(I_1 - 3)^i (I_2 - 3)^j + \sum_{i=1}^{N} \frac{1}{D_i}(I_3 - 1)^{2i} \qquad \text{Equation 4.12}$$

where:

- D_i: describes the compressibility and is ignored for fully incompressible rubber;
- c_{ij}: accounts for deviatory behaviour that governs the isochoric shear behaviour;
- W_e: strain energy density (the strain energy potential), that is the potential energy stored per unit of reference volume.

In the presence of the incompressibility assumption, the compressibility term $\frac{1}{D_i}(I_3 - 1)^{2i}$ is omitted like for the Ogden model as below:

$$W_e = \sum_{i+j=1}^{N} c_{ij}(I_1 - 3)^i (I_2 - 3)^j \qquad \text{Equation 4.13}$$

This model is recognised as the Taylor's expansion of the fundamental energy potential form, where the formulation is expressed in terms of strain invariants instead of principal stretch ratios in Ogden model. In fact, the polynomial representation of hyperelasticity is of a similar form to the Ogden model in which the principal stretch ratios are substituted with

strain invariants. This simplification decreases dependency of the strain energy potential on lesser independent variables and coefficients.

Like the Ogden model, the number of coefficients in polynomial form is an issue inasmuch as it increases the complexity of the material model and leads to more expensive numerical costs in the parameterisation procedure for characterisation of the model in order to be calibrated using experimental data. Moreover, the dependency of polynomial models on a comprehensive set of test data remains and three directional experimental stress-strain data should be used for characterisation. In spite of difficulties in model deployment, the polynomial method established a fundamental basis to develop reduced versions of itself to achieve efficiency in computation.

Mooney-Rivlin model

The Mooney-Rivlin model for nearly incompressible elastomers is obtained from the infinite series of polynomial model when the compressibility term including parameter D is neglected:

$$W_e = \sum_{i+j=1}^{N} c_{ij}(I_1 - 3)^i (I_2 - 3)^j \qquad \text{Equation 4.14}$$

The first order Mooney-Rivlin model is a particular form of the polynomial or Ogden model when the counter of summation is $N = 1$ in the polynomial form or the constants are $N = 2$, $\alpha_1 = 2$, and $\alpha_1 = -2$ in Ogden model. Subsequently, the equation is reduced to a quadratic form in equation 4.15 with consideration of compressibility coefficient:

$$W_e = c_{10}(I_1 - 3) + c_{01}(I_2 - 3) + \frac{1}{D_1}(I_3 - 1)^2 \qquad \text{Equation 4.15}$$

and in the incompressible form when the compressible term including I_3 is removed:

$$W_e = c_{10}(I_1 - 3) + c_{01}(I_2 - 3) \qquad \text{Equation 4.16}$$

This model is widely used for rubber application, specifically when subjected to bi-directional loading condition and the model is valid for lower than 200% deformation. The model accuracy in large deformation is an issue when this reduced order Mooney-Rivlin is employed for prediction of stress-strain behaviour. Since Mooney-Rivlin and Ogden models are empirical phenomenological models and physical parameters are not inherently used in their formulation, a characterisation procedure is required to obtain the parameters and coefficients based on experimental data and this is accounted as a disadvantage for these models.

Neo-Hookean model

Neo-Hookean model (Treloar, 1943) is one of the earliest physical based forms to simulate the large deformation in polymeric networks. This model has its origin from the micro-mechanical interaction of long polymer molecules in an integrated construction. In a simpler way, the Neo-Hookean model is practically obtained when $c_{01} = 0$ in equation 4.16 for incompressible mode:

$$W_e = c_{10}(I_1 - 3) \qquad \text{Equation 4.17}$$

and

$$c_{10} = \frac{1}{2} n K_b T \qquad \text{Equation 4.18}$$

where:

- n: chain density per unit of volume
- K_b: Boltzmann constant

- T: absolute temperature

The Neo-Hooke model in compressible form is:

$$W_e = \frac{1}{2} n K_b T (I_1 - 3) + \frac{1}{D} (I_3 - 1)^2 \qquad \text{Equation 4.19}$$

Although this model does not require load-deflection experimental data, the accuracy is an issue at large deformation mode due to the simple first order equations of elongation. In addition, a weak prediction of hyperelastic behaviour is obtained under different loading modes.

Reduced polynomial model

In the reduced polynomial model, the polynomial model order is reduced to one invariant (I_1: the first invariant of Cauchy-Green tensor) in response to the continuous efforts for simplification of models by decreasing the number of variables and parameters for characterisation of hyperelasticity through the strain energy potential function. The reduced polynomial model in compressible and incompressible modes is expressed in equation 4.20 and 4.21 respectively as below:

$$W_e = \sum_{i=1}^{N} c_{ij} (I_1 - 3)^i + \sum_{i=1}^{N} \frac{1}{D_i} (I_3 - 1)^{2i} \qquad \text{Equation 4.20}$$

$$W_e = \sum_{i=1}^{N} c_{ij} (I_1 - 3)^i \qquad \text{Equation 4.21}$$

This model enjoys a simplified structure in formulation and an acceptable accuracy for the unidirectional load cases. However, this model still has too many coefficients to be parameterised using the load-deflection experimental data. On the other hand, bi-directional loading may enable the prediction in extrapolation modes that may not provide

consistent result in the direction that the model is not tuned for and experimental data is not available.

Arruda-Boyce model

Arruda-Boyce model has been developed based on a physical micro-mechanical approach. This model reflects the Arruda and Boyce efforts to develop models of large deformation in elastomers (Boyce & Arruda, 1990), (Arruda & Boyce, 1993), (Boyce, 1997), and (Boyce & Arruda, 2000). This model is also known as the Eight-Chain model, which was derived from an elementary cubic cell with eight springs connecting the centre of cube to its corners according to the non-Gaussian network theory. The eight directions of the centre point in connection to the cube vertices are to resemble the orientation of molecular chain distribution within the elastomer structure.

In this model, the influence of the second invariant is dependent on the first invariant, so that the first invariant I_1 forms the fundamental equations of Arruda-Boyce model and the third invariant is employed when the incompressibility assumption is invalidated. The strain energy potential in this model is defined as in Equations 4.20 and 4.21 in compressible and incompressible modes:

$$W_e = G_0 \sum_{i=1}^{5} \frac{c_i}{{\lambda_m}^{2i-2}} \left({I_1}^i - 3^i\right) + \frac{1}{D}\left(\frac{{I_3}^2 - 1}{2} - \ln I_3\right) \qquad \text{Equation 4.20}$$

$$W_e = G_0 \sum_{i=1}^{5} \frac{c_i}{{\lambda_m}^{2i-2}} \left({I_1}^i - 3^i\right) \qquad \text{Equation 4.21}$$

where:

- $[c_1, c_2, c_3, c_4, c_5] = [\frac{1}{2}, \frac{1}{20}, \frac{11}{1050}, \frac{19}{7000}, \frac{519}{673750}]$
- G_0 : initial shear modulus

- λ_m: locking stretch, i.e. the point in stress-strain curve where the stiffness changes significantly.
- $D = \frac{2}{K_b}$: Double the inverse bulk modulus at small strain
- K_b: Boltzmann constant

The physical based methods such as Arruda-Boyce model have recently attracted more attention in modelling of hyperelasticity since not only are the parameters to be determined less than the phenomenological models, but less experimental data is needed to be collected for the characterisation of the model. The other advantage of physical models is that these models exhibit no common instabilities such as singularity or negative inclination in stress-strain curves as long as the configuration parameters are obtained from the physical properties of the material. Along with the inaccuracy arguments around this method in highly nonlinear deformation region, the Arruda-Boyce model and similar physical approaches suffer uncertainty in prediction of the rubber properties, that is, the behaviour of rubber varies from its original character with slightly different constructional elements such as the carbon black filler or other add-ons.

Van der Waals model

Van der Waals model is a physical based model that was initially introduced by Kilian (Kilian, 1980) on the molecular interpretation of deformation in polymers using the parameters of the van der Waals equation of state for the polymeric chains, and then, the modelling was further extended to derive the governing formulation on general deformation in elastomers (Enderle & Killian, 1987). Later, the large deformation of molecular network was investigated to develop the Van der Waals model for hyperelasticity (Kilian, et al., 1987).

The strain energy potential for modelling hyperelasticity in Van der Waals model was suggested in this form:

$$W_e = \mu\left\{-(\lambda_m^2 - 3)[\ln(1-\eta)+\eta] - \frac{2}{3}a\left(\frac{\tilde{I}-3}{2}\right)^{\frac{3}{2}}\right\} + \frac{1}{D}\left(\frac{{I_3}^2-1}{2} - \ln I_3\right) \qquad \text{Equation 4.22}$$

where

$$\tilde{I} = (1-\beta)I_1 + \beta I_2 \quad \text{and} \quad \beta = \sqrt{\frac{\tilde{I}-3}{\lambda_m^2-3}} \qquad \text{Equation 4.23}$$

The parameter μ represents the shear modulus and the parameters D and a concerns the compressibility of Van der Waals model in equation 4.22 and global interaction in equation 4.22 respectively. The equation shows that when the generalised invariant $\tilde{I}$ tends to the locking stretch λ_m^2, β and $\tilde{I}$ approach 1 and I_2 respectively according to equation 4.23, and by replacing these into equation 4.22, the network potential tends toward infinity (Seibert & Schöche, 2000). Therefore, the global strain invariant in Van der Waals model should be kept under the locking stretch to avoid the generation of infinite potential energy in Van der Waals equation. This limits the model validity to predict very large strain due to large deformation when subjected to tensile load.

Yeoh model

According to the experimental result (Yeoh, 1990), Yeoh found that the dependency of strain energy density function on the second invariant $\frac{\partial W_e}{\partial I_2}$ is generally much weaker rather than the first invariant $\frac{\partial W_e}{\partial I_1}$, particularly more applicable for deformation larger than 20% of initial length (Yeoh, 1993). As a result, like the Arruda-Boyce and Neo-Hookean models, Yeoh model is independent of the second invariant. A cubic relationship between the strain

energy density W_e and the first invariant I_1 represents an appropriate approximation for replication of the S-shape stress-strain curve in response to the large deformation of rubber as observed in experimental data. This model is expressed through the following equations 4.24 and 4.25 for compressible or incompressible assumptions of rubber behaviour:

$$W_e = \sum_{i=1}^{3} c_{i0}(I_1 - 3)^i + \sum_{i=1}^{3} \frac{1}{D_i}(I_3 - 1)^{2i} \qquad \text{Equation 4.24}$$

$$W_e = \sum_{i=1}^{3} c_{i0}(I_1 - 3)^i \qquad \text{Equation 4.25}$$

Yeoh model is classified as a phenomenological model since the parameterisation procedure is essential for determination of the model parameters. In fact, the Yeoh model coefficients can be characterised with minimum unidirectional data where the lack of data and test facility is an issue. At the same time, the model is consistent enough in prediction of stress-strain behaviour under alternative loading modes particularly in large deformation condition. Moreover, the model requires fewer coefficients for parameterisation, so that the fitting procedure requires less calculation efforts in comparison with models with more parameters. Therefore, the FE models demand less expensive computational resources and the solution convergence is faster.

Marlow model

The Marlow model, first introduced by (Marlow, 2003), was presented in continuation of efforts to explore a simplified shape for the strain energy density function whilst the model is applicable with satisfactory accuracy in different modes of deformation. Similarly to the Yeoh and Arruda-Boyce models, the effect of second invariant is neglected in the Marlow model because of its weak dependency to form S-shape changes in stress-strain curves from

large deformation unidirectional tensile data, so that a simpler form of the strain energy density function was derived in terms of the first invariant. Therefore, first invariant in terms of principal stretches can be expressed as follows:

$$I_1 = {\lambda_1}^2 + {\lambda_2}^2 + \frac{1}{{\lambda_1}^2{\lambda_2}^2} \qquad \text{Equation 4.26}$$

According to equation 4.26, I_1 varies from minimum 3 to maximum infinity. If the equation is rewritten for the unidirectional tension:

$$I_1 = \lambda^2 + \frac{2}{\lambda^2} \qquad \text{Equation 4.27}$$

The same range of change from minimum 3 to maximum infinity is perceived for the first invariant. It can be concluded that the sole unidirectional experimental data can be used for calibration of coefficients in strain energy density function. Practically, when the first invariant is a function of the three-directional stretch ratios, the equivalent unidirectional stretch ratio can be extracted to form the strain energy density function as follows:

$$W_e(I) = \int_0^{\lambda(I)-1} \sigma(\epsilon) d\epsilon \qquad \text{Equation 4.28}$$

where the σ and ϵ are nominal stress and strain of unidirectional tension respectively, which are directly obtained from the experimental data. To fulfil the incompressibility assumption in rubber behaviour, the invariant $I_3 = 1$ and the compressible term in the equations is omitted. In the Marlow model unlike the other models introduced so far, an explicit equation does not exist to represent the relation between the strain energy density and strain invariants. In this model, the strain energy potential is obtained through

unidirectional equations by resemblance of material deformation in three-dimensional mode.

4.2.2.3 Models for viscoelasticity

As discussed regarding the viscoelastic property of rubber, viscous materials exhibit a time and rate dependent characteristics principally due to the internal friction of molecular level rearrangements in polymeric structure within deformation mechanism. Viscoelasticity is apparently a property of material that cannot be modelled solely by the elasticity or viscosity. According to the literature (Fatt & Bekar, 2004), the pure nonlinear elasticity is well suited for either quasi-static or very high rate of strain deformation condition. Whatever condition occurs in between is considered as the large (finite) strain or small strain viscoelasticity.

In rheology, the resistance force against the motion is commonly modelled as the rate of distortion or relative velocity of moving object multiplied by the viscosity constant; on the other hand, the deformation in rubber is fully recoverable given adequate time. The inter-molecular viscous behaviour suggests the idea of relating the macroscopic behaviour such as the generated force or displacement with rate-dependent excitation applied by the displacement or load respectively. The instantaneous springiness and delayed response of material due to viscosity are combined in rubber through different configurations to build a baseline model that is independent of the applied loads of any kind and can ideally respond to arbitrary loading conditions. In this case, the behaviour of rubber under different conditions such as relaxation, creep, and cyclic loading can be simulated through a single model and calibrated using one particular static or dynamic characterisation procedure.

Unlike hyperelastic models, linear viscoelastic behaviour in material can be practically modelled through its resemblance to a combination of spring and dampers from a mechanical standpoint. However, the nonlinear rheological models in conjunction with large strain theories such as hyperelasticity are able to resolve the deficiency of the model in prediction of induced stress or strain in large elongation situation. Different configurations of linear viscoelastic models are explained as below:

Maxwell model

Maxwell model is considered as a rheological model, in which the instantaneous (Hookean spring) and rate-dependent (Newtonian dashpot) components are arranged in a series configuration, as shown in figure 4.6.

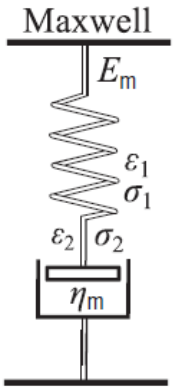

Figure 4.6. Maxwell model for viscoelasticity

The mechanical response of the Maxwell model can be modelled through the following equation:

$$E_m\dot{\varepsilon}(t) = \dot{\sigma}(t) + \frac{1}{\tau}\sigma(t) \qquad \text{Equation 4.29}$$

where $\tau = \eta/k$ is the relaxation time constant, and η and k represent the dashpot viscosity and spring stiffness respectively. The model response to a constant strain was solved and the relaxation behaviour is shown through the following equation:

$$\sigma(t) = \sigma_0 \exp(-\frac{t}{\tau}) \qquad \text{Equation 4.30}$$

Kelvin-Voigt model

In Kelvin-Voigt model (figure 4.7), the dashpot and spring are configured in parallel together in order to replicate the creep behaviour in viscoelasticity. The mathematical constitutive equation is derived as below:

$$\sigma(t) = E_v \varepsilon(t) + \eta \dot{\varepsilon}(t) \qquad \text{Equation 4.31}$$

The model's response to the constant stress is demonstrated through the following equation:

$$\varepsilon(t) = \frac{\sigma_0}{E_v}(1 - \exp(-\lambda t)) \qquad \text{Equation 4.32}$$

where $\lambda = \frac{E_v}{\eta}$ is called the rate of relaxation.

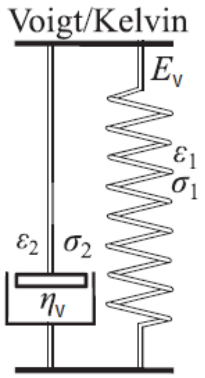

Figure 4.7. Kelvin-Voigt model for viscoelasticity

Standard linear Solid

The spring and dashpot in standard linear solid model are connected in both parallel and series arrangements as shown in figure 4.8. The constitutive equations are illustrated as shown below:

$$\dot{\varepsilon}(t) = \frac{\dot{\sigma}(t)+\frac{E_m}{\eta}\sigma(t)-\frac{E_m E_v}{\eta}\varepsilon(t)}{E_m+E_v} \qquad \text{Equation 4.33}$$

This model represents the most accurate prediction of viscoelastic behaviour among simple rheological models.

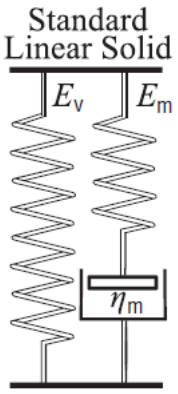

Figure 4.8. Standard Solid model for viscoelasticity

Generalized Maxwell-Wiechert Model

The generalised Maxwell models, that is also known as the Wiechert model, is an expansion to the standard linear solid model with repeated Maxwell model added in a parallel configuration.

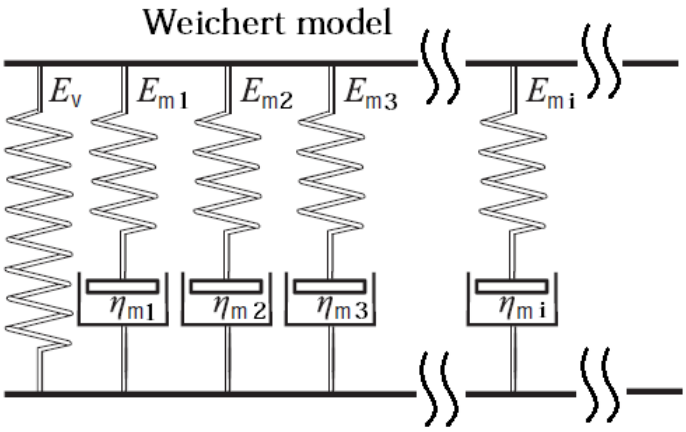

Figure 4.9. Weichert model for viscoelasticity

The constitutive equation to represent the Wiechert model is shown through the following equation:

$$\sigma(t) = \sigma_v(t) + \sum_{i=1}^{N} \sigma_m(t) \qquad \text{Equation 4.34}$$

where:

- $\sigma_v = E_v \varepsilon$
- σ_m: Maxwell stress according to $\sigma(t)$ in equation 4.29

Prony series model

The Prony series model is regarded as one of the most popular approach for modelling viscoelasticity among the FE packages primarily due to integrity, accuracy, and computational efficiency (Chen, 2000). Unlike the previous rheological models, the Prony series is a pure numerical method whose constants are calibrated using gradient-based fitting methods for stress-strain experimental data under relaxation or creep. There are three different representations of material viscoelasticity for creep, stress relaxation, and cyclic loading. The entire Prony series models initially begin with the baseline representation

of the applied stress or strain in terms of the induced strain and stress. The viscoelastic equations are formed based on the definition of each procedure as follows:

$$Creep\ form: \epsilon(t) = J(t)\sigma_0 \qquad \text{Equation 4.35}$$

$$Relaxation\ form: \sigma(t) = E(t)\epsilon_0 \qquad \text{Equation 4.36}$$

where the $E(t)$ and $J(t)$ are generally the elastic and compliance modulus respectively for creep and relaxation procedure, while $\sigma_0 and\ \epsilon_0$ denote the constant applied stress and strain respectively according to the stress relaxation and creep procedure definition. In cyclic dynamic experiment, the strain is normally applied through the cyclic form $\epsilon(t) = \epsilon_0 \sin(\omega t)$ and the resultant stress is expressed as below (Pioletti, 1997):

$$Dynamic\ form: \sigma(t) = \epsilon_0[G'(\omega)\sin(\omega t)\ + G''(\omega)\cos(\omega t)] \qquad \text{Equation 4.37}$$

where the G' and G'' are the storage and loss moduli. These equations can be generally rewritten as the $[\sigma(t)] = [E(t)][\epsilon(t)]$ in tensor form. The common point in these equations is the time-dependent elastic modulus $E(t)$ that can be extended to finite terms of exponential forms using the Prony expansion method. The rubber model for this application is assumed to behave like a general Maxwell solid, in that the stress eventually relaxes to a constant value at infinite time. The first step in formulating the viscoelasticity is to find out the range of validity of viscoelastic models. The governing models of viscoelasticity are expressed in *small* or *finite* (large) deformation regimes, where a high strain value usually greater than 40% is recognised as the separating condition for these regimes (Holzapfel, 1996). The linear viscoelasticity governs the behaviour in small strain regime while the nonlinear viscoelasticity offers an improved accuracy in prediction of stress-strain data for large strain regime (Petiteau, et al., 2013).

In small deformation, the time-dependent (convolution integral shape) and instantaneous elasticity are separable and a Boltzmann superposition of these terms forms the linear viscoelasticity equation, which can be described in its general state of deformation modes as below (Truesdell & Noll, 2004):

$$\sigma(t) = \sigma_\infty + \int_{s=0}^{\infty} G(s-t)\dot{\varepsilon}(t)dt \qquad \text{Equation 4.38}$$

where σ can be any element of the stress tensor; σ_∞ is the equilibrium stress term when the time tends to infinity and $\varepsilon(t)$ is the corresponding element in strain tensor. In creep and relaxation modes, $H(t)$ is substituted with creep function $K(t)$ and relaxation function $F(t)$ respectively. This relation for shear is expressed with the following equation:

$$\tau(t) = \tau_\infty + \int_{s=0}^{\infty} G(s-t)\dot{\gamma}(t)dt \qquad \text{Equation 4.39}$$

where $\tau(t)$, $G(t)$, and $\gamma(t)$ are the shear stress, shear modulus, and shear strain of a solid element under shear loading condition. If the convolution integral is normalised for the stress tensor elements and estimated by the numerical Prony time series in exponential shape function, the constitutive linear elasticity relation is formed, as described below for the shear modulus:

$$G(t) = G_\infty + \sum_{i=1}^{N} G_i\, e^{-t/\tau_i} \qquad \text{Equation 4.40}$$

where $G(t)$ expresses the time-dependent shear modulus and G_∞ is a constant to represent long term shear modulus in relaxation test; i.e. the $G(t)$ converges to G_∞ when time tends to infinity. The parameters τ_i and G_i denote the relaxation time constant and Prony series coefficients for each term that are determined through the minimisation of fitting error. The current representation of the shear modulus requires an adequate amount of time to converge to its final value and the settling time is variable for each material. In response to

this challenge, the time-dependent shear is rearranged accordingly in a way that the equation features the initial shear modulus G_0 as shown below:

$$G(t=0) = G_0 = G_\infty + \sum_{i=1}^{N} G_i \qquad \text{Equation 4.41}$$

Therefore,

$$G(t) = G_0 - \sum_{i=1}^{N} G_i \left[1 - e^{-t/\tau_i}\right] \qquad \text{Equation 4.42}$$

To generalise the usage of Prony series in relaxation mode to comprehensive deformation modes, the equation 4.42 is normalised by dividing the right and left hand of the equation by G_0, as demonstrated in equations 4.43 And 4.44:

$$g(t) = 1 - \sum_{i=1}^{N} g_i \left[1 - e^{-t/\tau_i}\right] \qquad \text{Equation 4.43}$$

Or:

$$g(t) = g_\infty - \sum_{i=1}^{N} g_i \, e^{-t/\tau_i} \qquad \text{Equation 4.44}$$

where $g_\infty = \frac{G_\infty}{G_0}$, $g(t) = \frac{G(t)}{G_0}$, and $g_i = \frac{G_i}{G_0}$.

The nonlinear viscoelastic theories dominate the constitutive equations at large strain regime, where the stress and strain are not separable to fulfil the superposition conditions. However, the constitutive nonlinear viscoelastic equations can be derived based on the generalisation of the small strain viscoelasticity as one of the available approaches. In this method, the deviatoric term of the instantaneous stress, like g_0 in the shear deformation mode, is estimated using a strain energy density based on the hyperelastic formulation discussed above. In this method that is also known as the convolution integral approach (Christensen, 1982), the time dependency of linear viscoelasticity is considered by an

incremental time function within a convolution integral. Therefore, a large deformation in relaxation and creep is directly handled by allowing multiple relaxation (creep) time constants and the Prony series for the relaxation (creep) function.

An advanced implementation of this approach is suggested by Bergstrom-Boyce model in (Bergstrom, 1999), (Bergstrom & Boyce, 1998), (Bergstrom & Boyce, 1999), (Bergstrom & Boyce, 2000), and (Bergstrom & Boyce, 2001). The Bergstrom-Boyce model is similar to the Standard Linear Solid configuration, which comprised of two parallel networks (figure 4.10): one network accounts for the equilibrium state which corresponds to the time-independent rubber behaviour and the other network contributes to the time-dependent deviation from equilibrium and gives the nonlinear rate-dependent term of the networks' resultant response. This model is widely used as the nonlinear large deformation viscoelastic model and a general representation of the model prediction is shown is figure 4.11.

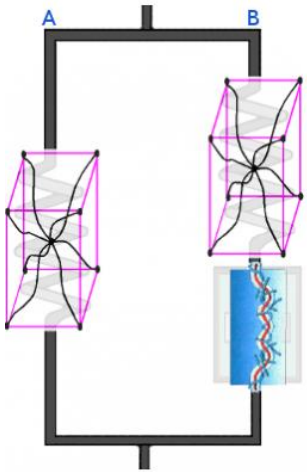

Figure 4.10. Network configuration in Bergstrom-Boyce model (Bergstrom, 1999)

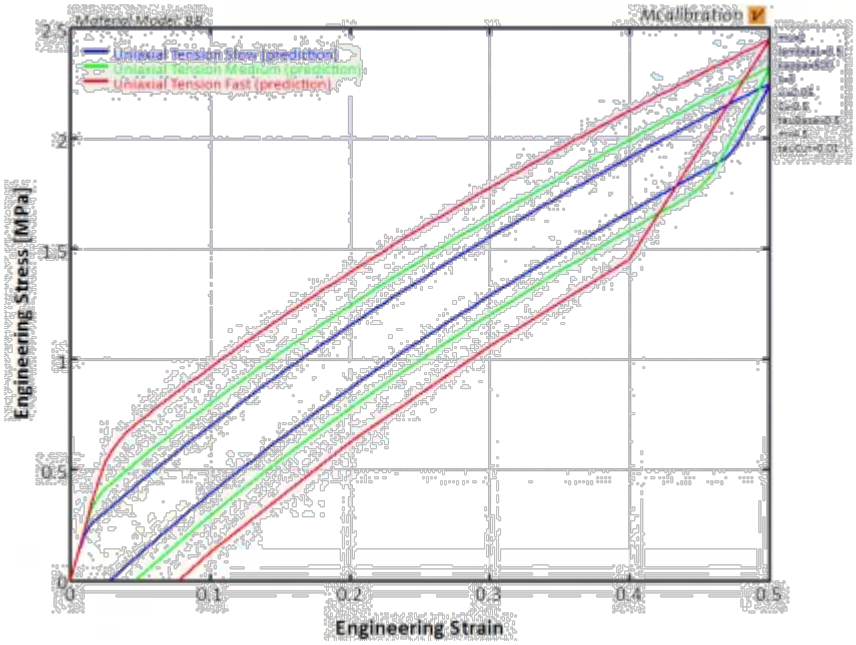

Figure 4.11. Stress-strain prediction of Bergstrom-Boyce model for nonlinear viscoelasticity (Bergstrom, 1999)

More nonlinear hyperviscoelastic models were offered by more researchers in (Liu, 2007), (Ghoreishy, et al., 2013), (Saleeb, et al., 2006), (Libertiaux & Pascon, 2010), (Puzrin & Rabaiotti, 2010), and (Bikard & Désoyer, 2001). In Ghoreishy's work, Marlow and Yeoh hyperelastic models were integrated with the linear Prony series and the nonlinear Bergstrom-Boyce viscoelastic models. It was demonstrated that the small strain viscoelastic models were unsuccessful to predict the accurate behaviour of relaxation in rubber at large strain, particularly when wider rubber samples were subjected to constant strain, but an acceptable prediction of strain-stress curves was obtained when the Yeoh model was used in conjunction with the Bergstrom-Boyce model. In this model, similar assumption in the Bergstrom-Boyce model for the network configuration was made. Then, the mechanical behaviour of the time-independent network was expressed with Yeoh and Marlow hyperelastic models.

To provide experimental data for characterisation of Prony series coefficients, various techniques are suggested such as relaxation test, creep test, and Dynamic Mechanical Analysis (DMA) test. Owing to the simplicity in implementation of relaxation test as well as its implementation in shorter timeframe, the stress relaxation form is known as the most popular representation of stress-strain data for viscoelasticity (Abu-Abdeen, 2010). Nevertheless, the creep data set can be used to characterise the rubber

4.3. Characterization of material models

In this section, the standard procedures to obtain the experimental data for hyperelastic behaviour of aircraft rubber are introduced. The viscoelasticity is not tested in this thesis and no sample was provided by Dunlop Aircraft Tyres Limited due to the confidentiality of the material and limitation of the facilities to test the viscoelasticity. For continuation of the thesis, the approximated hysteresis curves according to the literature are used to establish the FE model for the demanded applications. Later in this section, the large strain data are presented for rubber and reinforcement and two appropriate models based on the explained criteria in the previous section are selected to represent the hyperelastic and viscoelastic behaviour. Eventually, the models are parameterised and their performance in prediction of stress and strain data is examined in comparison with the experimental data through a virtual simulation.

4.3.1 Instrumentation and Standard procedure

4.3.1.1 Rubber testing

The instrumentation, rubber sample preparation, and standard procedures to obtain the hyperelastic experimental data are discussed in the following. The test facility is located in Dunlop Aircraft Tyres Limited (DATL) at Birmingham, UK. The tensile facility is a high force

floor standing “Tinius Olsen” instrument, which is branded as a popular machine for electromechanical material testing, as shown in figure 4.12. The machine features the force accuracy of ± 0.5% of applied load, displacement resolution of 0.001 mm, and Speed resolution of 0.001 mm/min. The test rig can be operated at speeds ranging from 0.01 mm/min to a maximum of 500 mm/min, which accommodates the operating procedure of ISO standard test. This test machine satisfactorily complies with the requirements of ISO 5893. For experiments, the tests were carried out at standard laboratory temperature near 27 °C.

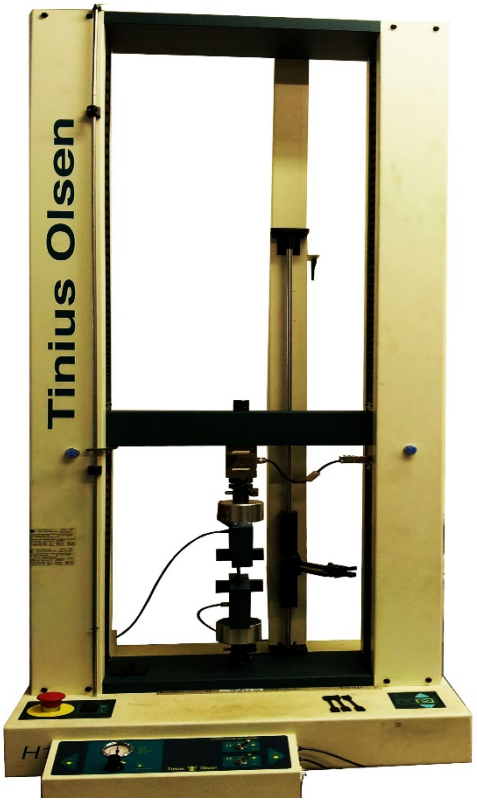

Figure 4.12. Tensile test machine to measure hyperelasticity

The tensile data were read and stored using data acquisition software QMAT 5.37 T-series, which is installed on a PC and connected to the test facility. The test machine is also commanded by the QMAT software as illustrated in figure 4.13. The working environment of the QMAT software is also shown is figure 4.14.

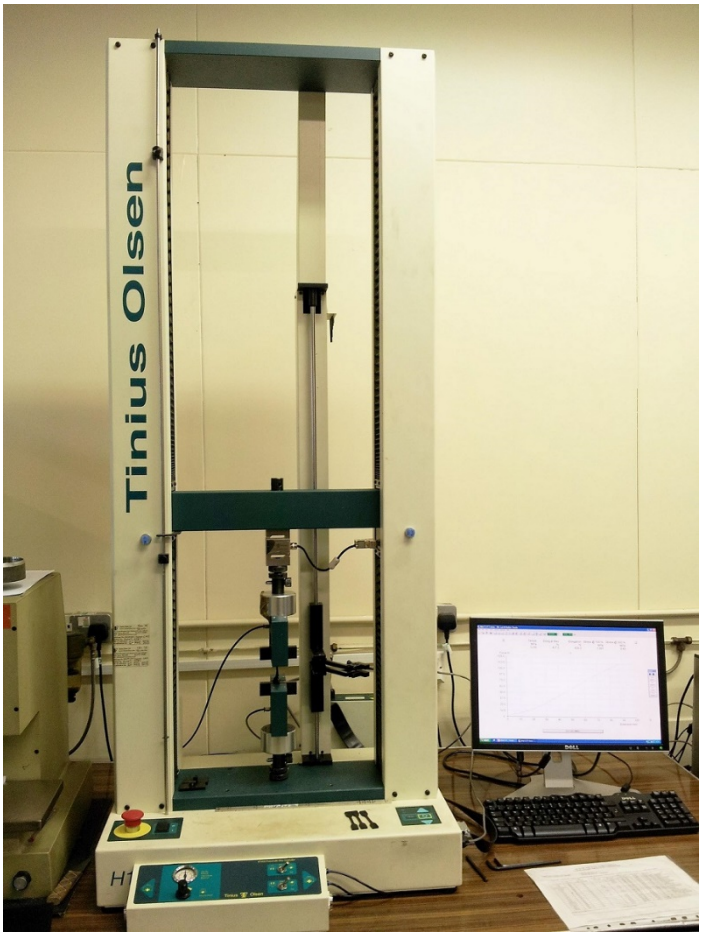

Figure 4.13. Tensile test machine to measure hyperelasticity

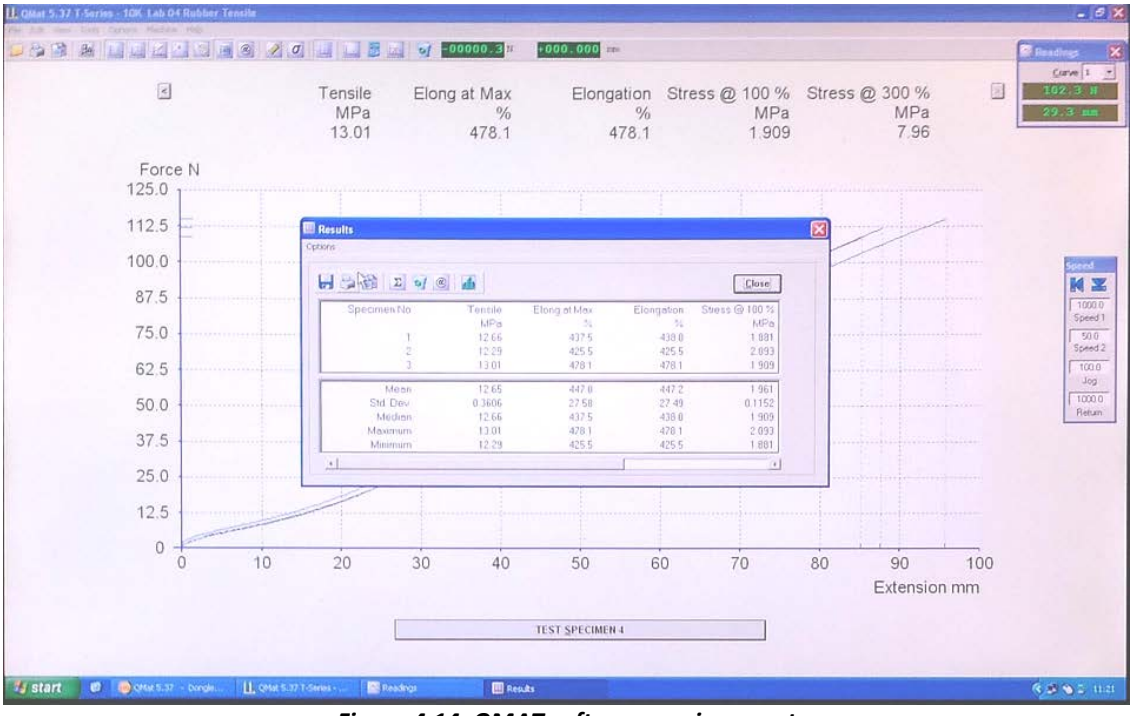

Figure 4.14. QMAT software environment

The samples were cut into Dumb-bell specimens (figure 4.15) based on the British standard *BS-ISO-37:2005* from a rubber sheet using the puncher shown in figure 4.16. The used dies and cutters were prepared in accordance with standard ISO 23529. According to the standard, the sample sizes were taken from the type 1A, in that the thickness of narrow sample should be 2.00 mm with ± 0.2 mm tolerance, the length is 20mm with ± 0.5 tolerance, and the 4mm size is set for width (20mm x 4mm x 2mm for [length]x[width]x[thickness]).

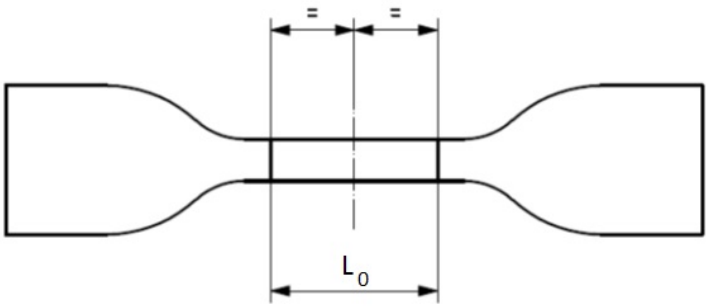

a. Dumb-bells specimen drawing

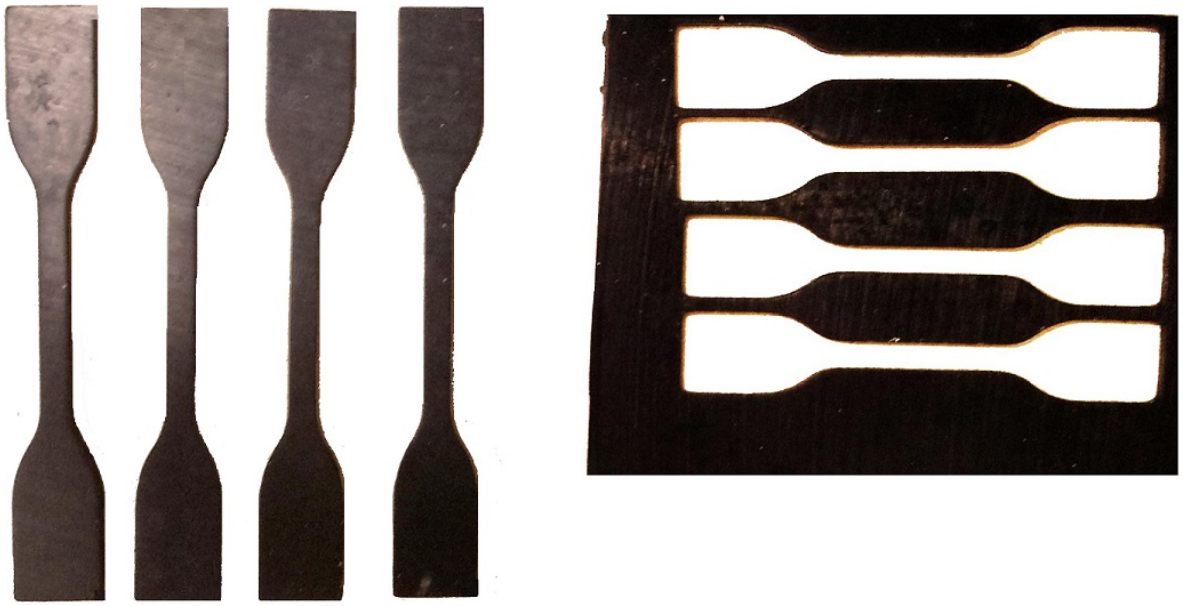

b. Punched dumb-bells specimen from the rubber sheet

Figure 4.15. Preparation of specimen for tensile test

a. Rubber sheet puncher machine

b. Rubber sheet puncher template

Figure 4.16. Rubber sheet cutter

In addition, a close shot of a sample mounted and securely gripped by metal grippers on the test machine is illustrated in figure 4.17. Three specimens were prepared to be tested by the suitable methods described in ISO 23529. Furthermore, the time between vulcanization and testing is more than 16 hours and less than 4 weeks as stated in the standard.

The test sample is inserted into the machine for tensile testing, while ensuring both end tabs are symmetrically gripped, so that the tension is distributed homogeneously over the

rubber cross-section. The moving grip is traversed at the nominal rate of 500 mm/min until the specimen breaks inside the test length. Any test in which the specimen is broken outside the allowed region (narrow part between notches) is discarded and the test is repeated with additional sample.

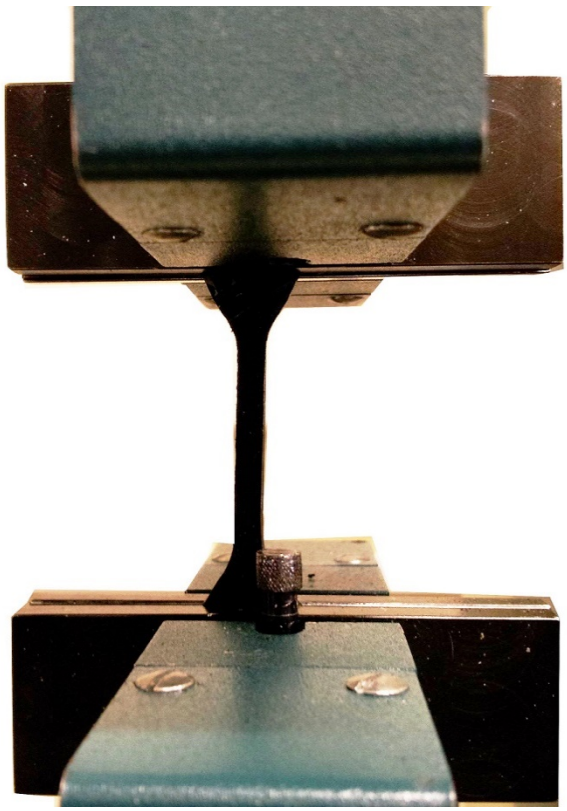

Figure 4.17. Mounted samples before experiment

A number of terms used for testing are defined as below in order to calculate the stress and strain based on the recorded load and displacement:

- Tensile stress: stress applied to stretch the specimen and is calculated based on the nominal stress, $\sigma_t = \frac{F_t}{A_0}$, where F_t is the tensile load and A_0 describes the nominal cross-section area.

- Elongation or tensile strain, expressed as a percentage of the sample length, produced by a tensile stress, $\varepsilon_t = \frac{100(L_t - L_0)}{L_0}$, where L_t is the sample length under tension and L_0 expresses the specimen initial length.
- Tensile strength: maximum tensile stress logged in extending the specimen at the breaking point

The stretched rubber sample on the tensile machine is shown in figure 4.18. Moreover, the broken rubber sample is also depicted in figure 4.19.

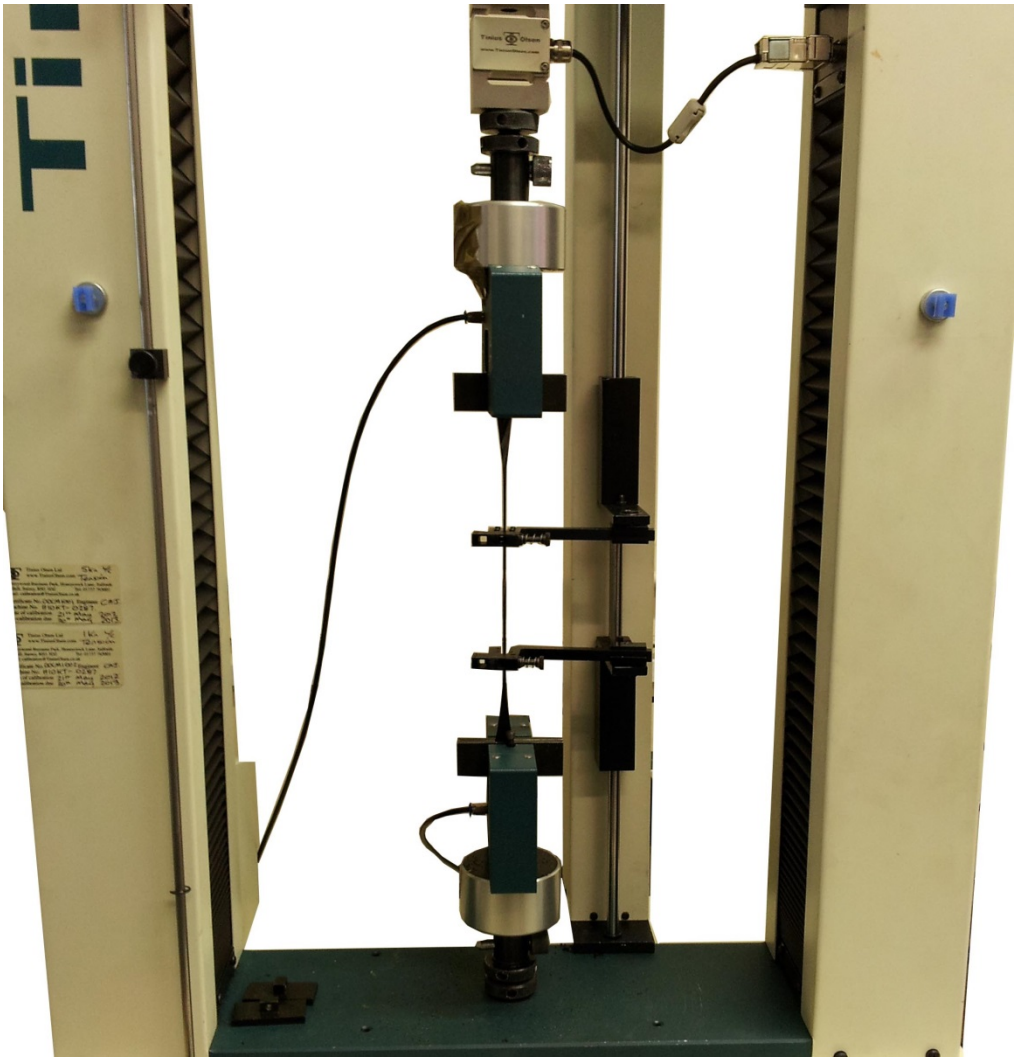

Figure 4.18. Rubber sample under tensile test

Figure 4.19. Broken specimen in comparison with the unused sample

4.3.1.2 Cord testing

Similar procedure to characterise the rubber specimen and the same apparatus was used for characterisation of the nylon cords. The main difference however was the size of specimen. Unlike the standard size for rubber samples, consistent cord length with different diameters is specified for civil and military tyre, as the length of 250 mm is cut for cords in both tyres and the diameter of different cords as are 0.54 mm, 1.00 mm, and 1.15 mm (American Society for Testing and Materials, 2014). According to the standard, the samples are placed around two pulleys (instead of being gripped) with a minimum tension and the moving pulley travels at 100 mm/min speed until the cord breaks.

4.3.2 Experimental data

4.3.2.1 Rubber and nylon cord

The hyperelastic test was conducted for both rubber and nylon cords. The rubber and cord labels and their specifications are listed in table 4.2 and 4.3 for military and civil tyres.

Table 4.2. Military tyre rubber and cords specification

Material	Code	Description
Military tyre 30x11.5R14.5 Rubber	M1436	Chafer
	M1450	Tread sheet compound
	M4305	Apex and Wrapping
	M4430	Inner lining
	M4495	Sidewall packing and cushion compound
	M4950	Insulation compound
	M8300	Sidewall compound
	MK017	Rubber topping for Band Belt Plies
Military tyre 30x11.5R14.5 Cord	P1694	Heal filler reinforcement
	N947	Band Belt Plies
	RP110	Cut, Breaker, and casing ply

Table 4.3. Civil tyre rubber and cords specification

Material	Code	Description
Civil tyre H41x16.0R20 Rubber	DC001	Tread & Suber tread & inner tread topping & insulation
	DC003	Bead Coat/Apex
	DC004	Inner liner
	DC005	Casing (topping compound) & clinch strips
	DC012	Sidewall
	DC018	Chafer
Civil tyre H41x16.0R20 Cord	DF014	Inner tread fabric
	DF022	Cut/Breaker
	DF023	Radial Casing/Breaker

The data are recorded in a format that can be easily loaded into Matlab for further post-processing. The load-displacement data are firstly averaged for three specimens, and then converted to the nominal stress-strain data using the formula introduced for tensile stress and strain in rubber and cords. The rubber and cords hyperelastic properties of civil aircraft tyre are demonstrated in figures 4.20 and 4.21 in terms of stress in MPa and unitless strain. The similar stress-strain curves are plotted for the military aircraft tyre in figures 4.22 and 4.23.

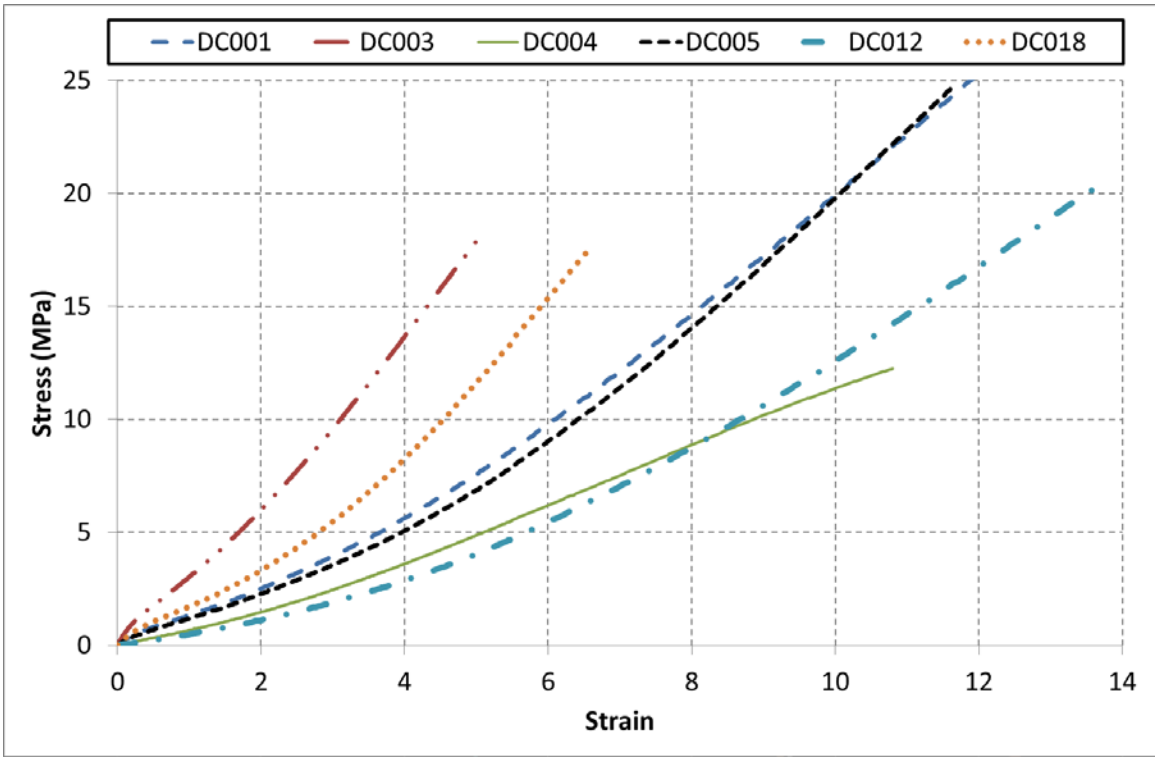

Figure 4.20. Hyperelastic behaviour for rubber compound of civil aircraft tyre

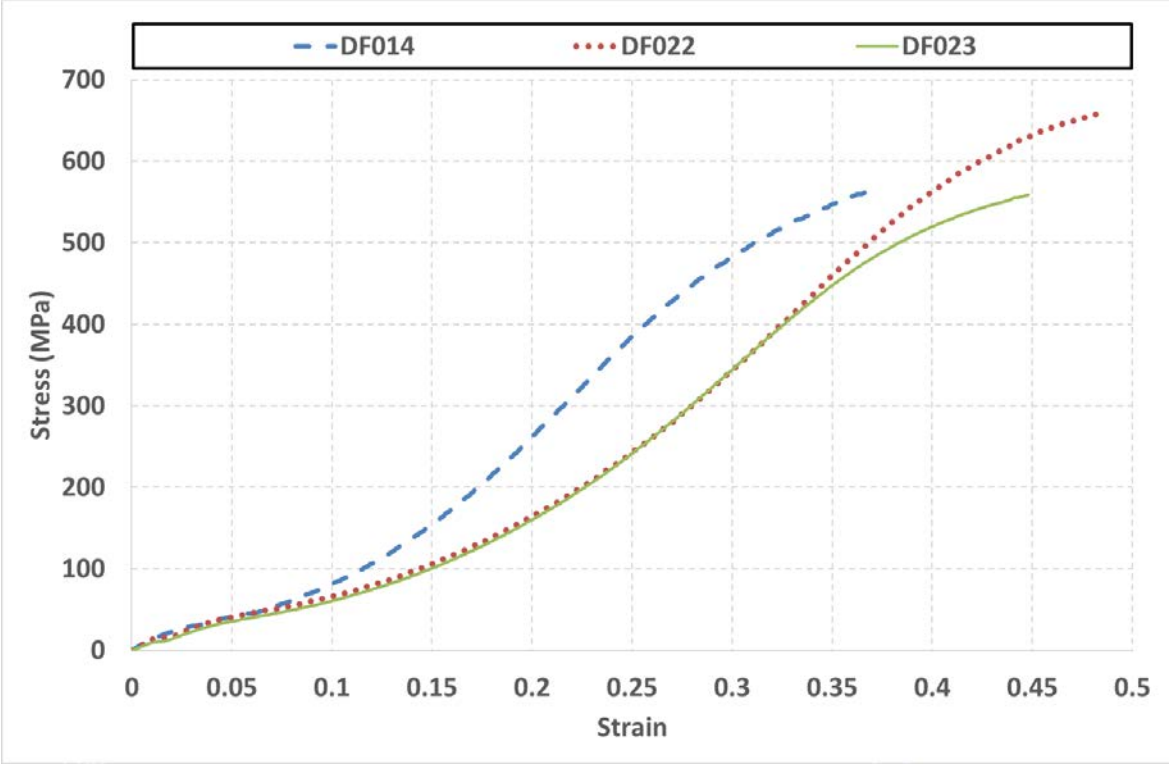

Figure 4.21. Hyperelastic behaviour for fibre cords of civil aircraft tyre

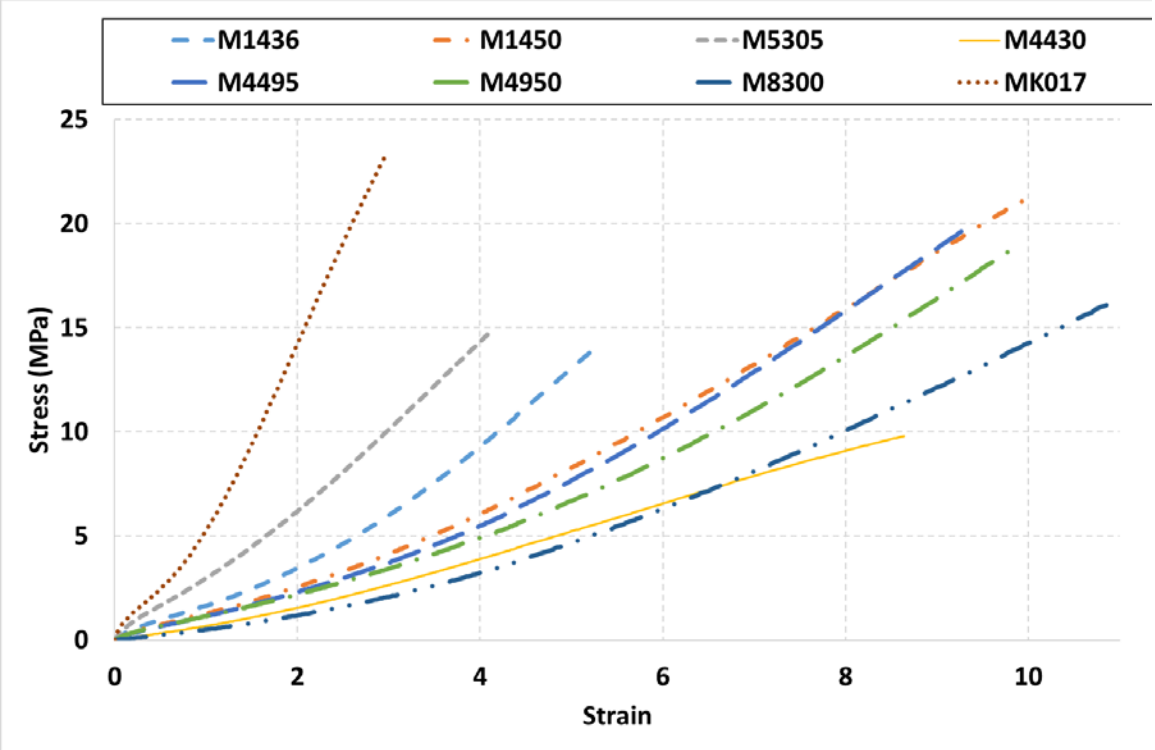

Figure 4.22. Hyperelastic behaviour for rubber compound of military aircraft tyre

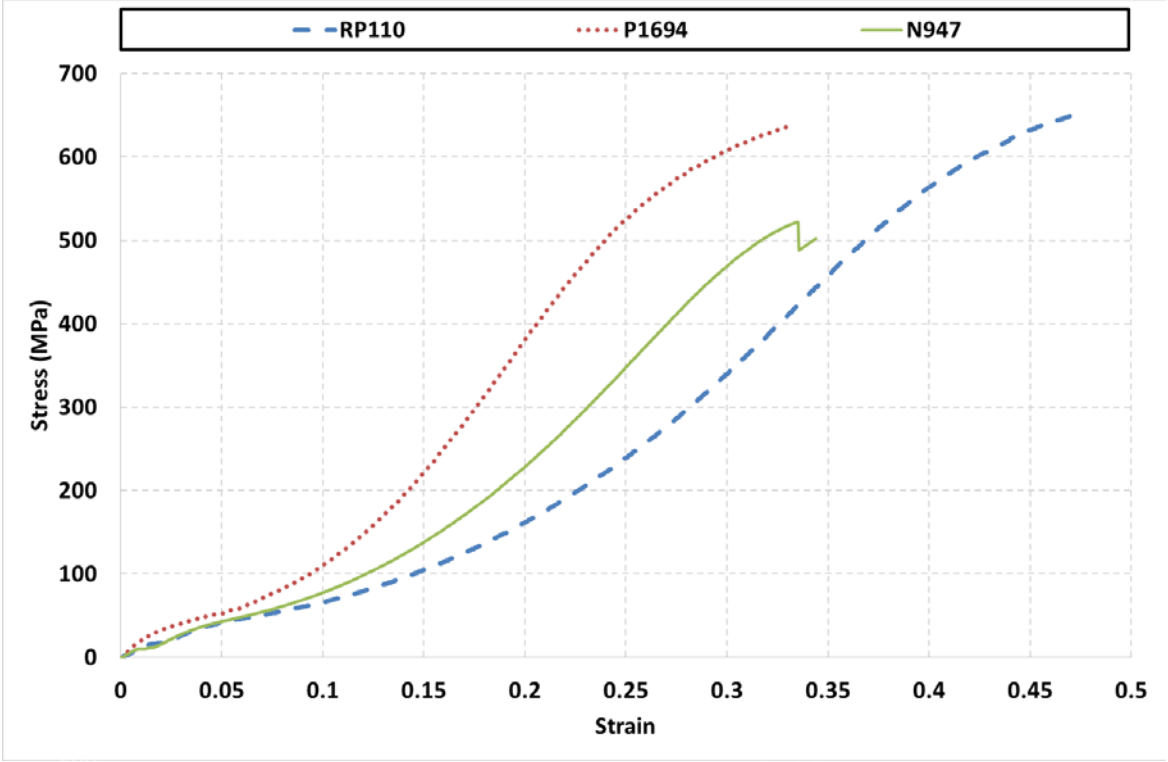

Figure 4.23. Hyperelastic behaviour for fibre cords of civil aircraft tyre

In order to ensure the repeatability of the high elongation load-displacement experiments, ten samples per nylon reinforcement cords in military aircraft tyre (RP110, N947, and P1694) were selected and subjected to similar loading condition. The results of applied force versus the generated strain for picked samples show a satisfactory repeatable procedure of tensile test for these materials, as reported in figures 4.24, 4.25, and 4.26.

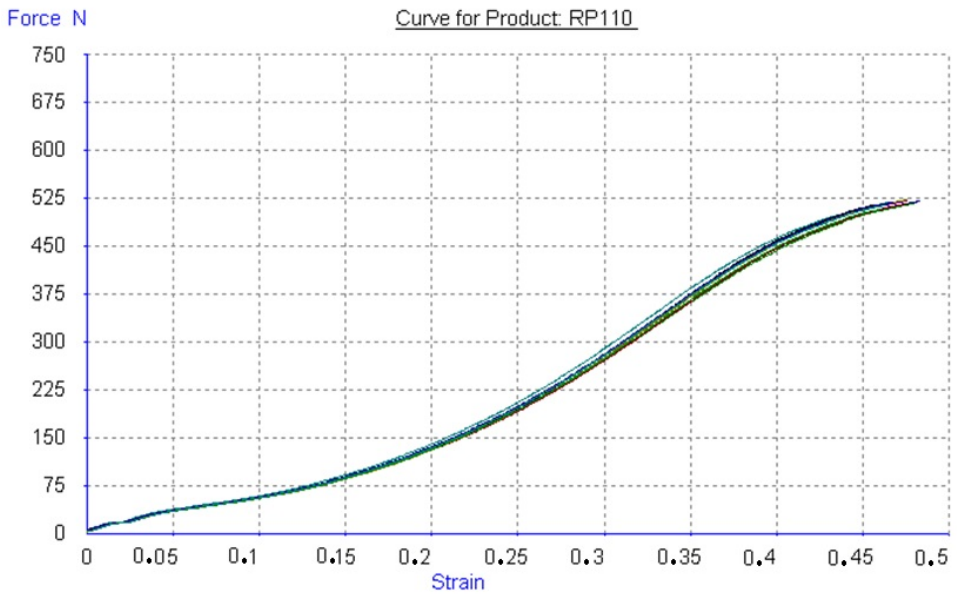

Figure 4.24. Repeatability check of force-displacement data for RP110

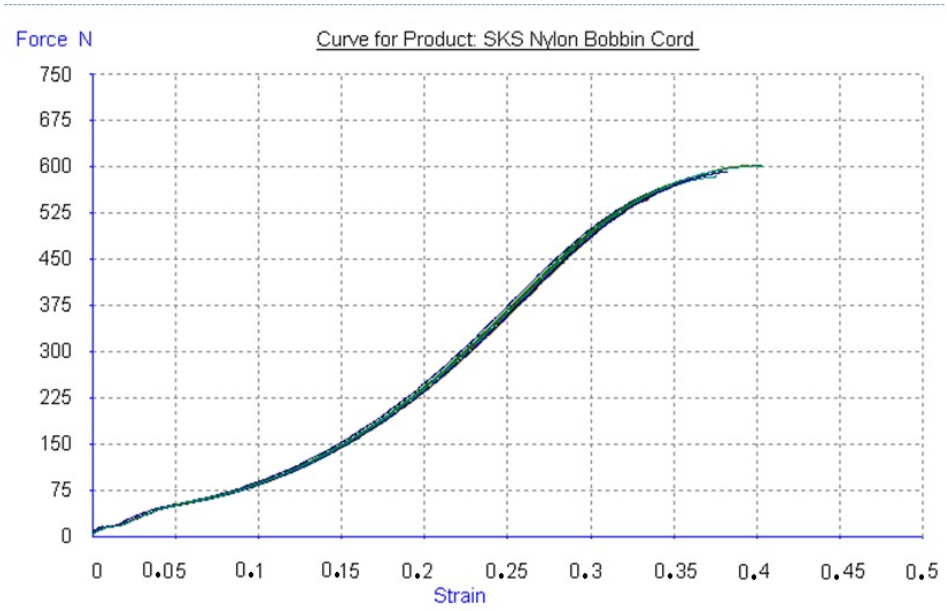

Figure 4.25. Repeatability check of force-displacement data for N947

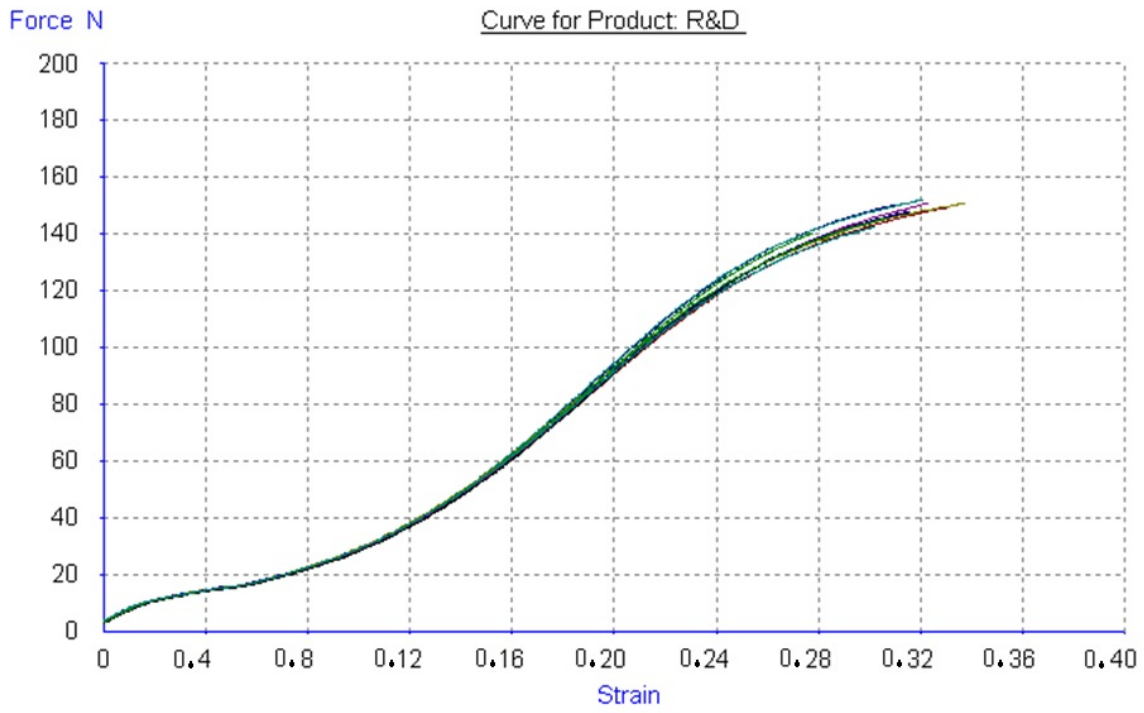

Figure 4.26. Repeatability check of force-displacement data for P1694

4.3.2.2 Bead

The cable bead in the military tyre application is composed of a 6 mm diameter steel cord enveloped by 52 twisted steel cords with 2 mm in diameter. The tensile strength of the 6 mm steel cable is in the range of 640 MPa to 710 MPa at 3.5 to 7 per cent of total elongation (Swanson, 1985) and the yield strength was measured around 625 MPa to 635 MPa, which was obtained from the manufacture (The Tire and Rim Association, 2007). In civil tyre application, the cable bead is constructed of one 5 mm steel cord that is surrounded by 76 steel cords which are sized 2 mm in diameter. The cable bead strength was characterised with the minimum theoretical breaking load of 459.2 kN.

4.3.3 Material model selection

In this section, the accuracy of material hyperelastic models are compared with the experimental data in order to obtain a selection criteria for the preferred model. For this

purpose, eight hyperelastic models were nominated as listed in table 4.4 including their parameters to be characterised.

Table 4.4. Hyperelastic models for accuracy study

Model	**Parameters**
Mooney-Rivlin (first order)	D_1, C_{01}, C_{10}
Polynomial N=2	$D_1, C_{01}, C_{10}, D_2, C_{02}, C_{11}, C_{20}$
Ogden N=3	$\mu_1, \mu_2, \mu_3, \alpha_1, \alpha_2, \alpha_3, D_1, D_2, D_3$
Neo-Hooke	D_1, C_{01}, C_{10}
Yeoh model	$D_1, C_{01}, C_{10}, D_2, C_{02}, C_{11}, D_3, C_{30}, C_{21}, C_{12}, C_{03}$
Arruda-Boyce	$\mu_1, \mu_0, \lambda_M, D$
Van der Waals	μ, λ_M, A, β
Marlow	No parameter needed

Abaqus material evaluation tool was employed to parameterise the models' coefficients and predict the hyperelastic behaviour. A sample comparison of model prediction using the described approaches is illustrated in figures 4.27 and 4.28 for rubber DC001 and cord DF023 of civil aircraft tyre in uniaxial, biaxial, and planar loading conditions respectively. The Arruda-Boyce method for cords is not applicable due to divergence issue in fitting solution. In addition, no test data is available to correlate the biaxial and planar models; however these figures help to track the overall trend of material behaviour to check it is located in a reasonable region.

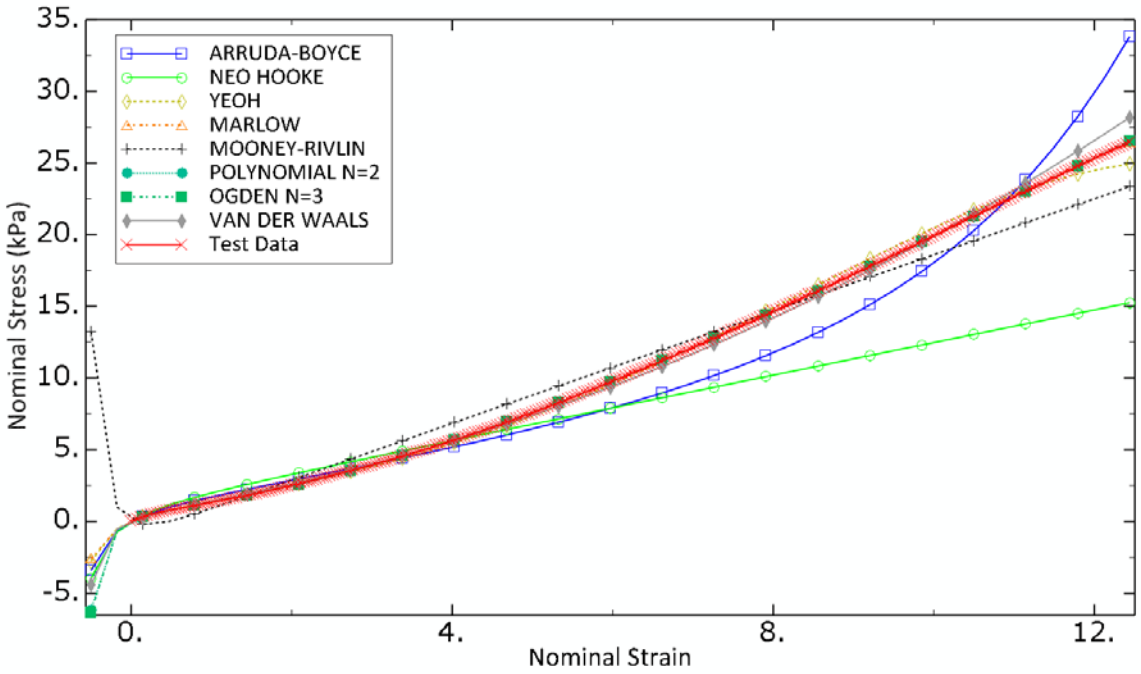

a. Uniaxial results

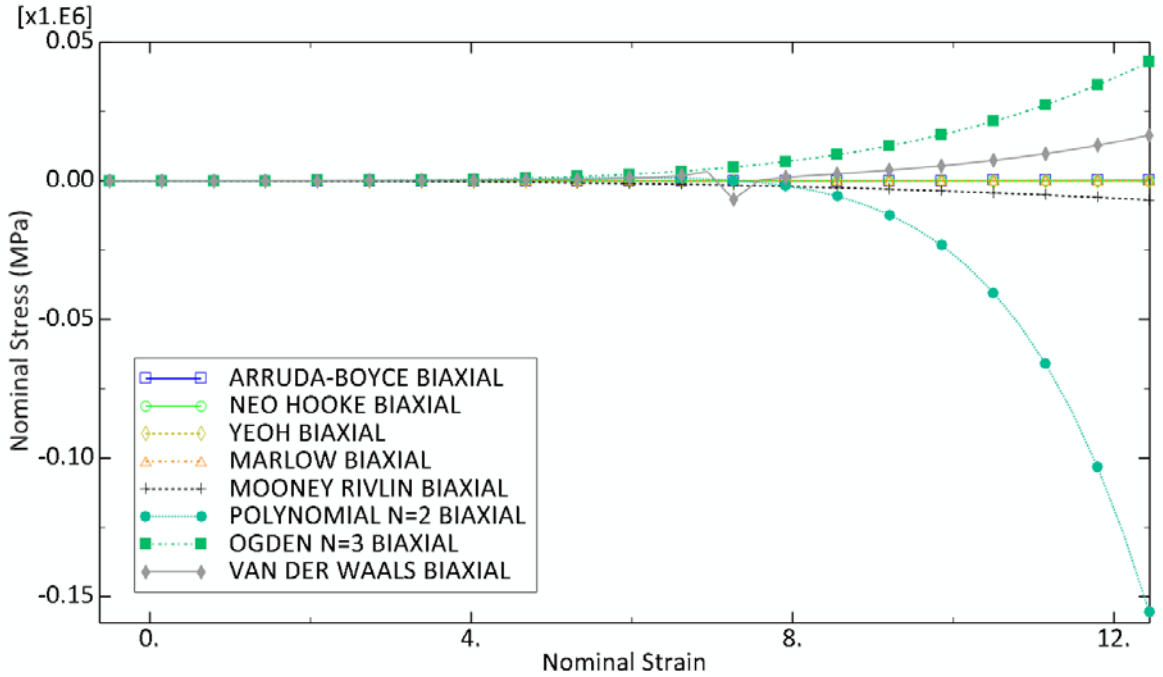

b. Biaxial results

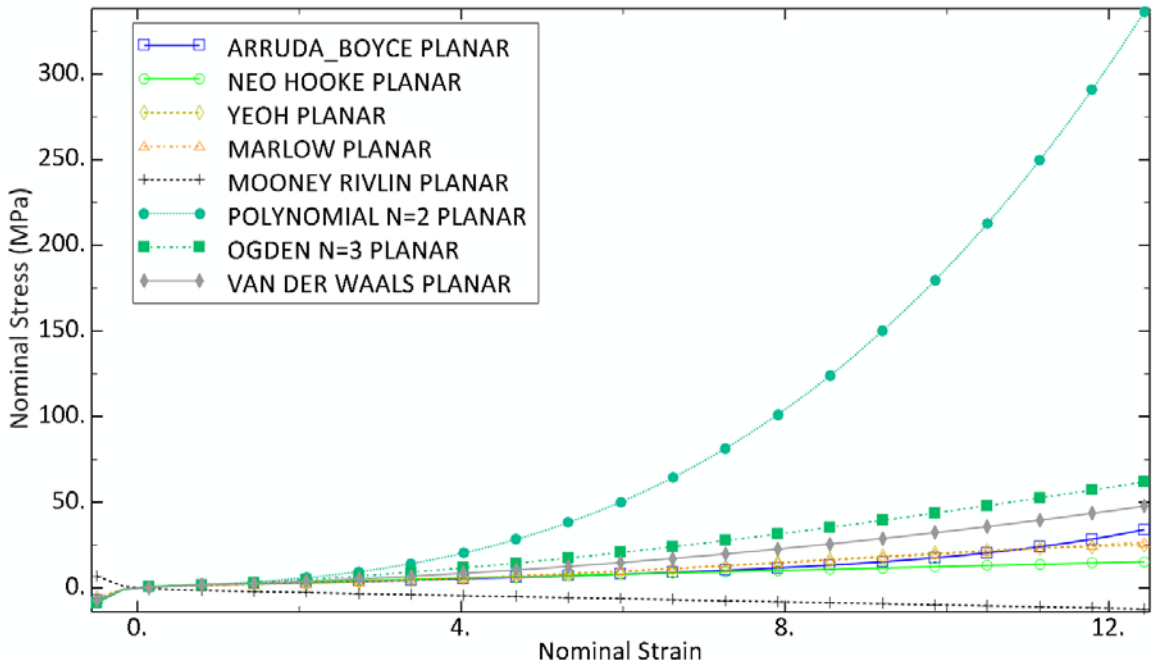

c. Planar results

Figure 4.27. Prediction of hyperelastic behaviour using different methods for rubber DC001

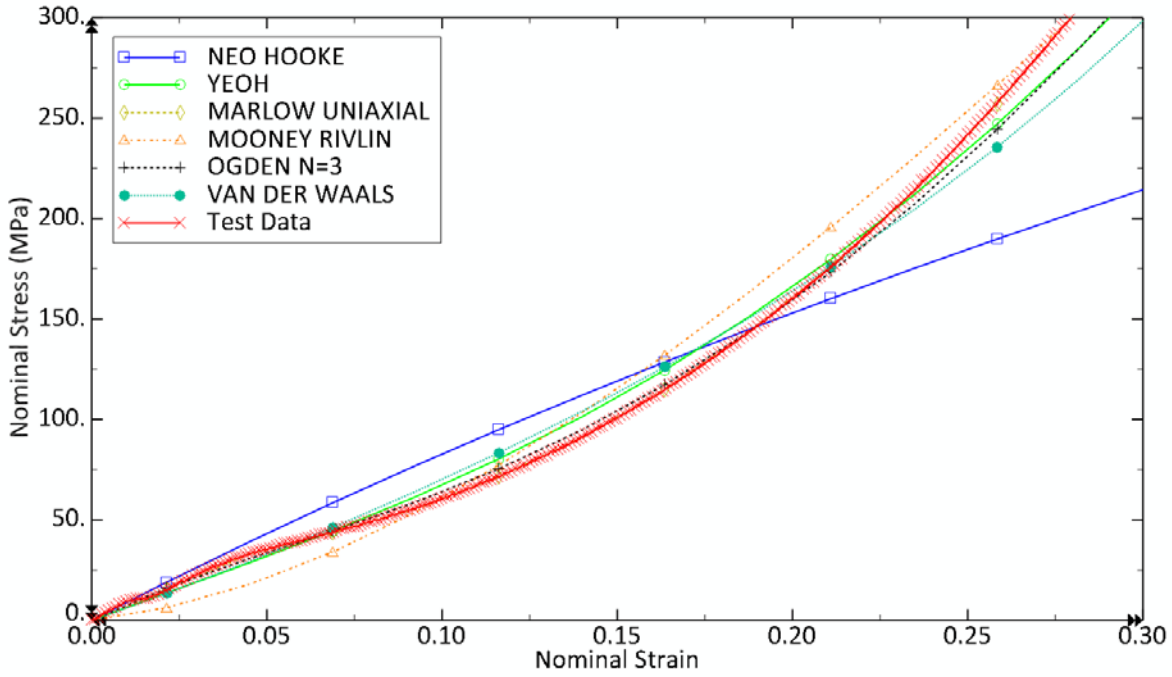

a. Uniaxial results

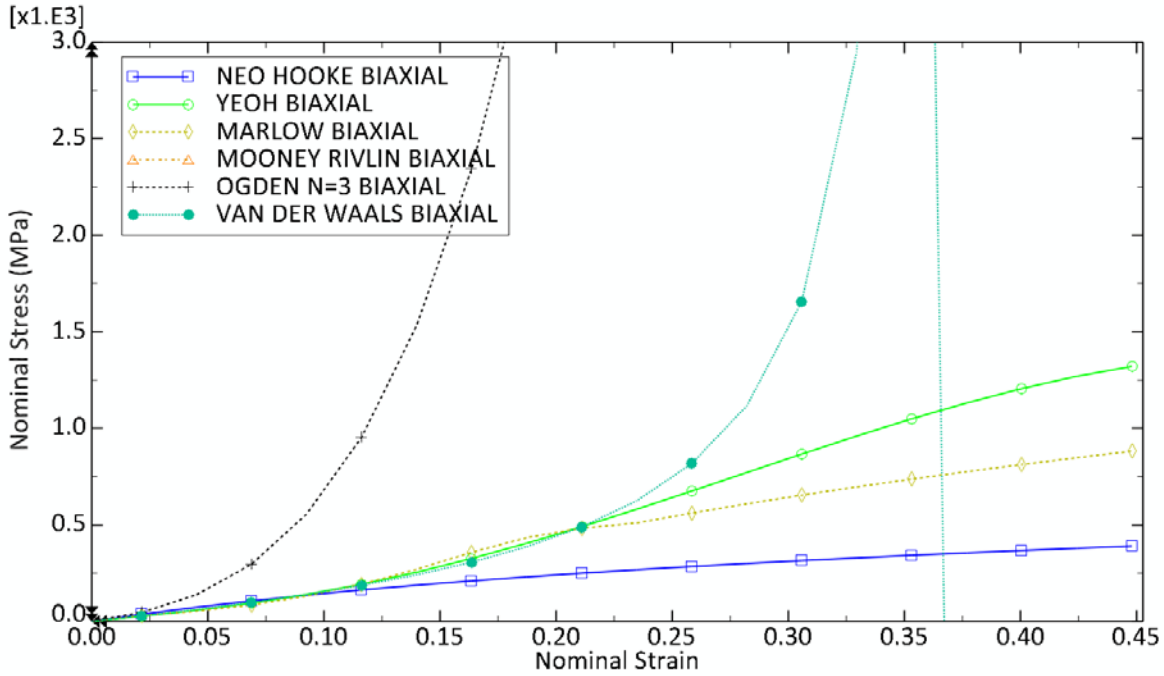

b. Biaxial results

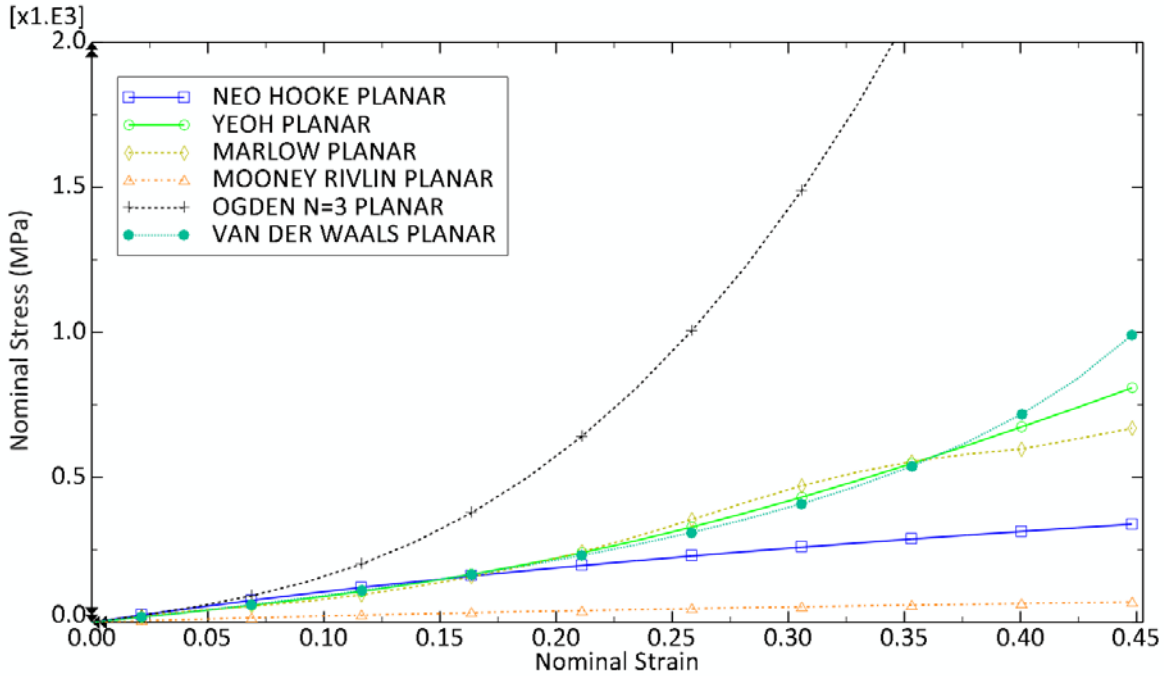

c. Planar results

Figure 4.28. Prediction of hyperelastic behaviour using different methods for cord DF023

Above methods were evaluated for use to model the rubber and reinforcement hyperelastic behaviour and their performances were examined. Yeoh and Marlow models were established as having the highest accuracy in uniaxial, biaxial, and planar deformation

modes among the other models. Since the Marlow method is not generally suggested to be used for the multi-axial loading condition, the Yeoh method is used to represent the hyperelastic behaviour of the rubber and reinforcements (Behroozi, et al., 2012). Further to the offered accuracy, this model offers lower computational cost due to the fewer parameters than the equivalent polynomial models because of model independency on the second invariant. The incompressibility condition is assumed for the rubber model and this leads to further simplification of the Yeoh model when the incompressibility term and consequently parameter D is omitted.

4.3.4 Parameterization of coefficients

The Abaqus solver was used in this research to parameterise the Yeoh coefficients for replication of the hyperelastic behaviour. These parameters were calculated for all rubber and reinforcements and the characterised coefficients of Yeoh models are listed in the table 4.5 according to coefficients from equation 4.25.

4.4. Summary

In this chapter, the importance of material modelling was initially presented. Then, the involved material behaviours in aircraft tyres were investigated and the differences with car tyres were discussed. Available models for elasticity, hyperelasticity, and viscoelasticity were explained. In conclusion, elasticity was chosen for steel beads because of small deformation in bead and hyperelasticity was selected to be employed for rubber and nylon cords due to large deformations specifically in sidewall and carcass plies. In section 3, the instrumentations and characterisation experiments based on standard procedures were described and corresponding test were carried out for modelling. The material properties were next parameterised using the characterisation tests and the most accurate models

with least parameters (Yeoh model) was used to replicate the hyperelastic material behaviour in rubber and nylon cords.

Table 4.5. Yeoh model parameters

Material	**Yeoh model coefficients**								
Military Aircraft tyre	C_{01}	C_{10}	C_{02}	C_{20}	C_{11}	C_{30}	C_{21}	C_{12}	C_{03}
M1436	0	0.449	0	1.2e-2	0	-4.2e-5	0	0	0
M1450	0	0.363	0	5.78e-3	0	-1.95e-5	0	0	0
M4305	0	0.7932	0	2.22e-2	0	-2.21e-4	0	0	0
M4430	0	0.1626	0	6.0e-3	0	-3.32e-5	0	0	0
M4495	0	0.3178	0	5.76e-3	0	-1.8e-5	0	0	0
M4950	0	0.3274	0	3.91e-3	0	-9.47e-6	0	0	0
M8300	0	0.1068	0	5.04e-3	0	-1.58e-5	0	0	0
MK017	0	1.1447	0	0.11	0	-1.83e-3	0	0	0
P1694	0	183.91	0	922.65	0	-1049.7	0	0	0
N947	0	133.60	0	403.83	0	9.054	0	0	0
RP110	0	123.187	0	208.99	0	32.499	0	0	0
Civil Aircraft tyre									
DC001	0	0.3869	0	3.85e-3	0	-8.75e-6	0	0	0
DC003	0	0.8368	0	1.63e-2	0	-1.25e-4	0	0	0
DC004	0	0.1724	0	4.1e-3	0	-1.52e-5	0	0	0
DC005	0	0.338	0	3.88e-3	0	-8.28e-6	0	0	0
DC012	0	0.1131	0	3.44e-3	0	-7.25e-6	0	0	0
DC018	0	0.4749	0	8.57e-6	0	-2.5e-5	0	0	0
DF014	0	134.93	0	614.27	0	-549.77	0	0	0
DF022	0	121.65	0	232.75	0	-10.022	0	0	0
DF023	0	107.73	0	274.39	0	-62.055	0	0	0

Chapter 5: Tyre Finite Element Modelling

5.1. Introduction

In this chapter, the finite element model for simulation of tyre behaviour is developed and its validity is examined against a number of standard verification procedures. First of all, a standard methodology for modelling, simulation, and analysis is explained based on the usage in aircraft tyres. The appropriate approach is explored on the basis of different aspects including the reinforcement-compound modelling in the tyre structure, the type of analysis, contact/friction modelling and type of meshing method. Following the section two, the methodology is implemented in section three through importing the tyre cross-section drawing into the Abaqus/CAE modelling environment, setting up the model geometry and boundary condition, meshing the tyre geometry, and eventually the configuration of solver parameters. Having implemented the FE model, the FE model is run for a number of standard simulations in section four and the results are verified through corresponding standard test procedures from the basic sizing measurement check to the legally mandatory burst test. In addition to validation tests, a number of simulations are carried out to measure the capabilities of the validated tyre behaviour in prediction of the tyre forces and moments as well as the tyre thermal behaviour due to viscoelastic dissipation during free rolling condition. Eventually in section five, the influence of tyre configuration parameters on its performance and general behaviour is investigated.

5.2. Methodology development for FE modelling

In this section, the available tyre geometries are initially presented and the components are introduced. Then, different possible approaches for composite modelling in Abaqus/CAE are discussed and the appropriate model is selected. The mathematical background of the analysis methods comes after and the simulation prerequisites for such analysis are

described. Next, the available mechanism to simulate the contact behaviour is discussed and the available friction model in contact is introduced. The aircraft tyre inflator behaviour is modelled as an ideal gas in sub-section six. As a part of boundary condition setup, the tyre rim and road surface are modelled, and finally, the mesh types and mesh density are investigated to obtain an efficient solution and accurate result.

5.2.1 Tyre geometry

There are different ways of extracting and importing the tyre geometry into the FE packages as one of the first steps in tyre modelling. When the drawing of a tyre cross-section is not accessible, the tyre can be cut in radial direction and a segment of the tyre profile is used to identify the tyre construction and sizing of the cross-section geometry. Moreover, the reinforcement spacing, cross-section area, and orientation through the rubber toppings in belt, tread, and carcass are specified, and rubber and reinforcement samples can be separated from the tyre cross-section in standard or available sizes for further characterisation tasks (Bolarinwa, 2004) (Yang, 2011). In this research, the high-detail CAD drawings from tyre design level are acquired through the collaboration with DATL and used to import into the Abaqus CAD environment.

The cross-section cut of the military tyre is shown in figure 5.1. The cross-section sketches of both military and civil tyres are shown in figures 5.2 and 5.3 with detailed construction components. In these two figures, the tyre components are assigned to the corresponding material properties as discussed in the previous chapter. The tyre components (rubber, reinforcement, and bead) and associated functionalities are presented in table 5.1 for both military and civil tyres with more details. The first point that becomes apparent in the

aircraft tyre is the number of layers in construction in comparison to the car tyres design and the first challenge is acknowledged through modelling such complicated construction.

a. Full geometry view

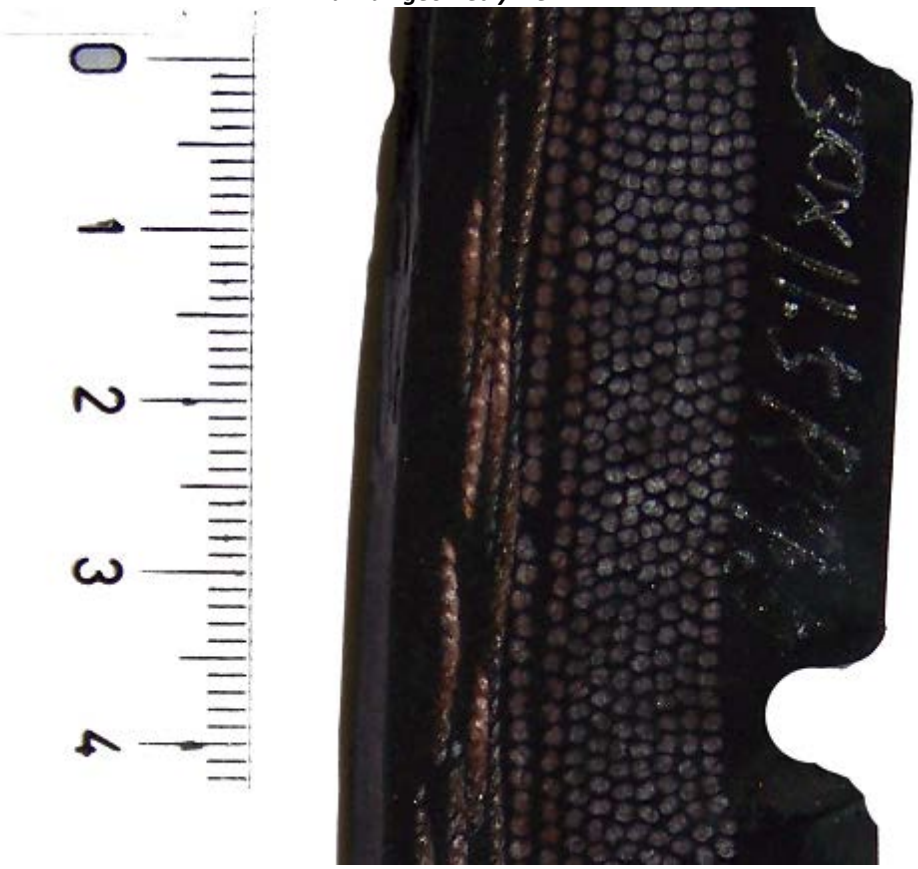

b. Tyre crown details

c. Tyre seating details

Figure 5.1. Military tyre cross-section

Figure 5.1.a shows a full geometry of radial military tyre in that the circumferentially-distributed fabrics appear as the spaced dots in figure 5.1.b. The carcass however is built of radial cords under the belt in figure 5.1.b, woven across the tyre profile, and appears as the extended continuous fabric cords that are twisted around the bead more clearly in figure 5.1.c. Furthermore, the bead is constructed of twisted steel cords although a number of them are missed in tyre segment sample.

Table 5.1. Aircraft tyre rubber and reinforcement specification

Material section	**Description of functionality**
Chafer	• Chafer cushions tyre contact on rim and seals tyre • Protects bead against debeading and rim abrasion • Resists chafing damage to both tyre and rim flange
Tread sheet compound	• Tyre contact point with runway that grips road • Designed to be wear resistant
Apex and Wrapping	• Rubber that fills above the bead located radially core between the plies and the turnup ply • Stiffens bead area for better durability
Inner lining	• Retain the compressed air inside the tyre • Resists the permeation of nitrogen and moisture into the casing.
Sidewall packing	• Protects the carcass against exposure and scratch • Provides softer ride
cushion compound	• Additional protection for belts to improve retreadability
Insulation compound	• Shields casing from tread heat
Sidewall compound	• Protects the casing plies from the weathering effects • Offers resistance to cuts and flexing
Band Belt topping	• Covers the belt
Heal filler reinforcement	• Extra protection for bead
Band Belt Plies	• Framework for whole tyre • Transmits the steering command to contact patch
Cut/Breaker/casing ply	• Casing plies are layers of fabric cord coated with hi-modulus rubber • Hold tread flat for superior traction and wear • Improves adhesion between tread and the casing plies
Bead	• Consist of bundles of high-tensile steel wires • Anchors the tyre to the rim and ensure an airtight seal

In figure 5.2, the military tyre construction material is shown in different colours. Rubber partitions are built of different material regions and each rubber region can be reinforced with fibres. In fact, the reinforced rubbers are toppings that wrap the woven nylon cords. The carcass ply, heel filler, and breaker/breaker-cut are the reinforced rubbery regions that build the main structure of an aircraft tyre. The number of plies toppings in carcass is indicative of the amount of vertical load that an aircraft tyre should withstand. The carcass

is pressurised and determines the inflated shape of deformed sidewall. Generally speaking, the aircraft is suspended on the inflated carcass and provides an air cushion to withstand its weight. The reaction forces and moments in landing gear are also transferred through the carcass to the contact patch. In addition, the breaker and under-tread plies provide dimensional stability and tread stabilisation, thanks to the breaker's stiff foundation for the tread's soft rubbery region. The breaker's stiffness directly influences the generation of the cornering forces and sustains the longitudinal and lateral forces and transfer the moments from contact patch to the landing gears.

The remaining rubber regions are responsible for filling the gaps between plies in the cross-section (apex and sidewall packing), protecting the tyre from external or internal damage to the belt and carcass (inner liner and sidewall rubber), and supporting the tyre either as a seat in tyre-rim interface (chafer) or friction surface and bumper in tyre-road interaction. The rubbery toppings have their role as the separator between the layup to prevent the cords from wearing and a media to transfer and distribute the shear forces along the belt and carcass cords.

Rubber regions are also shown in figure 5.3 for the civil aircraft tyre with similar components, but different number of plies, cord and rubber material, and layup configuration. In both tyres, the tread is not patterned, so that the maximum grip is provided because of bigger effective footprint, and the liquids are also guided towards the grooves in case of snowy or wet runway condition.

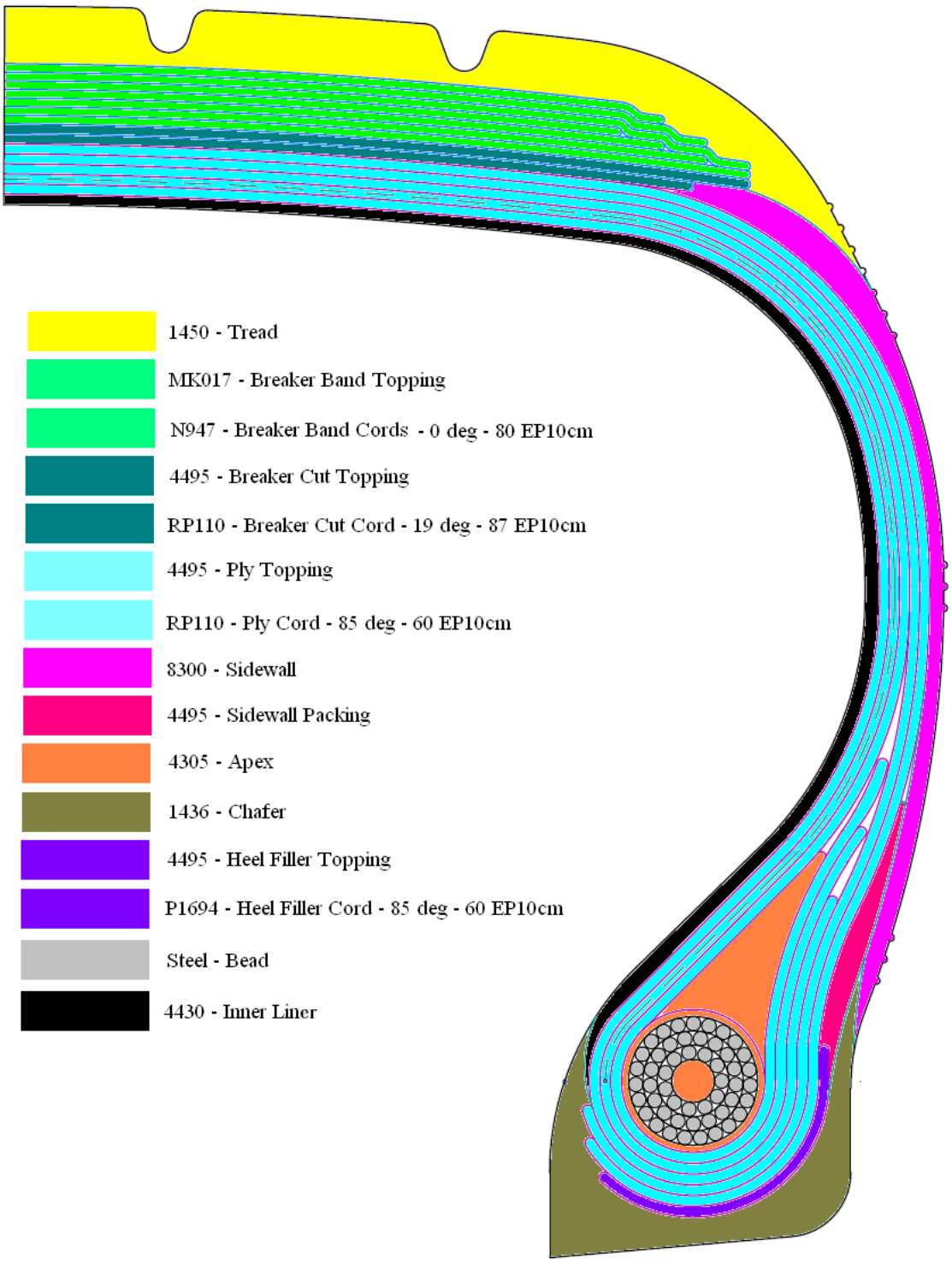

Figure 5.2. Military aircraft tyre cross-section drawing and detailed components (Dunlop, 2013)

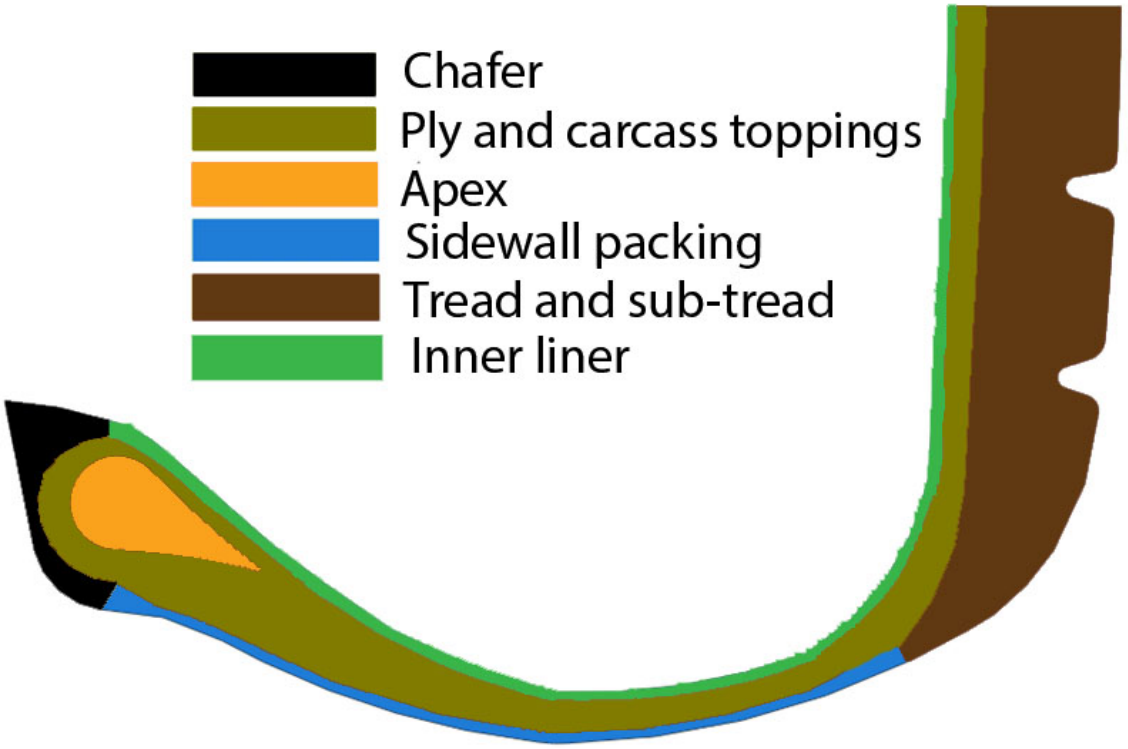

Figure 5.3. Civil aircraft tyre cross-section drawing and detailed components (Dunlop, 2013)

Having imported geometries into Abaqus/CAE, there are two approaches to split the tyre section into rubbery regions: *partitioning* of the section into regions or to *tie* the split regions together in order to build the tyre section. The difference between these approaches is generally related to the dependence or independence of seeding procedure, which is described as the geometrical discretisation of edges and boundaries as an initial step in the FE modelling. In partitioning method, the tyre cross-section is split into regions with common edges while the regions with individual edges are combined to form the tyre full section.

The mesh density in boundaries and interior discretisation is a result of the number of seeds along the edge of the region. In the partitioning approach, seeding dimension along the geometry edges is independent of the region size, but it is predefined for the whole

connected region, while the seeding size can be individually determined for each split rubber area in the tie approach. The latter seems to benefit the flexibility in selection of seeds for geometry discretisation procedure based on the area size and demanded accuracy for a specific analysis, but this causes inconsistency in matching nodes along the boundary of connecting regions; i.e. the nodes are not necessarily overlaid regarding to the refinement level. This requires establishing a separate algorithm to merge the nodes in neighbourhood and can consequently influence the solution performance. On the other hand, the interaction between layers to study the separation based on failure criteria can be deeply studied using the "tie method".

In this research, the "partitioning" approach is used instead of the "tie" approach. This is because of less complication in seeding rubber edges and consequently simpler implementation and meshing, the inconsistency in merging nodes along the common edges in "tie" approach, and stronger integrity elements. Moreover, the deformed common edges can be highly distorted by separation or overlapping using the "tie" concept to connect the rubber region when subjected to the extreme loading, which can be physically meaningless and inefficient.

5.2.2 Reinforcement modelling

5.2.2.1 Rebar element vs. composite layups

Tyre mechanical behaviour as a composite structure can be modelled using two approaches: *Composite Layup* and *Rebar Elements*. A composite layup approach is convenient for modelling a composite structure that is comprised of separable laminates. It is assumed that each single laminate is defined by a material, whose thickness has significant contribution in the section's total thickness. This configuration is used when the model contains several

laminates and each single laminate is composed of several layers. A layer represents a directionally strengthened arrangement of material that is moulded during the composite's manufacturing process. Composite layup approach in Abaqus/CAE is developed to help analysts manage a large number of plies in traditional composites (Simulia, 2013). This modelling approach is convenient for such composite parts which are now commonly used in aircraft body structure.

Rebar elements are used to define layers of uniaxial reinforcement in membrane, shell, and surface elements (such layers are treated as a smeared layer with a constant thickness equal to the area of each reinforcing bar divided by the reinforcing bar spacing) (Simulia, 2013). In this modelling methodology, rebar elements are considered as embedded surfaces with negligible thickness in comparison with their topping thickness in order to increase the strength of the whole layer. The host region often has the role of giving a stable shape to the whole body, whereas the embedded region is mostly constructed of very thin layers. This strategy gives a much closer representation for modelling composite materials such as tyres than the layup approach which is more suited to composites with the same range of thickness in layers. In tyre modelling, reinforcements are actually fabrics (plies) embedded in rubber compounds and are composed of cords which are laid at angles.

5.2.2.2 Rebar elements

As described, a layer of cords arranged in parallel rows and topped in rubber compound composes the so called layups or plies, which is attributed by its direction, spacing between cord, and cord's cross-section area specifications. Plies are commonly woven in various directions to provide appropriate strength to resist directional deflections such as bending and stretching, so that the longitudinal and cornering forces and moments are generated to

react the applied forces and moments from the landing gear to the contact patch. These embedded reinforcements in the rubber region are well known as “rebar elements” in Abaqus/Standard. Rebar elements are represented as zero thickness elements that can be used in conjunction with shell, membrane, and surface sections. In rebar concept, the cord orientation with respect to circumferential direction, spacing, cross-section area, material type, and the number of plies should be specified. Rebar elements in tyres are considered to be embedded in rubbery region to reinforce its host. In definition of rebar elements, it should be noted that the rebar elements are assumed to be unidirectional and individual reinforcing bars in continuum solid. An arbitrary position of the rebar elements inside the host is illustrated in figure 5.4, in which the spacing and orientation angle of rebar elements are depicted.

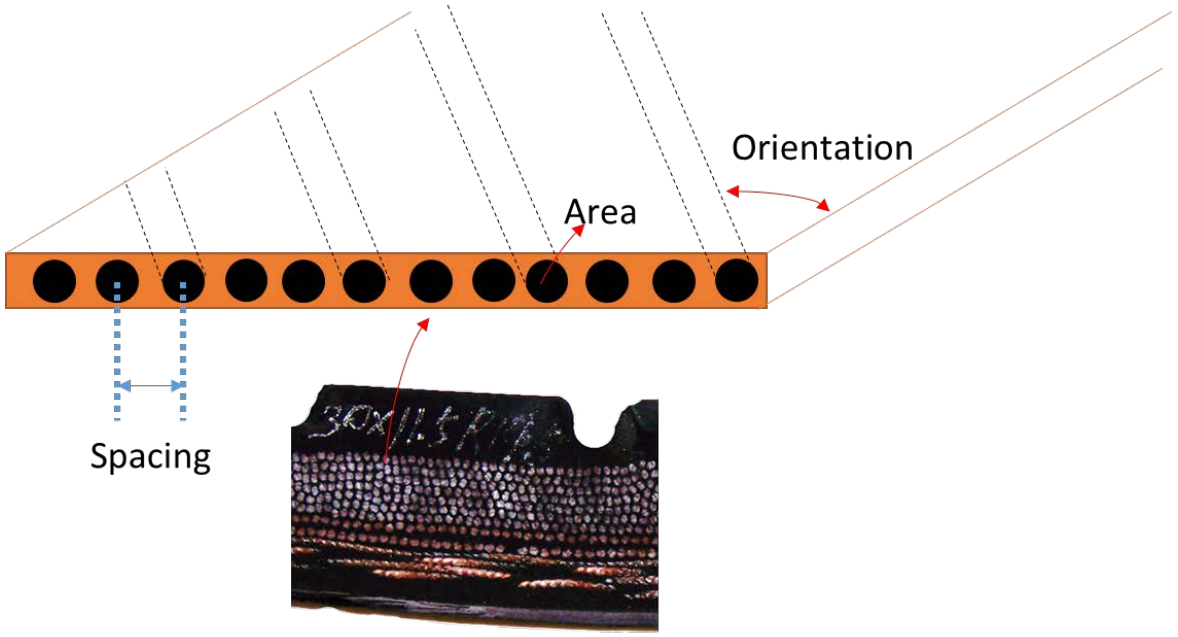

a. Schematic of a rebar layer

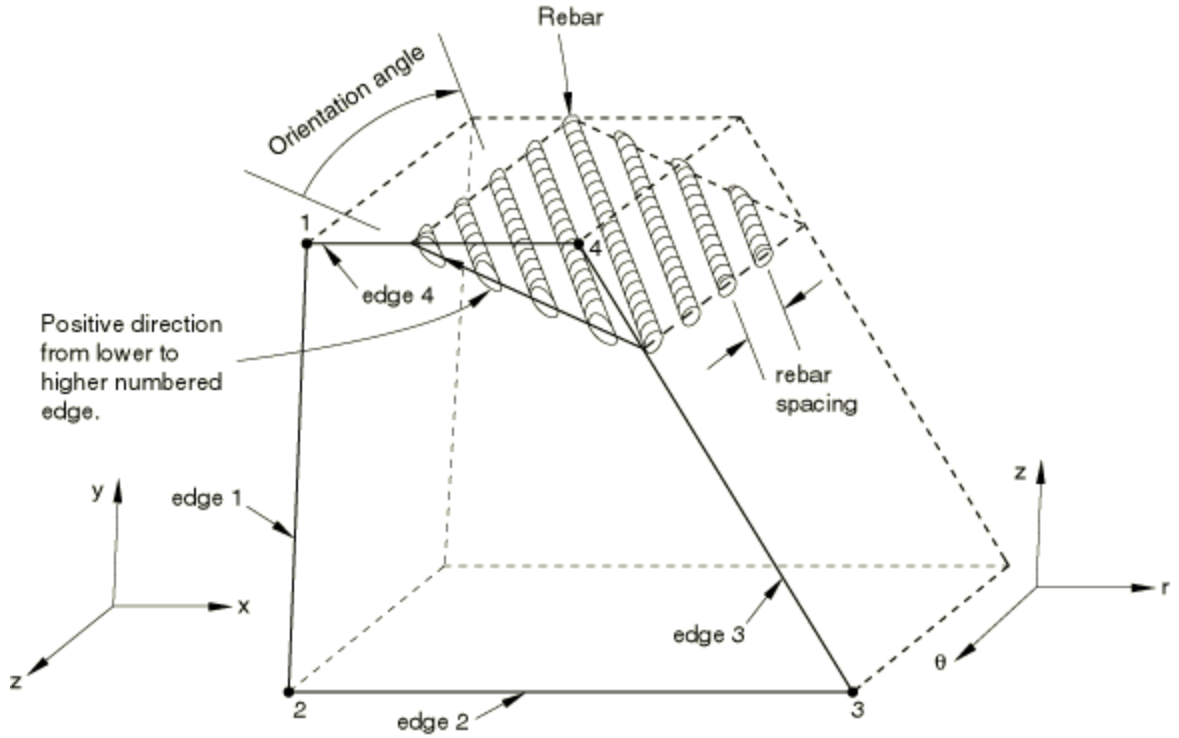

b. Position of rebar elements in a solid element (Simulia, 2013)

Figure 5.4. Rebar elements

The orientation of aligned cords in plies has probably the most important role in shaping the tyre cross-section profile under loading and inflation. Tyre mechanical behaviour can be considerably deviated from the normal design when the configuration of plies is varied even if it is solely cords orientation. In figure 5.5, two shapes of the tyre section with exactly the same material and configuration, but different angles of rebar elements in carcass are shown, which can explain the importance of cords orientations in unloaded inflated tyre to the same pressure. In grey cross-section, radial and circumferential plies are oriented in perpendicular directions 0 and 90 degrees in respect to the normal vector of cross-section, while half of the plies are oriented in 30 degrees and the other half in -30 degrees in respect to the same normal vector.

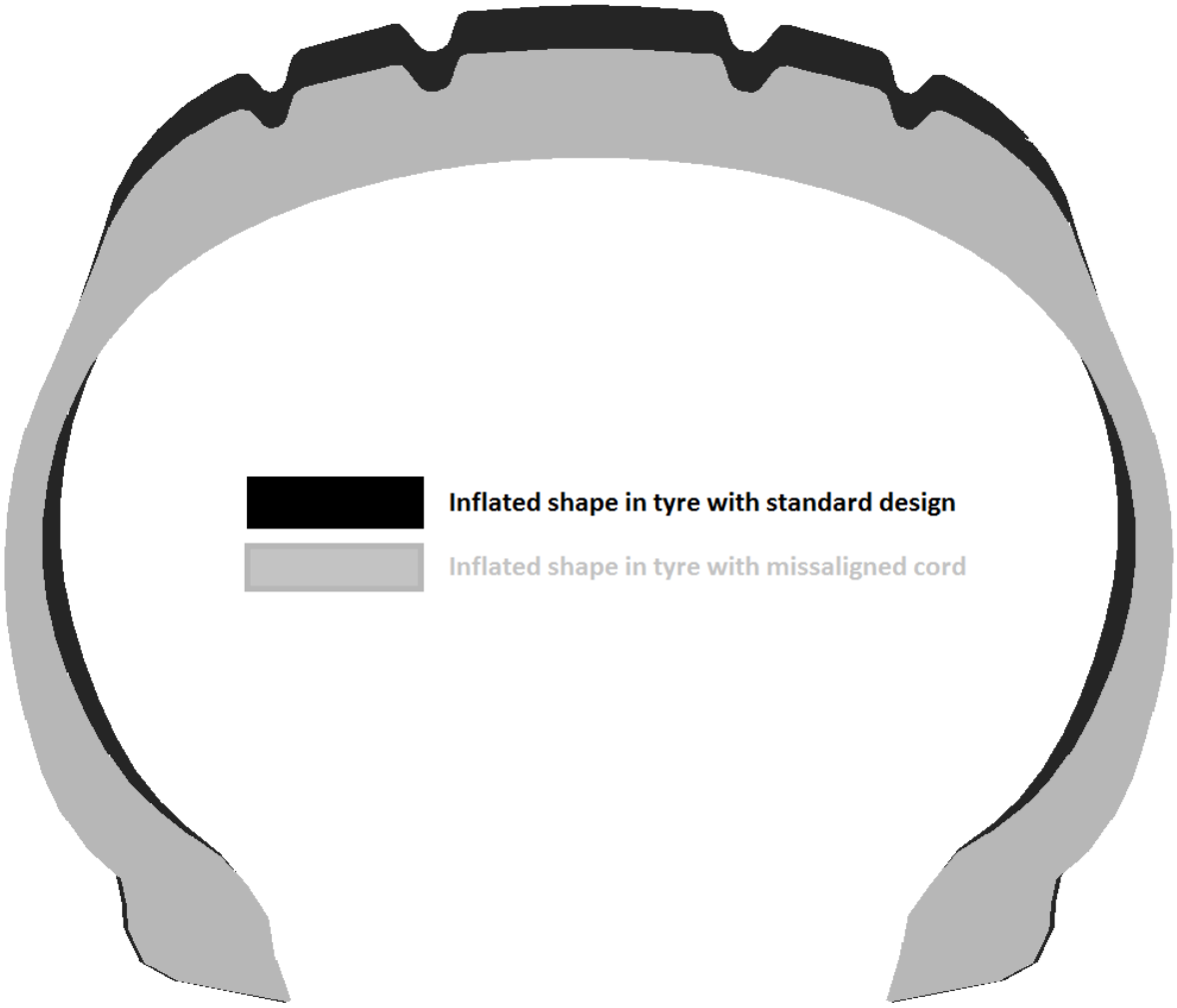

Figure 5.5. A comparison between two tyre configuration in terms of change in cord orientation in carcass construction subjected to 1.3 MPa inflation pressure

In Abaqus, rebar elements are embedded into a host region of material (rubber region) where translational and rotational motions are constrained according to a geometric tolerance. The embedding algorithm searches for the geometric constraints between nodes of the embedded and host regions. In case a node of an embedded element lies within a host element, its degrees of freedom are eliminated and the translation of each node is interpolated based on the corresponding degrees of freedom in the host element (Simulia, 2013).

5.2.3 Analysis type

To simulate the tyre mechanical behaviour, a number of analyses are available that will be presented in the following sections, and appropriate tyre analysis is selected to satisfactorily obtain the desired efficiency and accuracy in tyre mechanical behaviour.

5.2.3.1 Static stress analysis

For such simulation that the tyre behaviour is governed by the low rate of changes in external load and boundary condition, or in other words governed by the nearly equilibrium condition, the static analysis meets the stated requirements with an acceptable accuracy and reduced calculation cost. The “low rate of change” condition is to emphasise on validity of the assumption, in which the inertia effects are neglected. In static stress analysis, the material property and stiffness matrix are assumed to be time independent, so that the matrix remains constant during the analysis. This does not mean the nonlinear effects are not included, but nonlinearity in geometry, contact mechanism, and material property are still applicable as long as the physical stability is satisfied. As a result, the creep, swelling, and viscoelasticity cannot be modelled by the static stress analysis, but the rate-dependent nonlinear properties such as the hyperelasticity for large deformation can be modelled during a static stress analysis. This step is appropriate for one-time instantaneous deformation to check the sizing of tyre profile after applied static inflation and vertical load.

5.2.3.2 Steady state dynamics

The steady state dynamics is a specialised analysis that ignores the transient effects in tyre simulation, and generally is used to study the steady-state behaviour of deformable cylinders rolling along a rigid surface (Simulia, 2013). Having transient and inertia effects removed from the analysis, the rolling simulation in traditional steady-state approach is

extremely expensive due to the partial differential equations of rolling tyre that should be added to the set of algebraic deformation equations for each element. Furthermore, the mesh should be refined to achieve an acceptable accuracy because the tyre has contact with the flat road along its circumference and the coarse mesh can misshape the circular pattern into a poor polygonal cylinder and causes the geometrical inconsistency in the contact problem.

The alternative approach is to define a separate reference frame attached to the axis of rotation that travels at the aircraft ground velocity, but does not rotate with the tyre. The one on this reference frame observes stationary finite element mesh, so that only the area of the tyre near to contact zone is required to be finely meshed. The refined meshing around the area of contact can substantially reduce the problem size. On the other hand, the kinematics of the moving contact patch is solved in an Eulerian manner; i.e. the mesh is stationary and the motion is handled by the material flow through the elements, while the elements deformation is still described using the ordinary Lagrangian method to describe the material deformation. The inertia forces and frictional effects are modelled in conjunction with the rate-dependent and rate-independent material property. This analysis offers an adequate match for prediction of the generated forces and moments (F&M) across the contact patch in cornering or driving/braking conditions.

The accuracy in the prediction of F&M using this method is directly associated with the quality of the friction models. The major shortcoming of using the FE method is the analysis insensitivity to the generated forces and moments in contact patch that can deform the tread area as well as the carcass package. This analysis step also ignores the effects of

material stiffening in belt and profile change due to the centrifugal forces, which becomes considerable at high rolling speeds.

5.2.3.3 Transient implicit and explicit

This analysis type chiefly considers the transient behaviour of the aircraft tyre in which the final solution to such dynamic problems is a combination of both transient and steady-state parts. A straight meaning of using this analysis is to incorporate the inertia force and its effects into the equilibrium equations. In this analysis, the rate-dependent, time-dependent, and nonlinear material behaviour as well as the nonlinear geometry are considered in the final solution and extraction of tyre kinematics and forces. Although the transient dynamic analysis seems to be a comprehensive approach to solve dynamic problems, the demanded simulation time for such analysis is a seriously challenging issue. The dynamic transient procedure can be compromised if the equilibrium condition in each time increment is not checked. Based on this fact, there are two methods to offer a solution for a transient dynamic problem: the implicit and explicit approaches.

In most FE simulation, the analysis is broken into progressive steps of load application due to the nonlinear nature of tyre geometry like contact problem and the material nonlinearity such as hyperelasticity. At the end of each step, the tyre structure is subjected to deformation due to the increasing load and the stiffness matrix should be refreshed for the spatial state, and then, fed into the successive analysis step to calculate deformation due to the developed load. This procedure is common for most analysis types that consider geometrical and material nonlinearity in the simulation. The explicit and implicit approaches were developed to support the second part of the procedure, which are to consider the criteria for equilibrium between the internal forces and external loads.

A deviation in prediction of deformation is initiated because of the incremental iteration approach to solve the dynamic FE problem. In implicit approach, the dynamic equilibrium situation is evaluated by comparing the resultant external loads and the internal forces. Then, the comprehensive dynamic equilibrium is enforced within the structure by amending the internal forces in elements through the iterative Newton-Raphson approach. In other words, the implicit approach solves the equation in time $t + \Delta t$ based on itself and the solution found at time t, and as a result, the solution is unconditionally stable and allows for larger time increments. Once the equilibrium condition is satisfied, the new stiffness matrix is formed based on the increased externally applied load, and the solution is continued until the load reaches its eventual magnitude. In explicit approach, however, the abovementioned procedure is ignored and the dynamic equilibrium is not checked, and consequently, the equilibrium is not necessarily satisfied unlike the implicit approach. Final result in explicit approach can deviate excessively from the exact solution. The number of increments should be adequately increased to ensure that the solution does not tend to drift from the correct solution.

Having noted the disadvantages of explicit, it should be noted that this method is computationally efficient by circumventing the time-consuming Newton-Raphson iterations to find the equilibrium point although the convergence of the solution is not mathematically guaranteed. For static equilibrium analyses where the computational efficiency is not an issue, the implicit approach through the *Dynamic Implicit Simulation Step* in Abaqus/Standard module can bring accuracy to the solution while the convergence is guaranteed due to the correction applied until the equilibrium conditions are met. In dynamic problems where the inertia effects are added, the calculation cost can be

excessively increased by the need for an additional equilibrium check and iterative correction procedure which can extremely influence the simulation time in implicit approach. The explicit approach effectively reduces the runtime and more load increments are demanded to obtain better equilibrium since this approach is conditionally stable during the solution.

In this research, the tyre behaviour under static loading is simulated with the implicit analysis to take advantage of its accuracy for such computationally efficient simulation. For simulation of dynamic behaviour which demands computational resources, the explicit approach offers a compromised approach to increase efficiency in solution while its accuracy is directly dependent on the time increment sizes.

5.2.3.4 Coupled thermal and displacement analysis

This analysis is required when the mechanical and thermal physics significantly affect each other's behaviour, and as a result, the solution of thermal and mechanical equations should be obtained simultaneously rather than sequentially. This analysis in Abaqus, although ignores inertia effects in implicit analysis due to their large contribution to additional calculation cost, is capable of simulating the transient as well as steady-state behaviours and modelling time/temperature material properties. In explicit analysis, where the simulation time can be saved due to shortened procedure in correction of internal loads for equilibrium, the inertia effect is added into simulation for a better representation of those phenomena engaged in the dynamic behaviour of the tyre structure in high rolling speed conditions. The general matrix representation of thermo-mechanical equation set is provided in the following:

$$\begin{bmatrix} K_{uu} & K_{u\theta} \\ K_{\theta u} & K_{\theta\theta} \end{bmatrix} \begin{Bmatrix} \Delta u \\ \Delta\theta \end{Bmatrix} = \begin{Bmatrix} R_u \\ R_\theta \end{Bmatrix} \qquad \text{Equation 5.1}$$

where the K expresses the mechanical stiffness and thermal coefficients or combination of both, and u and θ are to represent the displacement and temperature variables. The R values stand for the boundary conditions and external loads or heat flux through the structure.

Thermo-mechanical problems can be implemented either fully or approximately. In exact solution, equation 5.1 is solved in analytically using available Gaussian elimination approaches. However, this implementation can be extremely expensive for the processor and it is highly recommended in case of a strong interaction between the mechanical and thermal behaviour. The thermo-mechanical implementation can be concisely expressed through the following sparse matrix in equation 5.2 when the thermal dependency of displacement and mechanical behaviour due to thermal effects are poorly associated. The solution of this matrix still solves the thermal and mechanical behaviours concurrently.

$$\begin{bmatrix} K_{uu} & 0 \\ 0 & K_{\theta\theta} \end{bmatrix} \begin{Bmatrix} \Delta u \\ \Delta\theta \end{Bmatrix} = \begin{Bmatrix} R_u \\ R_\theta \end{Bmatrix} \qquad \text{Equation 5.2}$$

According to Abaqus documentation (Simulia, 2013), the solver time can be reduced by a factor of two through this implementation in comparison to full implementation. On the other hand, the convergence rate in the modified form generally needs more iteration to obtain the equilibrium through solution using the Newton-Raphson method.

5.2.4 Contact modelling

The contact mechanism is generally defined between two opposing surfaces to prevent penetration of elements of one surface by another one. To be more specific, the contact

mechanism is usually conducted through three approaches: the traditional node-to-surface penetration, general contact method (edge-to-surface), and surface contact method (surface-to-surface).

In node-to-surface method, the slave nodes are prevented from penetrating into the master surface by making geometrical constraints between nodes of slave solid and element surfaces on master solid, as shown in figure 5.6. However, no restriction is determined for penetration of the master nodes into the slave surfaces.

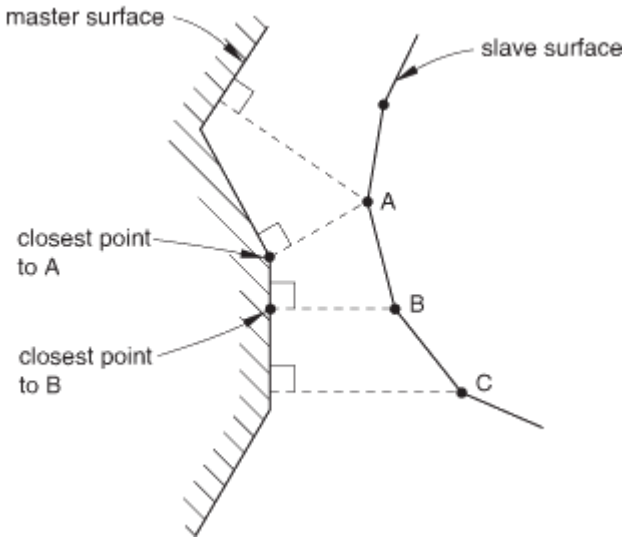

Figure 5.6. Node-to-surface contact interaction (Simulia, 2013)

In general contact method, the deformable/rigid surfaces, generated from the outer element surfaces, resist penetration of *feature edges* into the smooth part of opposing surface. The "feature edges" are construction edges that are used in meshing solids and determine the primary mesh boundary. The feature edges are defined as edges of solid surfaces, of which normal angle differs with respect to the neighbour edges at least as large as the specified *feature angle* (figure 5.7). This analysis is efficient due to the size of the added contact problem and more effective when there is an oblique angle between the

normal of facets in opposing surface with respect to the normal of the probable contact surfaces that are attached to the feature edges.

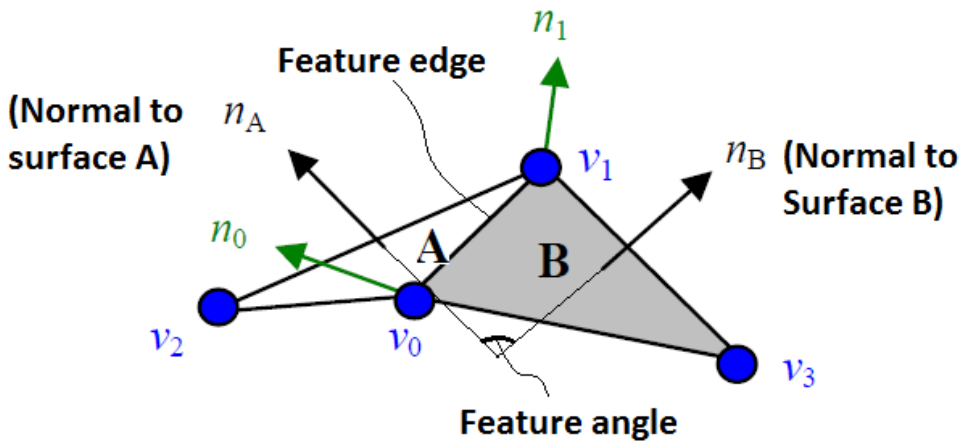

Figure 5.7. A demonstration of feature edge between to surfaces with feature angle (McGuire & Hughes, 2004)

The shape of both slave and master surfaces is considered in the surface-to-surface approach. In this method, the contact condition is enforced between a group of adjacent nodes in slave and master surfaces and provides a better enveloping and more accurate contact interaction.

The edge-to-surface method does not provide the best solution for the contact mechanism in tyre-terrain interaction since the normal of two surfaces are parallel to each other. In addition, the node-to-surface method may cause localised penetration of master nodes into the slave surfaces, and as a result, stress concentration can be generated. The surface-to-surface benefits of an averaging sense in contact interaction between opposing surfaces due to having more nodes involved in contact and offers a better accuracy in prediction of contact pressure and penetration mechanism. Therefore, the surface-to-surface approach was selected to be employed as the contact model in this thesis (Konyukhov & Schweizerhof, 2013).

5.2.5 Friction modelling

Friction mechanism between the road and tyre contact patch is the key parameter in prediction of the forces and moments produced along the contact area. Since an independent test for characterisation of the road and rubber surfaces was out of the scope of this research, predefined magnitudes of friction coefficient are considered for simulation of aircraft tyres. On the other hand, the coefficient of friction can significantly vary for different surfaces from polished ice to dry concrete. Moreover, the coefficient of friction is a function of sliding velocity, contact pressure and temperature. Therefore, the reference friction coefficient equals to 1 can be assumed for the modelling and simulation of tyre on interacting road surfaces, and the generated forces and moments can be scaled for different friction values based on sliding velocities and surface pressure on each contact elements.

The friction behaviour can be also modelled either linearly or nonlinearly. In the linear approach, the Coulomb model is used to describe the linear relation of induced forces along the elements with respect to normal load on the patch as follows:

$$F_{\mu} = \mu F_{z} \qquad \text{Equation 5.3}$$

where F_z and F_{μ} are the normal and friction forces and μ represents the coefficient of friction, which can be pressure, slip rate, and average surface temperature dependent. The force terms are usually addressed as shear stress τ at element level. Similar to friction force formulation, the shear stress is expressed as a linear relation of pressure and coefficient of friction in equation 5.4.

$$\tau_{\mu} = \mu p \qquad \text{Equation 5.4}$$

where p is the average pressure across the element contact surface, and τ_μ is the resultant of the shear stresses across the element surface, as depicted in equation 5.5.

$$\tau_\mu = \sqrt{{\tau_{\mu x}}^2 + {\tau_{\mu y}}^2} \qquad \text{Equation 5.5}$$

where $\tau_{\mu x}$ and $\tau_{\mu y}$ are the shear stress components along the x and y coordinates on the element surface coordinate system. The maximum achievable shear stress is obtained by taking the minimum shear stress from the following equation:

$$\tau_\mu = \min(\mu p, \tau_{max}) \qquad \text{Equation 5.6}$$

where the τ_{max} is the maximum allowable shear stress on the element surface, which is calculated based on the occasion where the relative motion is built up and the shear stress is saturated. Practically, τ_{max} is treated as a predefined parameter.

5.2.6 Inflator modelling

The inflator gas inside the tyre is typically modelled as a constant pressure applied throughout the inner wall. This assumption is due to negligible change in tyre volume under loading condition for most regular manoeuvres. Nevertheless, the constant pressure is not a valid assumption for application in aircraft tyres owing to the fact that the tyre pressure can change by 20% to 30% (figure 5.8) under the rated vertical load. Furthermore, the inflator temperature increases while aircraft is taxiing to the runway/terminal because of rolling resistance moments and tyre-road frictional heat that intensify temperature build-up across the tyre compounds. The temperature increase can change the pressure and air cavity volume and indirectly affects the tyre mechanical behaviour.

In figure 5.8 plotted based on the data from DATL, it is shown that by changing vertical load on the civil aircraft tyre from zero to maximum allowable 350 kN, the inflation pressure is

considerably increased by nearly 20% in comparison to the rated magnitude at unloaded condition. This significant increase in inflation pressure affects the tyre cross-sectional profile, footprint, and vertical stiffness. Therefore, inflator is modelled to avoid deviation in prediction of the tyre size after inflation/loading and footprint area and pressure.

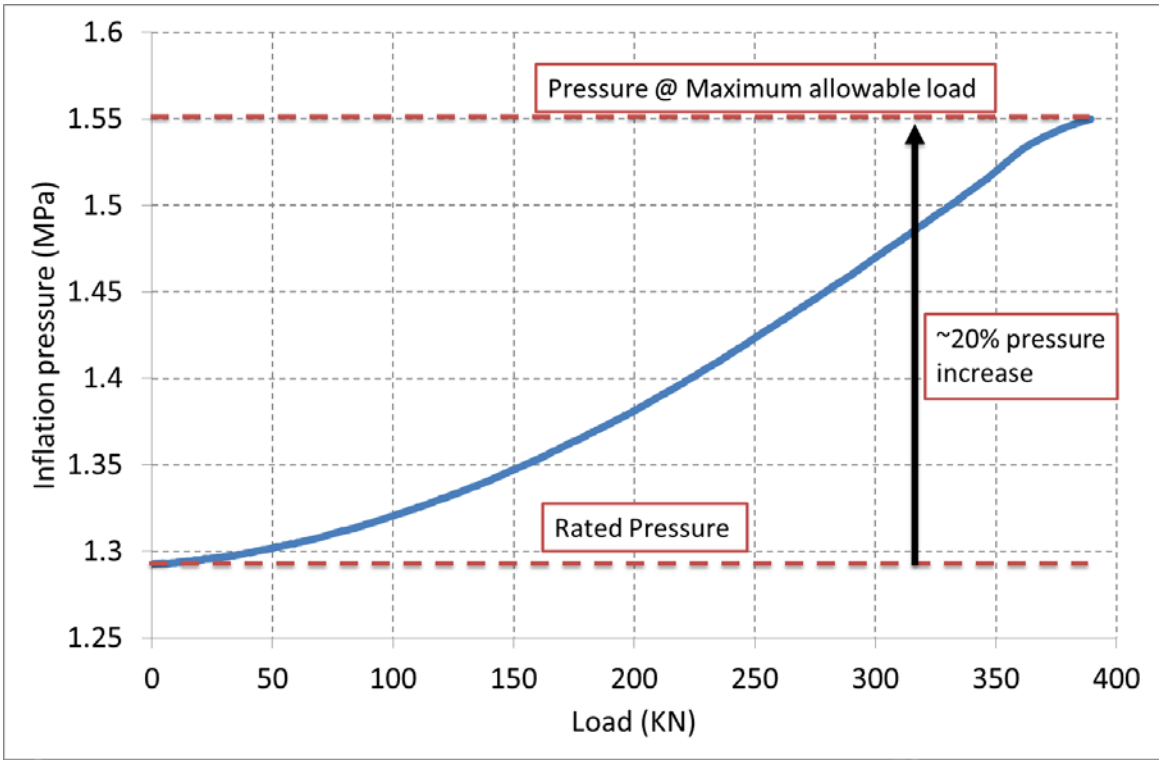

Figure 5.8. The inflation pressure change in civil aircraft tyre due to applied vertical load

There are a number of assumptions that should be made prior to implementing the inflator gas equations in the model. The air inside the tyre can be modelled as an ideal gas since the air still operates in normal condition. Moreover, the intermolecular forces and molecular sizes are negligible and the molecular interactions can be neglected. It is also assumed that an insignificant amount of heavy gases such as water vapour is mixed with the inflator gas. In addition, an isothermal process assumption will be valid in a static test procedure. Finally, it is assumed that the pressure gradient inside the fluid tends to zero.

The following equation can be extracted from an isothermal process based on the assumption made in the last paragraph (Simulia, 2013):

$$p = -K\left(\frac{V(p,\theta)-V_0(\theta)}{V_0(\theta_I)}\right) = -K\rho_R\left(\rho^{-1}(p,\theta) - {\rho_0}^{-1}(\theta)\right) \qquad \text{Equation 5.7}$$

where:

- K: Fluid bulk modulus
- p: Fluid pressure
- θ: Current temperature
- θ_I: Initial temperature
- $V(p,\theta)$: Current fluid volume
- $V_0(\theta)$: Fluid volume at zero pressure and current temperature
- $V_0(\theta_I)$: Fluid volume at zero pressure and initial temperature
- $\rho(p,\theta)$: current fluid density
- $\rho_0(\theta)$: density at zero pressure and current temperature
- ρ_R: Reference fluid density

5.2.7 Rim and road modelling

The rim in an aircraft tyre is built of a strong material to sustain the heavy loads during take-off and landing. The rim is built from high strength still and is much stiffer in deformation in comparison to the tyre compound so that rigidity is a good assumption to consider for its behaviour. A drawing of the military aircraft rim is illustrated in figure 5.9. The road can be treated in a similar way since the runway is usually made of tough concrete and reinforced foundations.

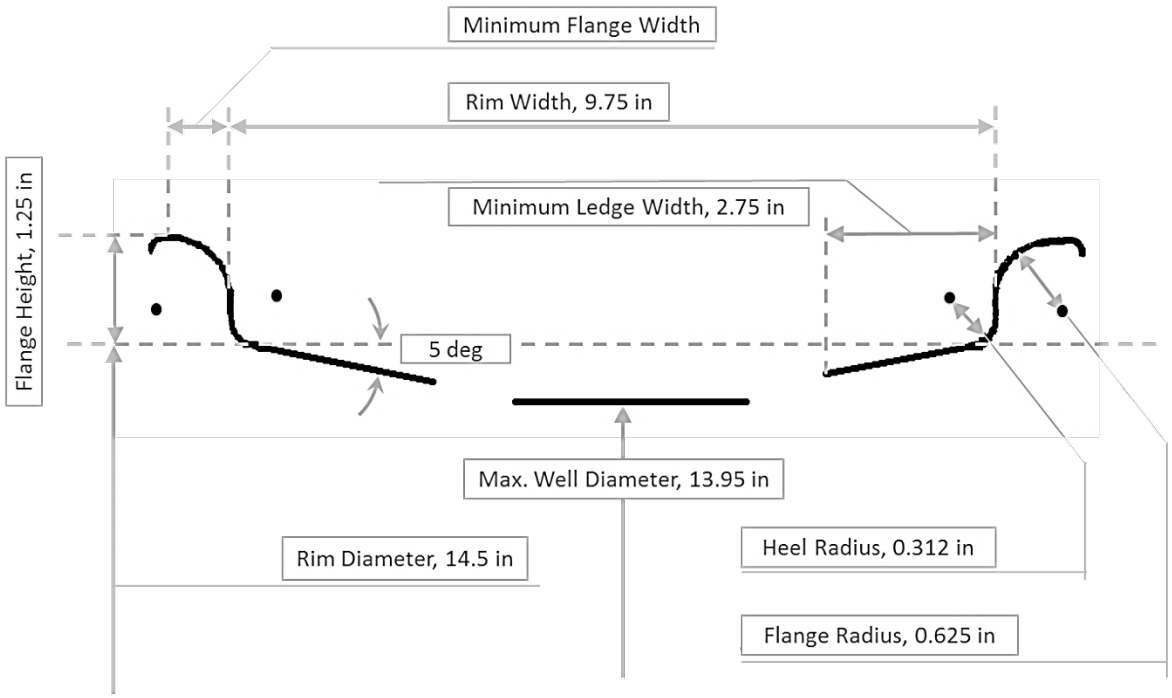

Figure 5.9. Rim design of the military aircraft tyre (Dunlop, 2013)

5.2.8 Meshing techniques

The available elements and meshing approaches are categorised in terms of their shape, application, efficiency, and accuracy. Generally, tetrahedral and hexagonal volume element shapes can be used to discretise the rubber tyre geometry, as shown in figure 5.10. Tetrahedron is a 4-node pyramid-like element that offers robust solution to a wide range of mechanical stress problems (Khennane, 2013). In the simplest form of this element, interpolation of displacements is conducted linearly, and consequently, stress and strain are constant in each element. The problem with tetrahedral elements is that it requires more refinement for the area where the stress gradient is noticeable, so that the problem size is increased to obtain a better accuracy. On the other hand, this element shape is not suggested in application for inelastic and nearly incompressible materials due to severe locking issues in nonlinear problems (Puso, 2006). Overall, meshing routines provide more robust meshing for triangular element since fewer nodes are associated with the

construction of tetrahedral elements. Hence, tetrahedral elements provide a better mesh for bodies with complex geometry while localised refinement is strongly advised to obtain acceptable precision.

The hexahedral element, although difficult to use for meshing due to higher 8-node flexibility, provides good accuracy for many elastomer-related problems with reasonable refinement (Benzley, et al., 1995). This element is traditionally integrated with the "Hybrid formulation" to reduce the instabilities in solution due to hourglass effects and volumetric locking in nearly incompressible material (Simulia, 2013). The "Hybrid formulation" can be employed in problems with incompressible material when an element is subjected to hydrostatic pressure and the volume is not changed in response to the applied load. As a result, the stress that is calculated based on displacement history is not obtained for that element. This formulation can improve the solution convergence in incompressible material by calculating the stress using alternative approach when volumetric locking occurs in an element. Furthermore, 8-node hexahedral element sides can be shaped into at least a 12-node element, which is called cylindrical hexahedral element (figure 5.11), and provide a better approximation of local stress in round edges. In general, the cylindrical hexahedral elements with "Hybrid formulation" offers the best performance in terms of the problem size and accuracy and is employed in this research to address the extreme nonlinearity of the tyre nature in both geometry and rubber material property.

a. Tetrahedron Element ***b. Hexahedron Element***

Figure 5.10. Tetrahedron and Hexahedron element shapes (Simulia, 2013)

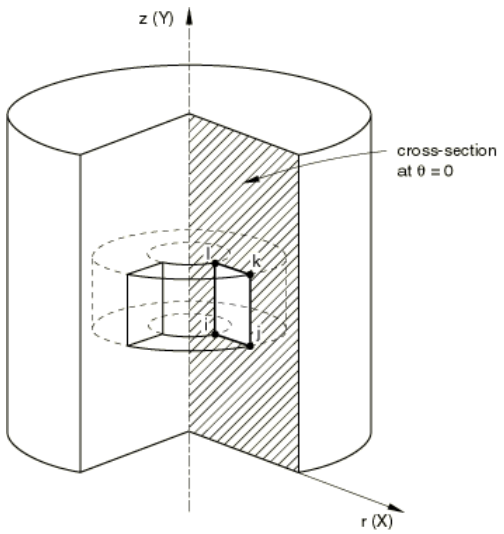

Figure 5.11. Cylindrical element (Simulia, 2013)

The rebar element, as explained in the reinforcement modelling section, is used to model the cord behaviour and has zero thickness elements when it is represented with surface elements which are embedded inside the rubber. Rubber topping performs the host role in rubber-reinforcement interaction model.

Beads are modelled using the hexahedron cylindrical elements with reduced integration. The reduced integration method reduces the number of integration points per element (usually around 3.5 times less), so that the generated stiffness matrix has less rows and columns and the simulation is carried out at less cost.

Finally, the whole tyre cavity, filled with inflator gas, is not meshed, but its constructing boundary should be defined using the *surface-based* or *element-based* approaches. In surface-based approach, the outside edges of inner liner elements are used to build a closed loop surface and the inflator gas is defined inside this cavity. In the alternative approach, the similar edges of inner liner are utilised to create *cavity elements* while their normal vectors

are pointing toward the inside of the cavity. The successive *cavity elements* should be formed in a closed loop similar to the surface elements in order to encircle the air inside cavity. The element-based approach is more suitable for two-dimensional modelling whist the surface-based approach was used in three-dimensional model for its simpler implementation.

5.3. Implementation

In this section, how the FE model was prepared in Abaqus/CAE for simulation and correlation study is described. Firstly, the strategy to solve a three-dimensional (3D) problem is determined and the modelling procedures are discussed. Then, how the mesh is generated and refined in the area of interest where the stress concentration is expected is presented. The boundary conditions are set in the next sub-section and the solver configuration parameters are discussed subsequently.

5.3.1 Two-dimensional (2D) and three-dimensional (3D) models

A special capability has been developed in SIMULIA/Abaqus for analysis of cylindrical and axisymmetric problems. This functionality allows reduction of the tyre modelling and simulation efforts to a great extent whereas the full 3D model is not essentially required to be created in the first instance.

Preparation of tyre FE model for simulation and analysis is initiated from building it as a two-dimensional (2D) axisymmetric problem from the full tyre's cross-section. This functionality can further reduce the full tyre cross-section into a symmetrical half tyre's cross-section model. In this approach, any boundary condition is treated as a full dimensional one throughout the circumferential direction, so that a 2D analysis merely supports symmetric and axisymmetric loading and boundary conditions. In the next step,

the nodal coordinates of half section model are mirrored around the axis of symmetry and a full section with symmetrical meshing is built. The idea behind having results transported from 2D half section into 2D full section model is to harmonise vertical response of the FE model mechanical behaviour when subjected to vertical loadings in right and left hand side of the cross-section in terms of nodal displacement and element stress content.

As explained in previous paragraph, only a 2D tyre model is required for certain types of analysis, e.g. tyre inflation, because of the axisymmetry of the tyre. However, a full 3D model is required to model the tyre behaviour when an asymmetric loading is applied. A 3-D model can be created from a 2D axisymmetric model by revolving the nodal coordinates around the tyre axis of rotation. The rubber partitions in tyre cross-section are also reflected into the 3D model in terms of both its structural complexity and mesh size. The complete revolution is constructed of revolved cross-section around the rotation axis and is so-called the mesh segment. The segment depth in revolution of nodal coordinates can be determined based on the desired refinement, which specifies the number of generated segments. The element types during the revolution can be formed either traditionally (with right edges) or cylindrically (with curved edges). The process from the half-section 2D to a full 3D FE model is illustrated in figure 5.12.

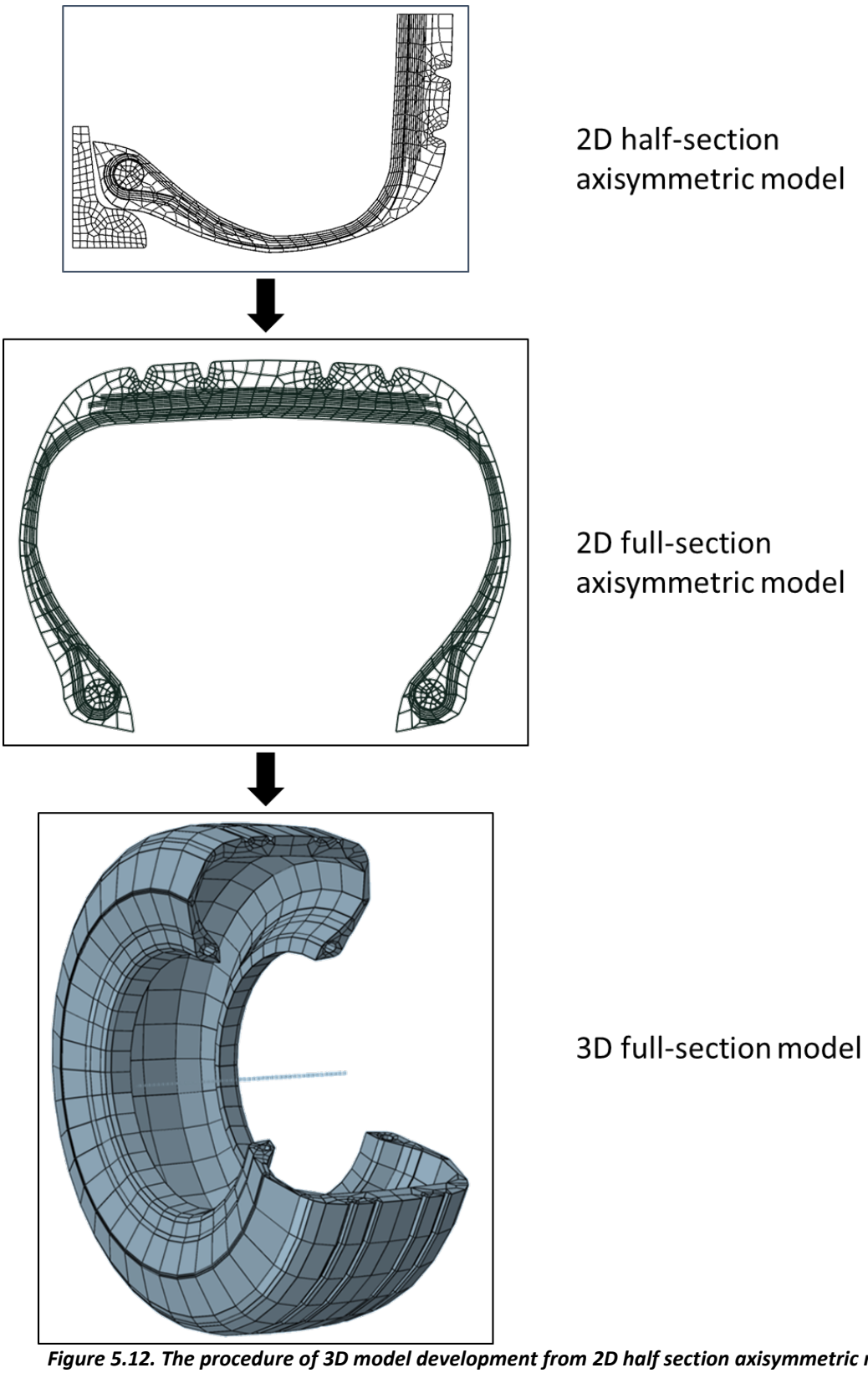

Figure 5.12. The procedure of 3D model development from 2D half section axisymmetric model

5.3.2 Tyre meshed section

A Hybrid-Cylindrical-Hexahedral element type is used to mesh the rubber cross section. The rebar element is meshed using the surface element and the Reduced Integration-Cylindrical-Hexahedron shape was chosen for beads. The element codes in Abaqus that are employed to mesh the tyre section are listed in table 5.2.

Table 5.2. Specification of DATL tyres under study

Region	**mode**	**Element type**	**Description**
Rubber	2D	CGAX4H/CGAX4HT	4-node bilinear axisymmetric quadrilateral, hybrid, constant pressure (T: Thermally coupled)
	3D	C3D8H/C3D8HT	8-node linear brick, hybrid, constant pressure (T: Thermally coupled)
Cord	2D	SFMGAX1	2-node linear axisymmetric surface element
	3D	SFM3D4	4-node quadrilateral surface element
Bead	2D	CGAX4/CGAX4T CGAX4R/CGAX4RT	4-node bilinear axisymmetric quadrilateral, reduced integration, hourglass control (T: Thermally coupled)
	3D	C3D8/C3D8T C3D8R/C3D8RT	8-node brick, tri-linear displacement and temperature, reduced integration, hourglass control (T: Thermally coupled)

Reduction in problem size and increased accuracy are usually opposite objectives to happen in terms of meshing technique. However, a trade-off can be obtained by local refinement of mesh in contact area and selection of coarser mesh for those off-contact segments. The meshed section 3D revolved model with refined segments near contact patch is illustrated in figure 5.13. Further details on the nodes specification can be found in (Simulia, 2013).

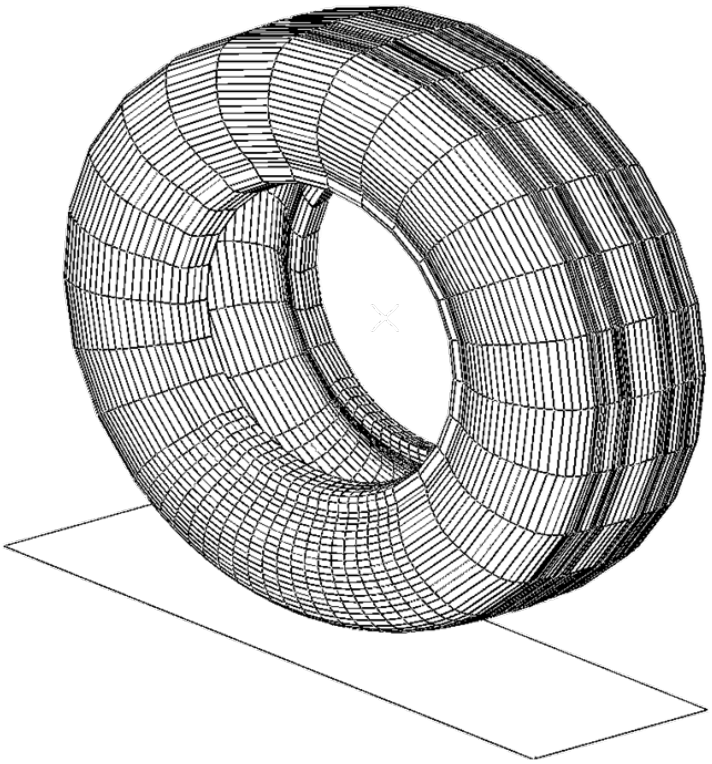

Figure 5.13. Meshed section of 3D FE model

5.3.3 Boundary condition setup

There are typically two geometrical boundary conditions that need to be determined: the rim-tyre interaction and road-tyre. In the case where the rim is modelled and is in contact with the tyre, the rim is then set fully-constrained to the ground. Alternatively, the sliding behaviour in rim-tyre interaction can be realistically neglected, so that the nodes in contact with the rim are constrained instead. In this situation, the boundary condition is however over-constrained and can be potentially reduced to restrict the translational motion in x (longitudinal), y (lateral), and z (vertical) directions of each node in tyre global coordinates according to SIMULIA/Abaqus legacy, as depicted in figure 5.14.

In case it is desired to recover the generated forces and moments in the contact patch, the seat nodes are rigidly tied into a reference node, of which the degrees of freedom should be entirely constrained. The rigid road is also fully-constrained in all rotational and translational

directions. Nevertheless, the z direction is set free when the road is loaded vertically to make an initial contact with the tyre for contact modelling and simulation of loading behaviour. Besides the displacement constraint, the initial pressure and temperature of the inflator air is set to the rated inflation pressure for each tyre and ambient 300° K respectively. The rated pressure for civil aircraft tyre is 1.29 MPa (187 psi) and in the military aircraft tyre it was determined to be 2.29 MPa (332 psi), as provided by DATL. The aircraft tyre pressure is almost 10 times higher than rated pressure in most passenger cars.

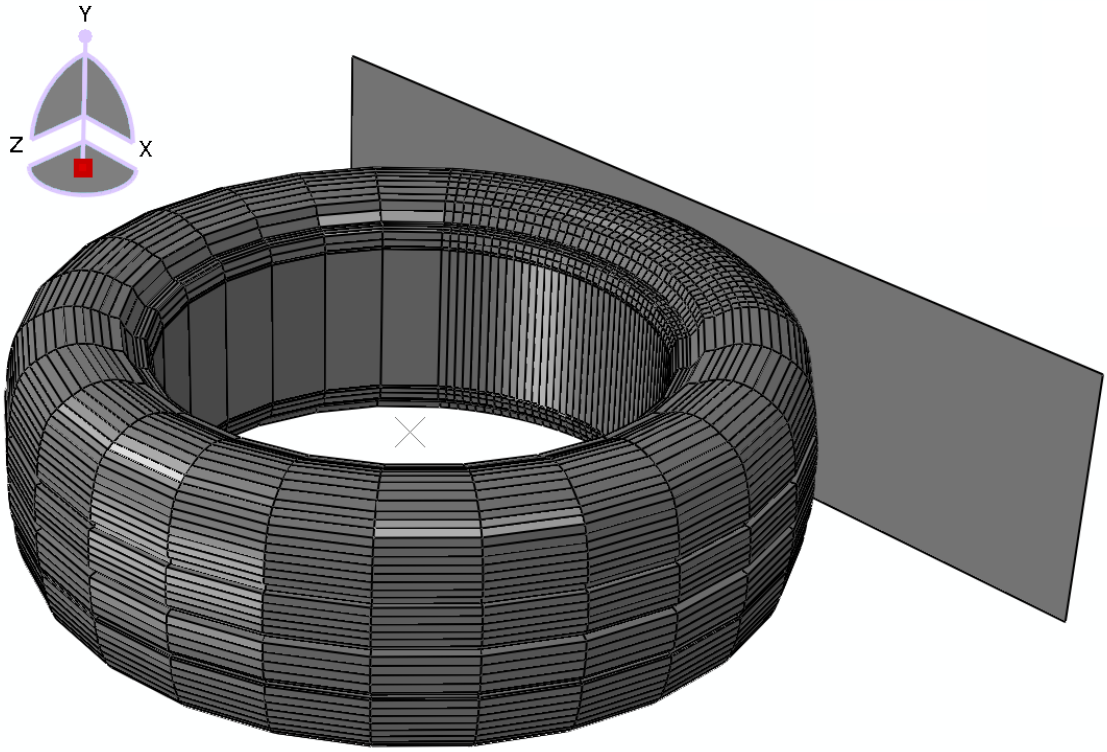

Figure 5.14. The Abaqus' global coordinate system

The simulation strategy is to ensure the equilibrium condition is met in each step for a more stable solution before any important nonlinear situation occurs. The initiation of tyre/road contact is one of those geometrical nonlinearities that can disturb the equilibrium condition and make the solution unstable. To prevent such instability, each particular event is essentially split into steps of simulations, and problematic events are preferably simulated

through displacement-controlled commands instead of force-controlled ones. Displacement-controlled approach provides a more stable solution to the problem since the stiffness matrix is not required to be inverted and the forces are calculated directly. Nevertheless, most physical loadings are force-controlled in nature. The displacement-controlled approach is used here to bring the tyre into initial contact with the road while the force-controlled approach is expected to accommodate the load change simulation in standard and explicit approaches. The comprehensive steps of simulation that are also extended to 3D steady-state transport analysis are illustrated in figure 5.15.

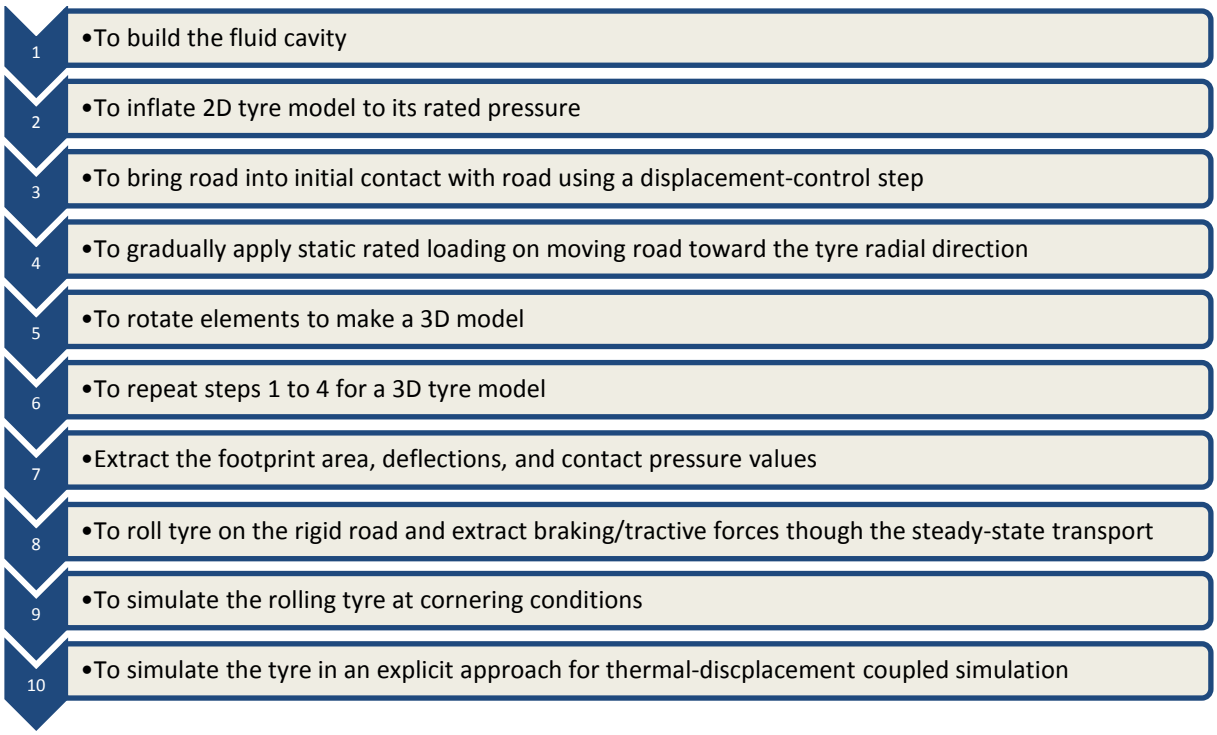

Figure 5.15. Simulation steps for tyre analysis procedure

5.3.4 Solver configuration parameters

5.3.4.1 Solver method

The solver can use *direct* or *iterative* methods to solve the $[K]\{u\} = \{F\}$ problem, where K, u, and F are stiffness matrix, displacement vector, and external force vector. Direct linear

equation is solved by implementing a sparse Gauss elimination method while iterative solver employs the domain decomposition based methods such as preconditioned conjugate gradient method (Simulia, 2013). Direct solver is selected as the preferred approach since the convergence of the iterative approach is conditional to the stop-iteration criteria.

A nonlinear problem requires updating the stiffness matrix at any iteration in nonlinear $[K]\{u\} = \{F\}$ problem. This problem can be solved using either full-Newton or quasi-Newton approaches. In full-Newton approach, the Jacobean matrix is formed at any iteration and used for approximation algorithm. This method is proven to take advantage of quadratic convergence rate, in that the final solution can be potentially obtained at a faster rate. However, the calculation of Jacobean matrix in big size problems is extremely expensive and sometimes it is even difficult to formulate in a close loop. For mildly nonlinear problem, where rate of nonlinearity can be avoided for a number of iterations, the quasi-Newton method is used, in which the Jacobean matrix occasionally updated when a change happens to be necessary (Simulia, 2013).

5.3.4.2 Parallel computing

The simulations were carried out on the "BlueBear" computation facility at University of Birmingham, University's High-Performance Computation (HPC) facility, with the specifications as shown in Table 5.3. The principal advantage of this facility is its capability to assign a job to more than one processing unit, so that the final solution is obtained in a shorter time.

Table 5.3. Computational features (University of Birmingham, 2013)

Component	**Specification**
Equivalent number of processing cores	848
Processing speed per core	2.2 GHz
Maximum available RAM per job submission	256 GB
Raw disk space	Over 150 TB

5.4. Post-processing of FE output

5.4.1 Introduction

Having prepared FE model for simulation, it is required to perform a mesh sensitivity analysis to find an optimum seed size for the tyre section discretisation. In this section, a mesh density sensitivity analysis is conducted to evaluate the appropriate number of mesh and the sensitivity of the solution to the quality and quantity of the meshing. Then, the FE model reduction to a simplified version is investigated for faster implementation and conditions are set for applicability of a simplified model.

The main application of 2D tyre model is to simulate the inflation behaviour of the tyre, i.e. to determine the inflated shape and simulate the tyre burst test for prediction of the critical pressure. Simulation of the inflated shape at rated inflation pressure does not normally pose a great challenge in terms of meshing of the tyre cross-section and stability in solution. Therefore, the model complexity can be explored from the points of view of both mesh size and structural complexity. However, there is a high chance of instability in simulation of burst in aircraft tyres, particularly at higher inflation pressures due to severe distortion of the elements unless the mesh size is carefully chosen and simulation procedure is adequately split into analysis steps. Through a trial and error procedure, the optimum mesh size was found for each 2D FE model, of which convergence could be obtained at the highest possible inflation pressure.

To ensure the quality of simulation in burst test, the FE model was studied for varying structural parameter, so that models with different complexity were developed. It should be noted that the structural complexity in tyre is solely based on rubber compounds owing to the fact that changes in ply configuration can considerably influence the tyre mechanical response and profile shape under similar load and inflation conditions. A pre-study was conducted on the effects of changes in fabric geometrical configuration to tyre mechanical properties, as demonstrated in figure 5.16. The tyre on the right hand side was configured with misaligned carcass cords to 45 degree in comparison to cord configuration at perpendicular angle in normal tyre on the left hand side. In this figure, it is clearly shown that the profile shape is inflated with different mechanisms under a constant inflation pressure of 3 MPa. The other advantage of this result is to demonstrate what parameters in the tyre can potentially be configured for design synthesis in development of future tyres.

Figure 5.16. A comparison between 2D FE models in terms of change in cord direction of construction fabrics of a sample tyre #2 at 3MPa inflation pressure

5.4.2 Mesh size study

Several 2D FE models were developed based on variation of element size and combination of mesh refinement in rubber, reinforcement, and bead. In this analysis, the tyre is prepared in identical boundary conditions and similar inflation pressure (at rated pressure); i.e. the chafer is in contact with the tyre rim, and the half section from the symmetry axis is constrained in rotation and motion perpendicular to the axis of symmetry, but the motion along the axis is unconstrained. Furthermore, the beads and cords were embedded into the rubber region to play their role as reinforcement. The mesh size, number of elements, solution time, stress, and deflection accuracy were measured and reported in this stage. The results were expected to demonstrate how the mesh size affects the maximum stress in the reinforcement and rubber components as well as the maximum deflection in the tyre. This simulation was conducted for the civil aircraft tyre.

The results of this simulation suggest that the accuracy of FE models is associated with the size of elements and level of local and global refinement. The efficiency, stability, and accuracy of an FE solution are factors that are affected by selection of mesh size in tyre FE modelling. A coarser element size enables simulation to be solved in shorter time, but can potentially deteriorate the prediction of stress and strain due to the higher possibility of excessive distortion in elements. On the other hand, the accuracy of stress is increased by using finer mesh sizes while the computational efforts rise. Element distortion is another important factor in selection of the element size for its mechanism in stability of solution. A higher rate of element distortion in solution can increase chances to break the simulation. Moreover, an excessive distortion potentially causes miscalculation of stress in the element. There is more chance of distortion in finer element sizes that are exposed to large deformation rather than coarser mesh size.

With regard to the large differences in the Von Mises stress of rubber and reinforcements in FE models with different mesh sizes, combinations of mesh sizes of bead, rubber and fabric components were employed to generate different 2D models of civil aircraft tyre as indicated in table 5.4. The combinations were obtained from three seed sizes for meshing bead, rubber and fabric regions. The FE models of civil aircraft tyre were inflated to the rated pressure of 1.29 MPa to check the sensitivity of FE simulation resulting from mesh size variation. For a fair comparison of the solution performance, simulations in each row of table 5.4 were carried out using a laptop with single processing core, whose specifications are shown in table 5.5. In addition, table 5.4 presents how the stresses and deflections vary with the changes in mesh size of the components. Figure 5.17 shows the prediction of von Mises stress distribution across two half sections with different element sizes in rubber region of the detailed model.

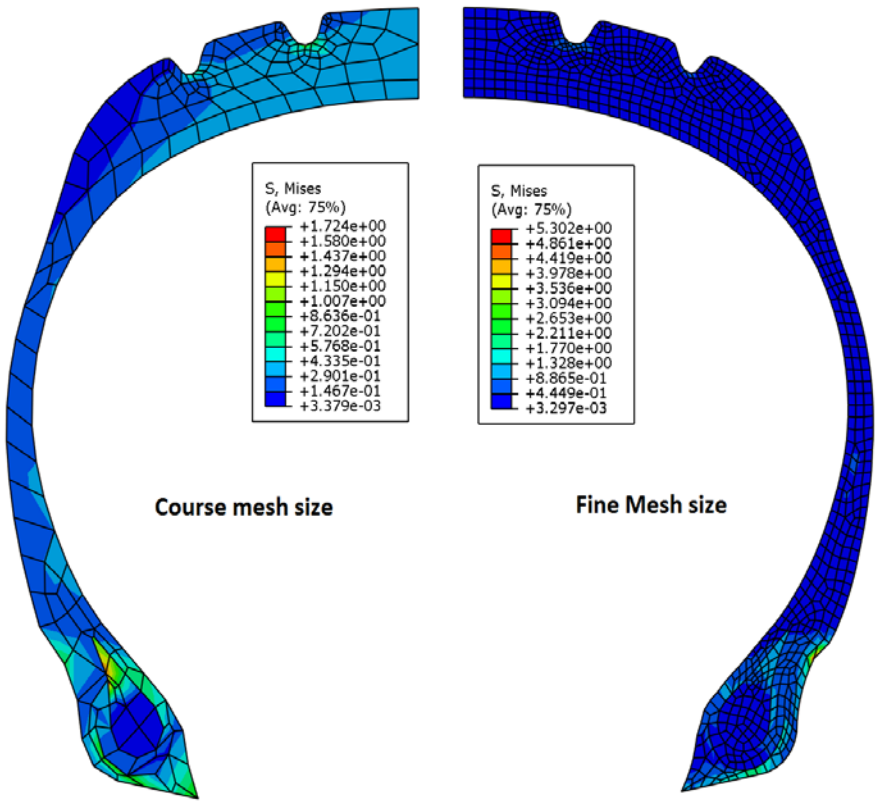

Figure 5.17. The von Mises stress in section of FE tyre models with different mesh size in rubber region

Table 5.4. Specifications of 2D FE models generated for mesh size study of civil aircraft tyre

BEAD Element size (mm)	RUBBER Element size (mm)	BELT Element size (mm)	Elements	Nodes	Variables	CPU Time (sec)	Maximum stress in Rubber (MPa)	Maximum Stress in fabrics (MPa)	Maximum deflection (mm)
2	6	2	2024	2132	4264	7.38	0.9548	81.49	44.39
2	6	5	1122	1230	2460	3.73	1.069	81.55	44.44
2	6	8	898	1006	2012	3.35	1.142	81.57	44.48
5	6	2	1938	2037	4074	7.23	1.085	81.86	44.54
5	6	5	1036	1135	2270	3.43	1.178	81.89	44.58
5	6	8	812	911	1822	3.06	1.256	81.91	44.62
8	6	2	1916	2012	4024	6.78	1.362	81.98	44.89
8	6	5	1014	1110	2220	3.58	1.565	82.06	45
8	6	8	790	886	1772	2.91	1.654	82.63	45.19
2	8	2	1890	1983	3966	7.01	1.017	81.01	44.20
2	8	5	988	1081	2162	3.50	1.039	81.02	44.26
2	8	8	764	857	1714	3.21	1.066	80.94	44.26
5	8	2	1804	1888	3776	6.86	1.087	81.12	44.25
5	8	5	902	986	1972	3.28	1.115	81.14	44.31
5	8	8	678	762	1524	2.91	1.121	81.03	44.30
8	8	2	1782	1863	3726	6.41	1.808	82.51	44.66
8	8	5	880	961	1922	3.35	1.900	82.27	44.77
8	8	8	656	737	1474	2.76	1.828	82.23	44.80
2	12	2	1784	1862	3724	5.14	0.7477	81.13	43.99
2	12	5	882	960	1920	3.06	0.7471	80.75	44.08
2	12	8	658	736	1472	2.61	0.7334	80.70	44.13
5	12	2	1698	1767	3534	4.92	0.7471	80.95	44.05
5	12	5	796	865	1730	2.83	0.7472	80.88	44.13
5	12	8	572	641	1282	2.39	0.7333	80.87	44.19
8	12	2	1676	1742	3484	4.77	0.7538	81.34	44.39
8	12	5	774	840	1680	2.98	0.7437	81.78	44.51
8	12	8	550	616	1232	2.53	0.7294	81.84	44.60
2	14	2	1735	1807	3614	4.92	0.6609	80.05	43.76
2	14	5	833	905	1810	3.21	0.6823	80.06	43.78
2	14	8	609	681	1362	2.53	0.7051	79.93	43.79
5	14	2	1649	1712	3424	4.70	0.6280	80.07	43.77
5	14	5	747	810	1620	2.68	0.6502	80.09	43.79
5	14	8	523	586	1172	2.31	0.6754	79.95	43.80
8	14	2	1627	1687	3374	4.32	0.5558	80.75	44.05
8	14	5	725	785	1570	2.83	0.5577	80.79	44.08
8	14	8	501	561	1122	2.31	0.5575	80.66	44.10

Table 5.5. Computational features of laptop used for mesh study

Component	**Specification**
number of processing cores	1
Processing speed per core	2.2 GHz
Maximum available RAM per job submission	4 GB
Raw disk space	160 TB

The FE simulation results, as reported in table 5.4, showed satisfactory consistency in deflection of components and acceptably comparable results for maximum Von Mises stress in fabric, but rather poor consistency in outputs of maximum Von Mises stress in the rubber region. The percentage of deviation from the average value is illustrated in Table 5.6 Maximum Von Mises stress in the cords and maximum deflection values are consistently within ± 2% of the mean value. It follows that mesh convergence criteria of FE models were satisfied for the bead and belt element sizes used at the rated inflation pressure. However, the maximum Von Mises stress in the rubber is much more sensitive to the variation in rubber component mesh sizes than maximum Von Mises stress in fabric. The Von Mises stress in the rubber tends to converge as the rubber element size is reduced. Therefore while the coarser mesh sizes for fabric and Bead are adequate for accurate prediction of the stresses in the reinforcement, smaller element size is required for accurate prediction of stresses in the rubber components.

Table 5.6. The range of deviation from average value in mesh sensitivity analysis of civil aircraft tyre

Description	**Percentage of deviation from average value (%)**
Maximum stress in cords under rated pressure	[-1.27, 1.91]
Maximum stress in rubber under rated pressure	[-38, 110]
Maximum deflection in rubbers	[-0.94, 1.4]

The calculation costs of 2D FE models indicated very modest computation costs, but it is evident from table 5.4 that an increase in the number of elements directly increases the computation time.

5.4.3 Detailed versus Simplified model

In view of the complexity of the aircraft tyre structure due to the high number of reinforcement plies, the element count for a detailed FE model will be extremely large. Considering that the aim is to apply the FE model for design and development purposes, it is essential that simulation of physical tyre tests can be carried out quickly. It is therefore important that the FE models developed should be capable of providing rapid (few minutes to few hours depends on the number of simulations), but reasonably accurate assessment of the performance of a new tyre design. It is also required that the models form the basis for automating the design analysis; hence, they must provide a capability for automation of the FE model generating process. Therefore in this study, several FE models of aircraft tyres have been developed in terms of varying structural detail to investigate the simulation times for different physical tests and the incurred accuracy in comparison with the highly detailed model.

The modern aircraft tyre consists of many parts including inner liner, bead, chafer, body plies, breaker plies, tread, apex etc., each with its own topping material and orientation of reinforcement cords where they exist. This diversity of material properties as well as reinforcement can be reflected to a greater or lesser extent in the complexity of the FE model. In addition, the element mesh size contributes to the complexity of the model. In this study, three levels of structural complexity were considered, namely *simplified*, *regular* and *detailed*.

In the simplified model, the rubber regions were aggregated as one region, and the property of dominant rubber region was used as the full region material property. The reinforcements were embedded in the topping material in similar positions. In the regular model, the cross-sectional structure was divided into four areas, the *filler* into which the bead is embedded, the *main body* into which the reinforcing cords of the body plies and breaker plies are embedded, and the *packaging cover* which consists of the un-reinforced outer covering of the tyre (inner liner, chafer, sidewall cover and tread). In this case, the rubber material properties of the aggregated parts were determined as the averages of their constituents. The reinforcing cords were embedded in the topping materials in the similar positions. In the detailed model, the individual topping materials, tread, packaging covers, and fillers were considered separately and meshed accordingly. The reinforcing cords were again embedded in the topping materials in the similar positions. For the military aircraft tyre, simple and detailed models were developed while for civil aircraft tyre, all three FE models (simple/regular/complex) were considered for simulation purposes.

It is obvious that the simplified model provides the least problem for meshing since the whole cross-sectional area is assumed to consist of a single topping material while the detailed model poses the greatest problem for meshing because of the requirement to match the meshes of the different sections made up of different topping materials.

2D FE models of a specific tyre can be developed from two points of view: mesh size and structural complexity. Since the major focus in 2D FE models is to represent tyre behaviour under inflation, models were created with different mesh sizes. It was found that at very high inflation pressure, solution convergence was sensitive to mesh size although this was not a problem at normal tyre operating pressure. This indicates that there is an optimum

mesh size for various 2D FE models in which the convergence of the solution can be obtained at the highest possible inflation pressure.

The configurations of the different models used in this study are as follows:

Detailed Model; all the six rubber components were considered separately in the construction of FE models namely: *Tread & Sub-tread & ITF topping & insulation*, *Bead Coat/Apex*, *Inner liner*, *Casing (topping compound) & clinch strips*, *Sidewall packaging*, and *Chafer*. The components are displayed in figure 5.18.a. for the military aircraft tyre and figure 5.18.b for the civil aircraft tyre.

a. Components of detailed model of military aircraft tyre

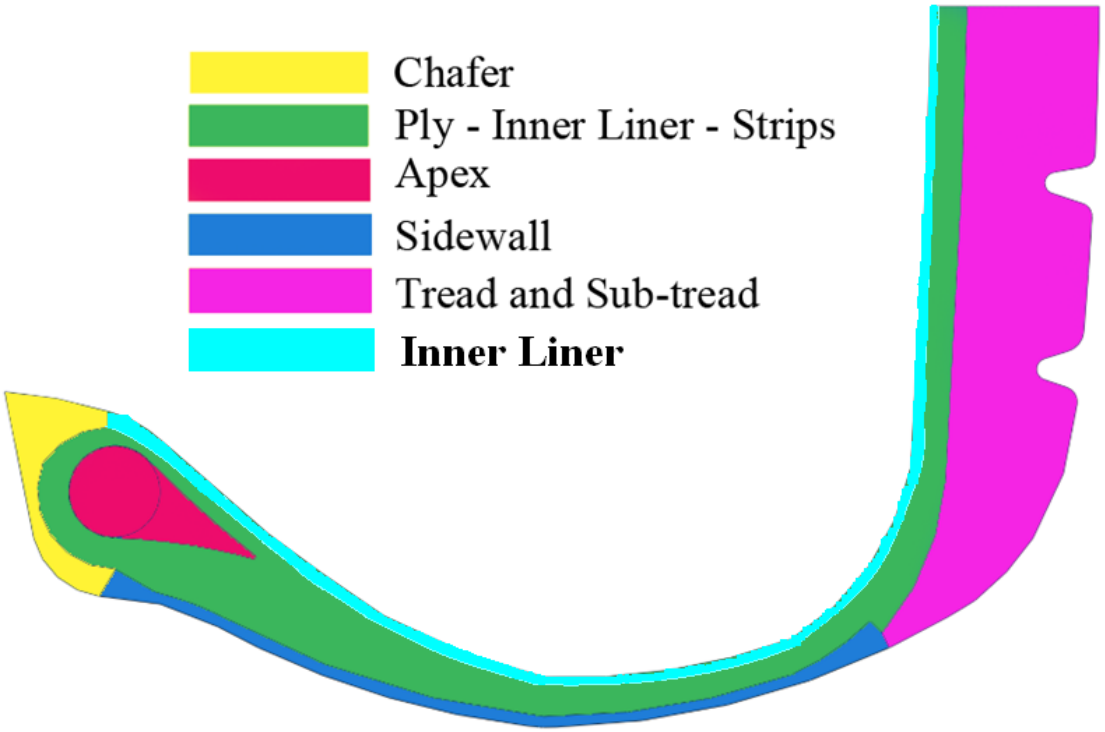

b. Components of detailed model of civil aircraft tyre

Figure 5.18. Detailed model of civil and military aircraft tyres

Regular Model; which is comprised of four dominant rubbery regions - *tread*, *carcass*, *apex*, and *chafer* in civil aircraft tyre, as illustrated in figure 5.19. In this model, *Inner liner*, *Casing (topping compound) & clinch strips*, and *Sidewall* that have comparable material properties were merged into one rubbery region. This combination is not expected to potentially produce a considerable difference in the model's mechanical response since the Inner liner and sidewall are thin components that are used as outer packaging and protection and contribute the least in overall stiffness of the tyre. Moreover, this combination of layers is not reinforced according to the original drawing of the tyre section. Material property of the *Casing* rubber (topping compound) was used for the combination of *Casing* and *clinch strips* components. No regular model is available for military aircraft tyre. In addition, most of

correlation studies were conducted on the simplified and detailed model for commercial aircraft tyre and the regular model was only used specifically for burst validation exercise.

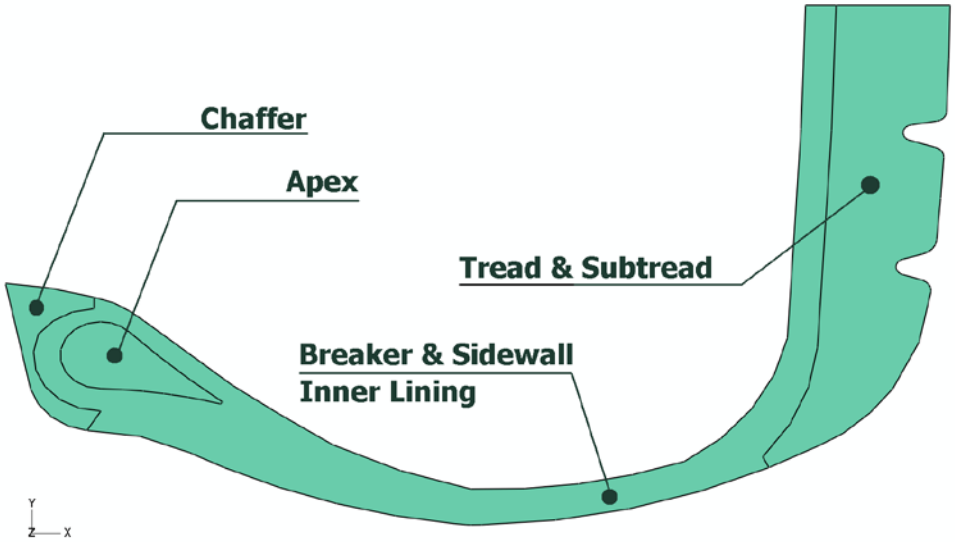

Figure 5.19. Components of regular model of civil aircraft tyre

Simplified Model; all the rubber components were considered to have the same hyperelastic properties. The material property of the *casing,* as the most dominant rubber component, was assigned to all rubber components since it has the most contribution in construction of the tyre.

The maximum Von Mises stress in cord and rubber of civil aircraft tyre that is subjected to a 3 MPa inflation pressure are shown in figures 5.20.a and 5.20.b. The result obtained from FE simulation of inflation suggests that the maximum Von Mises stresses in cords of the simple and detailed models have closer magnitudes rather than the maximum stress results in rubbery regions. The difference can be interpreted in two ways: firstly, an increase in the number of rubber components has led to thinner regions and higher aspect ratios in elements; secondly, each rubber region has its own material properties, i.e. while the solution has continuity in element displacements, it causes discontinuity in stress and less

stiff regions are under higher stress. An illustration of this discontinuity in stress is evident as it can be seen in figure 5.20. The maximum deflection under inflation occurs in the crown area inside the tyre for both simple and detailed models, as plotted and compared in figure 5.20.c. Both simple and detailed models demonstrate close trends in terms of crown displacement. It can be concluded that the diversity of material property does not influence the tyre mechanical response, but the stress in rubbery regions is seriously affected. It follows that partitioning FE model into its major components should produce more realistic results for cases when a precise assessment of stress in rubbery regions and interfaces is demanded.

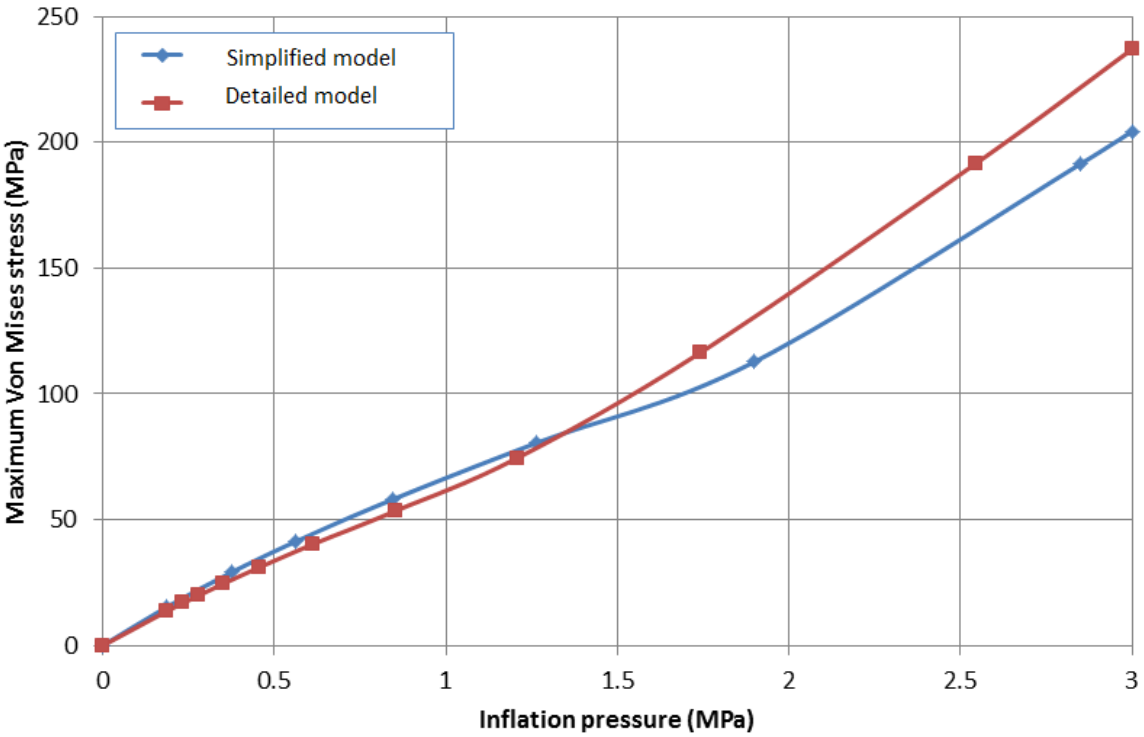

a: Maximum Von Mises stress in cords subjected to a 3 MPa inflation pressure in civil aircraft tyre

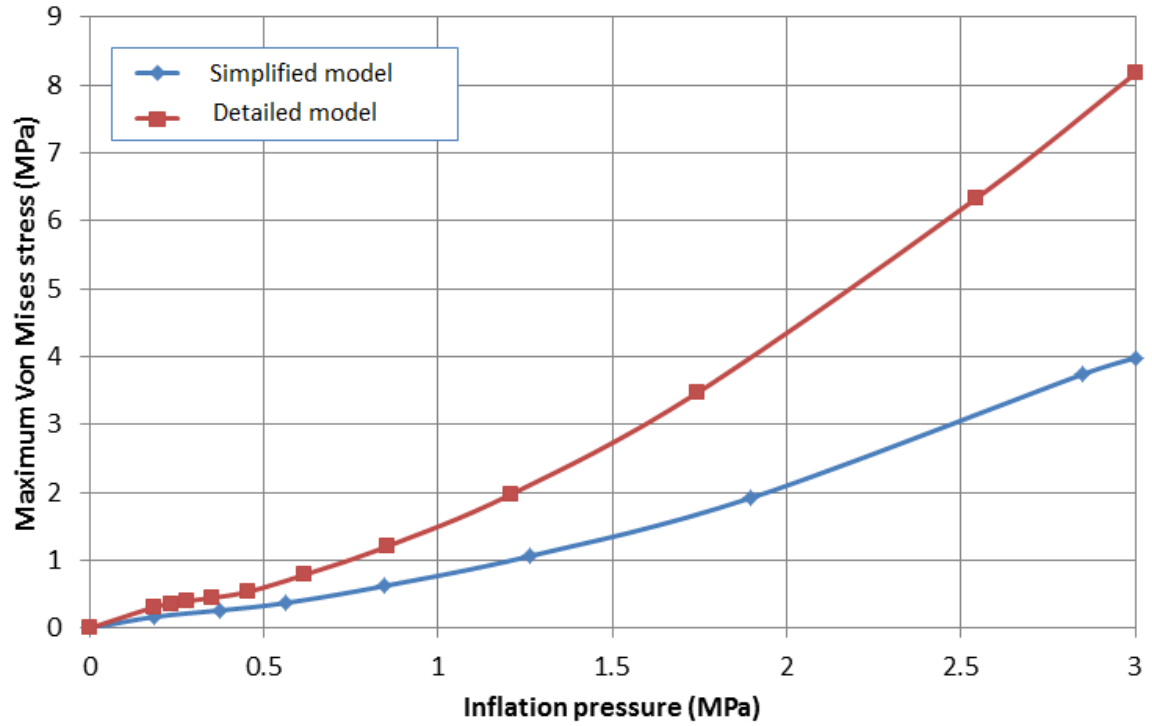

b: Maximum Von Mises stress in rubbers subjected to a 3 MPa inflation pressure in civil aircraft tyre

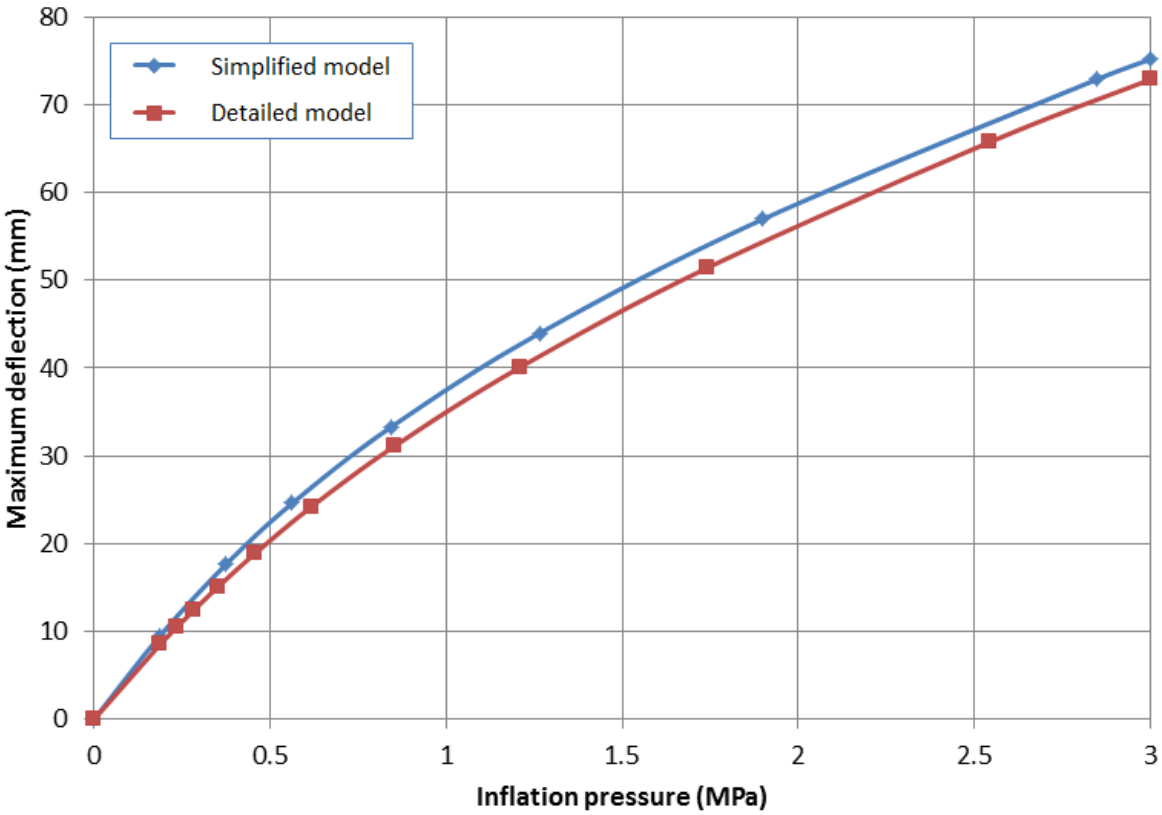

c: Maximum deflection of civil aircraft tyre subjected to a 3 MPa inflation pressure

Figure 5.20. Stress and displacement in inflated civil aircraft tyre

The discontinuity in stress in boundaries of material regions are shown in figure 5.21 due to the discontinuity in material properties of neighbour rubbers.

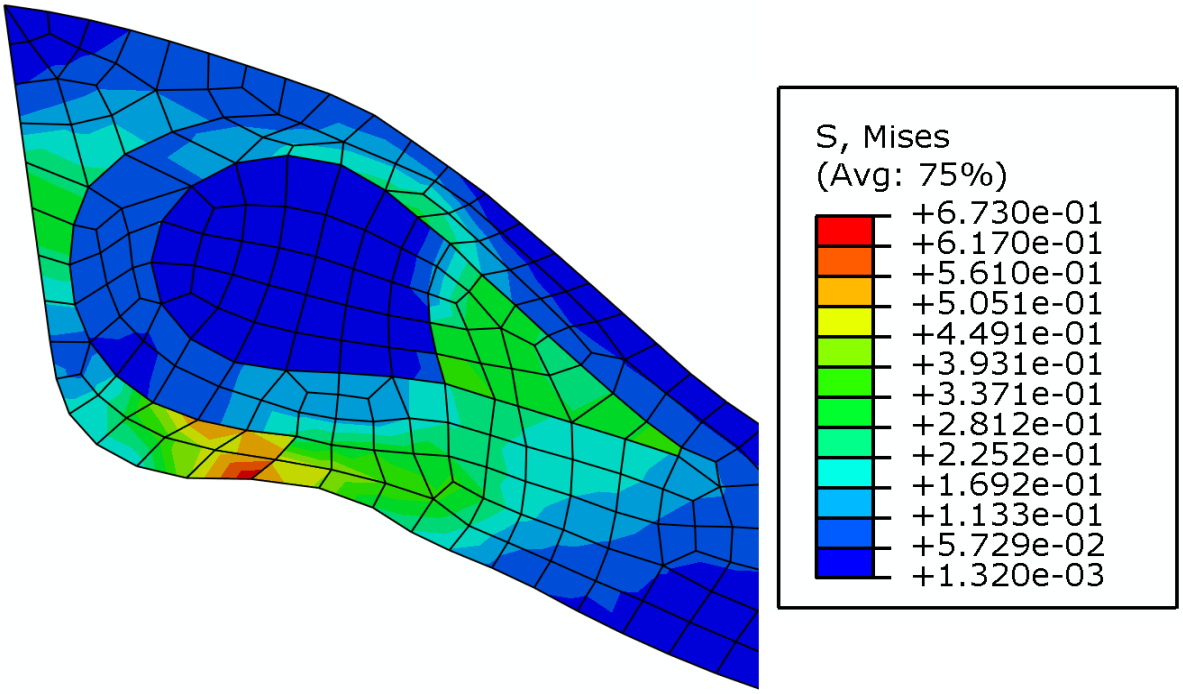

Figure 5.21. Stress distribution in detailed modelled as shown in figure 5.18.a

5.4.4 2D and 3D FE models

The 3D FE model was generated from the 2D axisymmetric model using the Abaqus INP file in order to check the deflection and stress results of civil aircraft tyre against that of the 2D model under 3 MPa inflation pressure. As shown in figure 5.22, maximum deflection of the 2D model coincides with 3D model maximum deflection in the tyre profile. As a result, the need for inflation simulation of a 3D model can be shown to be unnecessary if the inflation data of a 2D model is available. A 2D axisymmetric model of a tyre is adequate to simulate tyre inflation simulation instead of a complex and expensive 3D FE model.

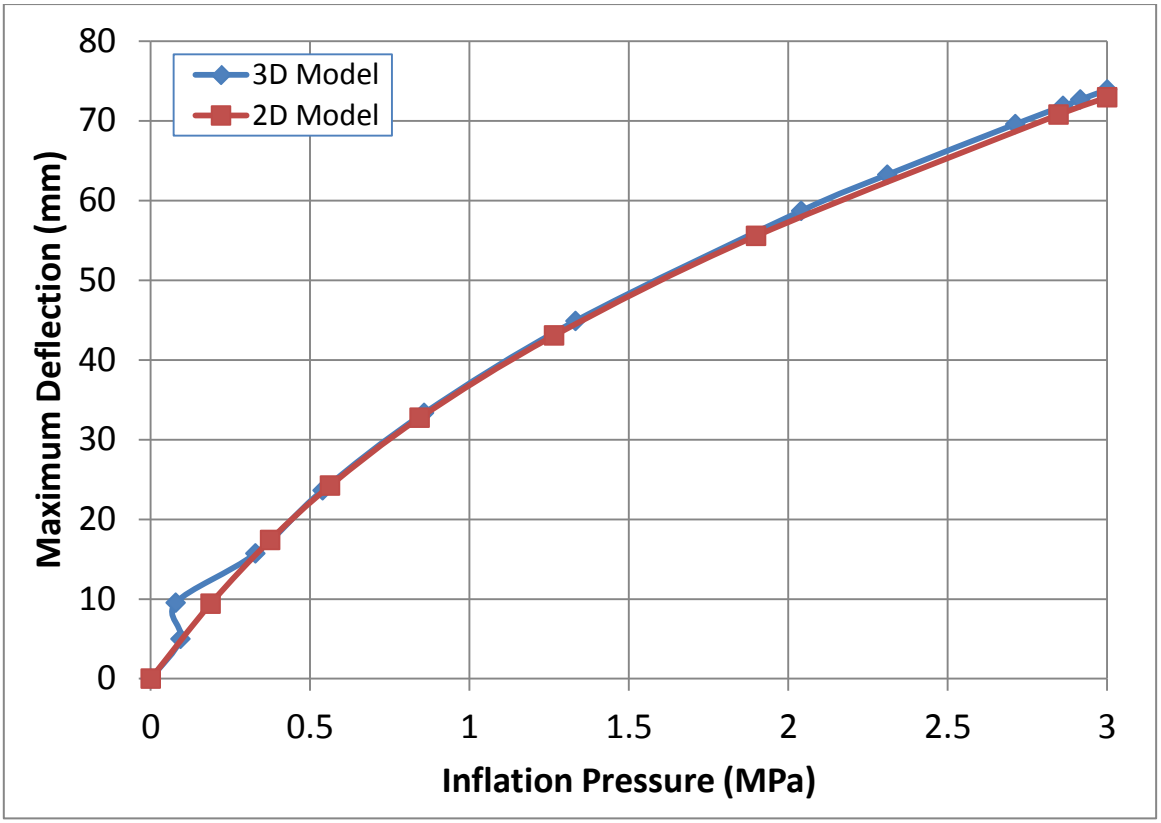

Figure 5.22. A comparison between 2D and 3D FE models subjected to 3 MPa inflation pressure in civil aircraft tyre

5.5. Simulation results and validation

The validation of the 2D FE model was conducted in three aspects: burst pressure, profile size check and footprint. After the tyre on the test rig was inflated to its rated pressure, a retractable flexible ruler was employed to measure the specified tyre size parameters immediately after the inflation as well as 24 hours after according to the standards manual. The standard measurements and sizing requirements will be discussed in the following sections.

In this section, the developed models in previous sections were utilised to validate against test measurements. The simulation was performed using the Abaqus/CAE for 2D FE models and Abaqus/Standard for 3D analysis of the FE model for static and steady-state test

procedures. The boundary conditions under which simulation was implemented in each step are as described in the previous section. Results obtained from the FE solver outputs were validated with measured deflection, footprint area and pressure, and burst pressure values to show the FE model accuracy. In this study, both civil and military aircraft tyres were used for simulation, representing two different tyre types to cross-validate and check the FE simulation repeatability.

5.5.1 Profile sizing check

The tyres were inflated to their rated operating pressures and profile check was carried out for both tyres. Also, comparison of 2D and 3D models under inflation and stress analysis of simplified and detailed 2D models were studied at this stage for the tyre where physical test data was available for comparison.

The tyre profile was expanded from deflated to inflated shape under the rated pressure of 2.78 MPa (403 psi) for military aircraft tyre and 1.29 MPa (187 psi) for civil aircraft tyre. The measurements from the inflated shape were obtained at provided inflation pressures and were used to check if the model is reliable in predicting tyre inflated shape. Three major dimensions were measured for validation of civil and military aircraft tyres: outside diameter, section width, and perimeter based on data availability by DATL. More measurements were obtained for military aircraft tyre, namely Tread Edge Diameter (TED), Tread Edge Width (TEW), A, B, and C, which are shown in figure 5.23 schematically. For civil aircraft tyre, the section width and tyre radius were measured, as shown in figure 5.24. A comparison of these values with FE model results demonstrates how close the predicted FE inflated shape of cross-section after pressurising inner chamber is in comparison with the measurements. The validation study results of military and civil aircraft tyres are shown

tables 5.7 and 5.8 respectively. The accuracy in prediction of tyre deformation is generally excellent because the deviation of simulation results from the test data was less than 1% for all FE models.

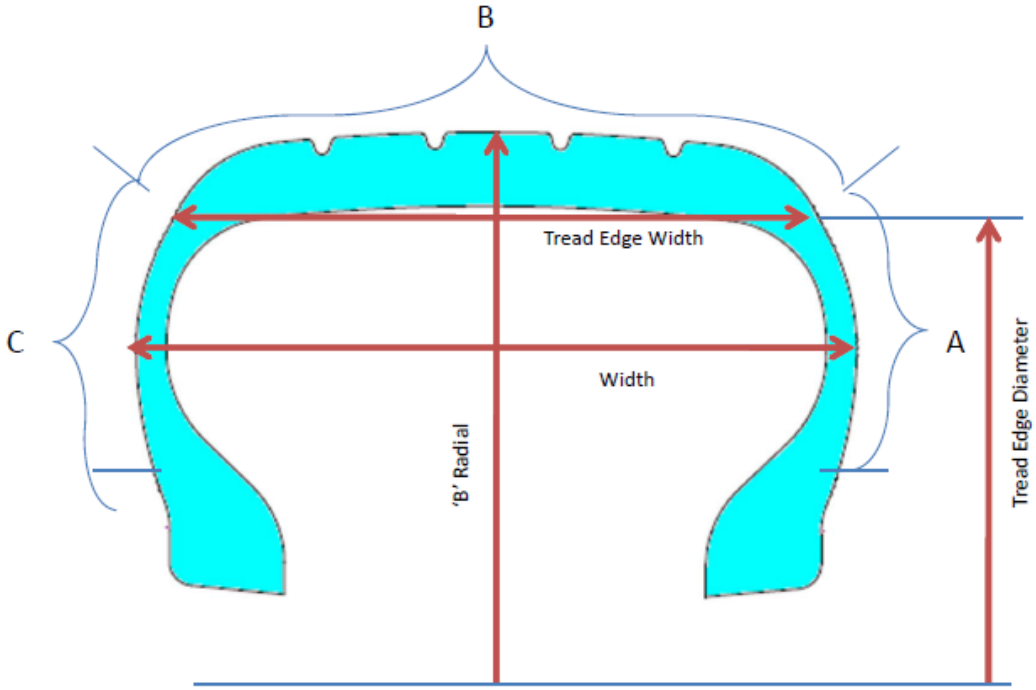

Figure 5.23. Parameters of tyre needed for profile check in military aircraft tyre

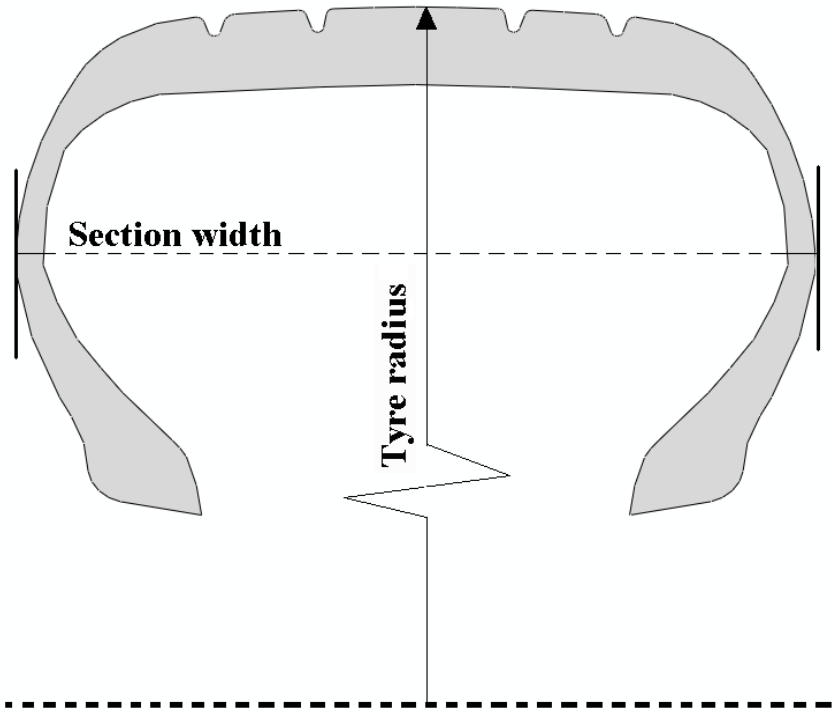

Figure 5.24. Parameters of tyre needed for profile check in civil aircraft tyre

Table 5.7. Profile check at the rated pressure of 2.78 MPa in military aircraft tyre

	Deflated on Rim		Inflated to 2.78 MPa			
	Real Measurement (mm)	Drawing Measurement (mm)	Real Measurement right after inflation (mm)	Real Measurement after 24 Hour (mm)	Measured after solution of Simplified FE Model (mm)	Measured after solution of detailed FE Model (mm)
*CBR	2128	2180	2350	2362	2381	2375
Width	263	262	280	284	283	274
*TED	650	652	677	679	679	679
*TEW	228	228	237	239	235	232
A	114	114	127	128	123	130
B	237	242	262	264	253	259
C	114	114	127	127	123	130

**** CBR: Circumference 'B' Radial, TED: Tread Edge Diameter, TEW: Tread Edge Width***

Table 5.8. Profile check at the rated pressure of 1.29 MPa in civil aircraft tyre

	detailed model	simplified model	Real measurement
Outside diameter (mm)	1060	1064	1049
Section width (mm)	333	328	349

5.5.2 Sidewall deformation

The tyre profiler is a moving laser measurement device to capture deflections of tyre in the sidewall. The tyre profiler is shown in figure 5.25. This test was carried out when the civil aircraft tyre was inflated to rated pressure of 1.29 MPa (187 psi) and vertically loaded to 146

kN (32825 lb). The 3D representation of civil aircraft tyre was used to simulate the sidewall deformation in FE model. The comparison of the sidewall profile is illustrated in figure 5.26.

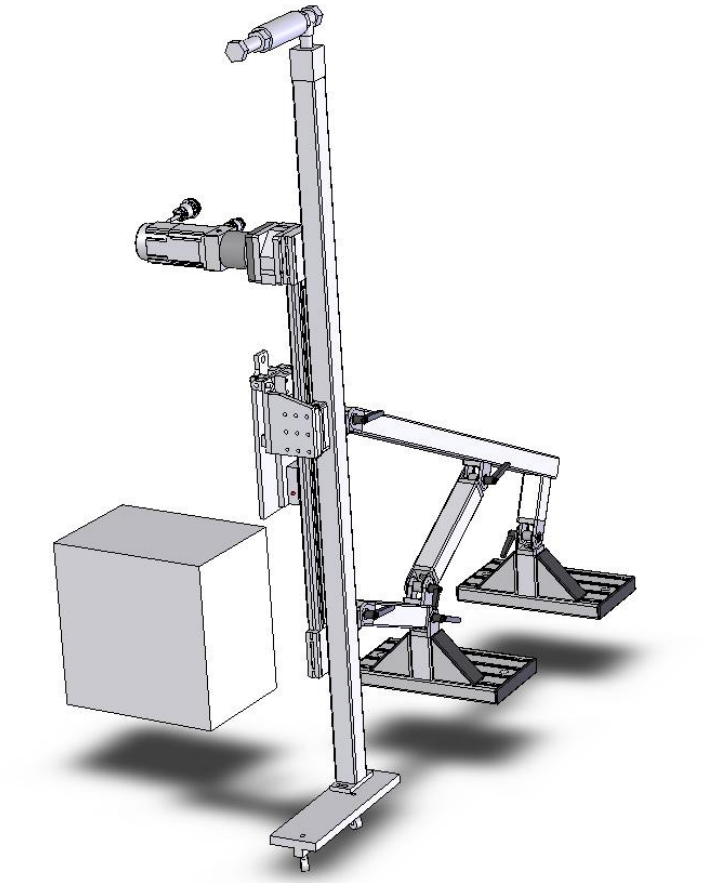

a. Tyre profiler mechanism provided by DATL

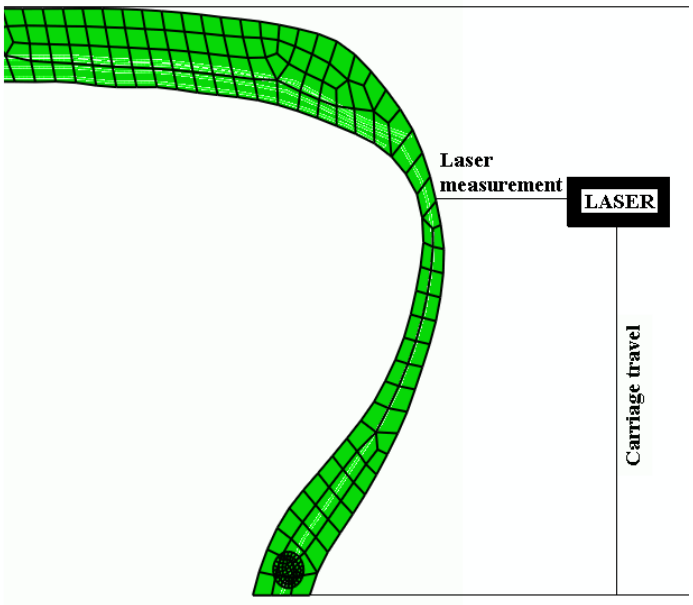

b. Tyre sidewall measurement

Figure 5.25. Tyre profiler

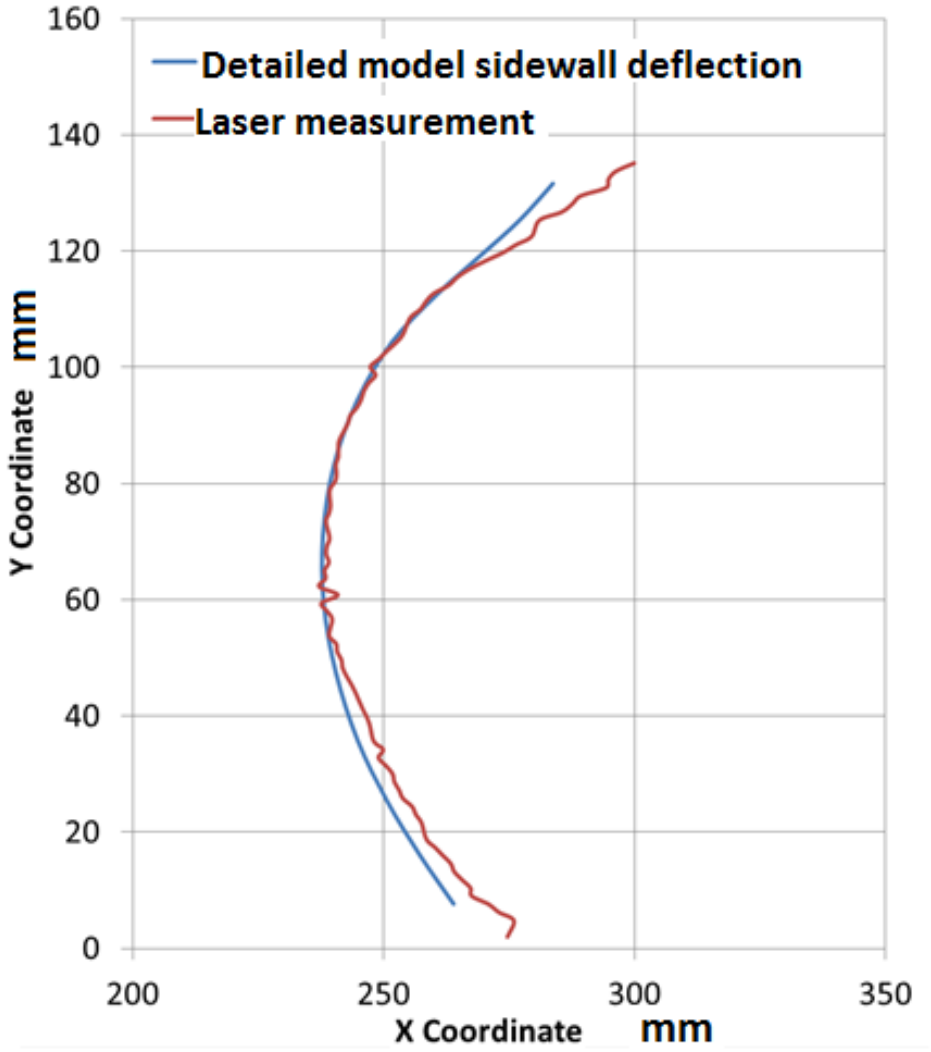

Figure 5.26. Sidewall deformation correlation between laser measurement and simulation

5.5.3 Tyre footprint

Tyre footprint under different loads and inflation pressure is another important criterion to judge the tyre design. The footprint correlation was carried out based on two measurements: the geometry of contact area and the contact pressure. The goal in tyre design is to obtain a consistent shape for contact area under load and inflation variation as well as a uniform contact pressure distribution for improved wear characteristic. To perform footprint correlation, both physical tyre and its 3D simplified/detailed model were exposed

to Inflation pressure of 1.29 MPa (187 psi) and loading of 146 kN (32825 lbs) in civil aircraft tyre. The procedure to obtain a footprint is to coat the top of the tread with black ink and insert a paper under the tyre before the contact is initiated with the road. After the prescribed pressure and load are applied, the tyre is unloaded and separated from the inked paper to reveal the contact area printed on the paper, as it is shown in figure 5.27. The contact area from the test was correlated with simulation in figure 5.28 for simplified and detailed 3D models with the yellow boundaries that represent the image-processed edges of inked footprint and the footprint from the FE simulation.

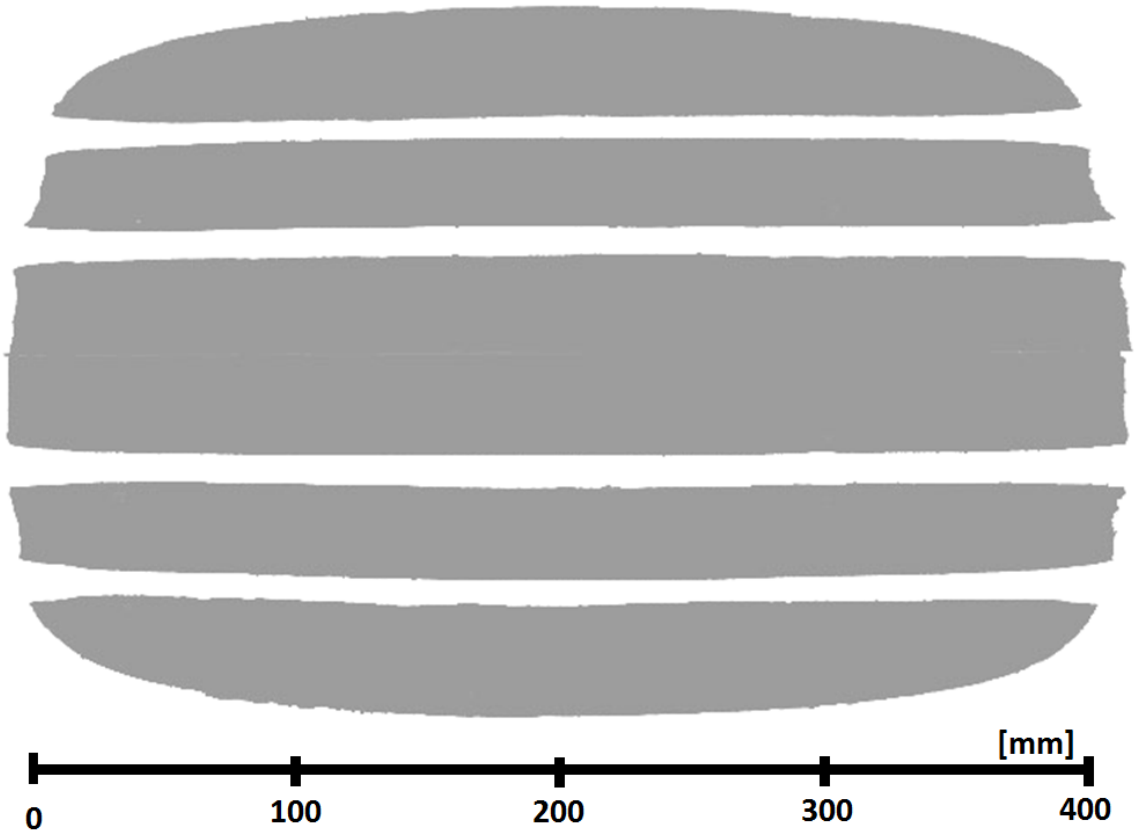

Figure 5.27. Tyre contact patch printed by ink on paper

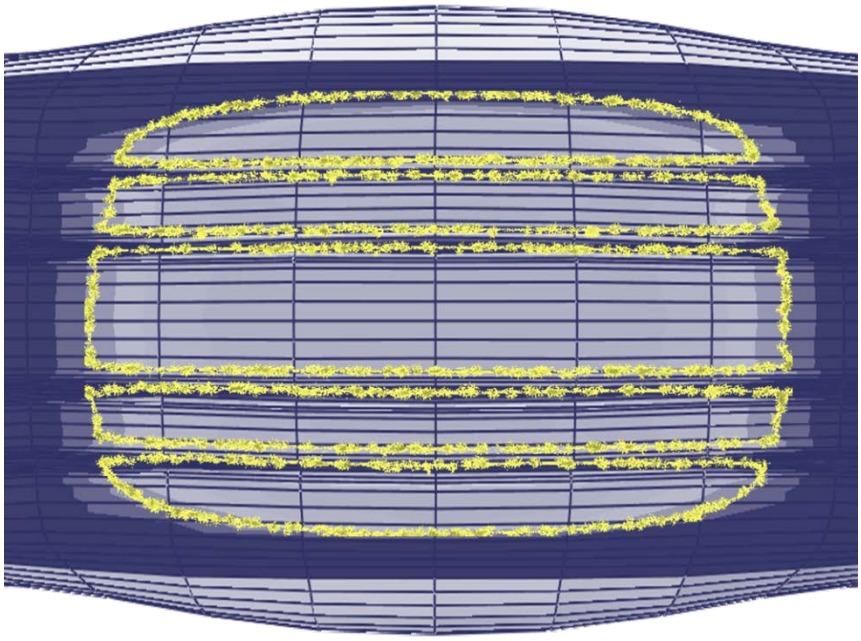

a. Correlation of footprint in simplified model

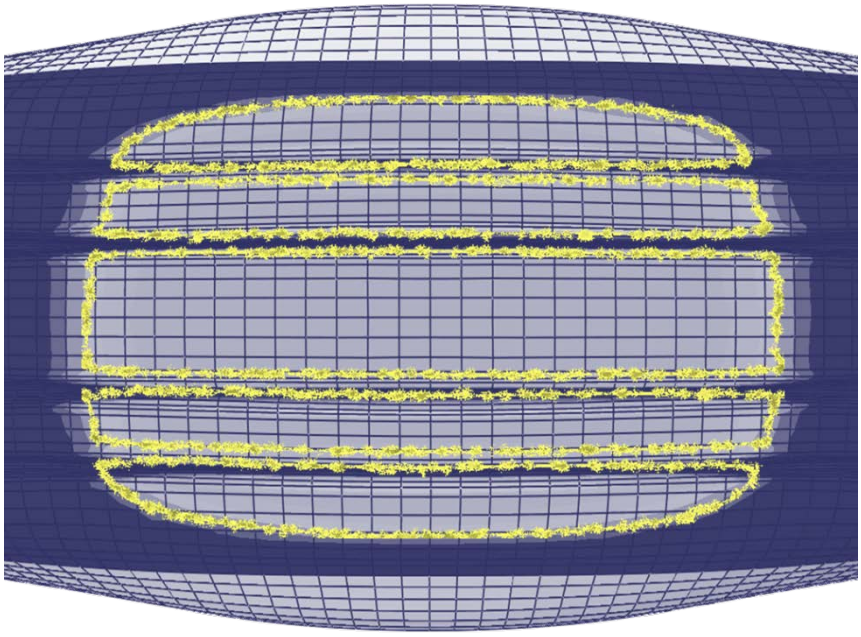

b. Correlation of footprint in detailed model

Figure 5.28. Correlation of footprint for simplified and detailed models

In addition, the contact pressure was measured and based on similar procedure the correlation results are demonstrated in figure 5.29 for simplified and detailed models. The correlation result for contact area and contact pressure is also shown in table 5.9 for models with different levels of complexity.

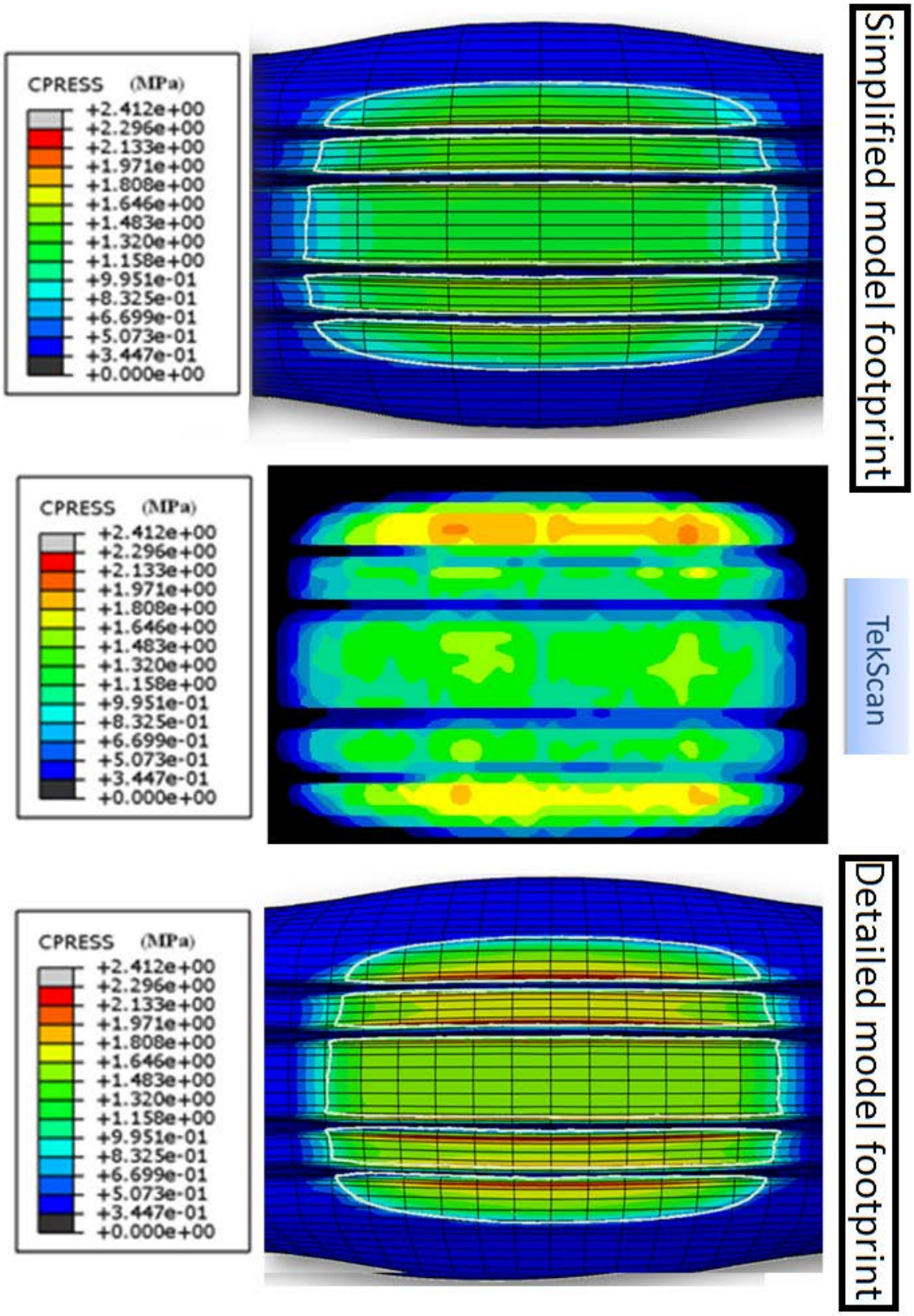

Figure 5.29. Correlation of contact pressure in simplified and detailed models

Table 5.9. Correlation of profile check for simplified and detailed model

	Contact Area (mm^2)	Percentage of deviation from test %	Max Contact Pressure (MPa)	Percentage of deviation from test %
Simplified model Constant inflation	115270	7.31	3.199	39.33
Detailed model Constant inflation	113150	5.33	2.414	5.14
Simplified model Varying inflation	114560	6.65	3.36	46.34
Detailed model Varying inflation	109782	2.20	2.31	0.61
Test Results	107419		2.296	

The correlation study resulted in an accurate prediction of the footprint area with less than 2% prediction error in the contact patch width and less than 5% deviation in contact patch length in all FE models. The contact pressure correlation is not generally good since the actual material property for tread is not used in simplified models. The detailed model with varying inflation pressure provides the highest accuracy among the rest of models in terms of contact area as well as the contact pressure. The reason for the excellent accuracy is the usage of actual tread material properties instead of a general rubber property in material definition, the more realistic contact area due to amended inflation pressure, and less distortion and stability in tread elements particularly near the grooves, where the elements were intentionally refined to avoid excessive distortion in that region.

5.5.4 Burst

The burst test is a legal requirement for certification of aircraft tyres and is an indication of the tyre to sustain the loads experienced in the landing/taking off manoeuvres. Each new tyre design has to pass the burst test to receive certification. The procedure of hydraulic burst test is based on pumping water into the tyre to increase its internal pressure until burst occurs starting from somewhere on the tyre profile – where the burst is initiated

depends on the tyre construction, material orientation, and material properties. Water was used to inflate the tyre cavity in order to provide safer test, stable inflation pressure because of higher density, and finally the leakage is effectively observable. The test location in DATL is shown in figure 5.30.

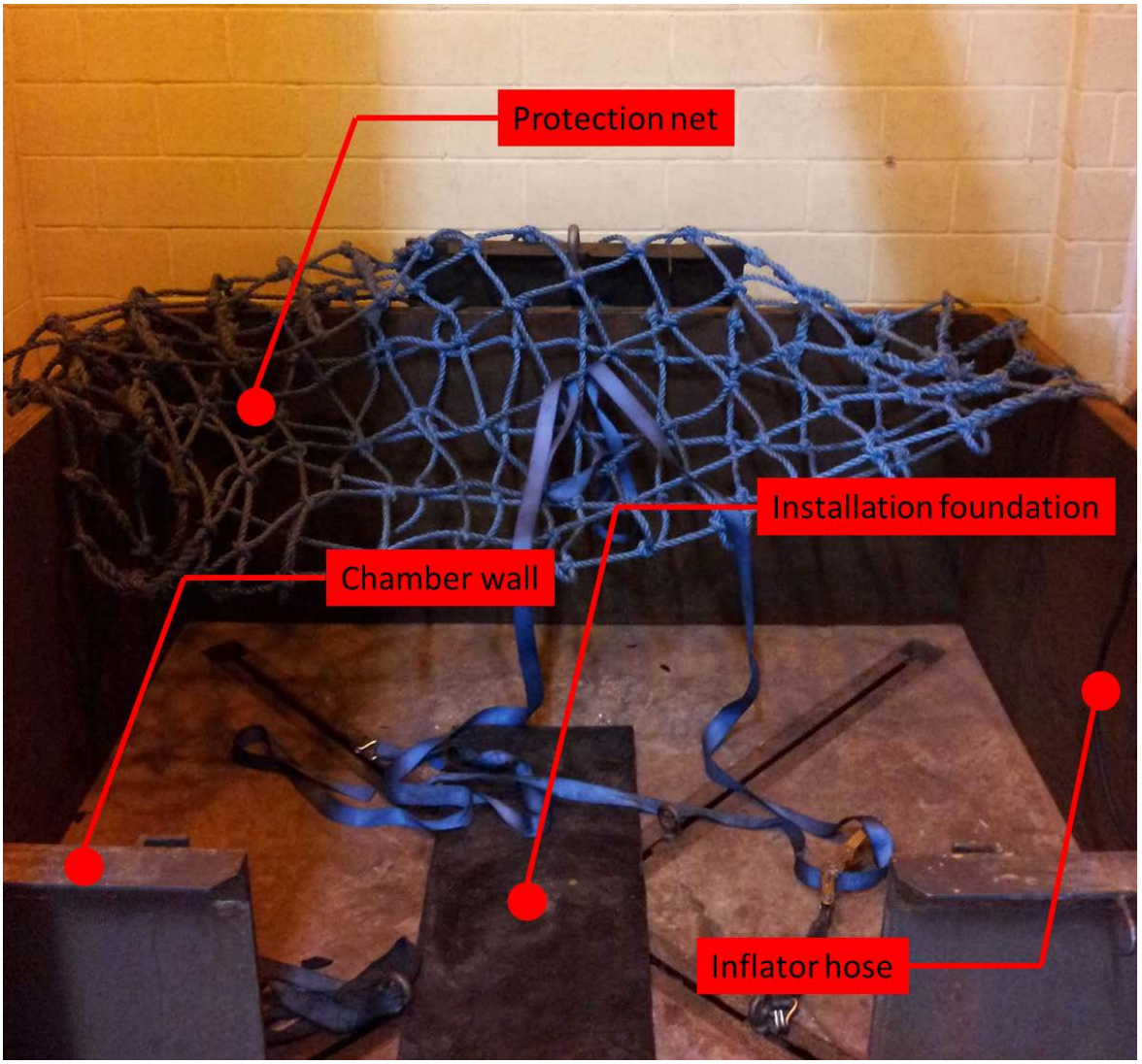

Figure 5.30. Test chamber facility in DATL to conduct burst test

For simulation of burst in finite element, the tyre inflation pressure that is applied on the inner liner was increased until it achieved a certain pressure where the burst criteria (normally 4 times of rated pressure) were satisfied. By definition, it is assumed that burst occurs in the condition that the Von Mises stress in cords exceeds the ultimate strength of

the cord material, as it was previously tested in material modelling chapter. It is rather simple to directly compare the normal stress in a cord with its ultimate strength since cords undergo unidirectional simple load only and bending stiffness can be neglected. The other failure modes such as fatigue, creep, or impact load do not apply since the burst test is performed under gradual incremental load at ambient temperature. A similar mesh density was assigned to the rubber region, cord, and bead elements in simplified to detailed models. The aim of this simulation was to understand if the simplified and detailed models were capable of simulating the real tests. To validate the reliability and accuracy of FE models, burst simulation results and failure mode were compared to what it was observed from the burst test.

The burst pressure in the physical burst test occurred at 7.8 MPa and 5.5 MPa inflation pressure for military aircraft tyre and civil aircraft tyre respectively. In simulation, the inflation pressure directly applied on inner liner of the tyres and the pressure was progressively increased in order to meet the failure criteria as discussed in above paragraphs. The step size in Abaqus/Standard for pressure increment was permitted to be calculated automatically owing to solver preferences for faster solution.

A similar mesh density strategy was configured for meshing the models with different rubber region models. This can lead to a more consistent result particularly in stresses although the mesh shape will not be identical due to geometrical partitioning in detailed models. The mesh seed size were configured to 2mm, 12mm, 2mm for bead, rubber and fabric respectively in military and civil aircraft tyre models. These sizes restrict the maximum edge size of each hexahedral element, but the minimum size of the elements are controlled by the geometry, partitioning, and sharp edges across the tyre section.

An input deck file (INP file) of model mesh and preferences containing necessary information for Abaqus solver was submitted to the Abaqus solver. The solution was reported to the Abaqus Visualisation mode in order to extract the stress and deformation results from nodes and elements. A demonstration of burst simulation for military aircraft tyre is shown in figure 5.31, in which the X and Y-coordinates represent inflation pressure in MPa and maximum Von Mises stress in MPa is shown as well. In this figure, the ultimate strength in cords was plotted in green to show the failure criteria, and the maximum pressure at burst test is the vertical line in purple. Figures 5.32 and 5.33 show the maximum displacement in the tyre structure and maximum von Mises stress respectively in FE simulation of civil aircraft tyre when the inflation was varied from deflated shape to 6 MPa. Three curves were plotted to show the comparison of maximum stress in cords and maximum deformation in tyre components for simplified, regular, and detailed FE models. The burst simulation for a 2D full section FE model is also illustrated in the same plot.

In general, the deformation in FE models are closely correlated and overlaid for models with different complexity in rubber compound since the considerable portion of tyre vertical stiffness comes from the inflator and cords configuration. However, the maximum von Mises stress in cords varies across FE models with different rubber compounds. The maximum stress is also sensitive to the mesh size inasmuch as the possible excessive distortion at badly meshed zones or extreme refinement in elements can generate local stress concentration and maximum stress rises.

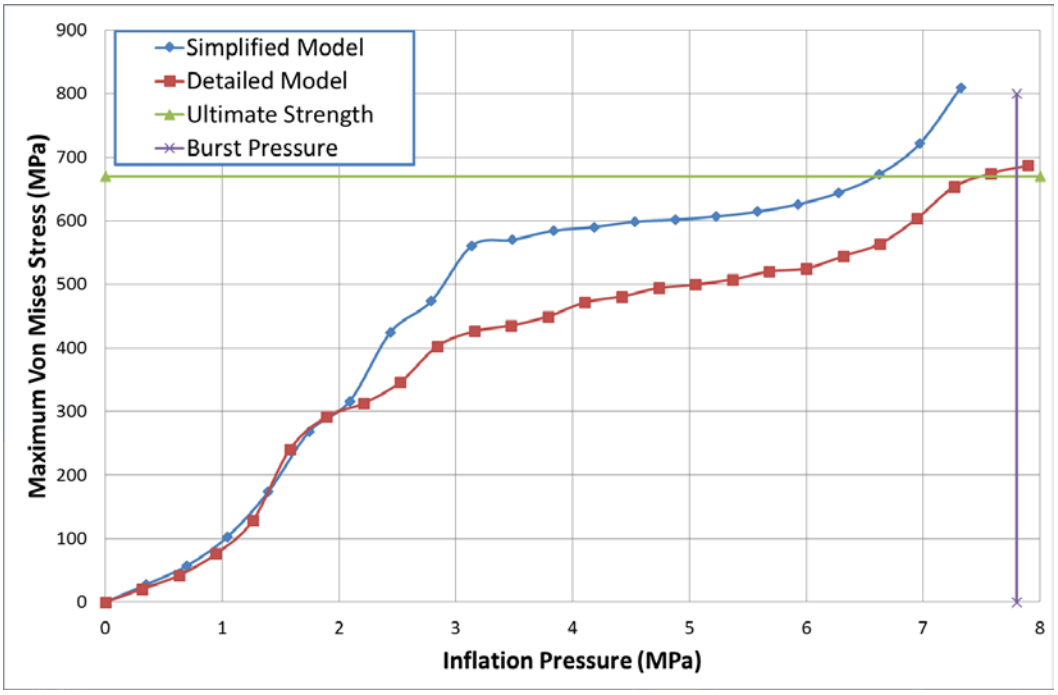

Figure 5.31. A comparison of max Von Mises stress in cords of simplified and detailed 2D models of military aircraft tyre

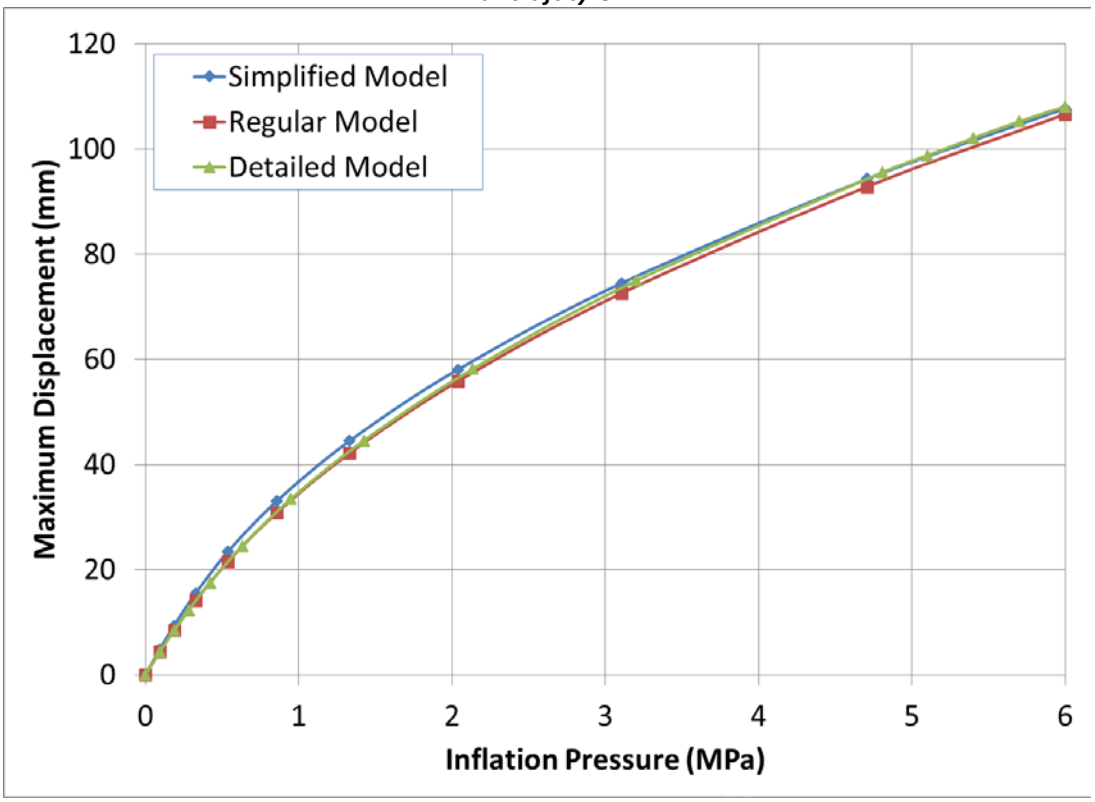

Figure 5.32. A comparison of max displacement in tyre components for simplified, regular, and detailed 2D models of civil aircraft tyre

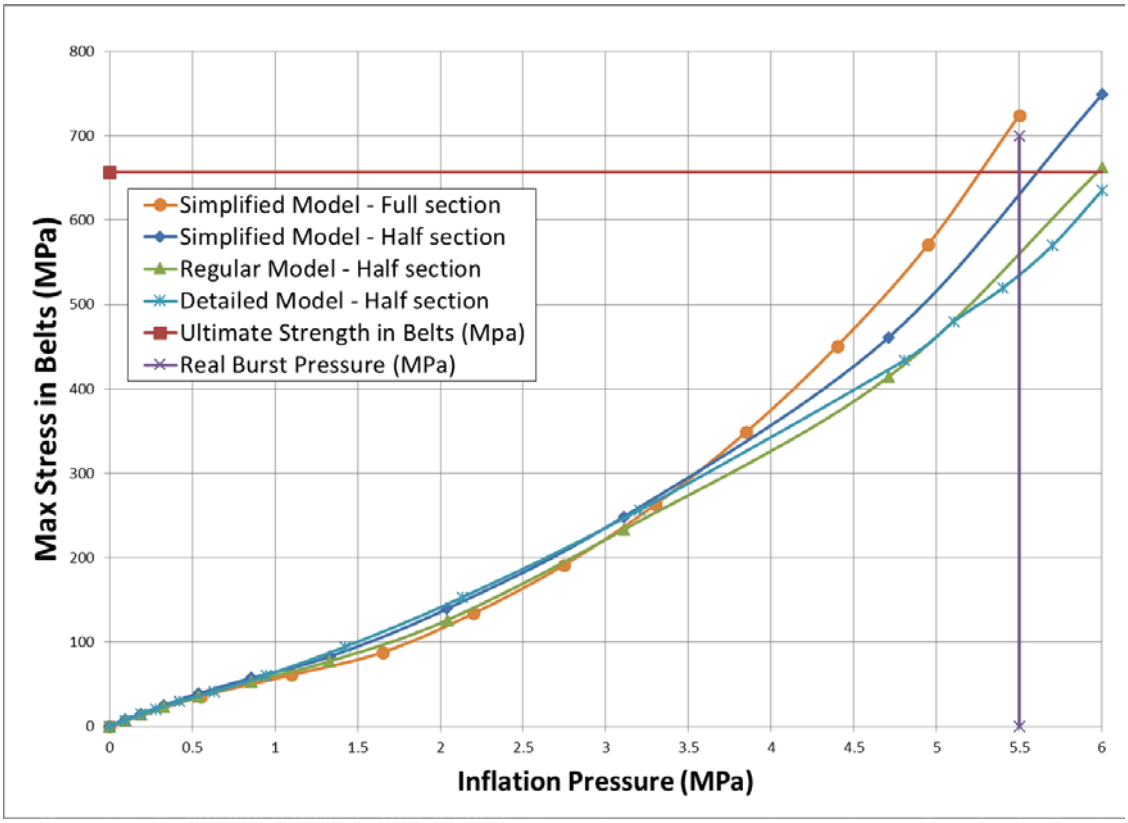

Figure 5.33. A comparison of max Von Mises stress in cords of simplified, regular, and detailed 2D models of civil aircraft tyre

A prediction of where burst initiates was also investigated through the FE simulation of both civil and military aircraft tyres. The von Mises stress in cords is shown in figures 5.34 and 5.35 for the civil and military aircraft tyres under the reported burst pressure at 5.5 and 7.8 MPa respectively. The figures indicates that the maximum von Mises stress occurs in sidewall for the civil aircraft tyre and crown for military aircraft tyre, which agrees with results obtained from burst test in DATL.

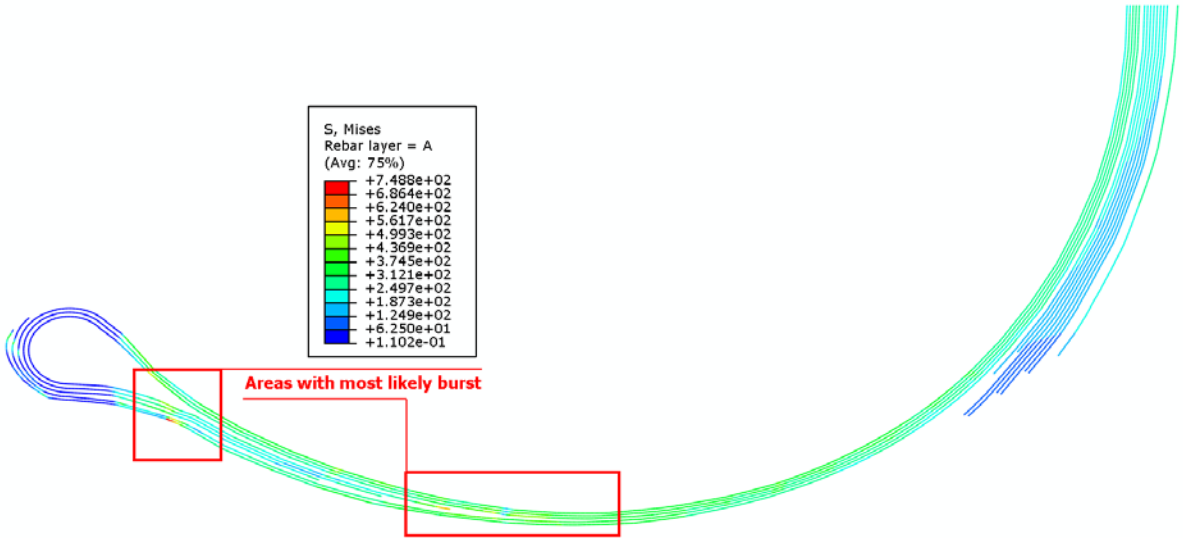

Figure 5.34. The von Mises stress in cords of civil aircraft tyre

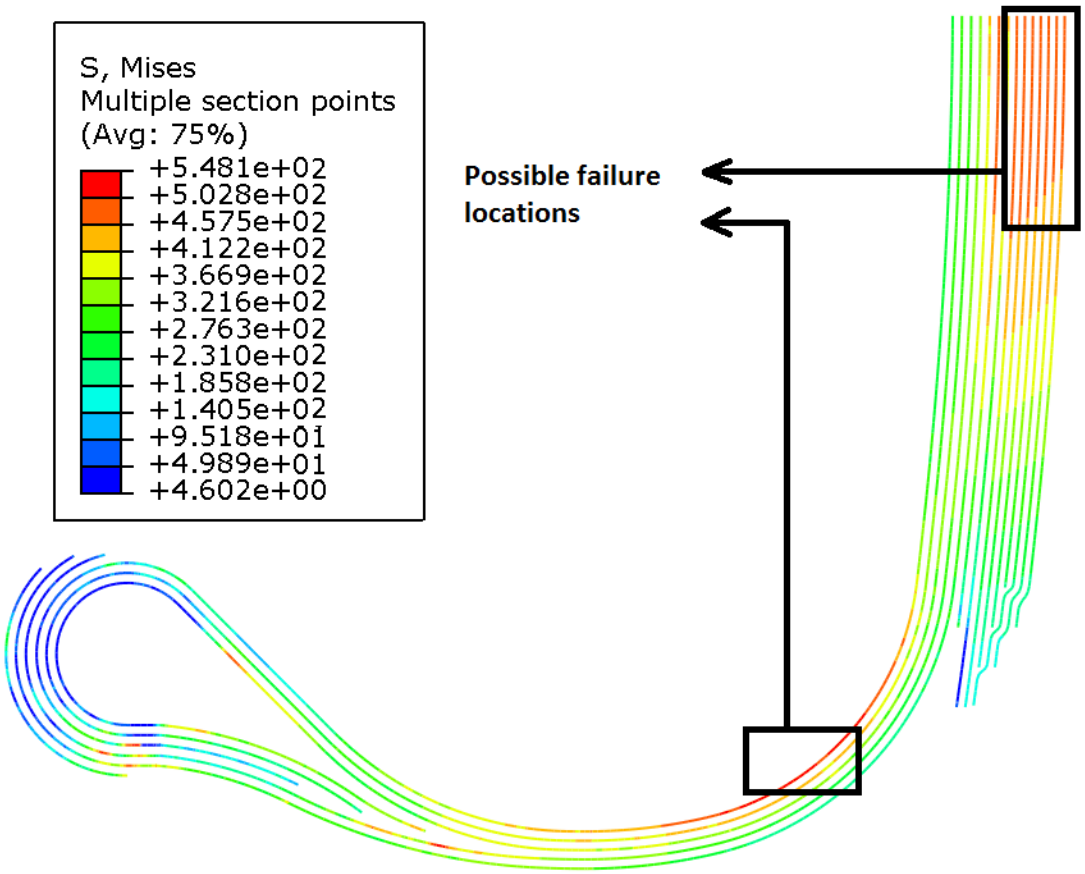

Figure 5.35. The von Mises stress in cords of military aircraft tyre

5.5.5 Inflation pressure

As previously indicated in inflator modelling section, the aircraft tyre pressure varies when load is applied due to severe change in tyre volume. The pressure was measured by the equipment in DATL. This change was simulated for the detailed FE model of 3D tyre, as shown in figure 5.36. Moreover, the improvement of load versus crown deflection in civil aircraft tyre is depicted in figure 5.37. The result shown in this figure describes the stiffening of tyre vertical response in the model with variable inflation pressure in comparison to the model with constant pressure. Furthermore, the footprint is affected since the loaded radius is compromised due to higher pressure in the tyre under similar load.

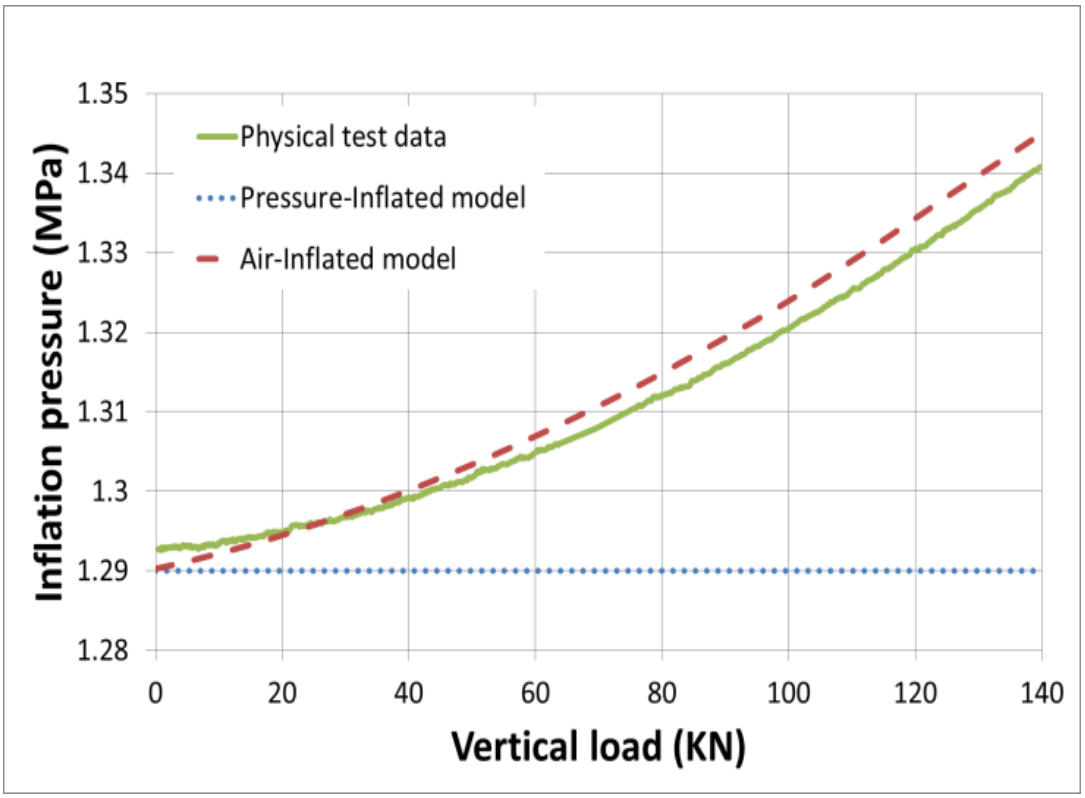

Figure 5.36. Correlation of inflation pressure change under load variation in civil aircraft tyre

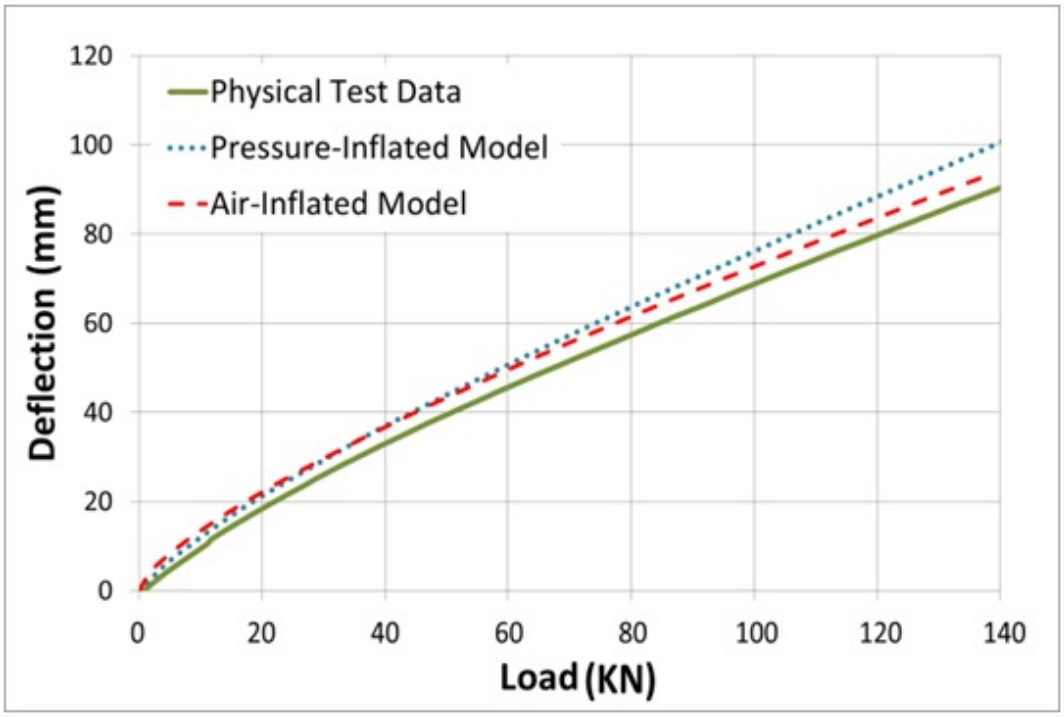

Figure 5.37. Correlation of load versus deflection simulation in civil aircraft tyre

5.5.6 Tyre forces and moments

The simulation of force and moment generation was carried out using a steady-state procedure in Abaqus, as described in analysis type section. The model procedure involves the calculation of tyre deformation under desired inflation pressure and vertical load using a static approach. The 3D deflected model was then restarted in the steady-state step where the element and node geometrical details were conditioned at the static step deformation, and the material was flown through the elements in circumferential direction of tyre. The braking/driving modes were generated by setting a constant traveling velocity for tyre on the road while the tyre rotation speed was virtually varied over a range from lower to higher than the free rolling condition where the tyre velocity and tyre loaded radius times the rotation speed are equal. In this simulation, the tyre is transferred from braking mode to driving mode and the free rolling condition is measured where the rolling force was equal to

zero ($v_x = R_l\omega$), as illustrated in figure 5.38 for the civil aircraft tyre. The results were obtained in the condition that the Coulomb friction was equal to one.

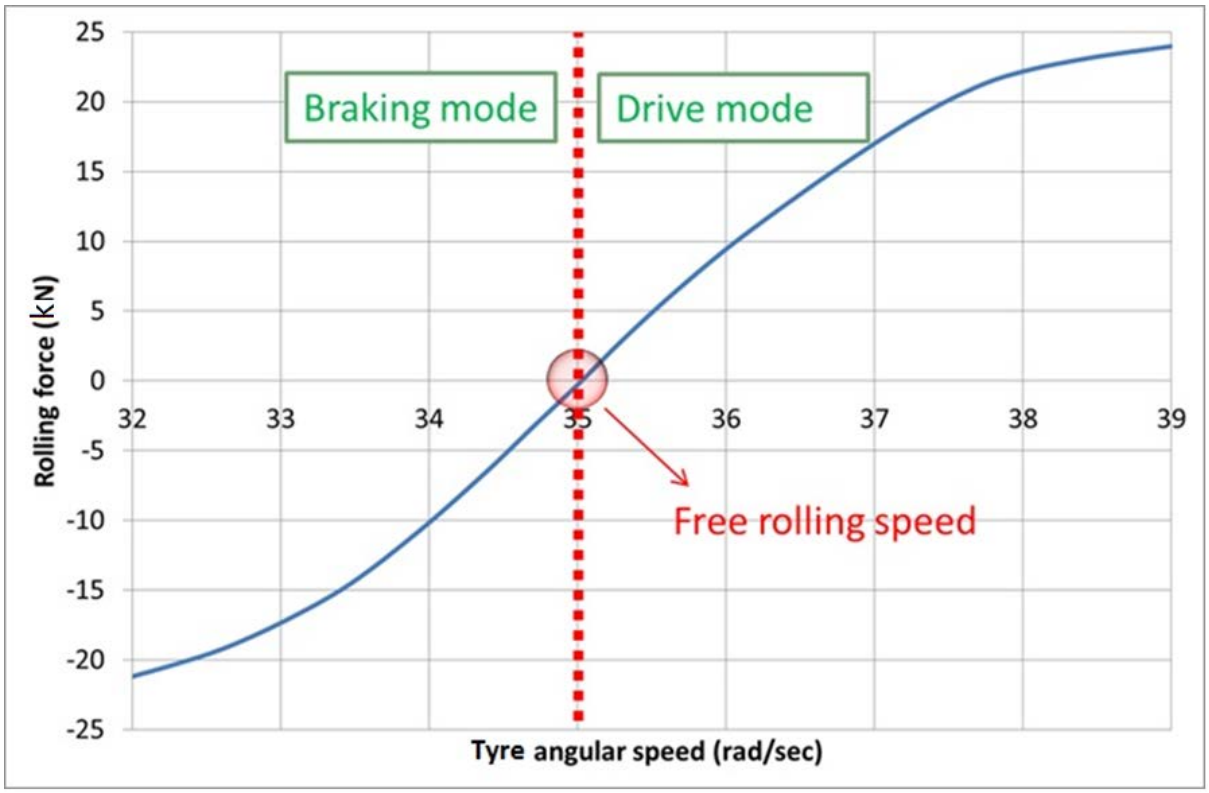

Figure 5.38. Tyre rolling simulation to find the free rolling condition

The slip ratio in free rolling condition is zero ($|v_x - R_l\omega| = 0$) and ideally the tyre is set to zero rolling moment. The details of this figure was taken from the civil aircraft tyre when it rolled under rated pressure 1.78 MPa and loaded condition of 100 kN, and the inflator was modelled in detailed 3D tyre for this simulation.

To simulate the cornering situation, the tyre was brought into the free rolling condition and was rotated around the normal to road direction to replicate the cornering condition in both positive and negative sides at tyre velocities of 1 km/h and 72 km/h. The convergence criteria was not met for the simulation at 1 km/h up to 90 deg slip angle and stopped around 30 deg according to the message received from the solver. However, the simulation

was completed at speed of 72 km/h and similar trend can be seen to the well-known tyre behaviour under cornering situation as presented in figure 5.39. This simulation was carried out under the rated inflation pressure, 100 kN vertical load, and coefficient of friction of one.

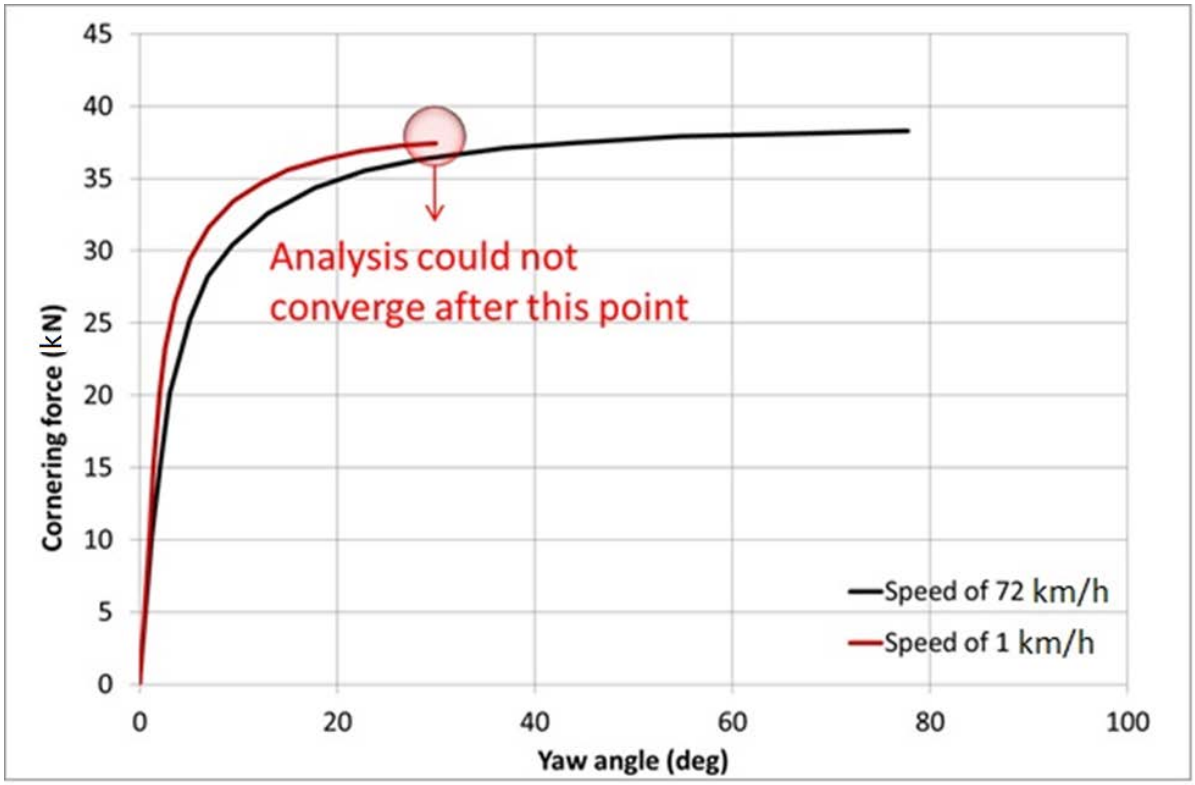

Figure 5.39. Simulation of cornering condition in civil aircraft tyre

The same simulation was carried out under vertical loads 20 kN, 40 kN, and 60 kN at speed of 10 km/h, and results are illustrated in figure 5.40. Aligning moments were also obtained under 100 kN vertical load and forward tyre velocities of 1 km/h and 72 km/h in figure 5.41.

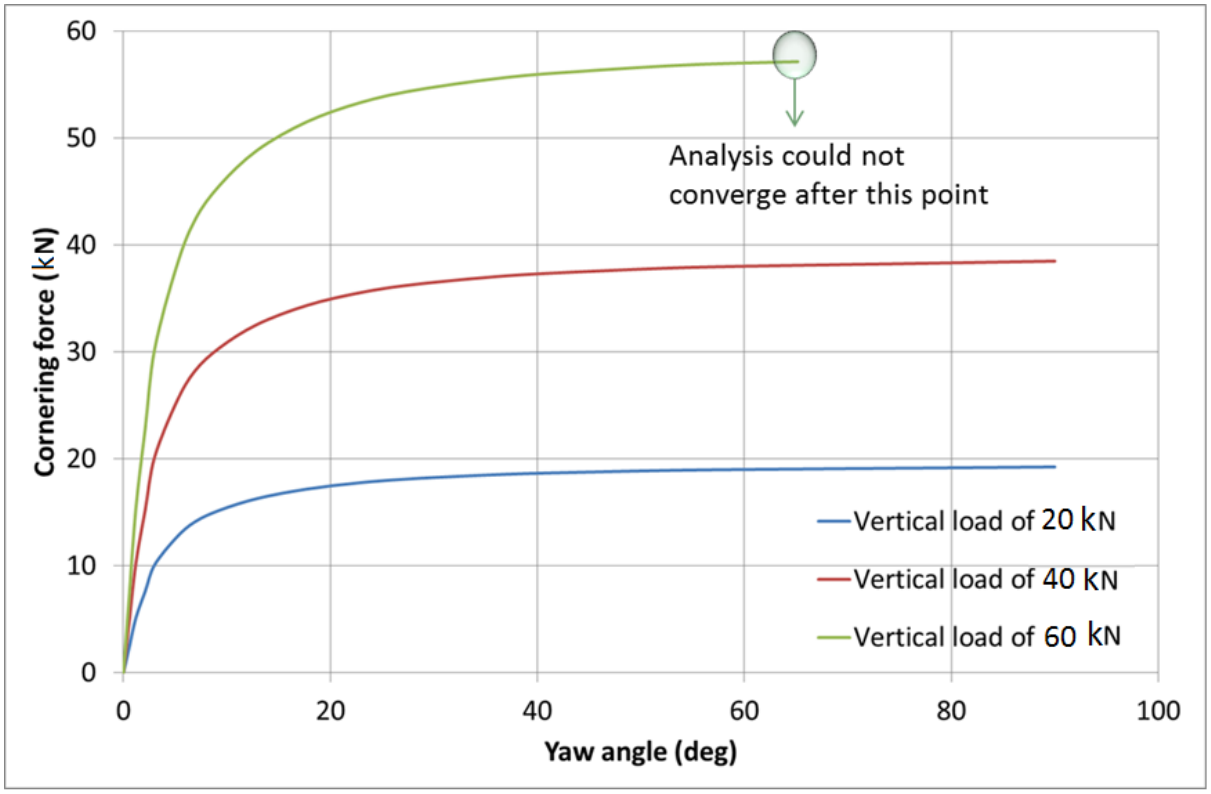

Figure 5.40. Simulation of cornering condition at different loads in civil aircraft tyre at 10 km/h

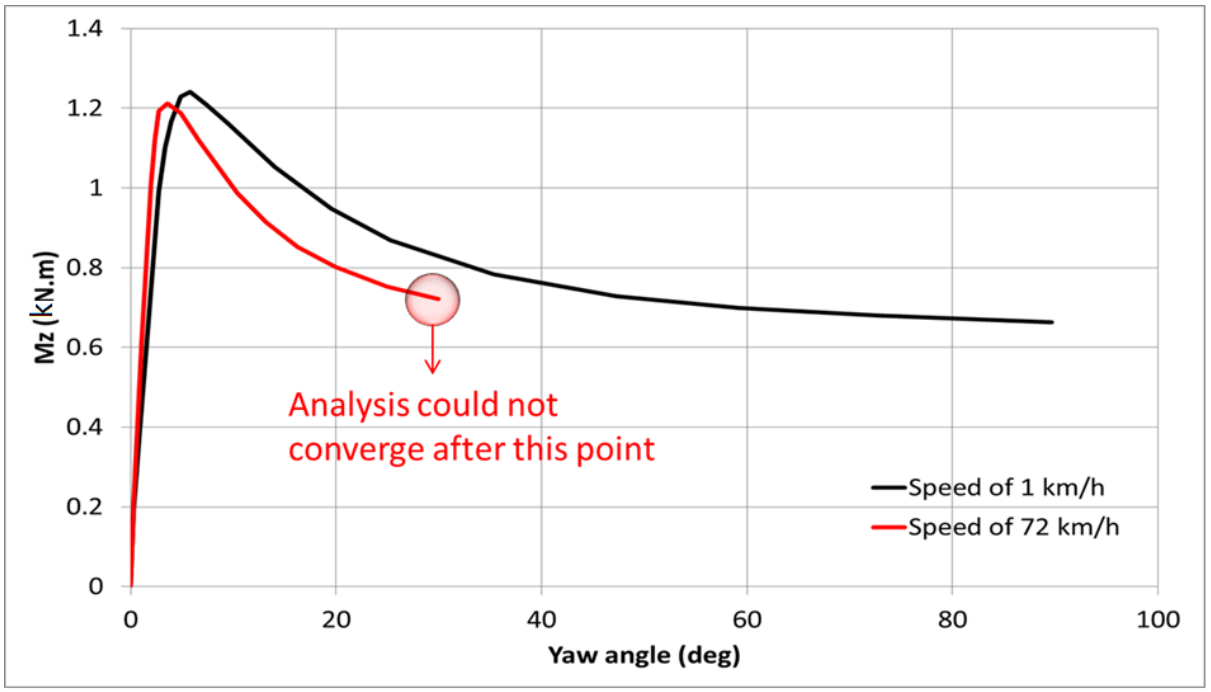

Figure 5.41. Aligning moment in civil aircraft tyre at 100 kN

5.5.7 Thermo-mechanical tyre model

The rolling tyre will stop after travelling a certain distance when it is freely rolled under vertical loading condition. This phenomenon is due to the kinetic energy dissipation from a number of sources such as air drag, rubber viscoelasticity, frictional and adhesive forces, and tyre/road geometry deformation. A combination of these forces is summed up to form the rolling resistance force against the tyre motion. The major resistance forces that make the most contribution to energy dissipation are friction force and material dissipative behaviour. The frictional forces become important when lateral or longitudinal slips are generated across the contact patch in cornering or braking/traction manoeuvres.

The hysteretic behaviour of rubber in deformation occurs where the tyre is in dynamic deformation under tri-axial loading condition and its magnitude is directly correlated with the rate and amplitude of deformation. In this research, the energy dissipation and heat build-up due to hysteretic behaviour of rubber were studied using the viscoelastic material behaviour, of which data was obtained from works at University of Birmingham (Yang, 2011). The relaxation test procedure, which conforms to SAE standard 6914 as described in material modelling chapter, was employed to characterise the Prony series modelling of viscoelasticity. Abaqus Material Evaluation toolbox was used to calculate the coefficients of Prony series. The relaxation test results and Prony series prediction of the viscoelastic behaviour in rubber is shown in figure 5.42 for tread and sidewall and figure 5.43 for sidewall.

The simulation was initially started with running tyre on the flat rigid surface without the thermal effects in order to get the stability in solution. This step is the essential in explicit analysis step in order to bring the tyre to equilibrium before the dissipative model is

deployed. The thermal effect by viscoelasticity was then added into the simulation to find out how the tyre temperature was built-up. The circumferential meshing segments were also refined and made uniform for this simulation since the tyre is supposed to roll on the rigid road and similar refinement level is required across the tyre circumference when the tyre rolls on the road unlike what was simulated in steady-state analysis procedure.

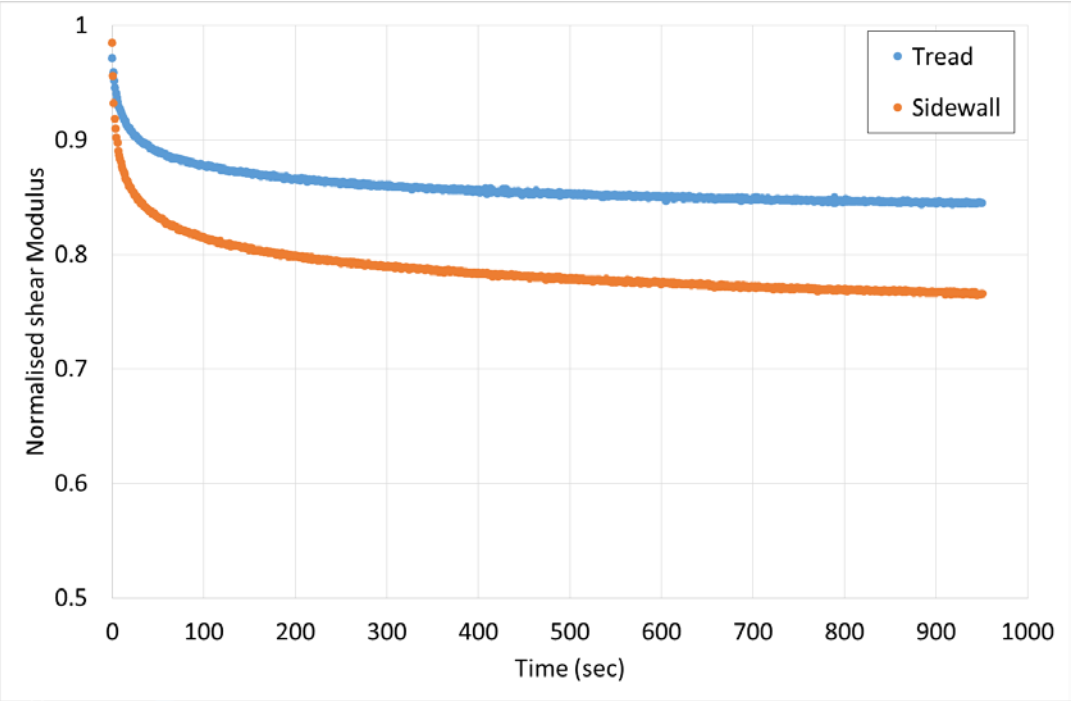

Figure 5.42. A sample relaxation test on tread and sidewall rubber (Yang, 2011)

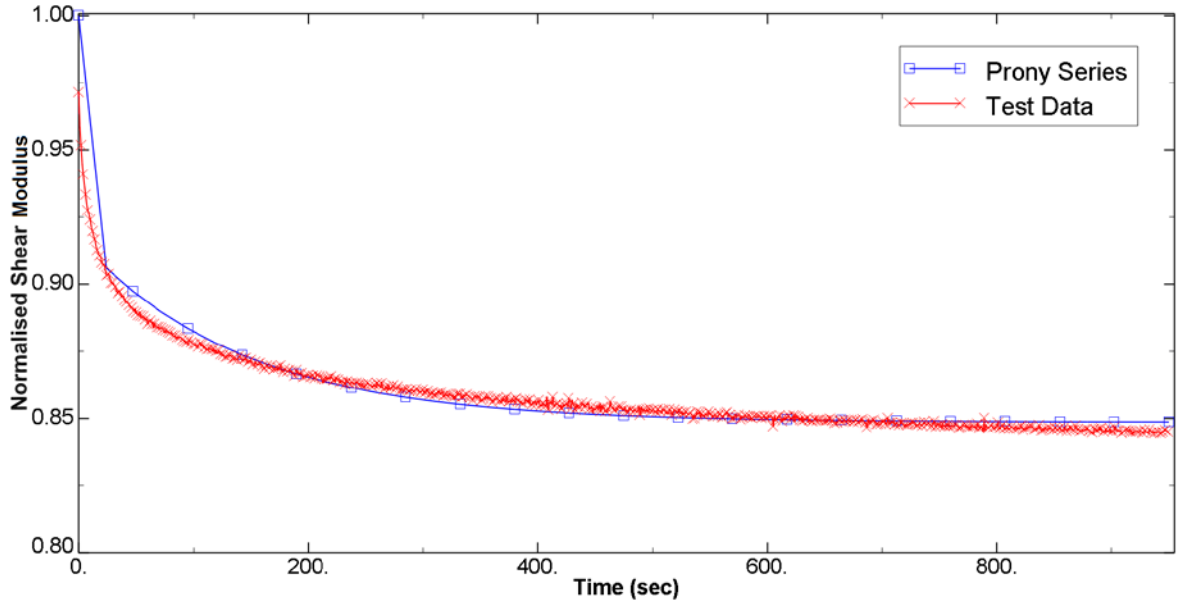

Figure 5.43. Characterisation of Prony series for tread rubber viscoelasticity

When the equilibrium condition was satisfied in free rolling explicit analysis, the new step was run while having the viscoelasticity implemented as material behaviour in the rubber compounds. The tyre was then rolled on an analytical flat road and a thermo-mechanical analysis was performed based on an explicit approach for 200 seconds under three vertical loads [50,100,150] kN, three speeds [10,30,50] km/h, and rated inflation pressure of 1.29 MPa.

The temperature in tyre cross section rises under the cyclic excitation because of the deflection mechanism when the tyre rolls under load. The temperature increase in tyre cross-section after 200 seconds of rolling is shown in figure 5.44 at 150 kN vertical load and 30 km/h traveling velocity. In rolling condition, the tyre cross section is frequently subjected to deformation/relaxation, so that the hysteretic loop is built in which the energy is dissipated in the form of heat. Here is where the viscoelastic material model is employed to compute the dissipated heat per cyclic deformation. As shown in figure 5.44, the more the tyre is deformed, the more the heat is build-up and temperature rises quicker in areas closer

to higher deformation. Mid-sidewall, shoulders and heel area are of the highest chance in temperature increase due to the bending deformation which occurs along.

Furthermore, figures 5.45 and 5.46 illustrate the maximum temperature increase in cross-section for different vertical loads and varying velocities. Figure 5.45 demonstrates that heat generation speeds up in higher loads. This is due to the higher deformation that the tyre cross section is exposed under higher vertical loads. In addition, the maximum temperature in cross section increases with higher rates when tyre rolls at higher speeds because of the quicker heat generation at higher frequencies, as shown in figure 5.46.

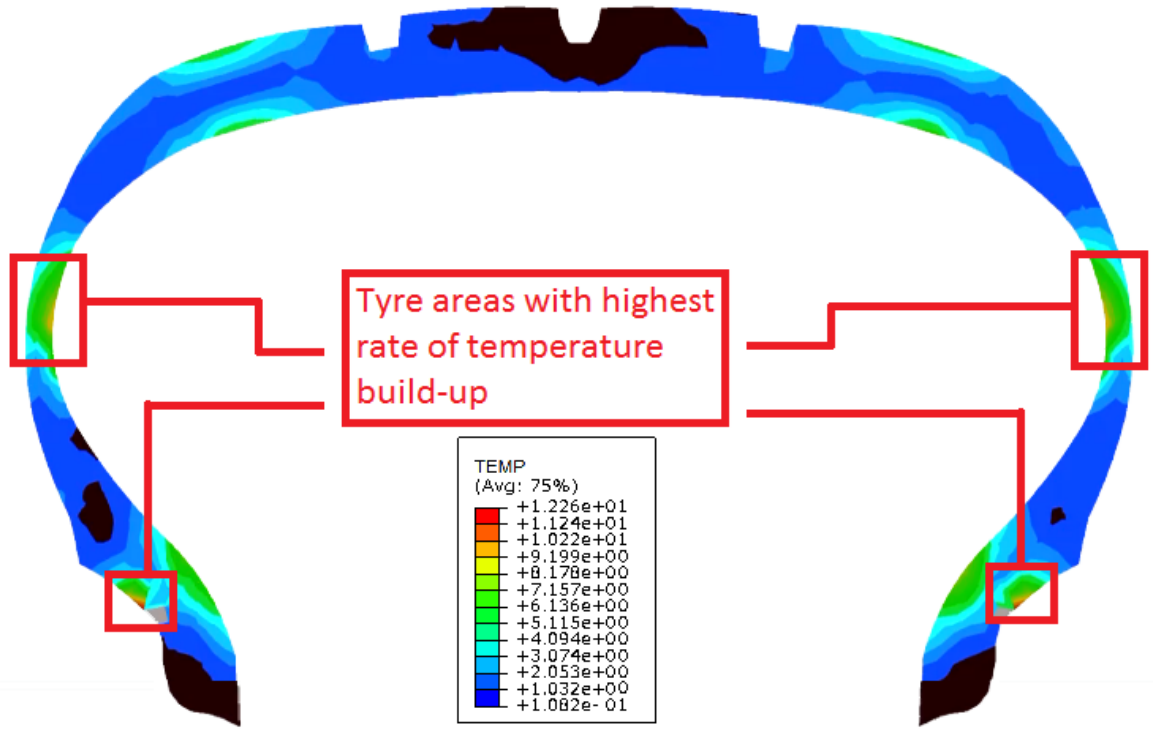

Figure 5.44. Temperature increase in rolling tyre after 200 seconds rolling

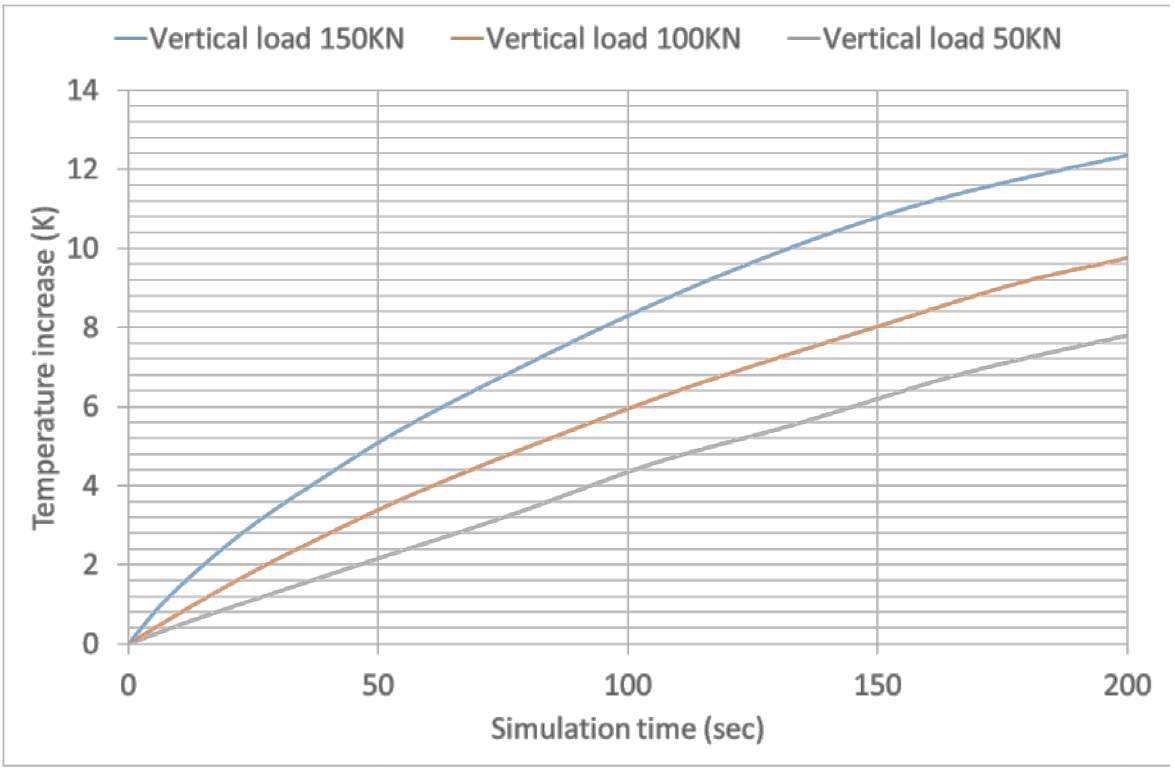

Figure 5.45. Temperature increase in time domain in varying vertical load and 30 km/h velocity

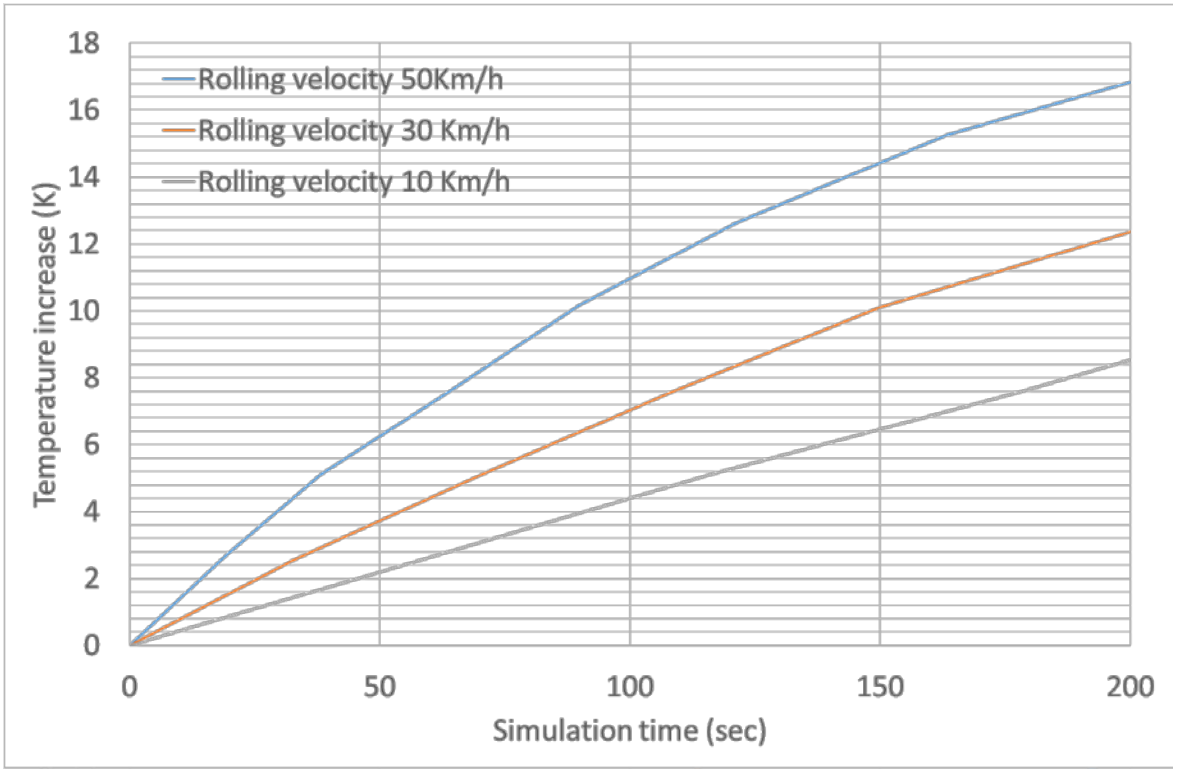

Figure 5.46. Temperature increase in time domain in varying velocities and 150 kN vertical load

To confirm whether the temperature rise trend from the FE analysis is correlated with relative experimentation from literature, the works by (Clark & Dodge, 1982) was used for comparison. As discussed in chapter 3, Clark et. al. mounted thermocouples inside the rubber compound in locations indicated with solid circles in figure 5.47 to measure the temperature build-up inside the tyre compound under the free rolling condition.

The tyre was then rolled for 200 seconds and the temperature rise was recorded for thermocouples inside the rubber compound at 6 representative locations A, B, C, D, E, and F. These locations are shown in figure 5.48, which each location includes three thermocouple spots in tread, carcass, and inner liner. The temperature rise in those spots is illustrated in figure 5.48.

Points C, D, and E demonstrated the highest rise between the locations according to the curves shown in figure 5.49. The temperature increase from the finite element solution as shown in figure 5.44 also confirms a similar trend in temperature build-up for the sidewall area as indicated in figure 5.49.

The magnitude of temperature rise does not match exactly the same magnitude as reported in literature due to the different structure, geometry, and rubber properties in the tyre used in this research and the one in Clark's works. However, a similar trend in the temperature rise was observed for both tyres as it can be seen from figures 5.45 and 5.49. The temperature rise in both tyres is not quite linear and a quadratic form is a better representation for what occurs during the heat build-up.

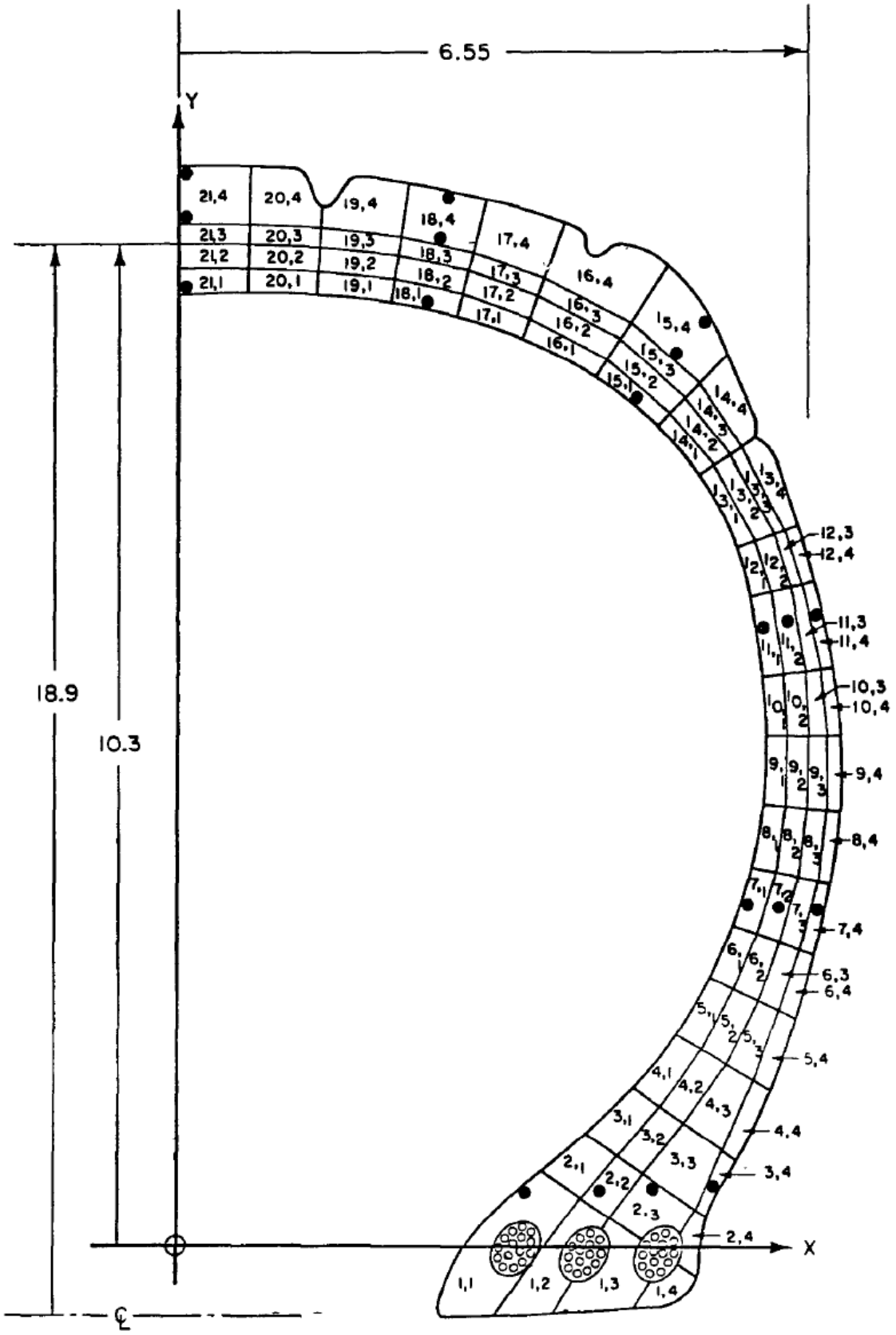

Figure 5.47. Tyre section used for temperature measurement (Clark & Dodge, 1982)

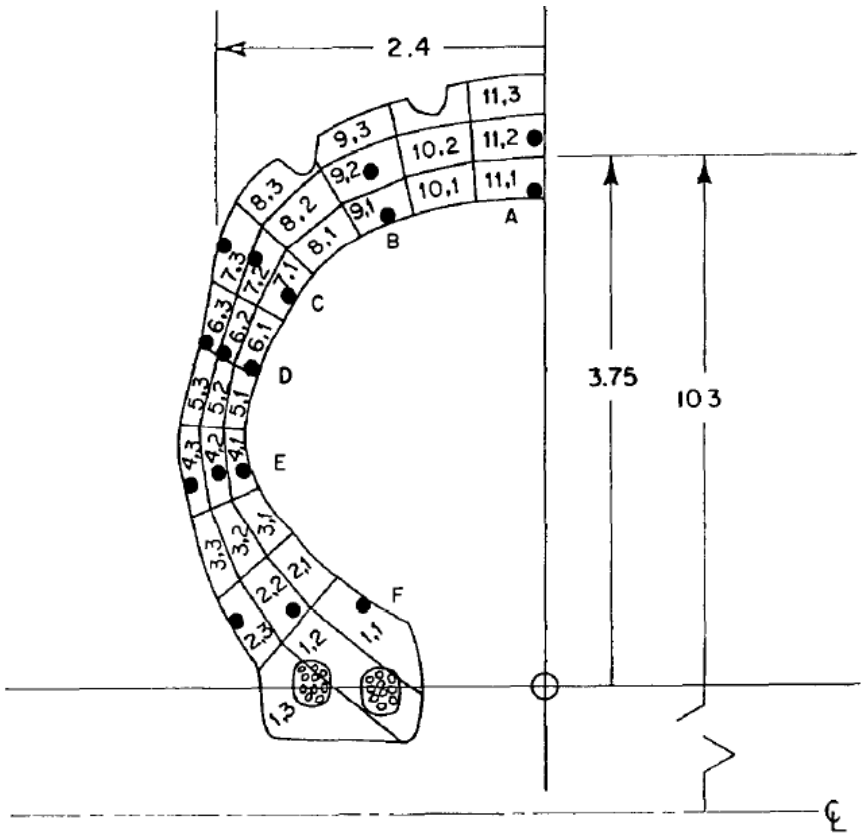

Figure 5.48. Locations in tyre section where the thermocouples were burried (Clark & Dodge, 1982)

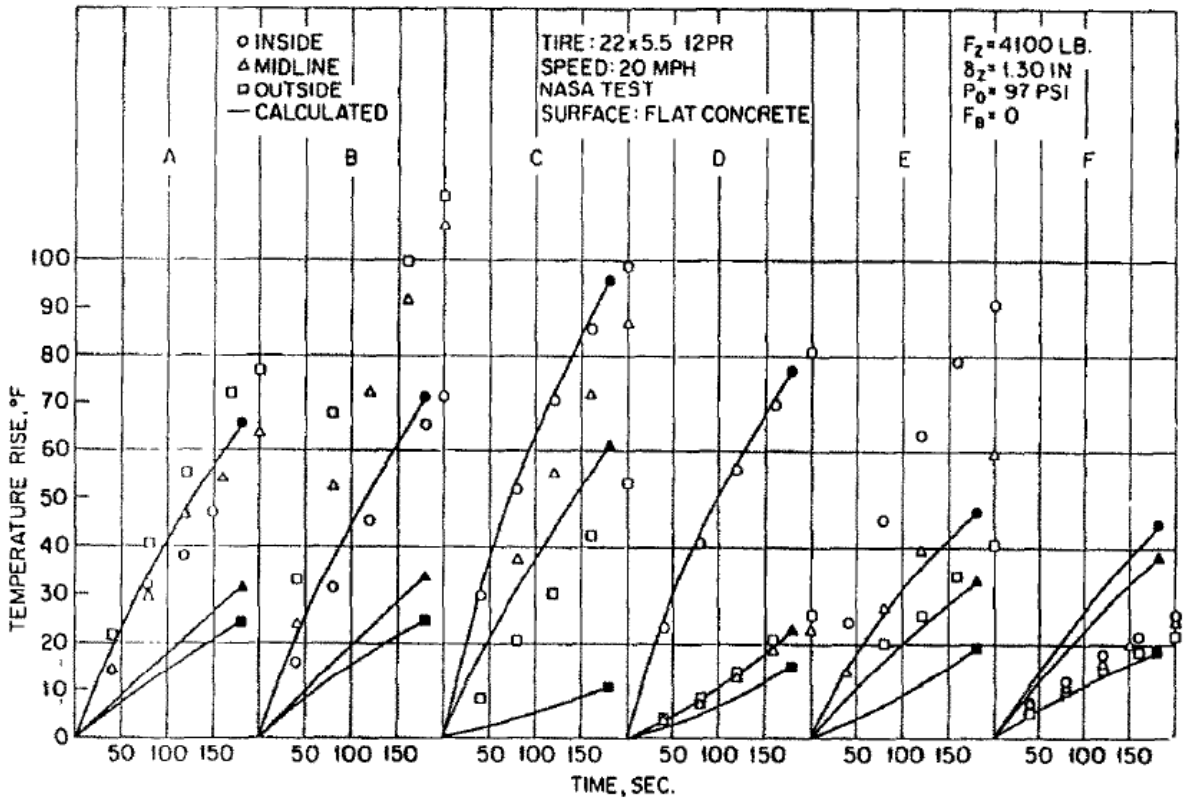

Figure 5.49. Temperature rise in thermocouples corresponding to the points indicated in figure 5.48 (Clark & Dodge, 1982)

5.6. Summary

In this chapter, the FE approach was explained to identify effective parameters and a wide range of FE simulations was implemented. Tyre structural detail was investigated to obtain a better understanding of the layer interaction and help in selection of the reinforced layer modelling in Finite Element. General approaches in modelling of tyre structure detail were studied and the rebar element approach was selected as the most appropriate technique for modelling of the uniaxial reinforcement in such a complicated structural configuration as aircraft tyres with many plies of cords and topping rubbers.

Moreover, the simplified and detailed representation of rubber compounds in civil and military aircraft tyres were developed to study the influence of rubber compound in tyre deformation and generated stresses and the tyre model was inflated into the same high pressure for comparison of models behaviour near burst. The result of simulations suggested that the influence of detail modelling of rubber region can be ignored while the stress varies to a high amount if the correct material property is not used to corresponding region as expected.

The correlation study was carried out in four steps: profile sizing check after inflation, burst test, sidewall deformation under vertical loading, inflator modelling, and tyre footprint. The FE models showed that it is capable of accurately predicting where and at what inflation pressure the burst occurs. The tyre profile was checked after inflation to correlate the cross-section measurements such as diameter and tread/sidewall extension after inflation, and tyre deformation in this simulation demonstrated excellent correlation for the sizing check. Footprint area and contact pressure were correlated to those from measurements. Both simplified and detailed models showed a good agreement in terms of the footprint shape,

but the detailed FE model presented a better correlation for the contact pressure. Inflator gas was modelled here as ideal gas using the hydrostatic elements and this definition helped to a better correlation of above parameters such as footprint and prediction of load-deflection mechanism.

Furthermore, a comparison study was carried out on the test results 2D and 3D FE models with symmetrical loading. Both model outputs in terms of structural deflections and stresses demonstrated a close agreement in trend and magnitude across a wide range of inflation pressure. This advantage can lead to the conclusion that the 2D FE model can be replaced for simulations such as burst test, in which the load is symmetrically applied in circumferential direction.

A mesh sensitivity analysis was conducted to find the appropriate mesh size in rubber, cords, and beads regions separately. A full matrix of civil aircraft tyre 2D models was generated with different mesh sizes, and the same simulation of tyre inflation up to the burst pressure was applied and submitted to the solver. The results suggested a good match between the different models in terms of the deformation, but the maximum von Mises stress deviation in all regions escalates at pressures higher than 3 MPa. This was thought to be due to the mesh disparity and dissimilar mesh grid distribution across the regions, so that dissimilar distortion in elements occurred and lead into deviation in the stress results of higher pressures.

Since the accuracy in prediction of tyre mechanical behaviour in FE model was validated through the correlation study, the simulation was extended further in order to predict the forces and moments generated across the contact patch. The overall trend of the predicted force and moments demonstrated a similar trend to those forces and moments generated

from the tyre test under lateral and longitudinal slip. However, the magnitude of the predicted forces and moments has a close relation with the employed friction model and its accuracy. Since a friction model is not available through tyre testing at DATL, the simulations could not be correlated with real-world test data.

In addition, the tyre thermal behaviour in free rolling condition was predicted using the idea of energy dissipation in hysteretic loops of rubber materials with viscoelastic behaviour. The models illustrated a load and velocity dependency; however, the velocity dependency of thermal behaviour can be ignored when the thermal data are plotted versus the travelled distance instead of time. The thermal model predicted the highest temperature increase in areas around the sidewall where the maximum deformation and relaxation occurs, and this prediction is in line with overall trends as reported in literature.

Chapter 6: Tyre Analysis Interface System

6.1. Introduction

In this chapter, the necessity of a specialised interface for design and development of brand new tyres is discussed. In section two, the algorithm to bring the FE and CAD capabilities together and integrate them for the benefit of the new tyre analysis package is explained. In continuation of section two, the algorithm of an automated tyre analysis interface is implemented and the user interface dialogue box and the software capabilities are introduced.

6.1.1 Motivation

The number of FE commercial package users is rapidly increasing within industry, academia, and research centres because of its huge reduction in the cost of designing new tyres by generating valued virtual prototypes, shortened time for product development and evaluation, and saved time, efforts, and dedicated personnel. However, very few commercial packages are available in the public domain that are exclusively equipped with tyre analysis toolboxes or specialised functionality, such as SIMULIA/Abaqus™ and FTire. On the other hand, effective use of such software requires a depth of knowledge in FE analysis techniques, so that non-expert users usually find difficulties to address the challenges in employing the available tools for tyre analysis.

In most cases, the interface of commercial packages themselves is not interactive and user-friendly due to focus on the analysis and complexity of models. As a case in point, SIMULIA/Abaqus provides a specialised interface for analysing the tyre mechanical behaviour, but most of the capabilities for analysis of tyre behaviour have been developed through the functions that are not visible in Abaqus/CAE. Three dimensional analysis of tyre requires codes to be manually written in INP deck files instead of being available in user

friendly dialogue boxes. This brings ambiguity and confusion for average users. Other software such as FTire™ and MF-Tyre™ do not provide the type of details that an FE package such as Abaqus™ can furnish in terms of design and analysis.

An evidence of the complexity of analysis using FE method is the number of online forums, consultants, and technical support departments that provide assistance and technical services to overcome such difficulties encountered by users in FE analysis. It follows that simplification of the user interface and hiding the tailored tyre analysis knowledge in the background will provide interactive tools for beginners, designers, and non-expert engineers to focus on design and development instead of struggling with commercial packages to make them work. The difference will be having results of FE analysis in a more reliable and efficient way in hand for further postprocessing and design synthesis. This can substantially improve the productivity by splitting the tasks to separate expert FE model developers and users of its application. On the other hand, the danger of a non-expert users being able to employ the professional environment of FE analysis is the concern when a working approach is generalised to the other tyres or operating scenarios while it requires deep investigation and understanding the comprehensive technical aspects. In addition, the required time to resolve the issues will decrease the overall productivity of the new product design procedure.

6.1.2 Objective

The goal in this chapter is to develop software which will make the capabilities of commercial FE tools such as Abaqus available through a simpler user interface which is designed specifically for tyre design analysis. The interface will benefit from the expertise and experience of a professional FE and tyre analyst in order to facilitate the use of the

software in a tailor-made manner for users. The user interface will be equipped with functionalities to automate the standard procedure of tyre mechanical and thermal analysis in a virtual environment.

6.1.3 Criteria

The software structure is expected to deliver an interface that satisfies a number of criteria: flexibility, simplicity, and reliability.

Flexibility. Analysis of a complex structure such as a tyre needs flexible tools to allow innovation by adaptation of practical knowledge. On the other hand, implementation of new ideas demands adaptable FE software for new tasks. As a case in point, the user interface is expected to be capable of offering alternative methods in modelling material for different applications.

Simplicity. The developed interface is desired to be simple and friendly for tyre designers who are unfamiliar with FE tools to employ this software for evaluation of brand-new designs or improvement of existing designs.

Reliability. Developed software must be checked for its validity over a reasonable number of sizing checks or manoeuvres in order to prove its reliability when it is employed on new designs.

6.2. Algorithm

The algorithm for tyre analysis interface was designed based on Abaqus capabilities; i.e. Abaqus is still used as the solver and core element in the whole analysis procedure. Following this approach, Abaqus functionalities are employed for meshing, providing solution to the problem, and post-processing of the results, which are successively executed

in an automated manner. The overall algorithm of the automated analysis procedures is demonstrated in figure 6.1. The user who can be a tyre designer or analyst provides the inputs to the input interface and determines what output from the FE simulation they are interested in. Once the input/output parameters are defined, possible errors in input/outputs are detected and corrected; the INP deck file is generated using the input geometry and input/output variables. The INP deck file is checked before it is submitted to the solver. The Abaqus Solver is employed to provide a solution to the submitted input deck file and the output is fed into the post-processing module. The desired outputs are plotted or saved based on the user orders and are then displayed in the output viewer interface. The whole procedure is planned, managed, controlled by the expert engine which is shown in the middle of the procedure chart in figure 6.1. Required inputs for generating an input deck file is illustrated in figure 6.2.

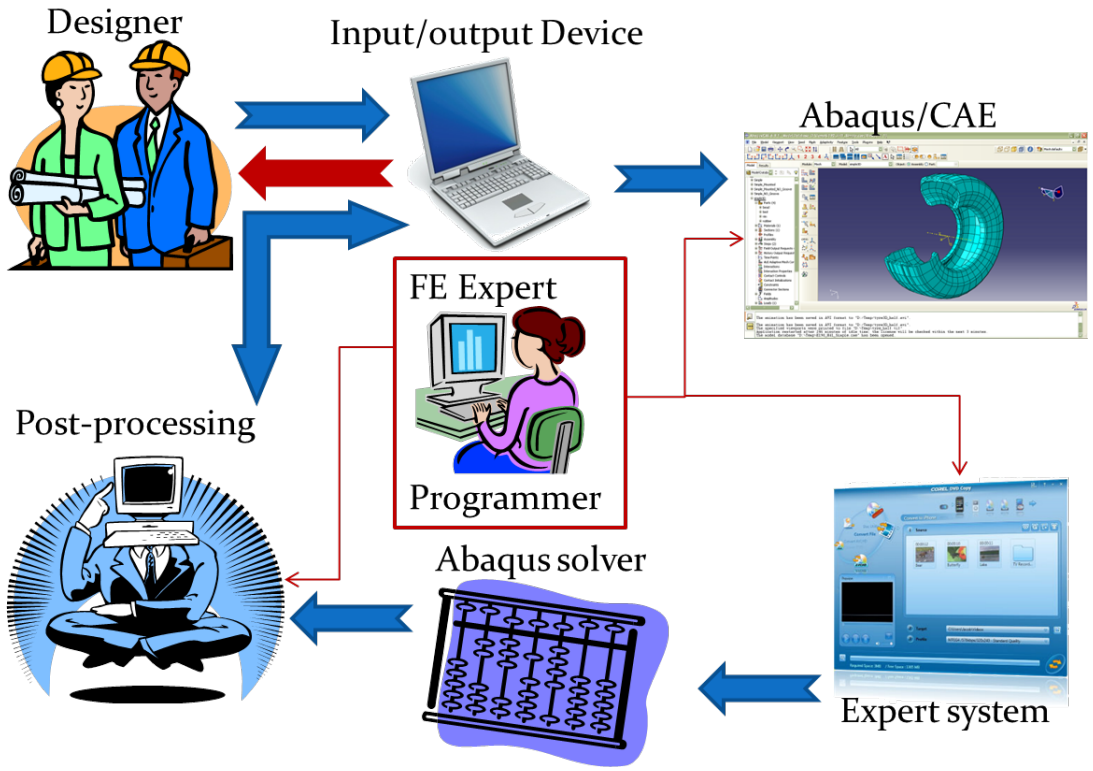

Figure 6.1. Automated procedure of tyre analysis interface

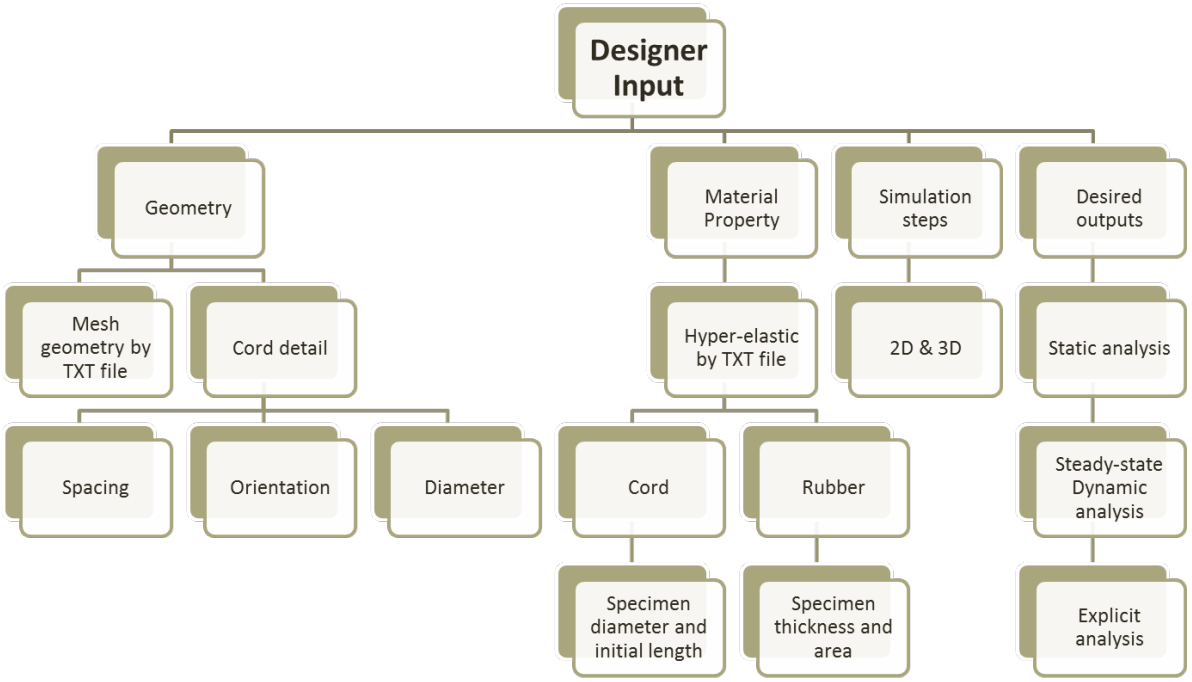

Figure 6.2. Required inputs for generating the INP deck file

The detailed procedure of automated analysis procedure is shown in figure 6.3. Generally, during the comprehensive analysis procedures, four programming languages are employed that each one is responsible for a task through the full procedure. The expert engine was coded in MATLAB that easily grants access to the Operating System commands in order to manage the operational tasks such as orders to read and write data. The user's input environment was developed using C++ to initially provide dialogue boxes to communicate with the user. Then, the interface requests for the input parameters such as material properties, simulation setup, and CAD cross-section profile.

Sub-tasks in the automated analysis interface are managed and ordered by Python as the core programming language in developing initial Abaqus functions. Amendment to the tyre geometry, tyre cross-section mesh, and generation of input deck file (INP file) are conducted by specific commands in Python through the Application Programming Interface (API) in Abaqus. The Python compiler is a built-in capability in Abaqus and debugs the commands

before it is processed into the input deck generator. Python scripts are also capable to perform parametric study when the influence of a physical variable is to be investigated. INP files will be generated by the Abaqus kernel based on the user's input parameters, mesh data and the desired inputs/outputs.

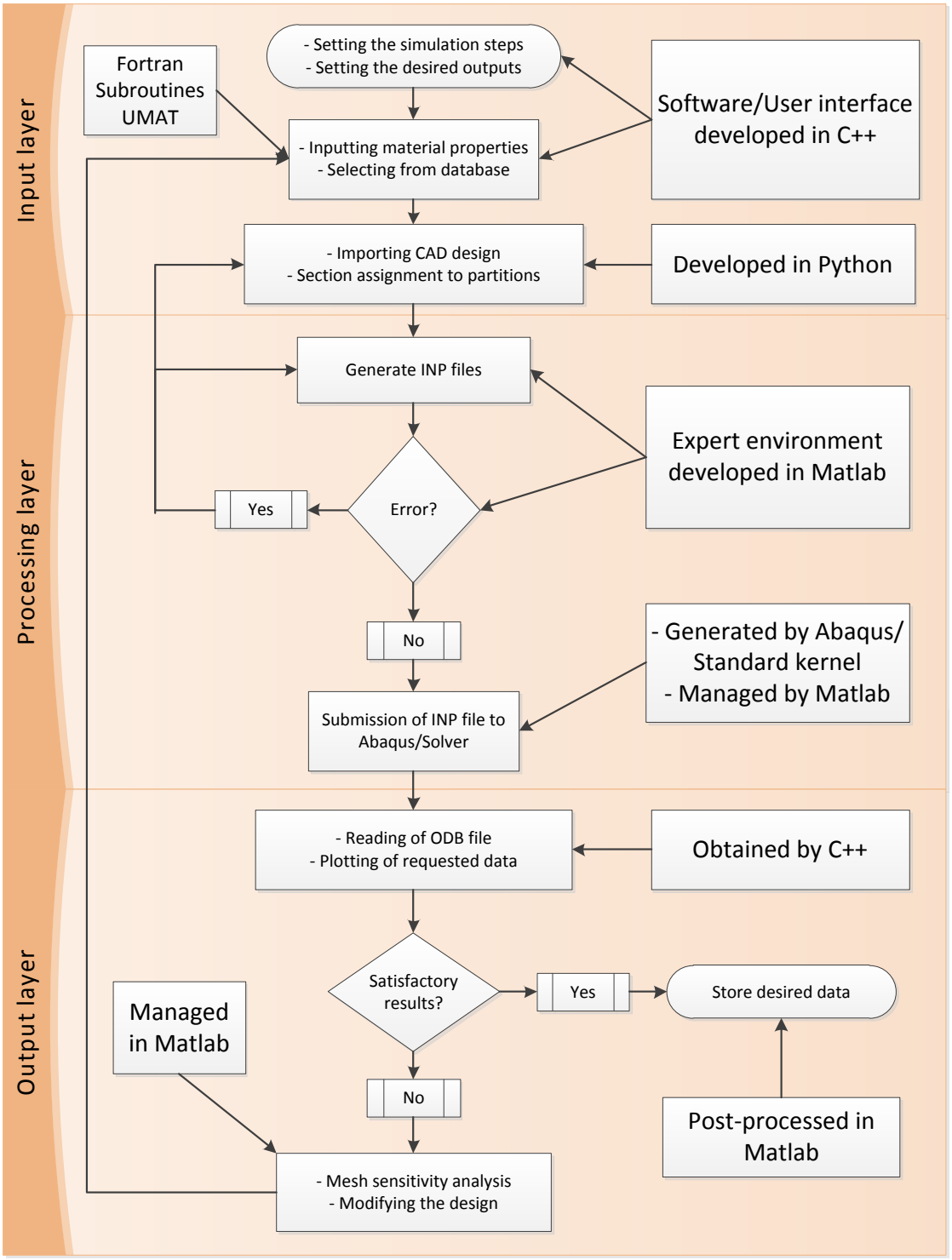

Figure 6.3. Flowchart of the data flow and procedure

For professional users and support, the user specific function, the FORTRAN codes that are written based on Abaqus instruction and are used to determine innovative material property or amend the analysis steps. Eventually, reading of ODB file is carried out with C++ as a standard API tool in Abaqus and the results can be stored or plotted by Matlab® on demand.

6.3. Interface development

In this section, the implementation of the algorithm and the structure of the Tyre Analysis Interface System (TAIS) are discussed. The main dialogue box in TAIS is composed of drop-down menus with standard functionalities and eight modules were developed on the main body of TAIS: geometry input interface, meshing module, material property module, simulation setup, Generate/Check INP file, Job conversion/submission to solver, post-processing toolbox, and export input/outputs and viewer. These modules in TAIS are shown in figure 6.4. Drop-down menus include file manager capabilities such as creating, opening, and saving models and help menu provides instruction manual and tutorial documents. In modules, a new window is pulled up by clicking on each button in order to take the user inputs and configure the solver and analysis. Figures 6.5 to 6.12 demonstrate the capabilities and available commands in each individual module.

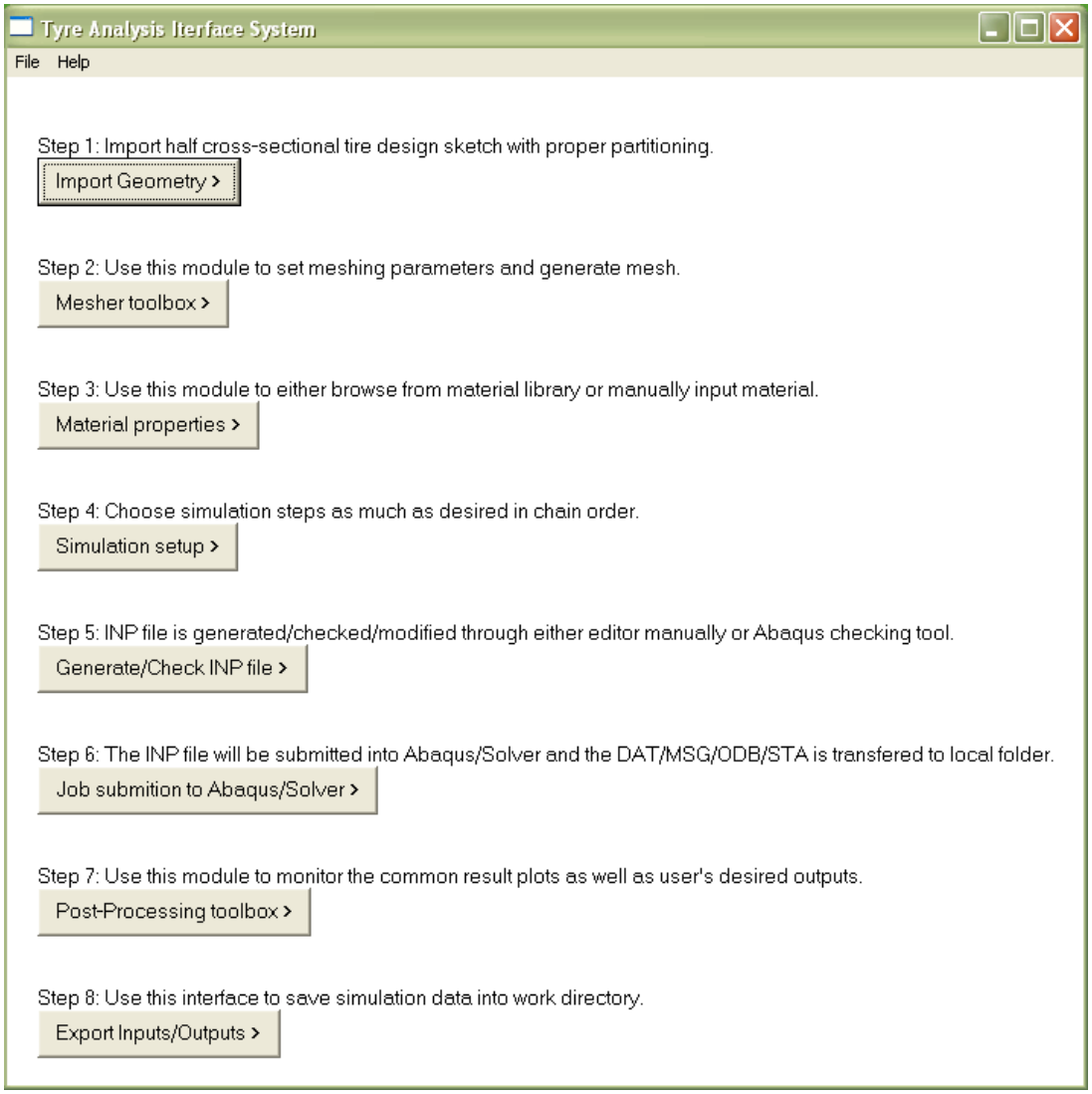

Figure 6.4. The structure of TAIS

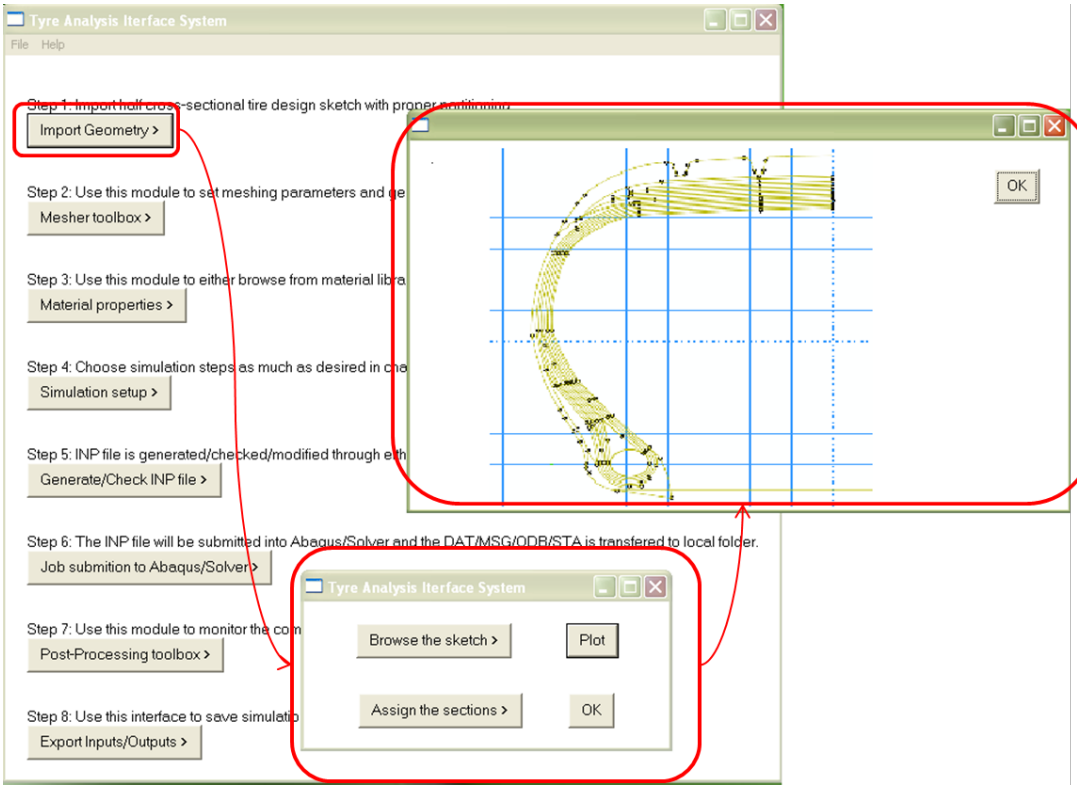

Figure 6.5. Geometry import module

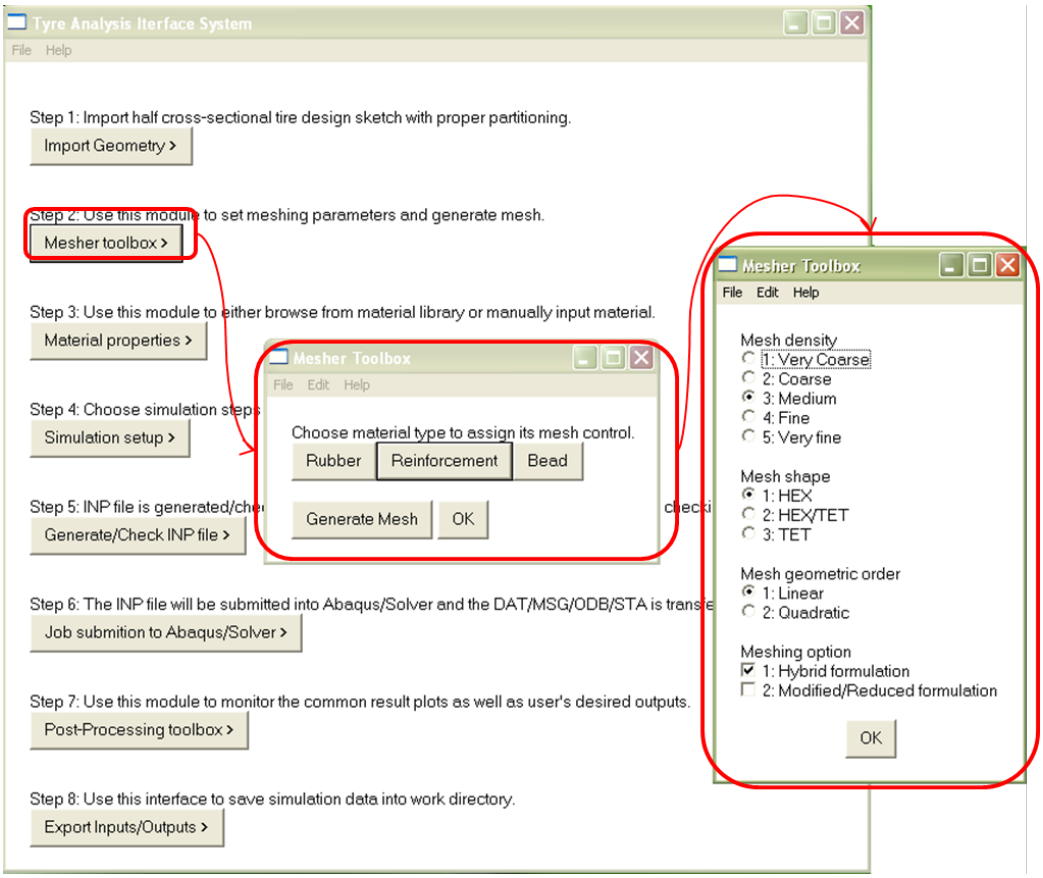

Figure 6.6. Meshing module

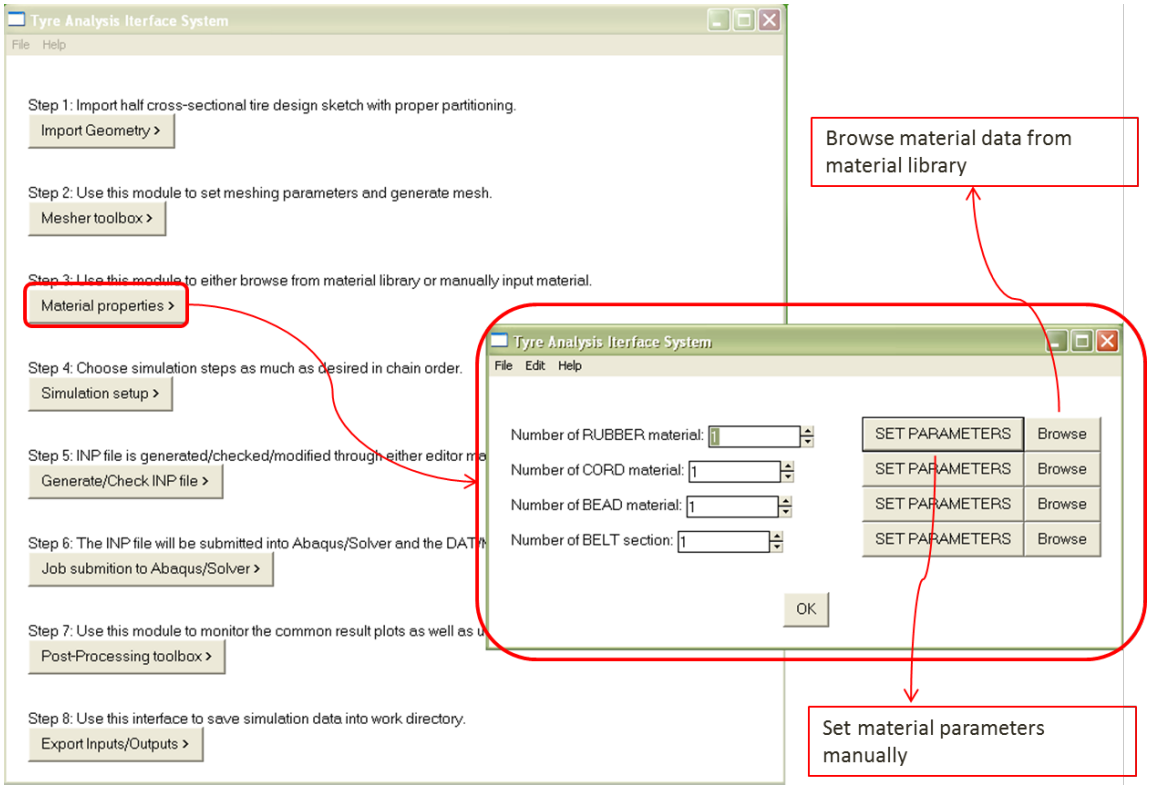

Figure 6.7. Material property module

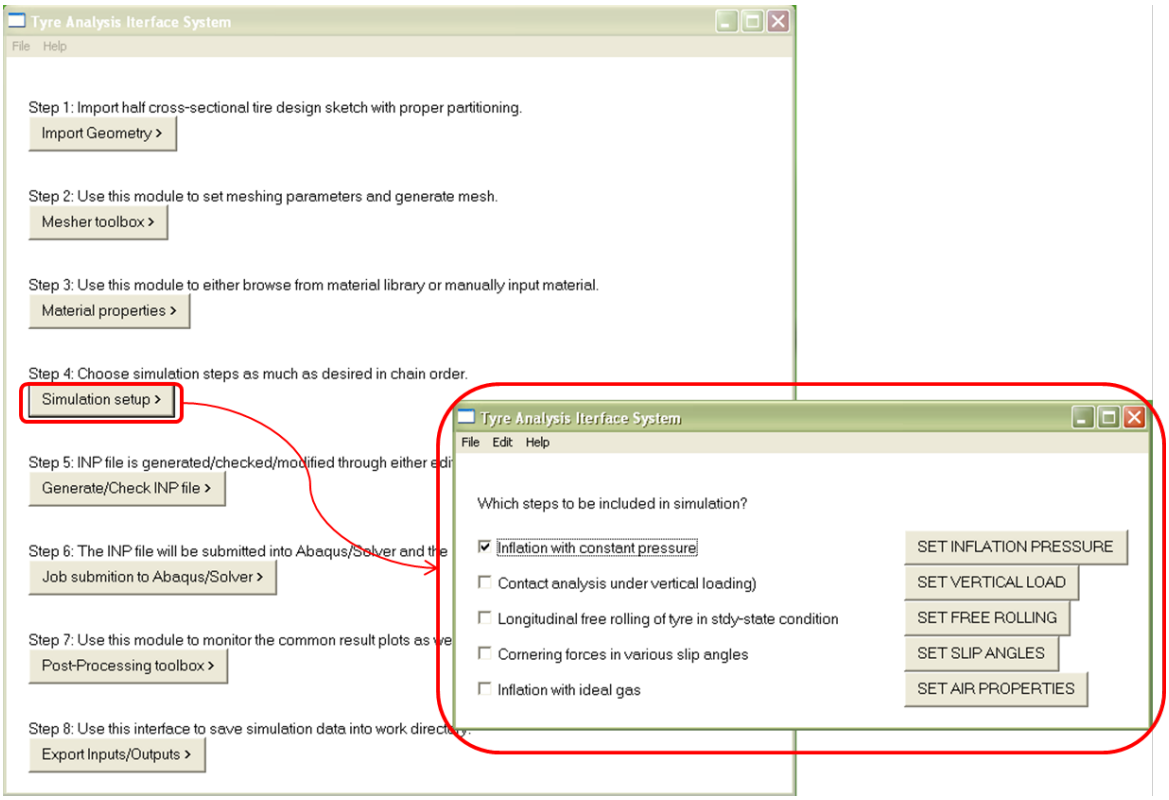

Figure 6.8. Simulation setup module

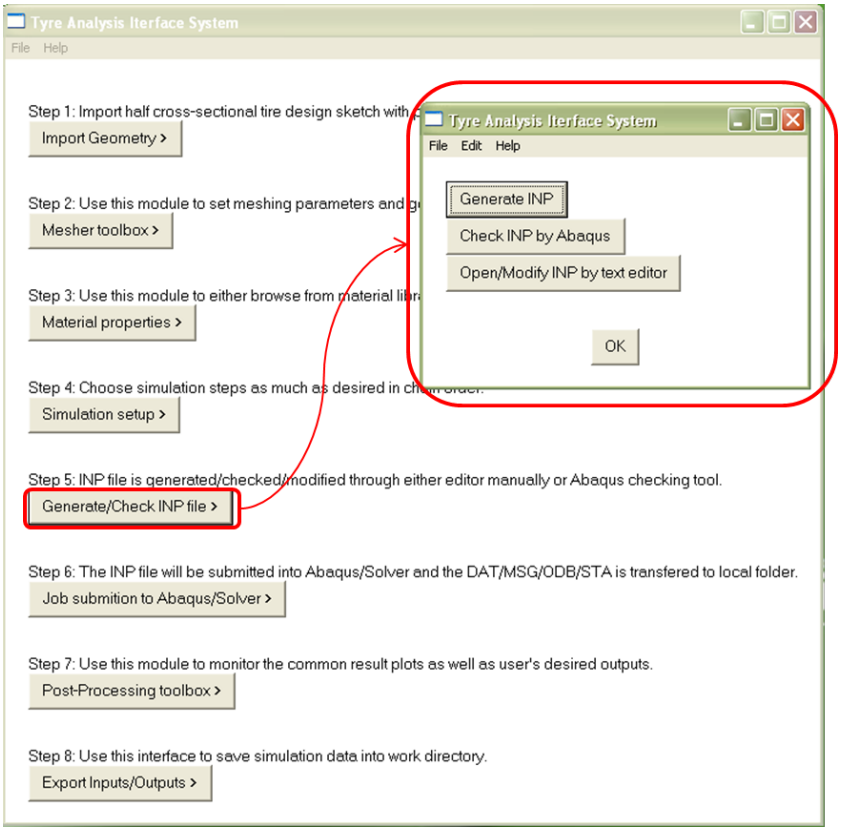

Figure 6.9. Generate/Check INP files module

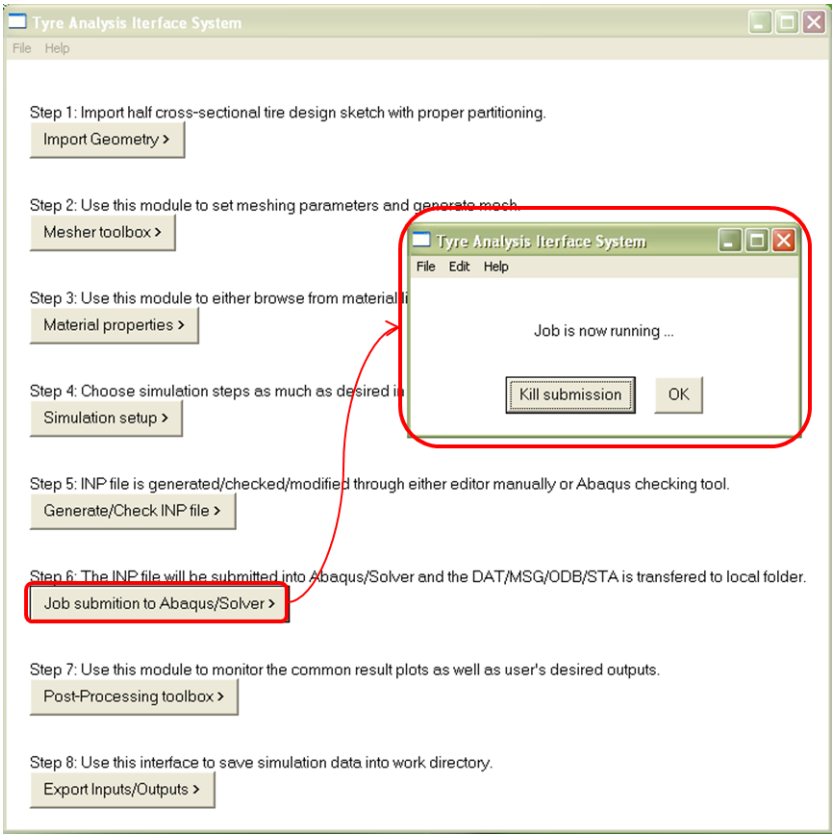

Figure 6.10. Job submission to Abaqus/Solver module

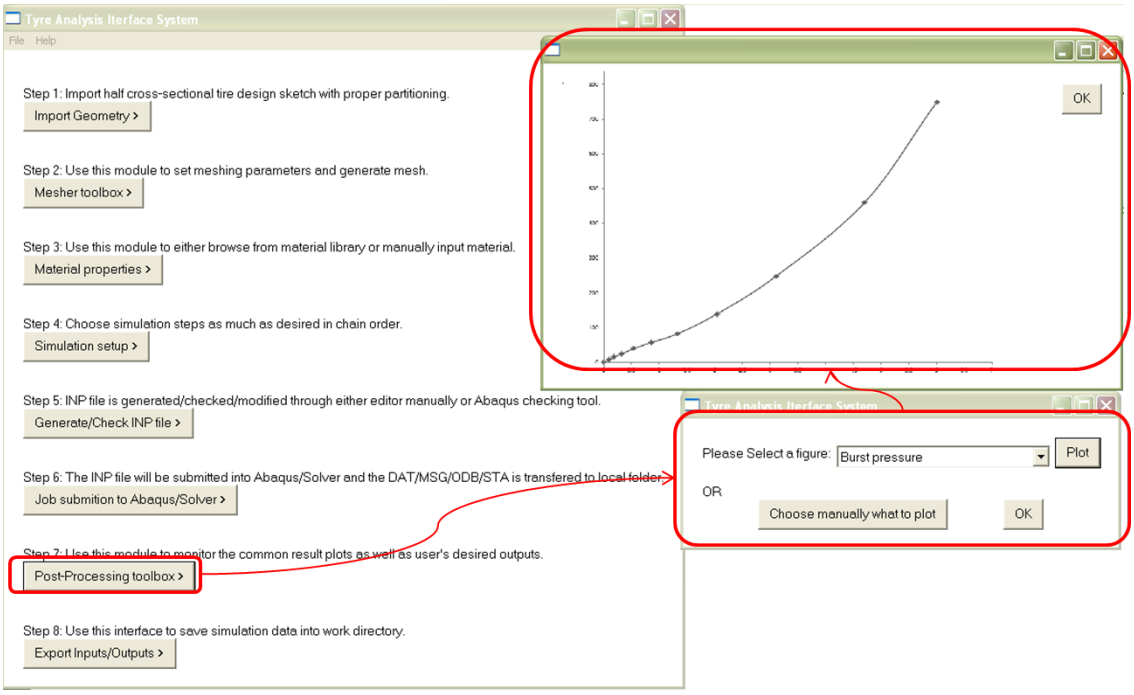

Figure 6.11. Post-Processing module

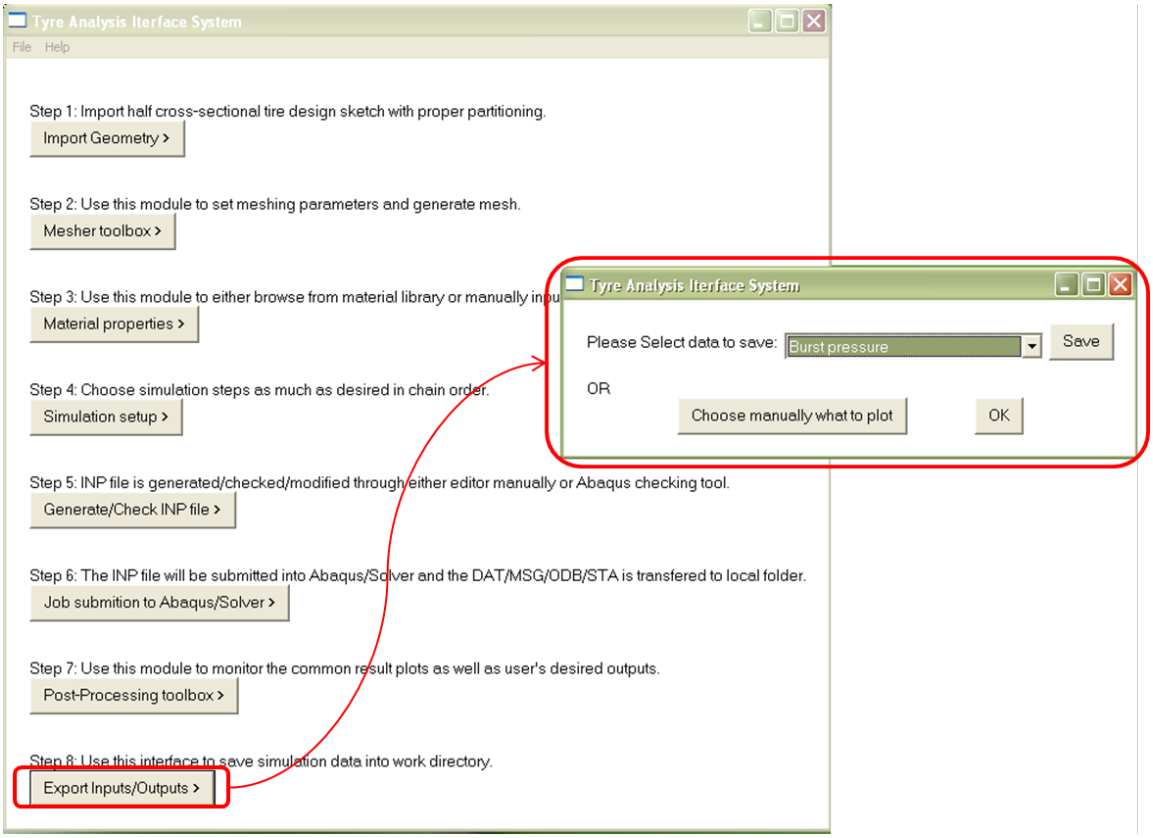

Figure 6.12. Viewer/Export results module

6.4. Summary

TAIS, Tyre Analysis Interface System, was developed based on the requirements and demands. TAIS is an input/output interface in tyre analysis for the non-expert FE users and benefits from material database builder which was initially developed in order to obtain the tyre mechanical properties. This interface is also capable of incorporating user's inputs, such as simulation steps and CAD design into the tyre simulation. The whole simulation process would be carried out automatically with a developed code in Matlab, while the interface is developed in C++. C++ also reads data lines from the output file and writes them into new files on demand. Abaqus commands are also run using Python scripts and demanded by the interface based on the user's demand.

The software is capable of doing a wide range of analysis from 2D to 3D profiles, appropriate for the most of standard simulations and requirement in academic and industrial environment. TAIS aims to help designers and R&D department to smoothly move their design into virtual environments and develop new product faster, more safely and more cost effectively.

Chapter 7: Conclusion and Future Works

7.1. Conclusion

7.1.1 Introduction

In this thesis, finite element analysis of aircraft tyres was investigated. The main goal was to develop a comprehensive modelling and simulation approach for analysis of mechanical behaviours in aircraft tyres. Within this research project, the tyre modelling capability was developed at Dunlop Aircraft Tyres Ltd (DATL) in order to improve tyre design process and develop tyre model for landing gear system and aircraft modelling/simulation required by customers such as Airbus. The tyre modelling accuracy in prediction of tyre mechanical behaviour was primarily evaluated by experimentation that was conducted and supplied by DATL. The results from the finite element analysis were employed to support developments of new tyre designs in DATL as well as safety assessment for the official tyre safety certification processes. Furthermore, the dynamic and thermal simulations of rolling tyres provided forces and moments (F&M) and tyre thermal behaviour, which are generated across the contact patch when the tyre was rolled, steered, and stopped during aircraft ground manoeuvres in taxiing, landing, and take-off.

A short description of each chapter is discussed in the next section. In section 3, the specific conclusions from the results and the contributions to the field of tyre simulation are described

7.1.2 Summary of chapters

In chapter 1, the motivation of conducting the current research was discussed and the research theme and the necessity of such research were broadly explained. Furthermore, the overall aims and objectives were presented in the third section to ensure the research was directed in line with the specified goals.

In chapter 2, the history of aircraft tyres was investigated to address the progression and importance of this industry. Then, the current research interests towards the tyre modelling and simulation were discussed and the importance of using modelling approaches in simulation of the tyre behaviour was explained. A description of tyre construction was provided to direct toward a better understanding of the rubber and cord composition which helps to understand the tyre behaviour due to design parameters and construction. Finally in section five, the tyre primary terms were introduced and defined to be used in the following chapters.

In chapter 3, the modelling objectives were explained in 5 categories, which include interface development, standardization of analysis procedure, optimised analysis procedure, improvements in simulation accuracy, and extrapolation; and the steps to achieve these goals was briefly described. The available literature was then discussed to set the direction of this research and identify gaps in current research. Furthermore, criteria to assess the productivity and efficiency of the available tyre models were discussed and finite element method was selected for the tyre modelling due to the most criteria matches found in this approach in comparison with other modelling methods to deal with the goals and objectives set for the thesis.

In chapter 4, the importance of material modelling was initially presented and available models for elasticity, hyperelasticity, and viscoelasticity were explained. The elastic property was chosen for steel beads because of small deformation in bead and hyperelasticity was selected for rubber and nylon cords due to large deformations specifically in sidewall and carcass plies. Next, the instrumentations and characterisation experiments based on

standard procedures were described and extracted for the Yeoh model, which was identified as the most efficient approach to model the rubber large deformation.

In chapter 5, a methodology for FE modelling and analysis of aircraft tyres was proposed and implemented. Tyre structural detail was investigated to obtain a better understanding of the layer interaction and help in selection of the reinforced layer modelling in Finite Element. The FE simulation was then implemented for the simplified and detailed representation of rubber compounds in civil and military aircraft tyres and the implementation was evaluated against a number of experiments such as sidewall deformation, burst test, footprint, etc. In continuation, a mesh sensitivity analysis was conducted to find the appropriate mesh size in rubber, cords, and beads regions separately. Finally in this chapter, tyre rolling was simulated on the road and the forces and moments because of steering and braking condition was extracted. The tyre was next used to simulate the heat generation in deformation cycles in free rolling condition.

In chapter 6, the tyre interface (TAIS) was developed for usage by DATL designers. The procedure to build such environment was discussed and presented in this chapter.

7.1.3 Accomplishments

The achievements of this research are discussed in this section. The highlight of accomplishments is listed below, which is discussed more in details in the following.

- Benchmarked available tyre and material models comprehensively
- Proposed procedures for testing and parameterisation of material properties
- Developed 2D/3D tyre models with different level of geometry complexity

- Optimised the tyre FE models based on the mesh size/tyre and solver configuration
- Verified the FE model accuracy in prediction of tyre mechanical behaviours against static experiments
- Implemented dynamic and thermal-deformation coupled simulations
- Developed tyre analysis interface for FE non-expert users

According to the explained criteria for model selection and benchmarking of available tyre models, the physical models proposed to be used for modelling of tyre mechanical behaviour. The selection was due to flexibility that the physical models offer, access to detailed analysis outputs, appropriate for the design synthesis, and extrapolation capabilities. Although the physical models require comprehensive inputs from material properties to detailed geometry and suffer a time-consuming solution especially in the Finite Element method, this selection is not influenced as long as the real-time implementation is not requested.

Material models and testing procedures were discussed in chapter four and the elastic, hyperelastic, and viscoelastic properties were comprehensively described. The Yeoh model was selected to use as the hyperelastic behaviour of rubber compound and nylon cords since a good correlation was found between the unidirectional experiment and Yeoh model predictions. In addition, it was found from literature that the reduced polynomial models such as Yeoh model are capable to predict the bi-axial and planar deformation in an acceptable range. As for the viscoelasticity, Prony series introduced the as the most accurate approach to replicate the viscoelastic behaviour in the operating condition in this problem.

Having a standard procedure developed for building 2D model to 3D one, a comparison study was carried out on the test results in 2D and 3D FE models in symmetrical loading condition (inflation only simulation). Both model outputs in terms of structural deflections and stresses demonstrated a close agreement in trend and magnitude across a wide range of inflation pressures. It was concluded that the 2D FE model can be replaced for simulations such as burst test, in which the load is symmetrically applied in circumferential direction.

In continuation, two different geometries of rubber compound were generally proposed in order to reduce the problem size and obtain a better mesh: the model with one rubber compound for the whole profile (simplified model) and the partitioned model to actual rubber regions (detailed model). The simplified and detailed models were exposed similar simulations and their performance was checked in terms of stress and deformation prediction. It was concluded the detailed model predicts more accurate trends and magnitudes for both stress and deformation, while the simplified model fails to predict the contact pressure and internal stress correctly while the deformation prediction was correlated within a reasonable range under %5 error tolerances.

The correlation study was carried out in four steps: profile sizing check after inflation, burst test, sidewall deformation under vertical loading, inflator modelling, and tyre footprint. The FE models showed that it is capable of accurately predicting where and at what inflation pressure the burst occurs. The tyre profile was checked after inflation to correlate the cross-section measurements such as diameter and tread/sidewall extension after inflation, and tyre deformation in this simulation demonstrated excellent correlation for the sizing check. Footprint area and contact pressure were also correlated to the data from measurement. It

is concluded that these static measurements are necessary for checking the accuracy in prediction of aircraft tyre models and are recommended to be represented as a standard procedure to evaluate the aircraft model validity.

Inflator gas was also modelled as ideal gas using the hydrostatic elements and this definition helped to a better correlation of above parameters such as footprint and prediction of load-deflection mechanism. It is concluded the usage of inflator in FE tyre models is necessary where the change in pressure due to the volume, mass, or temperature variations is considerable.

A mesh sensitivity analysis was conducted to find the appropriate mesh size in rubber, cords, and beads regions separately. A full matrix of civil aircraft tyre 2D models was generated with different mesh sizes, and the same simulation of tyre inflation up to the burst pressure was applied and submitted to the solver. The results suggested a good match between the different models in terms of the deformation, but the maximum von Mises stress deviation in all regions escalates at pressures higher than 3 MPa. This was thought to be due to the mesh disparity and dissimilar mesh grid distribution across the regions, so that dissimilar distortion in elements occurred and lead into deviation in the stress results of higher pressures. It is included that the mesh size sensitivity needs to be performed for each particular case separately as it may lead to different judgements when the tyre structure changes to obtain an optimized mesh size.

Since the accuracy in prediction of tyre mechanical behaviour in FE model was validated through the correlation study, the simulation was extended further in order to predict the forces and moments generated across the contact patch. A procedure to find the free rolling speeds at specific loading condition was developed by varying either the road or wheel

speeds and the slip ratio consequently. Then, the tire was steered at the free rolling condition to obtain the generated lateral forces due to cornering manoeuvres. The overall trend of the predicted force and moments demonstrated a similar trend to those forces and moments generated from the tyre test under lateral and longitudinal slip from the most literatures (Pacejka, 2012). However, the predicted forces and moments are strongly dependent to the applied friction regulation in the FE model. Since a valid friction model was not available through tyre testing in DATL, the simulations could not be exactly correlated with the real-world test data.

In addition, the tyre thermal behaviour in free rolling condition was predicted using the idea of energy dissipation in hysteretic loops of rubber materials with viscoelastic behaviour. The models illustrated a load and velocity dependency; however, the velocity dependency of thermal behaviour can be ignored when the thermal data are plotted versus the travelled distance instead of time. The thermal model predicted the highest temperature increase in areas around the sidewall where the maximum deformation and relaxation occurs, and this prediction is in line with overall trends as reported in literature.

Finally, a tyre analysis interface was developed within the thesis by using programming languages Python, Matlab, and C++. The software package is capable of doing a wide range of analysis from 2D to 3D profiles, appropriate for the most of standard simulations and requirement in academic and industrial environment. TAIS aimed to help designers and R&D department to smoothly move their design into virtual environments and develop new product faster, more safely and more cost effectively. TAIS was successfully tested and run through a number of simulation and similar outputs was obtained with this toolset. A

standard procedure to introduce the inputs/outputs to the GUI was introduced through the operating flowchart that can be used as a base for future developments.

7.1.4 Summary of contributions

This thesis contributes to the numerical modelling and analysis of mechanical behaviour in aircraft tyres. Specifically, it introduces standard procedures and novel techniques to the fields of finite element modelling, material testing and modelling, and analysis interface development in general. The primary objective of this thesis is to test the hypothesis that:

- Modelling of ideal gas as inflator increases the model accuracy in prediction of the contact area and pressure;
- Yeoh model for the rubber compound and nylon cord provides a reasonable prediction of material behaviour with quite faster implementation in comparison to complicated high degree material models;
- Simulation of burst pressure can be used as a predictor tool rather than physical burst testing in early product development and is capable to predict where the failure occurs;
- Tyre Analysis Interface System facilitates the task of tyre analysis using finite element method for inexpert designers in the field of FE analysis;
- Thermal-displacement coupled modelling of viscose heat dissipation in free rolling tyre is capable to predict the heat generation in cyclic deformation;
- The solution of FE tyre models with many layups and material/geometrical nonlinearities is converged and overcomes the convergence issues encountered;

- The thesis propose two different partitioning geometry with low and high detailed compound for the rubber region that offers a faster implementation by low detail model versus more accurate approach with high fidelity rubber region;
- Modelling cords helps to achieve aircraft tyre models with better convergence and higher accuracy in prediction of mechanical behaviour. In this thesis, the nylon cords were tested and implemented in FE package by the nonlinear hyperelastic materials, which was necessary due to the large deformation encountered in aircraft applications;
- The 2D FE model of aircraft tyres successfully predicts the tyre behaviour under symmetrical loading conditions like what occurs in burst test. This implementation is much faster in comparison to 3D model setup and less convergence issues is encountered;
- The optimized mesh size/tyre provides an FE model with a better prediction of mechanical behaviour and helps to a better convergence and as faster implementation as possible.

In cases that was listed above, thesis offers a contribution either in the field of analysis in general or specifically in the field of aircraft tyre analysis, which latter has the most contribution in this thesis.

7.2. Future works

A number of developments and researches are suggested in the following in continuation to the current research in order to further increase the applicability and accuracy of the models as listed in the following.

The current development of heat generation in rubber compound due to cyclic heat dissipation assumes that the material property does not change in response to varying temperature. This assumption is valid for a limited range of temperature change. However, the assumption should be reconsidered when the property change significantly due to temperature change in compound particularly when the frictional heat is added into the simulation. Therefore, material dependent data can be used in conjunction with coupled thermo-mechanical analysis in tyre simulation when the tyre temperature is largely changed due to material damping or frictional forces from road-tyre interaction.

In this thesis, the explicit approach was employed to solve the coupled thermal-displacement problem to predict the heat generation in aircraft tyre exposed to the free rolling condition and cyclic deformation consequently. The prediction of temperature change in the tyre model can be conducted with an implicit approach to potentially increase the accuracy in prediction of heat generation and temperature build-up since this approach ensures about the energy balance at any iteration.

An important aspect of tyre modelling is to model the behaviour of rubber-road interaction in sliding conditions. The current Coulomb-Mohr friction model considers inaccurate but enough and reasonable for tyre-road interaction. However, the friction is a complicated phenomenon that can be dependent on the surface temperature, contact pressure, surface roughness, and sliding velocities. For a better approximation of the forces and moments generated in contact patch, the friction effects should be modelled with highest fidelity to replicate the tyre behaviour during taxiing, take-off, and landing due to low speed cornering and braking and high speed free rolling conditions. Moreover, a precise friction model helps to accurately predict the heat generation in contact patch due to frictional forces.

Aircraft tyres are normally operate in high speed condition during landing and take-off. In this research the tyre was simulated for speeds under 100 km/h that is not representing for what happens in those conditions as it might be nonlinear phenomena occurs at extremely high speed. Belt stiffening phenomenon is of those nonlinear behaviour that can be seen in higher speeds and can affect the tyre mechanical performance due to high centrifugal forces and belt extension. Therefore, the extremely high speed simulation in explicit analysis is suggested to predict the tyre behaviour in landing and take-off conditions.

Finally, a number of amendments can be performed on TAIS in order to increase its productivity. The current development is capable to perform simulations including the pure inflation to steering at free loading conditions, which can be extended to offer more comprehensive ones such as heat build-up in cyclic deformation, high speed free rolling and high speed cornering/braking conditions. The material library needs to be upgraded in response to the requirements from the analysis. On the other hand, the environment itself has not been developed based on standard IT requirements and it has been a practice development rather than a standard OEM toolbar. Therefore, more developments are needed to change the TAIS to a professional appearance.

Appendix A: Tyre models

As discussed in chapter 3, several approaches have been developed on the modelling of tyre mechanical behaviour by many researchers so far, which are used for various applications where appropriate. As part of the benchmarking was conducted in this research, these approaches were widely investigated. The purpose was to gain insights toward a desirable tyre modelling according to the aims and objectives that were initially deliberated. The aim of this appendix is to introduce the modelling approaches of tyre mechanical behaviour in more details so that the usage of the FE is clearly distinguished between the other available approached. In this section, three categories of modelling approaches are discussed: analytical-physical models, empirical models and numerical physical models, as mentioned in chapter 3.

A.1. Analytical-Physical models

In these models, an analogous behaviour to what is observed for tyres under similar operating conditions[2] and inputs based on physical concepts is explored through a pool of known physical events, so that the picked models are capable of mimicking the tyre behaviour partially or comprehensively under specific regimes. The more physics that is added to the model, the more complexities and variables are required to formulate the mechanical/thermo-mechanical properties in order to initiate a prediction of tyre behaviour, but the model is equipped with more powerful tools so that more accurate estimation and better coverage of the mechanical performance are obtained.

The tyre can be represented by physical models ranging from an introductory flexible shell as the tread and carcass with equivalent bending and axial stiffnesses connected to a rigid rim, to a detailed model with extreme details in the geometry, complication in

[2] In this chapter, the “operating condition” means the inputs such as the slip ratio, slip angle, inclination angle, vertical force etc. that the tyre model used to generate the forces and moments in output.

representation of the material behaviour, and combination of coupled physical phenomena. In this section, popular tyre physical models are briefly introduced from the simplest to the most complicated one and the pros and cons of each are discussed.

A.1.1 Beam model

The beam model was initially introduced by (Pacejka, 1971) and (Soedel, 1975) as "tyre shell model" and later a more advanced version was released by (Clark, 1991). This method represents a physical approach in tyre modelling in which the tread block is modelled as connected massless thin beams. The equivalent axial and lateral (bending) stiffnesses are calculated mathematically based on the beam theory in mechanics, as shown in equations A.1 and A.2:

$$k_{axial} = \frac{AE}{L} \qquad \text{Equation A.1}$$

$$k_{lateral} = \frac{3AE}{L^3} \qquad \text{Equation A.2}$$

The beam elements in two directions construct the beam model: the *radial* beams in radial direction that are nearly the size of the tyre loaded radius subtracted from the tyre seat radius and are connected to the tyre rigid rim (figure A.1). The radial beams represent the tyre stiffness in radial direction. The short circumferential beams are interconnected to form the tread block circumferentially to form a net, and also mimic the road/tyre interaction. The friction at the tyre/road interaction is modelled in between the beam tip points through the circumferential beam. The entire beam structure was not formed of displacement elements, but generally acts as the force elements, and as a result, the rotation around the wheel axis is not supported by beam model since there is no mass associated with the beam elements and cannot be considered as a dynamic system. The beam elements are deflected

under the applied vertical load and steered angle on cornering and overall displacement of the tread block is formed. Furthermore, this configuration is assumed to allow friction physics between the beam end points, where connected with other beam ends, and ground. Hence, the longitudinal and lateral flexibilities for slip in x and y directions are allowed to induce longitudinal and lateral forces across the contact patch (Schmid, 2011).

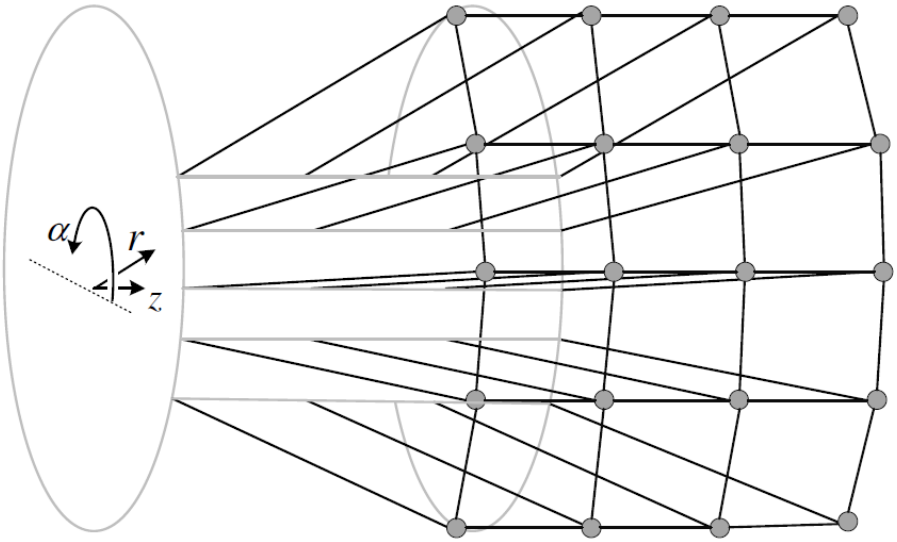

Figure A.1. A representation of the beam model (Schmid, 2011)

This discrete model has its origin from the physical concepts and a properly extended and fine-tuned model is capable of predicting the lateral and longitudinal forces along with the corresponding displacements. The model provides a decent understanding on how the tyre deflection mechanism works laterally and vertically and exhibits the mechanical performance of the modelled tyre under encountered load and cornering manoeuvre. Obtaining prediction of the tyre performance with details in structural displacement is independent of delivering the tyre experimental data in advance although initial parameter fine-tuning procedure is required to verify the validity of the model against a number of tests. If the model validity is passed in non-linear regions, this physical model has the

potential for being employed to extrapolate over the comprehensive variation of input parameters with acceptable accuracy in comparison to the empirical models that are not characterised for such operating range; e.g. the physical model does not encounter limitation in prediction of generated forces in higher load, while the empirical models should not extrapolate the generated forces for the range of loads that are not characterised for. This can increase modelling uncertainty in prediction using empirical models while an anticipated suitable behaviour is expected from physical models. The number of parameters that represent the model behaviour is minimal in the beam model likewise the other physical models. Therefore, the efforts in model setup particularly for the fine-tuning procedure is minimal in comparison to the empirical models, where an analogous shape function should be initially identified and a methodical procedure for optimisation of a large number of parameters is required.

Since the structural details are not modelled and the stiffness of thin beam element is indirectly associated with the rubber and fabric material property, the beam model is not considered a suitable tool to investigate the variation of stress in the reinforcement cords across layers and stress distribution in the tyre under extreme loads. In addition, the friction in beam model delivers the basic Coulomb-Mohr friction concept along with the elementary discrete point contact, and consequently, prediction of accurate frictional forces is a point for technical arguments due to inaccuracy caused by a simplistic representation of predicted forces and moments in the form of static and dynamic frictions.

A.1.2 Ring model

The ring model was initially introduced by (Pacejka, 1971) and (Soedel, 1975) as “tyre shell model” and was developed for tyre frequency response analysis based on the thin shell

theory (Tuononen, et al., 2012). This model is used for the dynamic structural behaviour and is capable of application for durability including noise, vibrations and harshness analysis under periodic vertical load caused by vehicle vertical dynamics and road unevenness - which is appropriate for the tyre ride models. This feature in the ring model is owing to the differential equation of motion derived for the belt motion. In early development of the ring model, the tyre sidewalls were represented as radial springs and the tyre belt including the tread, sub-tread, and carcass are modelled as a thin ring based on the shell theory and with radial, tangential, and torsional stiffnesses. The radial springs, spread circumferentially around the tyre and linked to the rigid rim, not only depicts the sidewall stiffness, but includes the influence of inflation pressure as an elastic foundation (Perisse & Hamet, 2000), as shown in figure A.2.

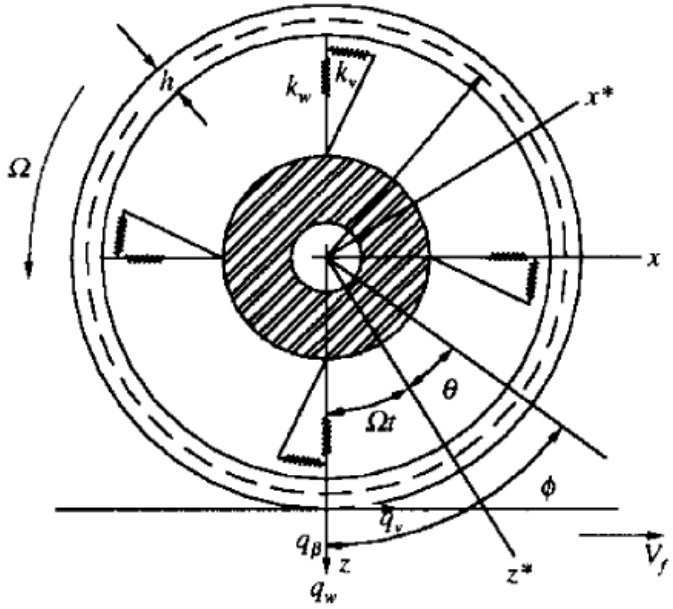

Figure A.2. Tyre ring model (Wei, et al., 2002)

This model offers a considerably accurate approach that is well established in its place among the vehicle ride and enveloping models using tyre as a flexible component. The

model historically looked after “dynamic stiffness” between the road and the road hub. The tread and belt compound can be modelled through more advanced ring models, and as a result, the verified model can be used to evaluate the developments of re-designed tyre and support the designer in assessment of new configurations. The physics-based model equations have their origin from the thin shell and layup theory and the equations are dynamically derived, so that an augmented physics such as the thermal effects can be integrated with the shell equations in order to take its influence into account.

Although the ring model suggests a well-established tool for dynamic and frequency analysis to obtain accurate radial forces, the governing equations for prediction of contact forces are not well developed so that the reliability of the model is not satisfactory for prediction of the lateral and longitudinal forces in tyre-road interaction. In addition, the model is not capable of accepting the direct compound properties as input to the model, and therefore, the belt configurations and material properties are not directly fed into the model for the comparative study of its performance and efficiency. As another drawback, the belt is assumed to be inextensible, so that the circumferential motions parallel to the belt surface are not captured. Moreover, owing to the complexity of the equations that are employed to meet the desired accuracy in the advanced ring model, parameterisation of coefficients requires a number of characterisation test that includes the “cleat” test, “coast down” test for calculation of the effective rolling radius, static tyre loaded radius and contact length measurement under varying vertical load, and steered free rolling test at very low speed to capture the tyre lateral stiffness.

A.1.3 FTire model

Flexible Ring Tyre Model, that is also well-known with its trade mark “FTire” developed by Cosin, is a full 3D nonlinear model for both in-plane and out-of-plane simulations (Gipser, 2013). This model is an extension to the rigid rim ring model, in which the assumption of inextensible belt in no longer valid and the belt axial stiffness is added into the formulation in conjunction with the spring and damper element for bending, radial, and torsional directions. Moreover, the more complicated force and damper elements were supplemented in order to improve the prediction of tyre behaviour particularly in nonlinear regions.

Figure A.3 demonstrates how the FTire model is constructed radially and circumferentially. The radial element is responsible for the vertical stiffness in the simulation and one end of the radial element is connected to a node on the belt and the other end is attached to a rigid rim. The tyre belt is divided into 80 to 200 (Gipser, 2005) segments that a lumped mass element sits at each end of the segments and shares the mass of connected segments. The tangential element delivers stiffness in torsional direction for the tyre. The belt elements are spread along the belt and are composed of the belt bending stiffness, which is strongly excited in contact patch boundaries, and the belt longitudinal stiffness, which particularly acts when the braking or tractive conditions are active.

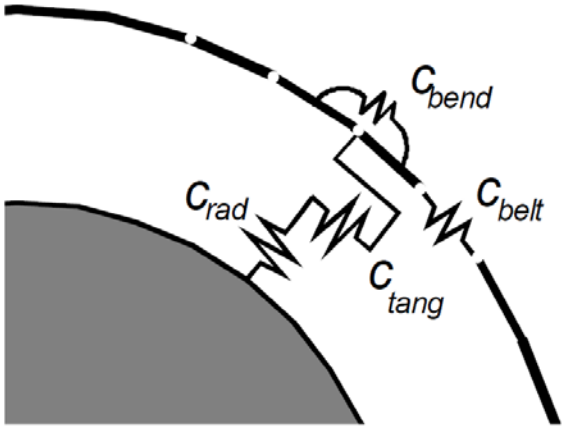

Figure A.3. Belt element model in FTire for in-plane application (Gipser, 2005)

In figure A.4, an advanced radial force element is illustrated in which both spring and damper are arranged in different configurations to individually represent a particular behaviour in tyre manoeuvres. The force element consists of the radial stiffness that is measured directly from the static test and has a nonlinear behaviour specially when there is no clearance between the tyre and rim, radial damping, dynamic spring and damping in Maxwell model arrangement that is subjected to the dynamic excitation condition, and eventually the spring-friction element that represents the elastoplastic (Gipser, 2005) behaviour of the material.

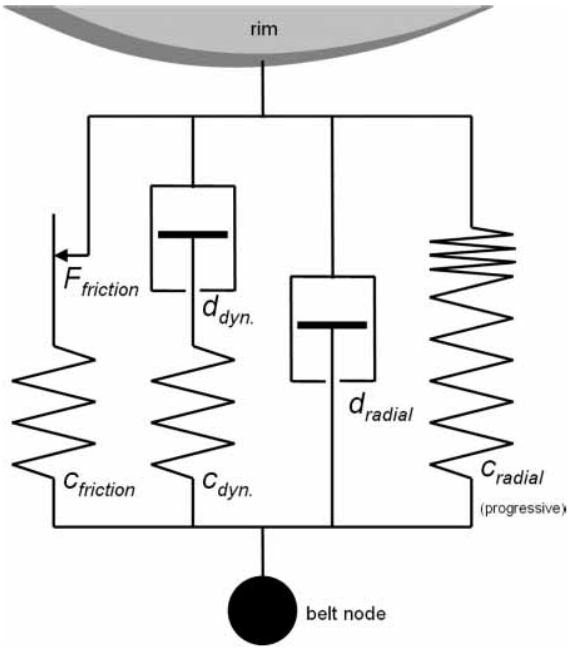

Figure A.4. The detailed radial force elements between belt and rim (Gipser, 2005)

Figure A.5 shows the general degrees of freedom available for each segment: the belt translational motion in which the belt axial stiffnesses parallel to the belt plane are involved, the torsional motion where the torsional stiffness is active, and the lateral bending. These motions are established to comprehensively cover the severe conditions that a tyre may come across in real world driving manoeuvres.

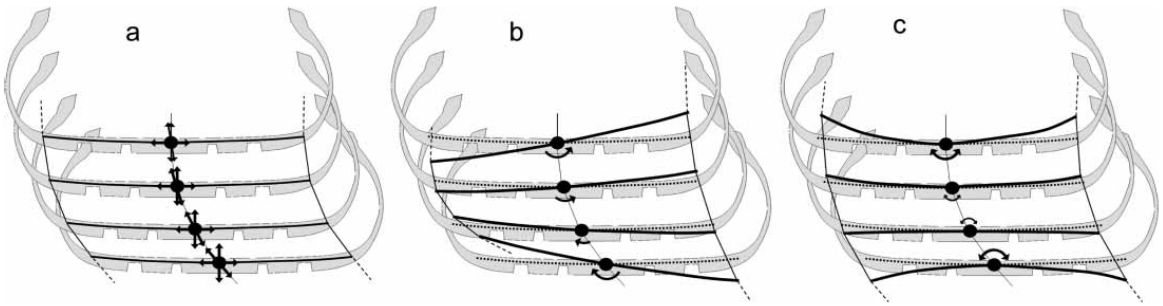

Figure A.5. Degrees of freedom of the belt segment: (a) translation; (b) torsion; (c) lateral bending (Gipser, 2005)

To sum up, the FTire is a physical model in which the tyre belt is discretised into equally angled segments, and from this standpoint, this method resembles a semi-numerical model.

The stiffness of sidewall and belt through each segment is broken into spring and damper elements with more than four degrees of freedom each. The FTire benefits from a built-in one dimensional thermal model to demonstrate the distribution of generated temperature exclusively across the contact area. The calculation cost is rather low and it is claimed to be appropriate even for real-time implementation based on a special version (Cosin, 2013). The model suggests a good accuracy for ride and durability analysis up to 200 Hz (Cosin, 2013), while tread pattern definition, durability analysis, and enveloping of uneven road is supported by this model.

The friction model in FTire to predict the generated forces and moments employs the well-known Coulomb-Mohr friction concept that is not regarded as an accurate approximation of friction coefficient in most literatures. Although amendments were put into practice on the current Coulomb-Mohr friction formulation to bring tread surface temperature, contact pressure, and sliding velocity dependency, the improvements would not necessarily provide a better approximation especially in nonlinear regimes. Moreover, the thermal model is not coupled with the deflection model. This is despite the fact that the thermal physics is actively involved in FTire through the heat generation model by means of frictional dissipations in contact patch to determine the distribution of temperature in contact patch area; i.e. the full tyre temperature change is only controlled by heat generation on account of the simplified frictional damping element and the influence of the tread block and sidewall deflection in tyre warm-up is ignored although its contribution cannot be neglected. In addition, the radiation and convection mechanism is not modelled for further simplification in one-directional heat transfer equations.

A number of characterising tests such as static load-deflection practice and dynamic cleat experiment should be carried out for parameterisation of coefficients. Concerning the design synthesis, FTire does not support the compound level analysis and therefore the verified FTire model should be re-parameterised for new configuration. A possible way to get over this issue is that the mechanical behaviour of a new tyre with altered stiffness and damping coefficients is evaluated against a number of standard test procedures, and the performance of new design is compared with the old configuration. Nevertheless, there will be a challenge to correlate the direct alteration of design parameters such as layup configuration with the indirect properties of tyre such as stiffness and damping coefficients.

A.1.4 Fiala model

The Fiala model is a popular physical tyre model and was a standard feature in early development of vehicle dynamic packages such as MSC.ADAMS owing to its simplicity, applicability, and satisfactory accuracy. This model focuses on the contact patch mechanism and the frictional forces generated in tyre/terrain interaction. Thus, the contact patch geometry is assumed to be known to establish the governing equations for connecting the amount of existing friction with the generated force through the contact area. Furthermore, pressure distribution is assumed to be uniform across the contact patch. Like the beam model with minimum input parameters, Fiala model needs 10 input parameters and these coefficients are directly linked with tyre physical properties such as the geometry and the stiffnesses, as reported in (Harty & Blundell, 2004).

Unlike the beam model, the Fiala model employs mechanical behaviour such as radial, longitudinal, and lateral stiffnesses that are measurable on the test rig based on non-destructive testing without cutting the tyre into specimens for the tensile testing as well as

the geometrical factors. Both slips in longitudinal and lateral directions form the fundamental basis of force calculation using the comprehensive slip, determined as equation A.3 (Fiala, 1952):

$$S_{comp} = \sqrt{(S_{long})^2 + (S_{lat})^2} \qquad \text{Equation A.3}$$

where:

- S_{comp} : Comprehensive Slip
- S_{long} : Longitudinal Slip
- S_{lat} : Lateral Slip

Then, the instantaneous friction coefficient for the road to tyre interaction is obtained by linear regression between the static and dynamic frictions through the equation A.4:

$$\mu = \mu_{sta} - S_{comp}(\mu_{sta} - \mu_{dyn}) \qquad \text{Equation A.4}$$

where:

- μ : Instantaneous friction coefficient
- μ_{sta} : Static friction coefficient
- μ_{dyn} : Dynamic friction coefficient

Having calculated the instantaneous friction coefficient, the critical friction coefficient is defined as below:

$$S^* = \left|\frac{\mu F_z}{2C_s}\right| \qquad \text{Equation A.5}$$

where:

- C_s : Longitudinal tyre stiffness

- F_z : Vertical load

The regime where the comprehensive slip is lower than the critical slip is called the elastic deformation state and where it is greater than the critical slip, it is referred to as the pure sliding state. Also, equation A.6 introduces the critical slip angle where the lateral force has different magnitudes at and beyond this threshold.

$$\alpha^* = \arctan\left|\frac{3\mu F_z}{C_\alpha}\right| \qquad \text{Equation A.6}$$

where:

- C_α : Lateral tyre stiffness

Longitudinal and lateral forces are calculated as below based on the critical slip ratio and critical slip angle:

$$\begin{cases} F_x = -C_s S_{comp} & if \quad |S_{comp}| > S^* \\ F_x = -sgn(S_{comp})\left\{\mu F_z - \left[\frac{(\mu F_z)^2}{4|S_{comp}|C_s}\right]\right\} & if \quad |S_{comp}| \leq S^* \end{cases} \qquad \text{Equation A.7}$$

$$\begin{cases} F_y = -\mu|F_z|sgn(\alpha) & if \quad |\alpha| > \alpha^* \\ F_y = -\mu|F_z|\left\{1 - \left[1 - \frac{C_\alpha|\tan\alpha|}{3\mu|F_z|}\right]^3\right\} & if \quad |\alpha| \leq \alpha^* \end{cases} \qquad \text{Equation A.8}$$

where:

- F_x : Longitudinal force
- F_y : Lateral force
- α : Slip angle

The Fiala model is computationally efficient. Other physics such as temperature effects can be modelled through a hybrid formulation that makes forces and moments calculated from the Fiala model dependent on temperature variation.

This model is not inherently equipped for camber angle sensitivity analysis. The physical parameters such as damping and stiffnesses are required to be measured prior to the modelling using a tyre test rig. Frequency and transient analysis are not supported in this model and also it cannot be used for ride analysis and road enveloping simulation. The model accuracy is always up for debate and reliability in nonlinear regions is poor in comparison to semi-empirical models (Pacejka, 2012). Fiala model suggests a poor "superposition method" for combined slip due to the fact that combined slip has a nonlinear effect in reality; accordingly it leads to poor correlation particularly in high slip condition. For the accuracy required in modelling, this model cannot provide enough reliability in prediction of contact patch forces and would be a good model for preliminary analysis stage due to its quick implementation.

A.1.5 Brush model

Tyre brush model is a phenomenological based model that mimics the physical events in tyre/terrain interaction. When the longitudinal and lateral forces are built up across the contact patch, the transversal deflection is progressively developed from the tread block tip with flexible mechanism and is transferred toward the inextensible sub-tread with stiffer foundation. This physical behaviour, modelled as elastic bristles that are perpendicularly attached to a rigid foundation which has been shaped deflected due to vertical load, as depicted in figure A.6 and A.7, represents the deflected belt profile under the applied vertical load. However, the deformation of bristles is due to the relative displacement of the bristle's tip to the imaginary rigid base attached to the top of the belt. The amount of relative deflection specifies whether the bristle tip is exposed to slip or stick region.

The expressed condition of bristles applies to the tyre when it rolls freely on a flat road, the slip angle is zero, and the tyre is not inclined with respect to the normal vector to the road. A free rolling condition in which the bristles are still normal is when the multiplication of effective rolling radius r_{eff} and tyre angular speed ω is equal to the wheel hub longitudinal velocity. In case that the multiplication of r_{eff} and ω differs from the vehicle forward velocity, that can be interpreted as the braking or drive mode and the sliding velocity V_{sx} is formed, the bristles near to the leading edge are still positioned rather vertically and the deflection is progressively developed along the contact patch toward the trailing edge.

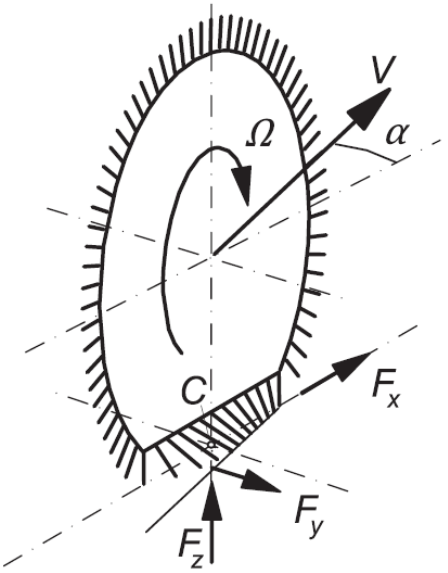

Figure A.6. The schematic of the tyre Brush model

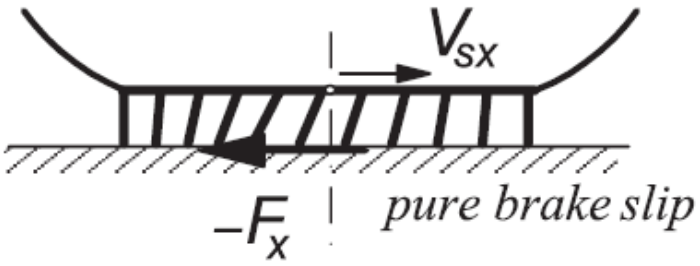

Figure A.7. Deflection in bristles under pure brake slip

As explained, the preliminary assumption in Brush model is the deflected geometry of the rigid ring as input to as this model is not equipped with a deflection mechanism

independently. The model uses sliding velocity, slip angle and vertical load. The pressure distribution is also assumed along the contact length to calculate developing angles in bristles based on the relative speed and bristle deflection mechanism. Then, the angles are compared with threshold angle such that the bristle proceeds from the sticking region, where the static friction law applies, to the sliding region, where the dynamic friction law is valid. As a result, bristles are divided into those in sticky or sliding region and the corresponding friction law applies for each region. The resultant longitudinal and lateral forces are then calculated based on the assumption for the forces in sliding and sticky regions.

Like the other physical models mentioned so far, the stiffness of the bristles in Brush model are required to be determined prior to the simulation setup. The difference however is the simplicity of the tests required to characterise fundamental parameters as only the quasi-static non-destructive procedures are carried out to measure the lateral and longitudinal stiffness in order to correlate with the required stiffness values. The shortcoming that still exists among the physical models so far, and which applies to Brush model as well, is the indirect relation of the detailed design of the rubber casing and embedded reinforcements with the observed performance and overall behaviour of the composite structure in response to imposed external operating conditions.

To sum up, this model represents an analytical approach in which a considerable amount of physics such as dynamic, multi-phase material and thermal regimes are involved to estimate the generated forces and moments generated across the sticky and sliding regions of the contact patch. In terms of model flexibility, since the tread package stiffness (bristle stiffness) is affected by tread and carcass temperature variation, the belt stiffness can be

mathematically correlated to the temperature development in the tread package. However, this analysis requires additional material testing in order to characterise the thermal dependency of the tread block. A new tyre model has been developed by Michelin in which both mechanical and thermal sub-models were coupled to build a thermo-mechanical model based on the Brush model. This model is so-called TaMeTirE, and according to the authors (Février, et al., 2010), (Février & Fandard, 2008) and (Durand-Gasselin, et al., 2010), the model demonstrates excellent accuracy in prediction of the force and moment in the presence of thermal effects. In TaMeTirE, the constructional compounds are defined to be temperature dependent and the forces and moments are compensated for thermal effects.

Computational-wise, a few physical parameters are needed in comparison to numerical and empirical models for calibration so that the model setup and implementation are fairly quick, so that it can be employed within an on-line estimation loop for a better approximation of overall friction. Moreover, this model can support combined slip condition based on calculation of the sticky and sliding regions.

Enveloping of road unevenness is not inherently supported in Brush model and it is assumed that the tyre rolls on a flat road. Probably the major drawback of the Brush model is its shortage of having a predefined deflection model in order to determine the tyre profile when the tyre load varies. As an outcome of this deficiency, the contact length is essentially assumed to be known to form the governing equations. However, the contact length can be proportionally correlated to the vertical force or inflation pressure. On the other hand, a shape function should be assumed for vertical pressure distribution across the contact length in order to determine where in the contact region is sticky and sliding. Finally, the brush model quality in prediction of force and moment is acceptable, but would not be

acceptable for desirable functionality in industrial end-user level where precision is very important unless a more comprehensive model like TaMeTyre is developed.

A.2. Empirical models

Generally, the empirical approach represents tyre modelling approaches that require tyre data measurements for the characterisation of parameters. This model is also referred to as the “black box” modelling approach. Two categories are recognised for this type of modelling: the shape function approach, and the regression models. Both models are based on curve fitting of test data but employ dissimilar tools for the same fitting problem. In the shape function approach, the overall measured behaviour is investigated and one or more shape functions, which most closely resemble the original shape and are also adaptable for varying operating conditions, are picked from a pool of functions. In the regression approach, the data targeted for fitting is broken into intervals and similar curves with dissimilar coefficients are used to interpolate the unknown data in between. Both methods are defined following this section and the advantages and disadvantages of each are separately discussed. The most famous candidate for the first category is the magic formula that will symbolise the rest of the empirical approaches in this study.

A.2.1 MF tyre

The MF-Tyre package that consists of the Magic Formula (MF) and SWIFT models were developed by TNO Automotive (TNO Automotive, 2010), and is the current iteration of initial works triggered by Professor Hans Pacejka at Delft University in Netherlands (Pacejka, 2012). MF-tyre consists of two separate modules: the force and moment module that is known as the Magic formula and the SWIFT module that predicts the enveloping path over uneven roads. Both models are discussed through the following sub-sections.

A.2.1.1 Magic formula

Magic Formula has been formed based on an empirical formulation, i.e. the general shape of the equation has been mathematically approximated based on observations from the overall trend of forces and moments curves derived from characterisation tests. The MF is well-known and popular among handling models and is practically a required option for most vehicle dynamics programmes and aircraft ground dynamic applications. The computational efficiency of the equations and the compact nature of a coefficient based model allow for straightforward implementation into iterative computer simulation.

The forces and moments are modelled in the MF through the similar generic form despite a distinct set of coefficients is applied to the same equation. That is probably why the MF equation was termed "magical", referring to its unique capability in mimicking the tyre forces and moments (F&M) behaviour by way of transformation into the desired shape through the observed F&M trend under the varying tyre states such as slip angle, slip ratio, inclination angle, and vertical load. Although the MF was derived empirically, its coefficients were purposely associated with both tyre physical parameters and states. Hence, the MF is generally a pure empirical model as it appears out of the box, but it is frequently addressed as a semi-empirical model when it is viewed in details.

The MF general form is shown through equation A.9 (Pacejka, 2012).

$$y = D\sin[C\arctan\{Bx - E(Bx - \arctan Bx)\}] \qquad \text{Equation A.9}$$

with:

- $Y(X) = y(x) + S_V$
- $x = X + S_H$

where:

- Y output variable F_x, F_y, and M_z
- X input variable $\tan\alpha$ or κ
- B stiffness factor
- C shape factor
- D peak value
- E curvature factor
- S_H horizontal shift
- S_V vertical shift

The way that the parameters affect the F&M shape is demonstrated in figure A.8. The left graph in figure A.8.a. demonstrates how the vertical shifting parameters move the curves around while the parameter D is taking care of the scalability of the curve. The right figure also explains how the general form of forces and moments shape is built through the trigonometric functions $\sin(\arctan(-))$. The influence of curvature and shape factors C and E is illustrated in figure A.8.b. This figure also indicates that the variation in the range of shape factors can make the MF curves consistent with the natural trends of F_x, F_y and M_z.

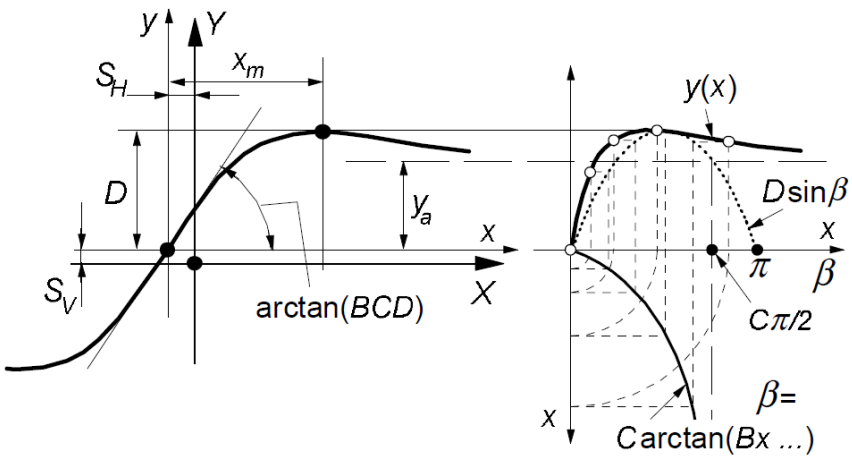

a. The influence of shifting coefficients S_V, S_H and scale parameter D (Pacejka, 2012)

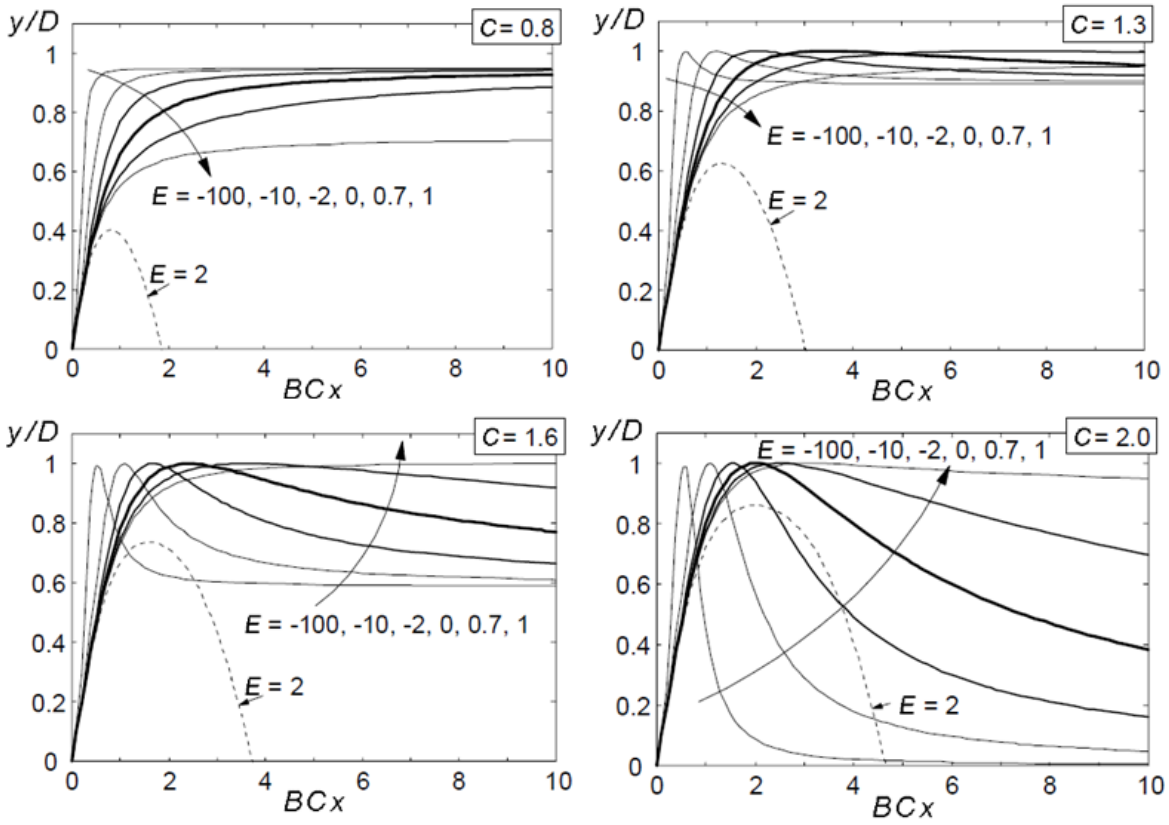

b. The influence of shape factor C and curvature parameter E

Figure A.8. The mechanism of MF parameters influence on the F&M shapes (Pacejka, 2012)

A.2.1.2 SWIFT model

The SWIFT model is a rigid ring tyre model to study the short wavelength and dynamic behaviour of the tyre on an uneven road and was developed at Delft University in Netherlands by (Maurice, 2000) and (Schmeitz, 2004). This model is listed under the semi-empirical models since the enveloping method is formed around two overlapped elliptical cams (figure A.9) that are pivoted in the tyre and moves along the rolling tyre. Each elliptical cam has a separate single point of contact with the road at the leading and trailing edges of the tyre contact patch. While the tyre travels along an uneven road, SWIFT mathematically averages the vertical motion of points on its own exclusive technique and represents it as the enveloped vertical motion. A practice of the SWIFT concept when facing a step road is

illustrated in figure A.10. However, the advanced tuned ring model runs the deflection mechanism in SWIFT. The interaction of these rigid rings and the two-ellipse models is shown in figure A.11.

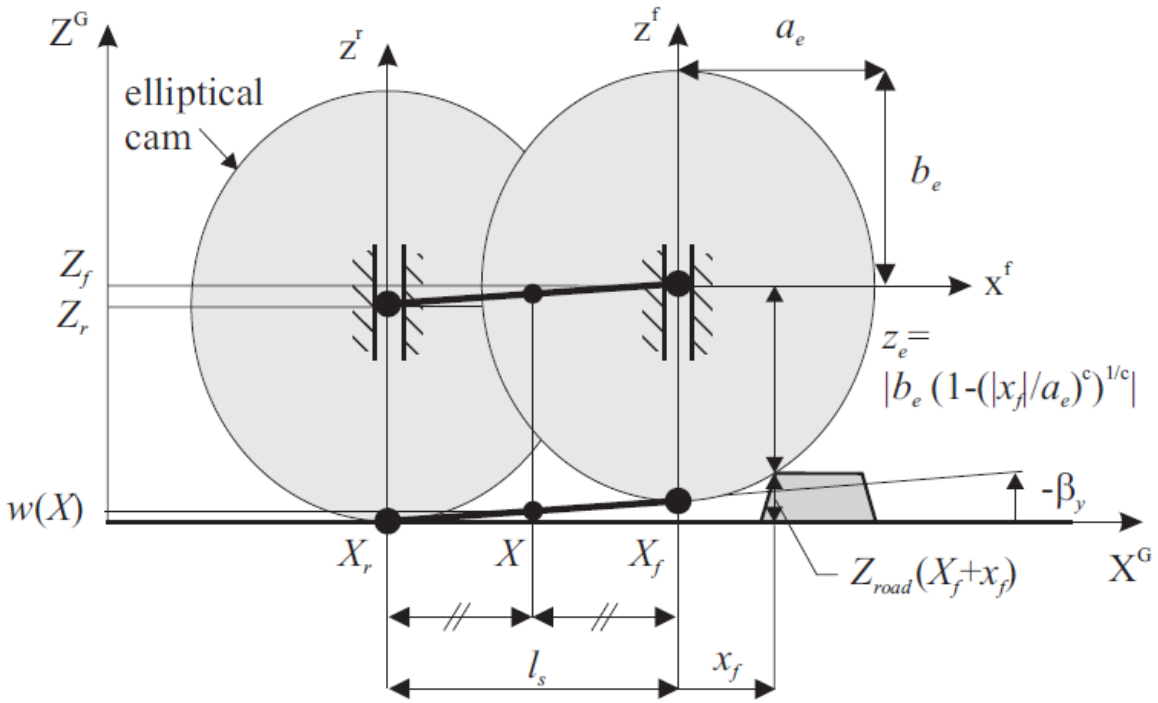

Figure A.9. The SWIFT enveloping conceptual model with elliptical cams (Schmeitz, 2004)

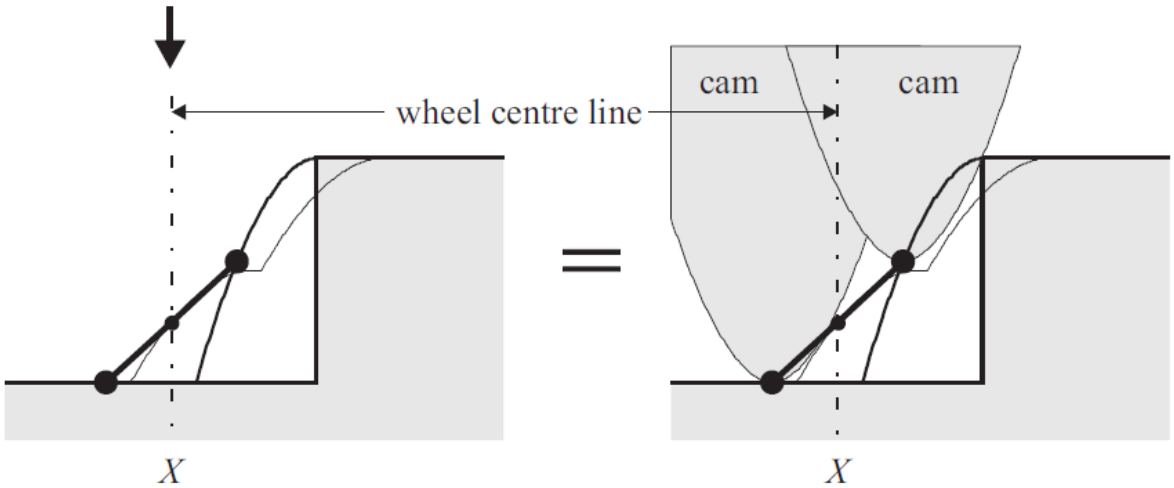

Figure A.10. A practice of SWIFT on step road (Schmeitz, 2004)

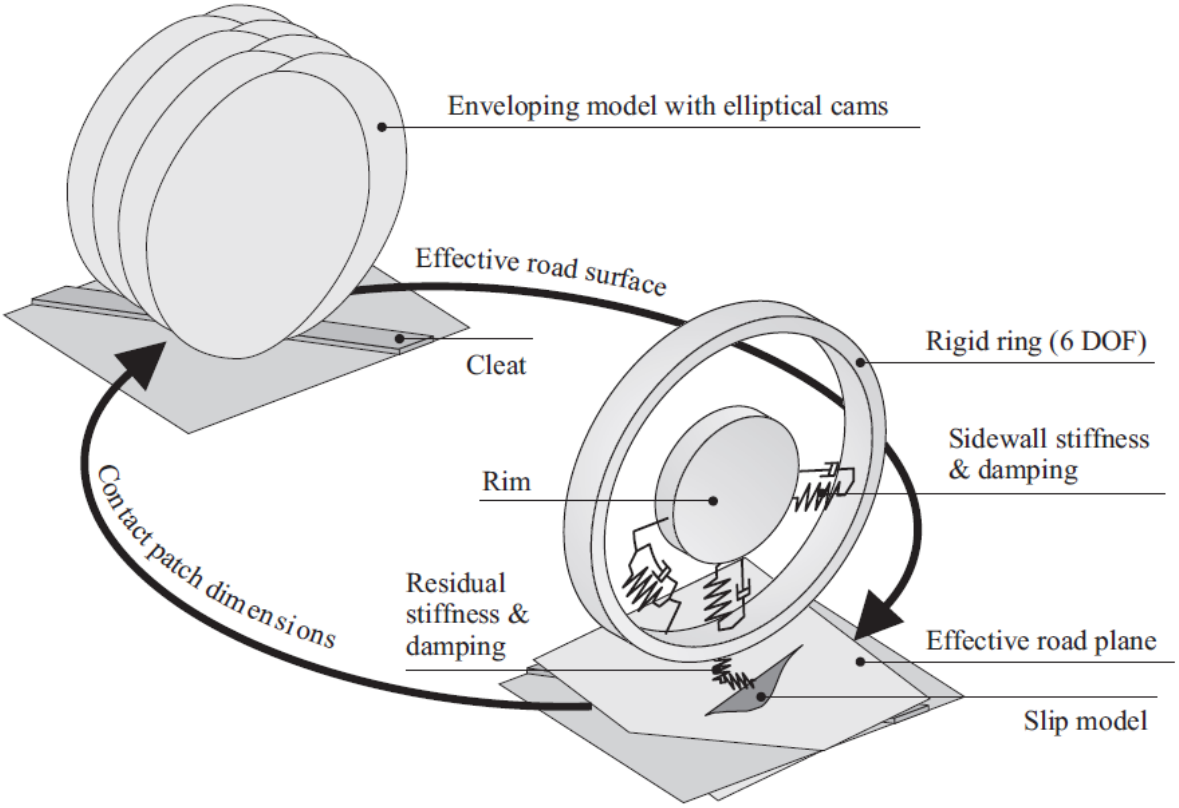

Figure A.11. The influence of shifting coefficients S_V, S_H and scale parameter D

Since the Magic formula disregards the deflection mechanism modelling, The SWIFT model covers its deficiency by employing the semi-empirical enveloping approach. The quality of the results is comparable with those discussed for FTire model.

Like the physical approaches, the SWIFT model needs experiments for parameterisation of stiffness in addition to determining the geometry of ellipses. TNO suggests a standard procedure to characterise the SWIFT parameters. It is time consuming if the SWIFT is desired to be run under a full operating range (Schmeitz, 2008).

A.2.1.3 Advantages and disadvantages of MF tyre model

Both MF/SWIFT are computationally efficient and appropriate for the hardware-in-loop and software-in-loop simulations. However, the optimization of parameters occasionally requires substantial effort and depends on parameter initialization and does not necessarily

provide unique tuned factors to the solution. A well fitted model can represent a good accuracy for a wide range of inputs in handling, ride, and enveloping up to 100 Hz. Durability analyses is also supported in the MF model.

Since MF tyre operates as a black box model, the outputs are only those for which the MF is tuned. In other words, a complete set of experimental data is essentially required, so that the parameters can be tuned based on the desired outputs and the rest of F&M data are interpolated/extrapolated. Nevertheless, the extrapolation may lead to wrong approximations of forces and moments. Since the straightforward prediction of behaviour without tuning of factors is not possible, this approach will not provide an appropriate tool to assist designers in the design synthesis prior to a prototype tyre being built.

Since the MF equations are available freely in public domain through manuals and books, the model setup is fairly quick and reasonable. Furthermore, the standard testing procedure to characterise the behaviour of tyres has been suggested by TNO automotive and are available through their online manuals on MF-Tool software, so that the efforts are the least for both equation setup and model characterisation of tyres. On the other hand, adding a supplementary factor based on an augmented physics like thermal effects is not straightforward according to the fact that the change should be seen throughout the model equation and the consistency of the MF model should be comprehensively studied. Although the model equations are freely accessible, the experiments can be very expensive (around $1500 hourly fee to use the MTS Flat-Trac in NTRC, Virginia USA) and time consuming to gather a quality database.

A.2.2 Regression models

The models based on regression use interpolation methods. Regression models are also referred to as the table-based model (CARSIM, 2013). Therefore, this method is considered as a pure empirical approach since no physics is involved in the coefficient of regression function. As pointed out in its title, this model requires a table of experimental data before it predicts the desired output. A number of references, (Smith, 2003) and (C. Fernandes, 2004), have implemented this method along with their vehicle dynamics codes.

The regression function can be either linear or nonlinear, in which an extrapolation is strongly discouraged. Thus, a table with extensive range of input parameter is required for a comprehensive applicability to avoid extrapolation. The accuracy of this method is highly tied with the quality of the table data and depends on how decent data are picked, and particularly, how much noise the data have. The next concern regarding its accuracy is due to the number of points for each force and moment curve to be interpolated. In fact, the more points selected, the better the interpolation follows the force and moment curves. However, it may over-follow the curve trends through the noises instead of circumventing them by passing through the noisy points and tracking the general trend of the curve instead, as expected. Therefore, a careful selection of quality data pool, properly post-processed and properly noise-rejected, is crucial to form the table of forces and moments. In addition, a trial procedure is necessary to determine the number of points that is supposed to be selected from each particular force and moment curve. The selection of the point's quantity depends on the level of discretisation and the type of regression function employed for the interpolation task. For a linear regression function, two coefficients are required to be characterised per interval between two successive discretised points while

for the well-known quadratic (second order) or cubic (equation A.10) (third order) B-Spline functions, three and four coefficients should be determined respectively (Boor, 2001).

$$Cubic\ (u) = a_3u^3 + a_2u^2 + a_1u + a_0 \qquad \text{Equation A.10}$$

According to the regression equation for cubic interpolation, four coefficients should be characterised in pure slip table of forces and moments per tyre individual load and position conditions at which the data are measured and one interval between two successive discrete points. By a simple calculation, the number of required coefficients at pure slip condition can be determined, and for a high precision in force and moment regression, a considerable number of coefficients are demanded. However, this method offers great computational efficiency owing to the fact that a simple cubic function with few math operations is employed for the prediction procedure. Like the MF, this method cannot be used for the design synthesis and it is functional where the table is not massive and a quick implementation is required.

A.3. Numerical-Physical models

In fact, these models are listed under the same category that analytical physical models are classified since the background of both methods has originated from mimicking physical phenomena of sophisticated tyre structure. However, these methods are categorised based on the level of complexity in physics and the level of physical details involved in modelling. The Finite Element Method (FEM) is known as the most common numerical method used to analyse the tyre performance under complicated loading and operating conditions. This method was described in details in section A.4.

References

Abu-Abdeen, M., 2010. Single and double-step stress relaxation and constitutive modeling of viscoelastic behavior of swelled and un-swelled natural rubber loaded with carbon black. *Material and Design,* Volume 31, pp. 2078-2084.

American Society for Testing and Materials, 2014. *ASTM book of standards: Standard Test Methods for Tire Cords, Tire Cord Fabrics, and Industrial Filament Yarns Made from Manufactured Organic-Base Fibers.* s.l.:s.n.

Arruda, E. M. & Boyce, M. C., 1993. A three-dimensional model for the large stretch behavior of rubber elastic materials. *Journal of the Mechanics and Physics of Solids,* 41(2), pp. 389-412.

Assaad, M. C. et al., 2008. Thin-Film Heat Flux Sensor for Measuring the Film Coefficient of Rubber Components of a Rolling Tire. *Tire Science and Technology,* 36(4), pp. 275-289.

Baeurle, S. A., Hotta, A. & Gusev, A. A., 2006. On the glassy state of multi-phase and pure polymer materials. *Polymer,* 47(17), pp. 6243-6253.

BEA, 2002. *BEA Report: Concorde accident on 25 July 2000 at La Patte d'Oie in Gonesse,* s.l.: Bureau Enquêtes-Accidents.

Bechira, H., Chevalierb, L., Chaouchec, M. & Boufalaa, K., 2006. Hyperelastic constitutive model for rubber-like materials based on the first Seth strain measures invariant. *European Journal of Mechanics - A/Solids,* 25(1), p. 110–124.

Behroozi, M., Olatunbosun, O. & Ding, W., 2012. Finite element analysis of aircraft tyre – Effect of model complexity on tyre performance characteristics. *Materials & Design,* Volume 35, pp. 810-819.

Bellonte, M., 2005. *Flight Operations Briefing Notes,* Cedex: s.n.

Benzley, S. E. et al., 1995. *A Comparison of All-Hexahedral and All-Tetrahedral Finite Element Meshes for Elastic and Elasto-Plastic Analysis.* Albuquerque, New Mexico, Sandia National Laboratories, pp. 179-191.

Bergstrom & Boyce, M. C., 1999. Mechanical behavior of particle filled elastomers. *Rubber Chemistry and Technology,* 72(10), pp. 633-656.

Bergstrom, J. & Boyce, M., 2000. Large strain time-dependent behavior of filled elastomers. *Mechanics of Materials,* 32(11), pp. 627-644.

Bergstrom, J. & Boyce, M., 2001. Constitutive modeling of the time-dependent and cyclic loading of elastomers and application to soft biological tissues. *Mechanics of Materials,* 33(9), pp. 523-530.

Bergstrom, J. S., 1999. *Large Strain Time-Dependent Behavior of Elastomeric Materials,* s.l.: MIT.

Bergstrom, J. S. & Boyce, M. C., 1998. Constitutive modeling of the large strain time-dependent behavior of elastomers. *Journal of the Mechanics and Physics of Solids,* Volume 46, pp. 931-954.

Bergstrom, J. S. & Boyce, M. C., 2001. Deformation of Elastomeric Networks: Relation between Molecular Level Deformation and Classical Statistical Mechanics Models of Rubber Elasticity. *Macromolecules,* 34(3), pp. 614-626.

Bikard, J. & Désoyer, T., 2001. Finite viscoelasticity, plasticity and damage of a class of filled elastomers: Constitutive model. *Mechanics Research Communications,* 28(6), pp. 693-702.

Bolarinwa, E., 2004. *Finite Element modelling of the pneumatic tyres,* Birmingham: University of Birmingham.

Bolarinwa, E. & Olatunbosun, O., 2004. Finite Element Simulation of the Tyre Burst Test. *Proceedings of the Institution of Mechanical Engineers Part D: Journal of Automobile Engineering,* 218(11), pp. 1251-1258.

Bolarinwa, E., Olatunbosun, O. & and Burnett, M., 2004. *A Study of Cornering Behaviour using a Finite Element Model.* Beijing, China, s.n.

Boor, C. d., 2001. *A Practical Guide to Splines.* s.l.:Springer-Verlag New York Inc.

Boyce, M., 1997. Direct Comparison of the Gent and the Arruda-Boyce Constitutive Models of Rubber Elasticity. *Rubber Chemistry and Technology,* Volume 69, pp. 781-785.

Boyce, M. & Arruda, E., 1990. An Experimental and Analytical Investigation of the Large Strain Compressive and Tensile Response of Glassy Polymers. *Journal of Polymer Engineering and Science,,* 30(20), pp. 1288-1298.

Boyce, M. & Arruda, E., 2000. Constitutive Models of Rubber Elasticity: A Review. *Rubber Chemistry and Technology,* 73(3), pp. 504-523.

Boyce, M. C. & Arruda, E. M., 2000. Constitutive Models of Rubber Elasticity: A Review. *Rubber Chemistry and Technology,* 73(3), pp. 504-523.

Bridgestone , 2006. *Bridgestone Aircraft Tire Application,* s.l.: s.n.

Bridgestone, 2013. *Revolutionarily Reinforced Radial (RRR).* [Online] Available at: http://www.bridgestone.com/products/speciality_tires/aircraft/rrr/index.html

Burke, A. & Olatunbosun, O., 1997. New Technologies in Tyre Modal Analysis using MSC/NASTRAN. *International Journal of Vehicle Design,* 18(2), pp. 203-212.

Burke, A. & Olatunbosun, O., 1997. Static Tyre/Road Interaction Modelling. *Mechanica,* 32(5), pp. 473-479.

C. Fernandes, E. P., 2004. *Tire Modeling for Model Validation.* s.l., SAE.

CAA, 2011. *CAA 'Significant Seven' Task Force Reports,* s.l.: Civil Aviation Authority .

Carroll, M., 2011. A Strain Energy Function for Vulcanized Rubbers. *Journal of Elasticity,* 103(2), pp. 173-187.

CARSIM, 2013. *Math models in CARSIM,* s.l.: Mechanical Simulation Corporation.

Chang, J. P., Satyamurthy, K. & Tseng, N. T., 1988. An Efficient Approach for the Three-Dimensional Finite Element Analysis of Tires. *Tire Science and Technology,* 16(4), pp. 249-273.

Chang, T., Saleeb, A. & Li, G., 1991. Large strain analysis of rubber-like materials based on a perturbed Lagrangian variational principle. *Computational Mechanics,* 8(4), pp. 221-233.

Chen, T., 2000. *Determining a Prony Series for a Viscoelastic Material From Time Varying Strain Data,* s.l.: U.S. Army Research Laboratory.

Chen, W. & Saleeb, A. F., 1982. *Constitutive Equations for Engineering Materials, Vol. 1, Elasticity and Modeling.* 1st ed. New York: Wiley.

Christensen, R., 1982. *Theory of Viscoelasticity: An Introduction.* 2nd ed. New York: Academic Press.

Clark, S., 1991. A Beam Model for Tire Critical Speeds. *Tire Science and Technology,* 19(2), pp. 113-120.

Clark, S. & Dodge, R., 1982. *Heat Generation in Aircraft Tires Under Free Rolling Conditions,* Langley, US: NASA.

Clark, S. & Dodge, R., 1984. *Heat Generation in Aircraft Tires Under Braked Rolling Conditions,* Langley, US: NASA.

Clark, S. K., 1974. *Rolling Resistance of Pneumatic Tires,* s.l.: The University of Michigan.

Clark, S. K. & Dodge, R. M., 1985. Tire modeling and contact problem - Heat generation in aircraft tyres. *Computers & Structures,* 20(1-3), pp. 535-544.

Cosin, 2013. *FTire Product Brief.* [Online] Available at: http://www.cosin.eu/

Danielson, K. T. & Noor, A. K., 1997. Finite Elements Developed in Cylindrical Coordinates for Three-Dimensional Tire Analysis. *Tire Science and Technology,* 25(1), pp. 2-28.

Dassault Systèmes Simulia Corp, 2012. *Abaqus Scripting User's Manual,* Providence: Dassault Systèmes.

Daws, J. W., Larson, R. E. & Brown, J., 2007. The Impact of Plus-Sized Wheel/Tire Fitment on Vehicle Stability. *Journal of Tire Science and Technology,* March, 35(1), pp. 23-40.

Dostal, H., 1939. The Statistical Theory of the Elasticity of Rubber. *Rubber Chemistry and Technology,* 12(1), pp. 56-63.

Driving Fast Inc., 2013. *Braking techniques.* [Online] Available at: http://www.drivingfast.net/ [Accessed 20 11 2013].

Dunlop Aircraft Tyre Limited, 2013. *Aircraft tyre technology.* [Online] Available at: http://www.dunlopaircrafttyres.com

Dunlop Tyres, 2013. *1923-1937: Early leader.* [Online] Available at: http://www.dunloptires.com/en-US/company/tire-history#1923-1937 [Accessed 20 August 2013].

Dunlop, 2008. *Tyre Care Manual,* Birmingham: Dunlop Aircraft Tyres Limited.

Dunlop, 2013. *1888-1922: Born ready to roll,* s.l.: Dunlop Aircraft Tyre Limited.

Dunlop, 2013. *Tyre reprository.* [Online] Available at: http://www.dunlopaircrafttyres.com/

Durand-Gasselin, B. et al., 2010. Assessing the thermo-mechanical TaMeTirE model in offline vehicle simulation and driving simulator tests. *Vehicle System Dynamics: International Journal of Vehicle Mechanics and Mobility,* 48(1), pp. 211-229.

Ebbott, T. G., 1996. An Application of Finite Element-Based Fracture Mechanics Analysis to Cord-Rubber Structures. *Tire Science and Technology,* 24(3), pp. 220-235.

Ebbott, T. G., Hohman, R. L., Jeusette, J.-P. & Kerchman, V., 1999. Tire Temperature and Rolling Resistance Prediction with Finite Element Analysis. *Tire Society and Technology journal,* 27(1), pp. 2-21.

EC, 2012. *EU transport in figures - Statiscal pocketbook ,* Luxembourg: European Commision.

Enderle, H. F. & Killian, G., 1987. General deformation modes of a van der Waals network. *Permanent and Transient Networks: Progress in Colloid & Polymer Science,* Volume 75, pp. 55-61 .

FAA, 1997. *Advisory Circular,* s.l.: Federal Aviation Administration.

FAA, 2000. *CERTIFICATION OF TRANSPORT AIRPLANE MECHANICAL SYSTEMS,* s.l.: Federal Aviation Administration.

FAA, 2006. *Inspection, Retread, Repair, and Alterations of Aircraft Tires,* s.l.: Federal Aviation Administration.

FAA, 2013. *Aviation Safety (AVS).* [Online] Available at: http://www.faa.gov/about/office_org/headquarters_offices/avs/

Faria, L. O. O. J. T. Y. B. T. W. W. B. J. M. B. E. B., 1992. Tire Modeling by Finite Elements. *Tire Science and Technology,* 20(1), pp. 33-56.

Fatt, H. & Bekar, M., 2004. High-speed testing and material modeling of unfilled styrene butadiene vulcanizates at impact rates. *Journal of Material Science,* 39(23), p. 6885–6899.

Feiertag, T., 2011. *Atlantic Sun Airways CAT C Pilot Procedure,* s.l.: Atlantic Sun Airways.

Ferry, J. D., 1980. *Viscoelastic Properties of Polymers.* 3rd ed. s.l.:Wiley.

Fevrier, 2013. *Method for the simulation of the physical behavior of a tire rolling on the ground.* Worldwide Network based patent registration, Patent No. 1516751.

Février, P. & Fandard, G., 2008. Thermal and mechanical tyre modelling for handling simulation. *ATZ worldwide,* 110(5), pp. 26-31.

Février, P., Hague, O. B., Schick, B. & Miquet, C., 2010. Advantages of a thermomechanical tire model for vehicle dynamics. *ATZ worldwide,* 112(7-8), pp. 33-37.

Fiala, E., 1952. Seitenkrafte am rollenden Luftreifen. *VDI-Zeitschrift*, 96(29), pp. 973-979.

Flory, P. J., 1967. *Principles of Polymer Chemistry.* 1st ed. Lincoln: Cornell University Press.

Flory, P. J., 1977. Theory of elasticity of polymer networks. The effect of local constraints on junctions. *The Journal of Chemical Physics,* 66(12), pp. 5720-5729.

Flory, P. J. & Erman, B., 1982. Theory of elasticity of polymer networks. *Macromolecules,* 15(3), pp. 800-806.

Fung, W. & Hardcastle, J. M., 2001. *Textiles in Automotive Engineering.* 1 ed. Lancaster(Pennsylvania): Elsevier.

Futamura, S. & Goldstein, A., 2004. Simplifying the Thermal Analysis of a Rolling Tire with the Deformation Index Method. *Tire Science and Technology journal,* 32(2), pp. 56-68.

Gent, A., 1996. A new constitutive relation for rubber. *Rubber Chemistry and Technology,* 69(1), pp. 59-61.

Gent, A., 2001. *Engineering with Rubber 2E: How to Design Rubber Components.* 2nd ed. New York: Hanser Publications.

Gent, A. & Thomas, A., 1958. Forms for the stored (strain) energy function for vulcanized rubber. *Journal of Polymer Science,* Volume 28, pp. 625-628.

Ghoreishy, H. R., Alimardani, M., Mehrabian, R. Z. & Taghvaei, S., 2013. Modeling the Hyperviscoelastic Behavior of a Tire Tread Compound Reinforced by Silica and Carbon Black. *Journal of Applied Polymer Research,* 128(3), pp. 1725-1731.

Giessler, M., Gauterin, F., Wiese, K. & Wies, B., 2010. Influence of Friction Heat on Tire Traction on Ice and Snow. *Tire Science and Technology,* 38(1), pp. 4-23.

Gillespie, T., 1992. *Fundamentals of Vehicle Dynamics.* 1st ed. Warrendale: Society of Automotive Engineers Inc.

Gillespie, T. D., 1992. *Fundomentals of vehicle dynamics.* s.l.:Society of Automotive Engineers (SAE).

Gipser, M., 2005. *FTire: A new fast tire model for ride comfort simulations,* s.l.: Esslingen University of Applied Sciences.

Gipser, M., 2005. FTire: a physically based applicationoriented tyre model for use with detailed MBS and finite-element suspension models. *Vehicle System Dynamics: International Journal of Vehicle Mechanics and Mobility,* Volume 43:sup1, pp. 76-91.

Gipser, M., 2013. *FTire - Flexible Ring Tire Model: Modelization and Parameter Specification,* Munich, Germany: Cosin Scientific Software.

Göktepe, S. & Miehe, C., 2005. A Micro-Macro Approach to Rubber-Like Materials. Part III: The Micro-Sphere Model of Anisotropic Mullins-Type Damage. *Journal of the Mechanics and Physics of Solids,* 53(10), pp. 2259-2283.

Goodyear aviation, 2013. *Goodyear Aviation Firsts,* s.l.: s.n.

Goodyear, 2011. *Aircraft Tire Care and Maintenance,* s.l.: s.n.

Guo, Z. & Sluys, L. J., 2006. Application of a new constitutive model for the description of rubber-like materials under monotonic loading. *International Journal of Solids and Structures,* 43(9), pp. 2799-2819.

Haisler, W. E. & Stricklin, J. A., 1970. *SNASOR II - A Finite Element Program for the Static Nonlinear Analysis of Shells of Revolution,* Houston: Texas A&M University.

Harty, D. & Blundell, M., 2004. *The multibody systems approach to vehicle dynamics.* 1st ed. s.l.:Oxford UK.

Haupt, P., 2000. *Continuum mechanics and theory of materials.* 1st ed. Berlin: Springer-Verlag.

Holscher, H., Tewes, M., Botkin, N. & Lohndorf, M., 2004. *Modeling of Pneumatic Tires by a Finite Element Model for the Development a Tire Friction Remote Sensor,* Bonn, Germany: Center of Advanced European studies and Research (Caesar).

Holzapfel, G., 1996. On large strain viscoelasticity: continuum formulation and finite element applications to elastomeric structures. *International Journal of Numerical Methods Application in Mechnaical Engineering,* 39(22), pp. 3903-3926.

Holzapfel, G. A., 2000. *Nonlinear Solid Mechanics: A continuum approach for engineering.* 1st ed. s.l.:John Wiley &Sons Ltd.

Hooke, R., 1676. *Description of Helioscopes.* s.l.:s.n.

Hughes, T. J. R., 2000. *Finite Element Method: Linear Static and Dynamic Finite Element Analysis.* 2nd ed. New Jersey : Dover.

Hunnekens, B., 2008. *Tire road frictional interaction: A physical approach,* Eindhoven: Eindhoven University of Technology.

IATA, 2013. *IOSA Standards Manual,* s.l.: International Air Transport Association (IATA) .

Isihara, A., Hashitsume, N. & Tatibana, M., 1951. Statistical Theory of Rubber-Like Elasticity. IV. (Two-Dimensional Stretching). *Journal of Chemical Physics,* Volume 19, pp. 1508-1512.

ISO, 1998. *Aircraft tyres and rims. Part 2. Test methods for tyres,* s.l.: International Organization for Standardization.

Jain, K. K. & Asthana, R. B., 2002. *Automobile Engineering.* 1st ed. Delhi: Tata McGraw-Hill Publlishing company limited.

James, H. & Guth, E., 1943. Theory of the elastic properties of rubber. *The Journal of Chemical Physics,* 11(10), pp. 455-481.

Kaga, H., Okamoto, K. & Tozama, Y., 1977. Stress Analysis of Tire Under Vertical Load by a Finite Element Method. *Tire Science and Technology,* 5(2), pp. 102-118.

Kaliske, M. & Rothert, H., 1997. On the finite element implementation of rubber-like materials at finite strains. *Engineering Computations,* 14(2), pp. 216-232.

Khennane, A., 2013. *Introduction to Finite Element Analysis Using MATLAB® and Abaqus.* s.l., Taylor and Frances.

Kilian, H. -G., 1980. A molecular interpretation of the parameters of the van der Waals equation of state for real networks. *Polymer Bulletin,* 3(3), pp. 151-158.

Kilian, H. -G., Schenk, H. & Wolff, S., 1987. Large deformation in filled networks of different architecture and its interpretation in terms of the van der Waals network model. *Colloid and Polymer Science,* 265(5), pp. 410-423.

Konyukhov, A. & Schweizerhof, K., 2013. Surface-To-Surface Contact – Various Aspects for Implementations within the Finite Element Method. In: *Computational Contact Mechanics.* Berlin, Germany: Springer Berlin Heidelberg, pp. 209-291.

Korunović, N., Trajanović2, M. & Stojković3, M., 2007. Finite Element Model for Steady-State Rolling Tire Analysis. *Journal of the Serbian Society for Computational Mechanics,* 1(1), pp. 63-79.

Korunović, N. et al., 2011. Finite Element Analysis of a Tire Steady Rolling on the Drum and Comparison with Experiment. *Journal of Mechanical Engineering,* 57(12), pp. 888-897.

Kuhn, W. & Grün, F., 2003. Statistical behavior of the single chain molecule and its relation to the statistical behavior of assemblies consisting of many chain molecules. *Journal of Polymer Science,* 1(3), pp. 183-199.

LaClair, T. J. & Zarak, C., 2005. Truck Tire Operating Temperatures on Flat and Curved Test Surfaces. *Tire Science and Technology,* 33(3), pp. 156-178.

Lee, C., Kim, J., Hallquist, J. & Zhang, Y., 1997. *Validation of a FEA Tire Model for Vehicle Dynamic Analysis and Full Vehicle Real Time Proving Ground Simulations.* s.l., SAE International.

Libertiaux, V. & Pascon, F., 2010. Differential versus integral formulation of fractional hyperviscoelastic constitutive laws for brain tissue modelling. *Journal of Computational and Applied Mathematics,* 234(7), pp. 2029-2035.

Lin, Y.-J. & Hwang, S.-J., 2004. Temperature prediction of rolling tires by computer simulation. *Mathematics and Computers in Simulation,* Volume 67, pp. 235-249.

Liu, M., 2007. *A Three-Dimensional Hyper-Viscoelasticity Constitutive Model for the Dynamic Response of Rubber,* Akron: University of Akron.

Luchini, J. R. & Popio, J. A., 2007. Modeling Transient Rolling Resistance of Tires. *Tire Science and Technology,* 35(2), pp. 118-140.

Mark, J. E. & Erman, B., 2005. *Science and Technology of Rubber.* 3rd ed. Amsterdam: Elsevier Academic Press.

Marlow, R. S., 2003. First-Invariant Hyperelastic Constitutive Model. In: J. Busfield & A. Muhr, eds. *Constitutive Models Rubber III.* Lisse: Swets & Zeitlinger, pp. 157-160.

Massy, A., 1991. Aircraft Tires: Bias or Radials?. *Aerospace Engineering,* September, 11(9), pp. 13-14.

Maurice, J. P., 2000. *Short Wavelength and Dynamic Tyre Behaviour under Lateral and Combined Slip Conditions,* Delft: Delft University of Technology.

McGuire, M. & Hughes, J. F., 2004. *Hardware-Determined Feature Edges.* Annecy, France, Proceedings of the 3rd international symposium on Non-photorealistic animation and rendering.

Meuniera, L. et al., 2008. Mechanical experimental characterisation and numerical modelling of an unfilled silicone rubber. *Polymer Testing,* 27(6), pp. 765-777.

Michelin, 2006. *Michelin certified tire expert program,* s.l.: s.n.

Michelin, 2013. *Michelin History: The time of significant disruptions.* [Online] Available at: http://www.michelin.com/corporate/group/history?l=en [Accessed 2013].

Michelin, 2013. *Michelin in aviation history.* [Online] Available at: http://www.airmichelin.com/history.aspx?id=148 [Accessed 2013].

Michelin, 2013. *Radial vs. Bias Technology.* [Online] Available at: http://www.michelinag.com/Innovating/Radial-vs.-Bias-technology

Michelin, 2014. *Michelin Tire Glossary.* [Online] Available at: http://www.michelinman.com/tires-101/tire-basics/glossary.page [Accessed 12 July 2014].

Miehe, C., Göktepe, S. & Lulei, F., 2004. A micro-macro approach to rubber-like materials--Part I: the non-affine micro-sphere model of rubber elasticity. *Journal of the Mechanics and Physics of Solids,* 52(11), pp. 2617-2660.

Miehe, C., Göktepe, S. & Lulei, F., 2004. A micro-macro approach to rubber-like materials—Part I: the non-affine micro-sphere model of rubber elasticity. *Journal of the Mechanics and Physics of Solids,* 52(11), pp. 2617-2660.

Miller, K., 2002. *Experimental Loading Conditions Used to Implement Hyperelastic and Plastic Material Models,* An Arbor, Michigan, US: axelproducts.

Mooney, M., 1940. A theory of large elastic deformation. *Journal of Applied Physics,* Volume 11, pp. 582-592.

Morris, N., 2014. *Wheel Tech, Part III: Wheel Diameter's Effect on Performance.* [Online] Available at: http://www.tuneruniversity.com [Accessed 14 07 2014].

Muhr, A. H., 2005. Modelling the stress-strain behaviour of rubber. *Rubber Chemistry and Technology,* 78(3), pp. 391-425.

Nah, C. et al., 2010. Problems in determining the elastic strain energy function for rubber. *International Journal of Non-Linear Mechanics,* 45(3), pp. 232-235.

Narasimha Rao, K. V., Kumar, R. K., Bohara, P. C. & Mukhopadhyay, R., 2006. A Finite Element Algorithm for the Prediction of Steady-State Temperatures of Rolling Tires. *Tire Science and Technology journal,* 34(3), pp. 195-214.

NFM Technologies, 2009. *AERONAUTICS: A SOLID PARTNERSHIP WITH AIRBUS,* Lyon: NHI Group.

NHTSA, 2001. *PROPOSED NEW PNEUMATIC TIRES FOR LIGHT VEHICLES,* s.l.: National Highway Traffic Safety Administration.

Oden, J. T., Lin, T. L. & Bass, J. M., 1988. A Finite Element Analysis of the General Rolling Contact Problem for a Viscoelastic Rubber Cylinder. *Tire Science and Technology,* 16(1), pp. 18-43.

Oertel, C. & Wei, Y., 2012. Tyre rolling kinematics and prediction of tyre forces and moments. *Vehicle System Dynamics,* 50(11), pp. 1673-1687.

Ogden, R., 1997. *Non-linear Elastic Deformations.* 1st ed. Dover, New York: Dover Publications.

Ogden, R. W., 1972. Large Deformation Isotropic Elasticity: On the Correlation of Theory and Experiment for Compressible Rubberlike Solids. *Proceeding of the Royal Society of Mathematical, Physical, and Engineering Sciences,* 326(1567), pp. 565-584.

Ogden, R. W. & Roxburgh, D. G., 1999. A pseudo-elastic model for the Mullins effect in filled rubber. *Proceeding of the Royal Society of London,* 455(1988), pp. 2861-2877.

Ogden, R. W., Saccomandi, G. & Sgura, I., 2004. Fitting hyperelastic models to experimental data. *Computational Mechanics ,* 34(6), pp. 484-502.

Ogden, R. W., Saccomandi, G. & Sgura, I., 2006. On worm-like chain models within the three-dimensional continuum mechanics framework. *Proceeding of the Royal Society of Mathematical, Physical, and Engineering Sciences,* 462(2067), pp. 749-768.

Olatunbosun, O. & Bolarinwa, E., 2004. FE Simulation of the Effect of Tire Design Parameters on Lateral Forces and Moments. *Tire Science and Technology jornal TSTCA,* 32(3), pp. 146-163.

Olatunbosun, O. & Burke, A., 2000. *Finite Element Modelling of Rotating Tires in the Time Domain.* Akron, Ohio, USA, Tire Society.

ONS, 2013. *Travel Trends: 2012,* s.l.: Office for National Statistics.

Pacejka, H., 1971. Shell model. In: S. Clark, ed. *Mechanics of Pneumatic Tires.* Washington: NBS Monograph.

Pacejka, H. B., 2012. *Tire and Vehicle Dynamics.* 3rd ed. Oxford, UK: Butterworth-Heinemann.

Park, H. C., Youn, S.-K., Song, T. S. & Kim, N.-J., 1997. Analysis of Temperature Distribution in a Rolling Tire Due to Strain Energy Dissipation. *Tire Science and Technology journal,* 25(3), pp. 214-228.

Perisse, J. & Hamet, J. F., 2000. *A comparison of the 2d ring and 3d orthotropic plate for modelling of radial tire vibrations.* Nice, France, s.n.

Petiteau, J.-C.et al., 2013. Large strain rate-dependent response of elastomers at different strain rates: convolution integral vs. internal variable formulations. *Mechincs of Time-Dependent Material,* 17(3), pp. 349-367.

Pioletti, D. P., 1997. Viscoelastic properties of soft tissues: application to knee ligaments and tendons. In: *PhD thesis .* Lausan: EPFL.

Puso, M., 2006. A stabilized nodally integrated tetrahedral. *Interntional Journal of Numerical Methods in Engineering,* 67(6), pp. 841-867.

Puzrin, A. M. & Rabaiotti, C., 2010. A thermomechanical framework for non-linear hyperviscoelastic materials. *Journal of Rheology,* Volume 54, pp. 619-643.

Rayna, J., 2004. Technically SPEAKING: When did you last ride on retreads?. *Real Questions, Real Answers*, 9(1).

Ridha, R. A., Satyamurthy, K. & Hirschfelt, L. R., 1985. Finite Element Modeling of a Homogeneous Pneumatic Tire Subjected to Footprint Loadings. *Tire Science and Technology,* 13(2), pp. 91-110.

Rievaj, V., Vrábel, J. & Hudák, A., 2013. Tire Inflation Pressure Influence on a Vehicle Stopping Distances. *International Journal of Traffic and Transportation Engineering,* 2(2), pp. 9-13 .

Rivlin, R. S., 1992. The Elasticity of Rubber. *Rubber Chemistry and Technology,* 65(3), pp. 51-66.

Rivlin, R. S. & Sawyers, K. N., 1976. The Strain-Energy Function for Elastomers. *ransactions of The Society of Rheology,* 20(4), pp. 545-557.

Saleeb, A., D.A. Trowbridge, T. W., Marks, J. & Vesely, I., 2006. Dynamic pre-processing software for the hyperviscoelastic modeling of complex anisotropic biological tissue materials. *Advances in Engineering Software,* 37(9), pp. 609-623.

Sasso, M., Palmieri, G., Chiappini, D. & Amodio, D., 2008. Characterization of hyperelastic rubber-like materials by biaxial and uniaxial stretching tests based on optical methods. *Polymer Testing,* 27(8), pp. 995-1004.

Schmeitz, A., 2004. *A semi-empirical three-dimensional model of the pneumatic tyre rolling over arbitrary uneven road surfaces,* Delft: Delft University of Technology.

Schmeitz, A., 2008. *Parameter Identification for SWIFT ,* Helmond: TNO Automotive.

Schmid, M., 2011. *Tire Modeling for Multibody Dynamics Applications,* s.l.: University of Wisconsin-Madison.

Seibert, D. J. & Schöche, N., 2000. Direct Comparison of Some Recent Rubber Elasticity Models. *Rubber Chemistry and Technology,* 73(2), pp. 366-384.

Shida, Z., Koishi, M., T. Kogure, l. & Kabe, K., 1999. A Rolling Resistance Simulation of Tires Using Static Finite Element Analysis. *Tire Science and Technology,* 27(2), pp. 84-105.

Sills, S., Vorvolakos, K., Chaudhury, M. K. & Overney, R. M., 2007. Molecular Origins of Elastomeric Friction. In: E. Gnecco & E. Meyer, eds. *Nanotribology: Friction and Wear on the Atomic Scale.* s.l.:Springer, pp. 659-676.

Simulia, 2013. *Abaqus Analysis User's Manual,* s.l.: Dassault Systèmes.

Skiba, R., 1999. Aircraft Tyres: Differences Between Aircraft and Automotive Tyres. *Pacific Flyer*, September.

Smith, N. D., 2003. *Understanding Parameters Influencing Tire Modeling,* s.l.: Colorado State University.

Soedel, W., 1975. On the Dynamic Response of Rolling Tires According to their Shell Approximations. *Journal of Sound and Vibration,* 41(2), pp. 233-246.

Svendenius, J. & Wittenmark, B., 2003. *Brush tire models with increased flexibility.* Cambridge, UK, Proceedings of the European Control Conference.

Swanson, S., 1985. A constitutive model for high elongation elastic materials. *Journal of Engineering Materials and Technology - ASME Transaction,* Volume 107, pp. 110-115.

Teodorescu, 2000. Influence Factors on Truck Tyre Rolling Resistance. *Scientific Bulletin, Series D: Mechanical Engineering,* 62(2), pp. 65-73.

The Tire and Rim Association, 2007. *AIRCRAFT YEAR BOOK 2007.* Copley, Ohio, USA: The Tire and Rim Association, INC.

Thomson, R. W., 1847. *Improvement in carriage wheels.* United States, Patent No. 5104.

Tielking, J. T., 1984. A Finite Element Tire Model. *Tire Science and Technology,* 11(1-4), pp. 50-63.

Tillerson, J. R. & Haisler, W. E., 1970. *SAMMSOR II - A Finite Element Program to Determine Stiffness and Mass Matrices of Shells of Revolution,* Houston, TEXAS, USA: Texas A&M University.

TNO Automotive, 2010. *MF-Tyre & MF-SWIFT equation manual,* Helmond, Netherlands: TNO.

Torenbeek, E., 1982. *Synthesis of Subsonic Airplane Design.* s.l.:Delft University Press.

Treloar, L. R. G., 1943. The elasticity of a network of long-chain molecules. *Transactions of the Faraday Society,* Volume 39, pp. 36-41.

Treloar, L. R. G., 1974. The mechanics of rubber elasticity. *Journal of Polymer Science: Polymer Symposia,* 48(1), pp. 107-123.

Treloar, L. R. G., 1975. *The Physics of Rubber Elasticity.* 3rd ed. Oxford: Clarendon Press.

Truesdell, C. & Noll, W., 2004. *The Non-Linear Field Theories of Mechanics.* 3rd ed. s.l.:Springer-Verlog.

Tseng, N.-T., 1987. Finite Element Analysis of Freely Rotating Tires. *Tire Science and Technology,* 15(2), pp. 134-158.

Tseng, N. T., Pelle, R. G. & Chang, J. P., 1989. Finite Element Simulation of Tire-Rim Interface. *Tire Science and Technology,* 17(4), pp. 305-325.

Tuononen, A., Hartikainen, L., Petry, F. & Westermann, S., 2012. *Parameterization of in-plane rigid ring tire model from instrumented vehicle measurements.* Seoul, South Korea, AVEC.

Tyre Press, 2014. *Dunlop Aircraft Tyres launches new radial products at Singapore.* [Online] Available at: http://www.tyrepress.com/2014/02/dunlop-aircraft-tyres-launches-new-radial-products-at-singapore/
[Accessed 14 07 2014].

University of Birmingham, 2013. *Bluebear.* [Online] Available at: https://intranet.birmingham.ac.uk/it/teams/infrastructure/fm/bear/bluebear/index.aspx
[Accessed 24 11 2013].

van der Steen, R., 2010. *Enhanced friction modeling for steady-state rolling tires,* Eindhoven, Netherlands: Eindhoven University of Technology.

Wakefield, I. & Dubuque, C., 2009. Exceeding tire speed rating during take-off. *Aero Magazine*, pp. 15-19.

Wang, M. & Guth, E., 1952. Statistical theory of networks of non-Gaussian flexible chains. *The Journal of Chemical Physics,* 20(7), p. 1144–1157.

Watson, G., 2005. Airbus' Biggest Gamble - The A380 Takes Flight. *Wings magazine*, July/August.

Way, T. R. et al., 2009. Tractor tire aspect ratio effects on soil bulk density and cone index. *Journal of Terramechanics,* 46(1), pp. 27-34.

Wei, Y., Fan, C. & Guan, D., 2002. *Ring Model for Pneumatic Tires.* s.l., IEEE, pp. 496-501.

Yang, X., 2011. *Finite element analysis and experimental investigation of tyre characteristics for developing strain-based intelligent tyre system,* Birmingham, UK: University of Birmingham.

Yang, X. & Olatunbosun, O., 2012. Optimization of Reinforcement Turn-up Effect on Tyre Durability and Operating Characteristics for Racing Tyre Design. *Materials & Design,* Volume 35, pp. 798-809.

Yang, X., Olatunbosun, O. & Bolarinwa, E., 2009. Generation of Tyre Cross-sectional Geometry for FE Tyre Model Using Image Processing Techniques. *International Journal of Engineering Simulation.,* 10(1), pp. 3-10, ISSN 1468-1137.

Yavari, B., Tworzydlo, W. & Bass, J. M., 1993. A Thermomechanical Model to Predict the Temperature Distribution of Steady State Rolling Tires. *Tire Society and Technology journal,* 21(3), pp. 163-178.

Yeoh, O. H., 1990. Characterization of Elastic Properties of Carbon-Black-Filled Rubber Vulcanizates. *Rubber Chemistry and Technology,* 63(5), pp. 792-805.

Yeoh, O. H., 1993. Some Forms of the Strain Energy Function for Rubber. *Rubber Chemistry and Technology,* 66(5), pp. 754-771.

Yeoh, O. H. & Fleming, P. D., 1998. A new attempt to reconcile the statistical and phenomenological theories of rubber elasticity. *Journal of Polymer Science Part B: Polymer Physics,* 35(12), pp. 1919-1931.

Yin, H. S. et al., 2006. Truck Tire Thermal-Mechanical FEA and DMA with Application to Endurance Evaluation. *Tire Science and Technology,* 34(4), pp. 220-236..

Yokohama tire, 2014. *Tire specifications.* [Online] Available at: www.yokohamatire.com [Accessed 14 07 2014].